Universitat Politècnica de València
Departamento de Máquinas y Motores Térmicos

An assessment of fuel physical and chemical properties in the combustion of a Diesel spray

Doctoral Thesis
Presented by:
Jean-Guillaume Nerva
Directed by:
Dr. José Vicente Pastor Soriano

Valencia, 24th May 2013

à la memoire de notre p'tite mamie

à mes parents, à ma famille

Doctoral Thesis

An assessment of fuel physical and chemical properties in the combustion of a Diesel spray

Presented by: Jean-Guillaume Nerva
Directed by: Dr. José Vicente Pastor Soriano

Examining Board:

President:	Dr. Jesús Benajes Calvo
Secretary:	Dr. José M. García Oliver
Examiners:	Dr. Gilles Bruneaux
	Dr. José E. Juliá Bolívar
	Dr. Magín Lapuerta Amigó

Valencia, 24th May 2013

Remerciements. À l'heure d'exprimer mes remerciements, je repense à ce long voyage et le refais à l'envers. Il a été long, difficile, pénible parfois même. J'ai la chance d'être arrivé au bout. J'y ai certainement beaucoup appris sur moi-même, mes vertus, mes limites, mes vices même. Il y aura indéniablement un avant et un après. Une chose m'apparaît comme évidente cependant: je n'ai pu en voir la fin que grâce à ceux qui m'ont accompagné et aux fructueuses rencontres que j'ai faites en chemin.

Je tiens donc à remercier en premier lieu le *Departamento de Maquinas y Motores Térmicos*, et en particulier, ses deux dirigeants, le Dr. Francisco Payri et le Dr. José María Desantes qui m'ont accueilli au sein de leur centre de recherche. Je remercie également le Ministère de la Recherche et de l'Innovation espagnol pour son soutien économique et matériel qui m'a permis de réaliser ce travail et l'élaboration de cette thèse.

J'associe évidemment à ces remerciements le Dr. José Vicente Pastor Soriano pour la confiance et la liberté qu'il m'a accordées. Si comme à l'image d'une plante, un tuteur n'aide pas directement à grandir, il aide avant tout à pousser dans la bonne direction. Ainsi, il a su recadrer mon travail aux moments opportuns, contenir mes enthousiasmes, me soutenir dans les moments plus difficiles. En cela, il a parfaitement rempli la tâche qui lui incombait.

Il serait difficile de ne pas citer ceux avec qui l'histoire a commencé : le Dr. José Galindo et Raúl Luján, avec qui j'ai réalisé mes premiers pas comme stagiaire, et qui m'ont en quelque sorte mis le pied à l'étrier. J'étais alors sans aucune maitrise de la langue, et ils ont eu la patience de m'enseigner leur métier et les joies de la programmation. Je les en remercie vivement. Elle s'est poursuivie par le master, la thèse, avec la participation de nombreux professeurs pour leur élaboration respective. Ainsi, je tiens à dire ma reconnaissance aux Drs. José María García Oliver, José Manuel Pastor, Jean Arrègle, Javier López, Ricardo Novella et Antonio García pour leur fine connaissance de la dynamique du jet Diesel et plus globalement des processus de combustion dans un environnement aussi hostile que celui d'une chambre de combustion. Ils ont représenté un soutien quasi-quotidien et leurs orientations bibliographiques m'ont été précieuses. Plusieurs tâches spécifiques ont nécessité le concours d'autres professeurs et chercheurs du Département. J'associe donc également à ces remerciements les Drs. Gabriela Bracho, Javier Salvador et Jaime Gimeno pour leur aide sur les taux d'introduction. Je remercie chaleureusement aussi les Drs. Jaime Martín et Pablo Olmeda pour leur éclairage sur le traitement du signal de pression et son filtrage, et enfin, les Drs. Bernardo Tormos, José Manuel Luján et tout particulièrement

le Dr. Yesid Gómez pour leur collaboration lors de la caractérisation physico-chimique des combustibles.

Dans le cadre de ma formation doctorale, j'ai aussi eu la chance d'effectuer trois séjours à l'étranger. Je remercie donc les Drs. Lyle Pickett et Caroline Genzale, Dave, Cherissa et Lisa de Sandia National Laboratory (Livermore, USA), le Dr. Tesuya Aizawa de Meiji University (Tokyo, Japon) ainsi que tous ses élèves, et enfin Rudolf Wimmer et Christian Brandhofer de BMW Motoren (Steyr, Autriche) de m'avoir accueilli au sein de leur établissement respectif. J'ai beaucoup appris à leur côté, à la fois techniquement et humainement.

Je tiens également à rendre un hommage appuyé à ceux sans qui une grande partie des données et résultats condensés dans cette thèse n'auraient jamais vu le jour. Ils restent malheureusement trop souvent dans l'ombre de nos publications et un grand mérite doit leur être reconnu. Je remercie donc le technicien Daniel Lérida avec qui j'ai partagé de nombreuses heures devant le moteur, ainsi que mes stagiaires, Axel, Carlos Bosch, Inma, Cesar, Céline, Sophie, Alexandre, Sébastien, Guillaume, avec qui j'ai partagé de nombreuses heures devant... Matlab. Un grand merci à eux. Leur aide me fut précieuse.

Il leur a parfois été difficile de prendre la pleine mesure de l'effort et de l'implication requis par la tâche, de là vient immanquablement tout leur mérite puisqu'ils ont fait preuve à mon égard d'un soutien sans faille. Ils sont à la fois la soupape de décompression et la bouffée d'oxygène de cette thèse. Je pense bien évidement à mes parents en premier lieu, Chantal et Christian, à ma soeur Christa, et sa petite tribu, Sylvain, Terry, Killyan et Eva. Je pense aussi à mes amis, les *Carmeneros* d'abord, à Diego, Monica, Alberto, Zenaida, Irene, Micha, Angela, Jorge, Pablo, Alejandro et María, mais aussi à Majo, Herminia, Bea, Edu, et tout particulièrement Ana, celle qui a partagé mon quotidien, mes voyages, mes doutes, mes joies, et donc vécu aux premières loges tout ce cheminement. Mes pensées vont également vers Amparo, Francisco et toute sa famille qui m'ont eux aussi beaucoup assisté et encouragé sur cette route de montagne.

Je remercie enfin mes collègues de *despacho*, Francisco Briceño, Gustavo Ramirez et Carlos Micó, mon collègue et colloc' Simon Arthozoul, et tous les autres collègues doctorants du CMT. Je remercie aussi Chris Kolodziej et Rob Pickering d'avoir éclairé certains points de cette thèse et leur expression dans la langue de Shakespeare. Je remercie enfin tout le personnel administratif de nous faciliter ces tâches parfois ingrates du quotidien, une aide qui n'est pas toujours de mise dans d'autres départements. J'espère que ceux que j'oublie me pardonneront.

À tous, une grande partie de ce travail vous appartient.

Agradecimientos. A la hora a expresar mis agradecimientos, echo la vista atrás y recuerdo el viaje realizado. Fue largo, difícil, incluso doloroso. Tengo la suerte de haber llegado al final. Sin duda, aprendí mucho sobre mí mismo, mis virtudes, mis limitaciones, incluso mis vicios. Obviamente, habrá un antes y un después. Sin embargo hay algo que es obvio, y es que solo pude ver su termino gracias a los que me acompañaron, y a aquellos que he conocido y me han ayudado a lo largo del camino.

Así pues, quiero dar las gracias en primer lugar al Departamento de Máquinas y Motores Térmicos, y en particular a sus dos dirigentes, el Dr. Francisco Payri y Dr. José María Desantes, por recibirme en su centro de investigación. También quiero agradecer al Ministerio de Investigación e Innovación Español por su apoyo económico y material, que me permitió realizar este trabajo, y por último, el desarrollo de esta tesis.

Incluyo evidentemente en estos agradecimientos al Dr. José Vicente Pastor Soriano por la confianza y la libertad que me ha dado. Como en una planta, un tutor no ayuda directamente a crecer, ayuda sobre todo a crecer en la dirección correcta. Fue capaz de recentrar mi trabajo en los momentos adecuados, de contener mis entusiasmos, me apoyó en los momentos difíciles, por lo que cumplió perfectamente con la tarea que le incumbía.

Sería difícil no hablar de aquellos con quien empezó la historia, el Dr. José Galindo y Raúl Luján, con quien hice mis primeros pasos como alumno de prácticas, y quienes de alguna manera, me han puesto el *"pied à l'étrier"*. Sin ningún conocimiento de la lengua, tuvieron la paciencia de enseñarme su oficio y las alegrías de la programación. Les doy las gracias por ello. Se continuó aquella historia con el master, la tesis, y la participación de muchos profesores en sus respectivos desarrollos. Así, doy las gracias a los Dres. José María García Oliver, José Manuel Pastor, Jean Arrègle, Javier López, Ricardo Novella y Antonio García por su fino conocimiento de la dinámica del chorro Diesel, y más en general de los procesos de combustión en un ambiente tan hostil como es el de una cámara de combustión. Constituyeron un apoyo casi-diario, y sus orientaciones bibliográficas fueron preciosas. Varias tareas específicas requirieron la contribución de otros profesores e investigadores del Departamento. Incluyo también en este agradecimiento a la Dra. Gabriela Bracho y los Dres. Javier Salvador y Jaime Gimeno por su ayuda en la tasas de inyección. Además me gustaría agradecer a los Dres. Jaime Martín y Pablo Olmeda por su ayuda en el tratamiento de la señal de presión y su filtrado, y por último, a los Dres. Bernardo Tormos, José Manuel Luján y particularmente al Dr. Yesid Gómez por su apoyo durante la caracterización físico-química de los combustibles.

Como parte de mi formación doctoral, también tuve la oportunidad de hacer tres estancias en el extranjero. Doy las gracias a los Dres. Lyle Pickett y Caroline Genzale, Dave, Cherissa y Lisa del Sandia National Laboratory (Livermore, EEUU), al Dr. Tetsuya Aizawa de la Universidad de Meiji (Tokyo, Japón) y a todos sus alumnos. A Rudolf Wimmer y Christian Brandhofer de BMW Motoren (Steyr, Austria), por darme la bienvenida en sus respectivas instituciones. He aprendido mucho de cada uno de ellos, tanto en el aspecto técnico como en el humano.

También quiero hacer un homenaje muy especial a los que me han ayudado a conseguir la mayor parte de los datos y resultados que aparecen condensados en esta tesis, y sin ellos no habría germinado. Por desgracia, se quedan muy a menudo en la sombra de nuestras publicaciones y un gran merito se les debe de reconocer. Doy las gracias al técnico Daniel Lérida con quien he compartido muchas horas delante del motor, así como a mis alumnos de proyecto: Axel, Carlos Bosch, Inma, Cesar, Celine, Sophie, Alexandre, Sébastien y Guillaume, con quien compartí muchas horas delante de... Matlab. Muchísimas gracias a todos por vuestra preciosa ayuda.

A veces ha sido difícil para ellos tomar conciencia del esfuerzo y del compromiso requeridos por el ejercicio, de aquí realmente viene todo su mérito, ya que me mostraron un apoyo incondicional en todo momento. Son a la vez la válvula de escape y el soplo de oxígeno de esta tesis. Pienso primero, por supuesto, en mis padres Chantal y Christian, mi hermana Christa y su pequeña tribu: Sylvain, Terry, Killyan y Eva. Y pienso en los "Carmeneros": Diego, Mónica, Zenaida, Alberto, Irene, Micha, Angela, Jorge, Pablo, Alejandro y María. También en Majo, Herminia, Bea, Edu, y especialmente en Ana, con quien comparto mi vida cotidiana, mis viajes, mis dudas, mis alegrías, y así vivió este pequeño viaje a la vanguardia. Tampoco puedo olvidar a Amparo, Francisco y toda su familia, que también me asistieron y me ayudaron mucho en este camino de montaña.

Por último, agradezco a mis compañeros de despacho Francisco Briceño, Gustavo Ramírez y Carlos Micó, mi colega y compañero de piso Simon Arthozoul, y el resto de doctorandos del CMT. Quiero agradecer a Chris Kolodziej y Rob Pickering por ayudarme en aclarar algunos puntos de esta tesis y su expresión en la lengua de Shakespeare. También dar las gracias a todo el personal administrativo, por ayudarnos con estas tareas a veces ingratas de lo cotidiano, ayuda que no siempre se brinda en otros departamentos. Espero que aquellos de los que me haya olvidado me perdonen.

A todos, una gran parte de este trabajo os pertenece y os esta dedicado.

Acknowledgment. Now that the time has come to express my thanks, I look back on this long journey and think about what has been achieved and who aided me in this process. It has been long, difficult, painful sometimes but I feel that I am lucky to have reached the end. I certainly learned a lot about myself, my virtues, my limits, my vices as well. There is definitely a before and an after but one thing appears fairly obvious to me nonetheless, I could only reach the finish line thanks to those who accompanied me, and the contributions they have made along the way.

I would like first to thank the *Departamento de Maquinas y Motores Térmicos*, and in particular its two leaders Dr. Francisco Payri and Dr. José María Desantes for hosting me in their research centre. I also thank the Spanish Ministry of Research and Innovation for its economic and material support that allowed me to perform my work and be able to carry out the research necessary for this thesis.

Naturally, I add to these thanks to Dr. José Vicente Pastor Soriano for the confidence and freedom he has given me. As for a plant, a *"tuteur"* (in french) may not directly help it to grow, it primarily helps in having that plant pushing in the right direction. He was able to reframe my work at appropriate times, to contain my enthusiasms, support me in difficult times, and therefore he perfectly fulfilled the task he was assigned to.

It would be difficult not to mention those with whom the story began, Dr. José Galindo and Raúl Luján, with whom I made my first steps as a student, and therefore who somehow set my foot in the caliper. Without any knowledge of the language, they had the patience to pass on to me their expertise and the joy of programming. I thank them for that. It then continued with the masters, the thesis, and the contributing participation of several other teachers whom I wish to thank for their help in this accomplishment. Thus, I thank Drs. José María García Oliver, José Manuel Pastor, Jean Arrègle, Javier López, Ricardo Novella and Antonio García for their detailed knowledge of Diesel jet dynamics and more generally the combustion processes in a hostile environment such as that of a combustion chamber. They represented an almost daily support and their bibliographical guidance has been precious. Several specific tasks required the contribution of other professors and researchers from the Department. So, I also add to these thanks Drs. Gabriela Bracho, Javier Salvador and Jaime Gimeno for their help with injection mass flow rates. I also warmly thank Drs. Jaime Martín and Pablo Olmeda for their help with the treatment of the pressure signal and its filtering, and finally, Drs. Bernardo Tormos,

José Manuel Luján and especially Dr. Yesid Gómez for their support during the physico-chemical characterization of the fuels.

As part of my doctoral training, I also had the chance to participate in three internships abroad. I thank Drs. Lyle Pickett and Caroline Genzale, Dave, Lisa and Cherissa from Sandia National Laboratory (Livermore, USA), Dr. Tetsuya Aizawa from Meiji University (Tokyo, Japan) and all his students, Rudolf Wimmer and Christian Brandhofer from BMW Motoren (Steyr, Austria) for welcoming me into their respective institutions. I learned a lot on their side, both technically and humanly.

I also want to pay tribute to those without whom much of the data and results summarized in this thesis would never have emerged. Unfortunately, they are too often in the shadows of our publications and a great credit must be given to them. I thank the technician Daniel Lérida with whom I shared many hours in front of the engine, as well as my undergraduate students, Axel, Carlos Bosch, Inma, Cesar, Celine, Sophie, Alexander, Sébastien and Guillaume, with whom I shared many hours in front of... Matlab. A big thank you to you all for your help.

It was sometimes difficult for them to take on board the full measure of effort and involvement required by the task, and from there actually comes their ultimate help as they continually supported me regardless. They are both the relief valve and the breath of fresh air of this thesis. I think of course about my parents first, Chantal and Christian, my sister Christa, and her little tribe, Sylvain, Terry, Killyan and Eva. I think about my friends the *Carmeneros*, Diego, Monica, Alberto, Zenaida, Irene, Micha, Angela, Jorge, Pablo, Alejandro and Maria, but also about Majo, Herminia, Bea, Edu, and particularly Ana, who shared my daily life, my travels, my doubts, my joys, and thus lived this little journey with me every step of the way. I also add thanks to Amparo, Francisco and her entire family who encouraged and assisted me on this mountainous road.

Finally, I thank my colleagues from the *despacho*, Francisco Briceño, Gustavo Ramirez and Carlos Micó, my colleague and roommate Simon Arthozoul, and all the other doctoral fellows from CMT. I also thank Chris Kolodziej and Rob Pickering for discerning certain points of this thesis and their expression in the language of Shakespeare. I also thank all the administrative staff who have assisted us with all of these sometimes ungrateful tasks, making our daily life easier. While this is not an exhaustive list, I hope that those whose names I have forgotten will forgive me.

To all, a large part of this work belongs to you.

Abstract. With the slow but ineluctable depletion of fossil fuels, several avenues are currently being explored in order to define the strategic boundaries for a clean and sustainable energetic future, while accounting for the specificities of each sectors involved. In regard to transport applications, alternative fuels may represent a promising solution, at least at short or middle term, such as the International Energy Agency foresees that their share could account for 9 % of the road transport fuel needs by 2030 and 27 % by 2050, with the potential resources to reach 48 % beyond. If they have already been included in significant blending proportions with conventional fossil fuel in most of the occidental countries, their introduction also coincides with a long-time established program of continuously more drastic standards for engine emissions of NO_x and PM, now even further demanding by the seek for combustion efficiency aiming at reducing CO_2 emissions.

While several works discuss the alternative fuels effect on exhaust emissions when used directly in production Diesel engines, results and analysis are sometimes contradictory, depending sometimes on the conditions in which they were obtained, and the causes of these results remain unclear. Therefore, in order to better understand their effect on the combustion processes, and thus extract the maximum benefits from these fuels in the optimization of engine design and calibration, a detailed comprehension of their spray and combustion characteristics is essential.

The approach of this study is mostly experimental and based on an incremental methodology of tests aiming at isolating injection and combustion processes with the objective to identify and quantify the role of both fuel physical and chemical properties at some key stages of the Diesel combustion process. After obtaining a detailed characterization of their properties, five fuels have been injected in an optical engine enabling a sharp control of the thermodynamic environment, and the application of optical techniques for spray measurements and characterization. Diagnostics applied to free jets in inert conditions allowed to discuss the fuel effect on the processes of atomization, vaporization and development of the mixture fraction field, while the reactive environment, by including the previous findings, enabled to assess their effect on ignition, soot formation and flame temperature.

As a result, empirical models have been developed in order to predict the liquid length of these fuels based on their properties measured by standards at ambient conditions. These correlations confirmed the minor effect of liquid atomization for fuel vaporization as stated in the Siebers mixing-limited hypothesis. They also revealed the significance of fuel latent heat well correlated by the fuel density. By extension of results obtained in another laboratory, the equivalence ratio at any point of the inert spray showed to be

likely modified by the unique difference in stoichiometry among fuels. Under reactive conditions, the key role played by fuel ignitability on the lift-off length establishment has been confirmed as well as the role of the latter on soot formation. The increase of flame sooting propensity showed to cool down the flame and produce lower flame temperature, a priori in favor of decreasing thermal NO_x formation. Such chain-reaction between ignition, lift-off, soot formation and flame temperature was already suggested in the literature although in separate studies. For the first time, these relationships were associated in the same test campaign with the objective to assess the effect of fuel properties on the spray reaction of combustion. By permitting a better understanding of the fuel effect and its consequences on key stages of the Diesel combustion, this study provides arguments to discuss the emissions results obtained with real production engines and beyond, also provides a database of both inputs and outputs for comparison with spray and combustion modeling. In that sense, it participates to the global effort on the way to improve the design of future engines in terms of efficiency and contamination.

Résumé. Avec l'épuisement lent mais inéluctable des combustibles d'origine fossile, plusieurs pistes sont actuellement à l'étude afin de définir les contours stratégiques d'un futur énergétique propre et pérenne, tout en prenant en compte les spécificités de chacun des secteurs concernés. En ce qui concerne le domaine des transports, les combustibles alternatifs peuvent représenter une solution prometteuse, au moins à court ou moyen terme, au point que l'Agence Internationale de l'Energie prévoie que leur part puisse représenter jusqu'à 9 % du carburant dédié au transport routier d'ici 2030 et 27 % d'ici 2050, avec les ressources potentielles pour atteindre 48 % au-delà. S'ils sont déjà présents dans d'importantes proportions sous forme de mélange avec le carburant fossile conventionnel dans la plupart des pays occidentaux, leur introduction coïncide également avec un programme établi de longue date, fixant des normes sans cesse plus drastiques pour les émissions des moteurs en termes de NO_x et PM, et dont le calendrier est rendu encore plus exigeant aujourd'hui par la recherche de meilleurs rendements de combustion visant à réduire les émissions de CO_2.

Alors que plusieurs études ont déjà traité l'effet de différents combustibles alternatifs sur les émissions de gaz d'échappement lorsque ceux-ci sont employés directement dans des moteurs Diesel de série, les résultats et les analyses sont parfois contradictoires, dépendant parfois des conditions dans lesquelles ceux-ci ont été obtenus, et les causes exactes de ces résultats demeurent encore incertaines. Par conséquent, avec pour objectif de mieux comprendre l'effet de ces combustibles sur les processus de combustion, et afin d'en extraire ensuite le maximum de bénéfices dans l'optimisation, la calibration et la future conception des moteurs, une compréhension détaillée de leur caractéristiques et de leur effet sur le jet Diesel est essentielle.

L'approche de cette étude est avant tout de type expérimental et est basée sur une méthodologie incrémentale d'essais visant à isoler les différents procédés d'injection et de combustion dans le but d'identifier et de quantifier le rôle des propriétés physico-chimiques du combustible à certaines étapes clés du processus de combustion Diesel. Après avoir obtenu une caractérisation détaillée de leurs propriétés, cinq combustibles ont été injectés dans un moteur optique permettant un contrôle pointu de l'environnement thermodynamique, et l'application de techniques optiques pour la mesure et la caractérisation du jet Diesel. Ces diagnostics appliqués au jet libre en conditions inertes ont permis d'analyser l'effet du combustible sur les processus d'atomisation, de vaporisation et de développement du champ de fraction de mélange, tandis qu'en milieu réactif, tout en tenant compte des conclusions précédentes, ils ont ainsi permis d'évaluer leur effet sur l'auto-inflamation, la formation de suie et la température de flamme.

Pour résultats, des modèles empiriques ont été développés afin de prédire la pénétration liquide de ces combustibles en fonction de leurs propriétés mesurées par des standards à conditions ambiantes. Ces corrélations ont confirmé l'effet mineur de l'atomisation dans le processus d'évaporation comme le suggère l'hypothèse de "contrôle par mélange" émise par Siebers. Ils ont également révélé l'importance de la l'enthalpie de vaporisation qui se trouve être bien corrélée par la densité du combustible. Enfin, par extension des résultats obtenus dans un autre laboratoire, la richesse en tout point du jet semble n'être modifiée que par la seule différence de stœchiométrie entre combustibles. En conditions réactives, le rôle clé joué par l'auto-inflammation du combustible dans l'établissement de la longueur de *lift-off* (décollement) a été confirmé, ainsi que le rôle de ce dernier sur la formation de suie. Egalement, les flammes plus enclines à former des suies ont montré un refroidissement dû à la radiation, réduisant ainsi les températures locales et suggérant en conséquence une réduction de la formation de NO_x d'origine thermique qui y est associée. Une telle réaction en chaîne entre l'auto-inflammation, le dosage au *lift-off*, la formation de suie et la température de flamme a déjà été suggérée dans la littérature, mais souvent séparément. Pour la première fois, ces relations ont été associées dans une même campagne d'essais et exploitées afin d'évaluer l'effet des propriétés du combustible sur la réaction de combustion du jet. En permettant une meilleure compréhension de ces effets et de leurs conséquences sur les étapes critiques de combustion Diesel, cette étude fournit des arguments pour discuter les résultats d'émissions obtenus avec ce type de combustibles dans des conditions réels mettant en jeu des moteurs de série. Au-delà, elle fournit également une base de données servant de référence pour comparaison avec des résultats de modélisation de jet. En ce sens, elle participe à l'effort global permettant d'améliorer la conception des futurs moteurs en termes de rendement et de contamination.

Resumen. Con el agotamiento lento pero ineludible de los combustibles fósiles, varias vías se están estudiando actualmente con el fin de definir los límites estratégicos para un futuro energético limpio y sostenible, al tiempo que representa las características específicas de cada uno de los sectores involucrados. En lo que respecta a las aplicaciones de transporte, los combustibles alternativos pueden representar una solución prometedora, al menos a corto o mediano plazo, tales como la Agencia Internacional de Energía prevé que su participación podría hacerse cargo de un 9 % del combustible necesitado por del transporte de carretera para el año 2030 y del 27 % para el año 2050, con los recursos posibles para llegar a 48 % más allá. Si ya han sido incluidos en importantes proporciones de mezcla con combustibles fósiles convencionales en la mayoría de los países occidentales, su introducción también coincide con un programa histórico fijando normas continuamente más drásticas de las emisiones de los motores de NO_x y PM, ahora aún más exigentes por buscar la eficiencia de la combustión y así reducir las emisiones de CO_2.

Si bien varios trabajos discuten del efecto de los combustibles alternativos en las emisiones de gases de escape cuando se utilizan directamente en motores Diesel de producción, sus resultados y análisis son a veces contradictorios, dependiendo a veces de las condiciones en que fueron obtenidos, y las causas de estos resultados siguen siendo poco claras. Por lo tanto, con el fin de comprender mejor su efecto sobre los procesos de combustión, y por lo tanto extraer los máximos beneficios de estos combustibles en la optimización del diseño del motor y de calibración, una comprensión detallada de sus características de chorro y combustión es esencial.

El enfoque de este estudio es experimental, y sobre todo basado en una metodología incremental de ensayos destinada a aislar a los procesos de inyección y de combustión, con el objetivo de identificar y cuantificar el papel de las propiedades físico-químicas del combustible, en algunas etapas clave del proceso de combustión Diesel. Después de obtener una caracterización detallada de sus propiedades, cinco combustibles se han inyectado en un motor óptico que permite un control agudo del entorno termodinámico producido, y la aplicación de técnicas ópticas para la medición y la caracterización del chorro. Diagnósticos aplicados a los chorros libres en condiciones inertes permitieron discutir del efecto del combustible sobre los procesos de atomización, de vaporización y de desarrollo del campo de fracción de mezcla, mientras que en su entorno reactivo, incluyendo los resultados anteriores, permitió evaluar su efecto sobre el auto-encendido, la formación de hollín y de las llamas temperatura.

Como resultado, modelos empíricos se han desarrollado con el fin de predecir

la longitud liquida de los combustibles en base a sus propiedades medidas por estándares en condiciones ambientales. Estas correlaciones confirman el efecto de menor importancia de la atomización de líquido para la vaporización de combustible como se indica en la hipótesis de chorro "controlado por mezcla" emitida por Siebers. También reveló la importancia del calor latente del combustible que correlaciona bien con la densidad del combustible. En fin, por extensión de los resultados obtenidos en otro laboratorio, la riqueza en todo punto del chorro inerte mostró ser modificada solamente por la relación de estequiometria entre combustibles. En condiciones de chorro reactivo, el papel clave desempeñado por la cualidad de ignición en el establecimiento de longitud de *lift-off* (despegue) ha sido confirmado, así como el de éste último en la formación de hollín. Además, las llamas más propensas a formar hollín mostraron un enfriamiento debido a la radiación, reduciendo así las temperaturas locales y por lo tanto, lo que sugiere una reducción en la formación del NO_x térmico asociado. Tal reacción en cadena entre el auto-encendido, dosado en el *lift-off*, formación de hollín y temperatura de la llama ya se sugirió en la literatura aunque de forma aislada. Por primera vez, estas relaciones se han asociado en la misma campaña de ensayos con el objetivo de evaluar el efecto de las propiedades del combustible en la reacción de combustión del chorro. Al permitir una mejor comprensión de estos efectos y sus consecuencias en las etapas críticas de la combustión Diesel, este estudio proporciona argumentos para discutir los resultados obtenidos con la emisión de este tipo de combustible en condiciones reales de motor. Además, también proporciona una base de datos que pueda servir de referencia para comparación con resultados de chorros modelados. En este sentido, contribuye al esfuerzo general para mejorar el diseño de los futuros motores en términos de rendimiento y de contaminación.

Resum. Amb l'esgotament lent però ineludible dels combustibles fòssils, diverses vies s'estan estudiant actualment per tal de definir els límits estratègics per a un futur energètic net i sostenible, alhora que representa les característiques específiques de cada un dels sectors involucrats. Pel que fa a les aplicacions de transport, els combustibles alternatius poden representar una solució prometedora, almenys a curt o mitjà termini, com ara l'Agència Internacional d'Energia preveu que la seua participació podria ser responsable d'un 9 % del combustible del transport per carretera necessari per a l'any 2030 i el 27 % per l'any 2050 amb els recursos possibles per arribar a 48 % més enllà. Si ja han estat inclosos en importants proporcions de barreja amb combustibles fòssils convencionals en la majoria dels països occidentals, la seua introducció també coincideix amb un programa històric fixant normes contínuament més dràstiques de les emissions de NO_x i PM als motors, ara encara més exigents per a buscar l'eficiència de la combustió i per a reduir així les emissions de CO_2.

Si bé diversos treballs discuteixen l'efecte dels combustibles alternatius en les emissions de gasos d'escapament quan s'utilitza directament en motors dièsel de producció, resultats i anàlisi són de vegades contradictoris, depenent de les condicions en que van ser obtinguts, i les causes d'aquests resultats continuen sent poc clares. Per tant, per tal de comprendre millor el seu efecte sobre els processos de combustió, i per tant extreure els màxims beneficis d'aquests combustibles en l'optimització del disseny del motor i de calibratge d'aquest, una comprensió detallada de les seues característiques i de la seua evolució al doll (polvorització) i a la combustió és essencial.

L'enfocament d'aquest estudi és experimental i sobretot es basa en una metodologia incremental de les proves destinades a aïllar els processos d'injecció i de combustió, amb l'objectiu d'identificar i quantificar el paper de les propietats del combustible, tant físiques com químiques en algunes etapes clau del procés de combustió Diesel. Després d'obtindre una caracterització detallada de les seues propietats, cinc combustibles s'han injectat en un motor òptic que permet un control òptim de les condicions termodinàmiques (ambientals), i l'aplicació de tècniques òptiques per a la mesura i caracterització del doll. Diagnòstics aplicats als dolls lliures en condicions permiteixen discutir l'efecte del combustible en els processos d'atomització, vaporització i el desenvolupament del camp de fracció de mescla, mentre que l'entorn reactiu, mitjançant la inclusió dels resultats anteriors, donarà l'oportunitat d'avaluar el seu efecte sobre el auto-encesa, la formació de sutge i de les flames temperatura.

Com a resultat, els models empírics han sigut desenvolupats per tal de predir la longitud líquida dels combustibles en base a les seues propietats mesurades en

condicions ambientals estàndards. Aquestes correlacions confirmen la menor importància de l'efecte de l'atomització de líquid per a la vaporització de combustible com s'indica en la hipòtesi de "control per mescla" emesa per Siebers. També van revelar la importància de la calor latent del combustible que correlaciona bé per a la densitat del combustible. Per extensió dels resultats obtinguts en un altre laboratori, la relació d'equivalència aire combustible local en qualsevol punt del doll inert va mostrar ser probablement modificada únicament per la diferència entre l'estequiometria dels combustibles. En condicions reactives, el paper clau desenvolupat per la capacitat d'ignició en l'establiment de longitud d'enlairament de la flama ha estat confirmada així com el paper d'aquestes en la formació de sutge. L'augment de la propensió de les deposicions de sutge mostrat per les flames, que es refredi la flama i produir una menor temperatura d'aquesta, a priori afavoreix la disminució de la formació de NO_x mitjançant la via tèrmica. Tal reacció en cadena entre l'encesa, l'enlairament, la formació de sutge i la temperatura de la flama ja es va suggerir en la literatura encara que de forma indirecta, però per primera vegada es van associar en la mateixa prova amb l'objectiu d'avaluar l'efecte de les propietats del combustible a la les etapes clau del procés de polvorització i de combustió. Permetent una millor comprensió de l'efecte del combustible i les seues conseqüències en les etapes crítiques de la combustió del dièsel, aquest estudi proporciona arguments per discutir els resultats obtinguts amb les emissions dels motors reals de producció i va més enllà, també proporciona una base de dades per a la comparació amb l'aerosol i el modelització de la combustió, i en aquest sentit, participa en l'esforç global en la manera de millorar el disseny dels futurs motors en termes d'eficiència i la contaminació.

Table of Contents

Index of Figures

Index of Tables

Nomenclature

Latin

A/F	Air-fuel ratio
A	Soot projected area ratio
	Nozzle area
A_a	Projected area soot aggregate considered
A_p	Projected area of the averaged primary particle
$c_{1\ or\ 2}$	Plank constants
C_a	Nozzle area coefficient
C_d	Nozzle discharge coefficient
C_M	Nozzle momentum coefficient
c_p	Specific heat capacity at constant pressure
C_v	Nozzle velocity coefficient
c_v	Specific heat capacity at constant volume
d	Exit diameter of the nozzle
D_f	Fractal dimension
d_p	Primary particle diameter
D_t	Thermal diffusion
Da	Damköhler number
E_a	Energy of activation
f_v	Soot volume fraction
h	Specific enthalpy per unit of mass
I	Laser intensity
	Spectral radiance
k_a	Absorption coefficient
k_e	Extinction constant

k_f	Pre-factor for soot morphology characterization
Ka	Karlovitz number
$K - factor$	Nozzle convergence
KL	Optical thickness with K, extinction coefficient and L, path length
L_v	Enthalpy of vaporization per unit of mass
m	Mass
$\dot{m}$	Mass flow rate
$\dot{M}$	Momentum flux
n	Polytropic index
n_p	Number of soot particles
n_{pxl}	Number of pixels per soot aggregate
P	Pressure
R	Universal gas constant
r	Distance between a pixel and the centroid of the particle
R^2	Coefficient of determination
R_g	Radius of gyration
Re	Reynolds number
s	Scattering
$S(t)$	Spray penetration as a function of time
s_L	Propagation velocity of the laminar flame
t	Time
T	Temperature
$T_{x\,\%}$	Temperature of the x % recovery from distillation
u	Spray axial velocity
V	Volume
X	Spray axial coordinate
Y	Mixture fraction

Greeks

α	Absorption
	Empirical coefficient accounting for particles overlapping effect
α_{sa}	scattering albedo
Δ	Variation/Increment
ϵ	Emissivity
η	Combustion efficiency
λ	Wavelength
ν	Viscosity

ϕ	Equivalence ratio
ρ	Density
σ	Standard deviation
τ	Ignition delay
	Transmittance
θ	Spray spreading angle

Subscripts

0	Relative to initial conditions
a or air	Relative to air (with standard composition)
ad	Relative to adiabatic conditions
adm	Relative to admision conditions
amb	Relative to ambient conditions within the test rig
app	Relative to apparent value
b	Relative to bulk conditions
$back$	Relative to back-pressure
bb	Black body
cl	Relative to spray center line
eff	Relative to efficient value
eq	Equivalent
$evap$	Relative to evaporation conditions
ext	Extinction
f or $fuel$	Relative to the fuel
geo	Geometric
inj	Relative to fuel injection
$inlet$	Relative to inlet conditions
int	Relative to intake conditions
l	Relative to liquid phase
max	Maximum value
min	Minimum value
noz	Relative to the nozzle
$outlet$	Relative to outlet conditions
spe	Specific
st	Relative to stoichiometric conditions
th	Relative to the theoretical value

vap	Relative to vapour phase

Acronyms

0-, 1-, 2- ,3-D	zero-, one- two, three-dimensional
2C	2-color
AHRR	Apparent heat release rate
ASI	Cf. (T)ASI
(A)SOE	(After) start of energizing
(A)SOI or (A)SoI	(After) start of injection
ASTM	American Society for Testing and Materials
(A)TDC	(After) top dead center
BD	Biodiesel
Bio-SG	Bio-synthetic gas
BSFS	Brake specific fuel consumption
BtL	Biomass-to-liquids
C_F	Fuel chemical properties
CAD	Crank angle degree
CCD	Cf. (I)CCD
(C)CI	(Calculated) Cetane Index
CFD	Computational fluid dynamics
CH	Methylidyne radical
$CI_{95\,\%}$	95 % confidence interval
CI	Cf. (C)CI
CMOS	Complementary metal-oxide-semiconductor
CN	Cetane Number
CoV	Coefficient of variation
CR	Compression ratio
D2	Diesel ♯2
DI	Cf. (HS)DI
DME	Dimethyl ether
DPF	Diesel particulate filter
ECU	Electronic control unit
EGR	Exhaust-gas recirculation

EoC	End of combustion
EoI	End of injection
EPO	Exhaust port opening
Eq.	Equation
EU	European union
EZ	Error zone
FAME	Fatty-acid methyl ester
FBP	Final boiling point
FID	Flame ionization detector
fps	Frames per second
FT(D)	Fischer-Tropsch (Diesel)
FWHM	Full width at half maximum
GUI	Graphical user interface
HC	Cf. (T)HC
HCCI	Homogeneous charge compression ignition
HD	High-density ambient condition: 800 K, 30 $kg.m^{-3}$
HHV	Higher heating values
HRL	Heat release law
(HS)DI	(high-speed) direct injection
HT	High-temperature ambient condition: 850 K, 26 $kg.m^{-3}$
HVO	Hydrotreated vegetable oil
IBP	Initial boiling point
(I)CCD	(Intensified) charge-coupled device
IEA	International Energy Agency
IMEP	Indicated mean effective pressure
IPC	Intake port closure
IQT	Ignition quality tester
IRDCI	Injection Rate Discharge Curve Indicator
ISO	International Organization for Standardization
LD	Low-density ambient condition: 800 K, 22 $kg.m^{-3}$
LHV	Lower heating value
LIF	Cf. (P)LIF
LII	Cf. (P)LII
LL	Liquid length

LOL	Lift-off length
LRT	Likelihood ratio test
LT	Low-temperature ambient condition: 750 K, 26 $kg.m^{-3}$
NO_x	Nitrogen oxides (NO and NO_2)
NO	Nominal ambient condition: 800 K, 26 $kg.m^{-3}$
NTC	Negative temperature coeffcient
OD	Optical density
OH	Hydroxyl radical
ON	Octane Number
P_E	Engine physical properties
P_F	Fuel physical properties
P_O	Oxidant physical properties
PAH	Polycyclic aromatic hydrocarbons
PDA	Phase Doppler anemometry
PID	Proportional-integral-derivative
(P)LIF	(Planar) laser-induced fluorescence
(P)LII	(Planar) laser-induced incandescence
PM	Particulate matter
PPCI	Partially-premixed charge Ignition
ppm	Parts per million
R&D	Research and development
RDG	Rayleigh-Debye-Gans
Rep.	Repetition
	Reprocessing
RME	Rapeseed-oil methyl ester
RMSE	Root mean square error
RoHR	Rate of heat release
rpm	Revolutions per minute
SAE	Society of Automotive Engineers
SCR	Selective catalytic reduction
SINL	Spatially-integrated natural luminosity
SMD	Sauter mean diameter
SME	Soy methyl ester
SoC	Start of combustion

SOE	Cf. (A)SOE
SoI or SOI	Cf. (A)SoI or (A)SOI
STP	Standard temperature and pressure
(T)ASI	(Time) after start of injection
TDC	Cf. (A)TDC
TEM	Transmission electron microscope
(T)HC	(Total) hydrocarbons
TSL	Two-stage Lagrangian model
UHC	Unburned hydrocarbons
US(A)	United States (of America)
UV	Ultraviolet
VGT	Variable-geometry turbocharging
WTI	West Texas intermediate

Chapter 1

Introduction

Contents

1.1. Introduction

As an introduction to this document, this chapter approaches the global context surrounding the specific and focused features of the research performed in this thesis. Different aspects such as history, technology, ecological and economical contexts are loomed. Finally, a list of current challenges and remaining issues are released. Following this description, the approach and the methodology of the study will be outlined as well as the essence of every chapter so the reader can get an overview of the document content beforehand.

1.2. Context and motivation of the study

1.2.1. The Diesel engine through history: a benchmark of efficiency

This was in 1892, when the French-German engineer Rudolf Diesel gave a consequent step on the way to the concept of ideal conversion energy cycle (adiabatic engine) formulated by Carnot in 1824 [1–3]. At this time, his new design of an engine based on fuel ignition by air compression was competing with the steam engine and the Otto cycle engine, better known as spark-ignited engine. The suppression of pumping losses and the use of higher compression ratios offered right away a significant improvement in terms of thermal and cycle efficiencies respect to the spark-ignited engine. The employment of Diesel engines first spread to high-power applications such as ships, electricity power plants, locomotives and trucks, until it first got implanted into a serial passenger car in 1936 on the Daimler-Benz AG 260 D (Cf. Figure 1.1) [4].

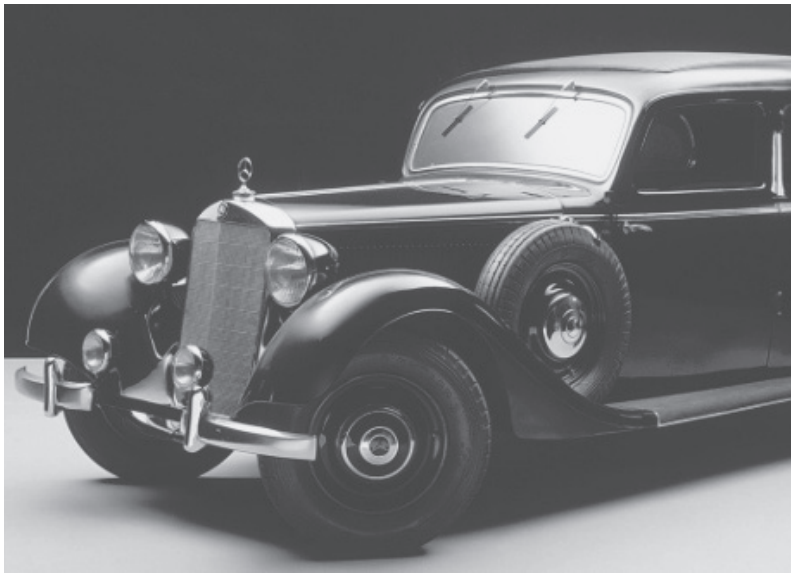

Figure 1.1. *Daimler-Benz AG 260 D, first car equipped with a Diesel engine in 1936.*

In the 70's, two major oil crises hit the occidental world constraining governments towards energy savings. In Europe, governments chose to encourage the implantation of Diesel engines on the market of passenger cars and light-duty commercial vehicles, by adapting their tax policy in favor of the compression-ignition technology. Research and engineering developed, and

rapidly permitted to improve both fuel consumption and engine drivability. Initial limitations of 2-stroke large and heavy power-plants working at low-speed under steady-state load conditions were pushed back, fitting the requirements of a light-duty engine for passenger cars, and offering a valid alternative to the spark-ignited technology in this sector. Figure 1.2 collects data presented in [4] and shows the chronological progression of the Diesel engines technology through the past century. From its first industrialization in 1912, the Diesel engine kept improving performance, fuel consumption and efficiency. Among the extensive milestones' list shown in [4], the major hits behind such improvements are most likely the following:

- **The turbocharger group (1978)** led to higher specific power and permitted to reduce engine size. By taking advantage of a turbine to recover the exhaust gas heat (instead of using the "expensive" energy like historical compressors used to), it enabled a better efficiency but also had the inconvenient to have a longer time of response. The onset of variable turbine geometry (quite at the same time as direct injection) and later double-stage turbocharging permitted to step over these limits.

- **The electronic control (1989)** of the engine enabled a more accurate, more reliable and more versatile management of the engine with respect to conventional mechanical systems, being probably carburation and combustion phasing the most glaring examples. As the versatility of engine control through any kind of mechanical systems is often quite limited, the Electronic Control Unit (ECU) opened a new field, multiplying the number of inputs, outputs and increasing the complexity of transfer functions. Nowadays, the ECU does not only control the engine but the whole vehicle and became a cornerstone of its design.

- **The in-cylinder direct injection (1989)** partially modified the combustion phenomenology while increasing both combustion and thermal efficiencies compared to engines with pre-combustion chambers (indirect injection).

Through the ages, the Diesel engine has been able to reassemble all the ingredients of the success recipe: economy, affordability and drivability. Although the design and the technology have tremendously improved its functioning, the fundamental concepts of a compression-ignition engine are still faithful to the original design imagined by Rudolf Diesel.

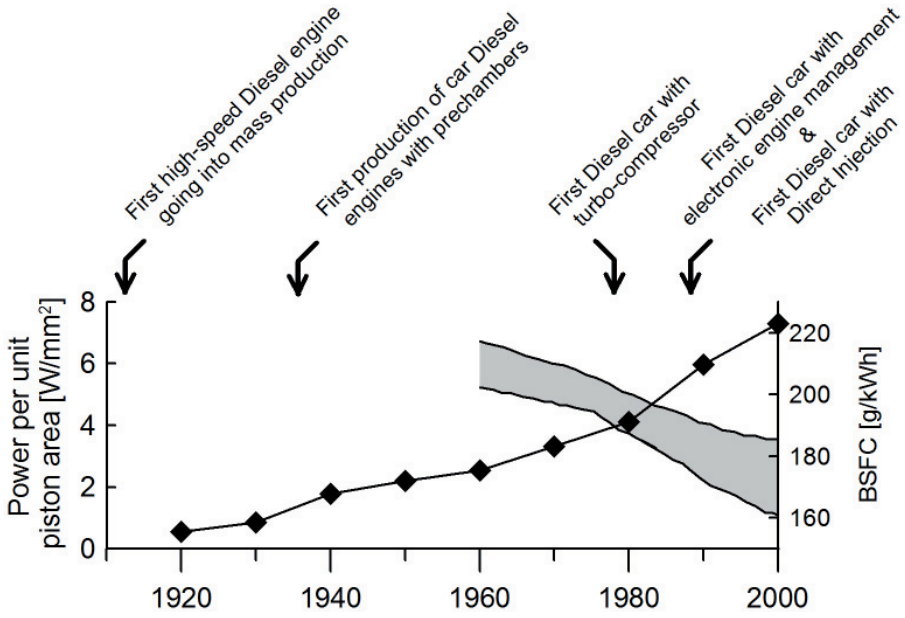

Figure 1.2. *Long-term technical and efficiency evolution of high-speed Diesel engines between 1910 and 2000. Adapted from [4].*

1.2.2. An important concern rapidly arose: exhaust gas emissions from internal combustion engine

In Europe, the commercial success of Diesel engines on the market of light-duty vehicles grew rapidly from the early 90's, as such Diesel and gasoline engines reached a point of equal shares in 2005 as illustrated by data of market penetration in Figure 1.3. In the rest of the world, the role of Diesel engines remains confined to heavy-duty applications nonetheless. In every instance, Otto and Diesel engines occupy today a leading position in the motion and propulsion of road transport, maybe up to a point finding echo in Hippocrates' words, *"Everything in excess is opposed to nature"*. Indeed, the massive use of both internal combustion engines promptly raised concerns about air quality, especially in dense populated regions. Pollutants such as Carbon Monoxide (CO), particles (PM), unburnt hydrocarbons (UHC), Sulfur Dioxide (SO_2) and Nitrogen Oxides (NO_x=NO+NO_2) have been identified

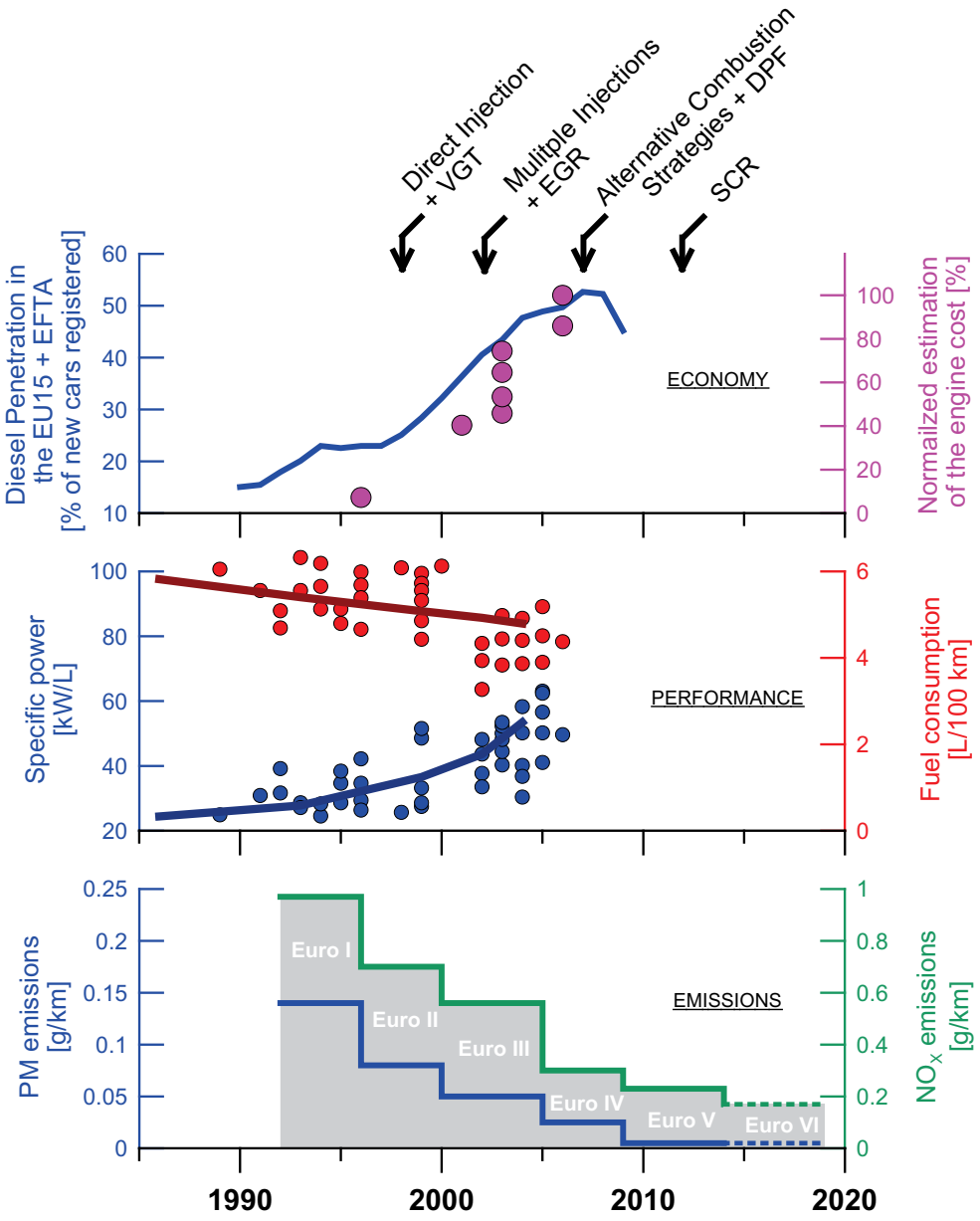

Figure 1.3. *Recent economical, technological, performance and emissions data for high-speed Diesel engines. Source: Economy [4, 5], Performance [4, 6], Emissions [7].*

as potentially harmful for human health and/or environment. Although their effect on human health remains hard to quantify, it seems quite accepted by the medical scientific community that a correlation exists between traffic air-related pollution and mortality [8, 9]. Episodes such as those at Donora, Pennsylvania (1948), London (1952), and New York (1966) led people to death due to excessive levels of SO_2 and particles [10]. In particular, PM and SO_2 are responsible for respiratory ailments aggravation, such as asthma, bronchitis and emphysema [11, 12]. The harm of nitrogen oxides (NO_x) is not clearly demonstrated for human health except for minor disease such as eye irritation. The issue of this particular contaminant is rather preoccupying for environment, causing acid rain and formation of smog clouds above cities. Historically, contamination productions of Diesel and gasoline engines are slightly different. While spark-ignited engines rather produce NO_x, CO and HC, compression-ignition engines are substantially associated to NO_x and PM emissions. As a consequence, worldwide air agencies initiated legislation programs specific of each engine technology during the 70's, aiming at a drastic reductions of their emissions *via* a rigorous process of homologation [7]. A stringent and challenging calendar was established in Europe as illustrated by Figure 1.3 while quite similar targets were also adopted in Japan and in the USA.

To face these severe limits, major technological improvements have been brought to the conventional Diesel technology along these past 20 years, as arrowed in Figure 1.3. Although they severely increased the cost and the complexity of Diesel engines, they also permitted to keep improving fuel consumption and specific power. The principal turn is certainly the development of flexible high-pressure injection systems which allowed the implementation of in-cylinder fuel direct injection -historically used on all heavy-duty applications- into a high-speed and small-sized engine. While making the engine more adiabatic, it also permitted a free mapping of critical parameters such as injection timing, injection pressure and rate of injection [13]. Thus, it enabled a sharp control of the fuel mass injected and thereby facilitated a significant reduction of fuel consumption. Soon, high-pressure direct injection spread to all light-duty engines and the possibility of this solenoid-actuated technology to operate three injections per cycle was exploited, using a pilot injection for noise reduction, while using a post-injection for PM reduction [6, 14, 15]. Nowadays, conventional piezo-electric and direct-acting piezo-electric injectors allow up to 8 injections per cycle, but the interest of such a number of injections is not fully established yet. In the meantime, the association of Diesel engine with turbocharging became more systematic, increasing specific power and efficiency, until the implementation

of Variable-Geometry Turbocharging (VGT) significantly improved engine drivability at transient loads.

Rapidly, a dilemma between NO_x and PM emissions emerged in Diesel combustion as both emissions appeared to be difficult to reduce simultaneously. Two possible paths to resolve what has been baptized the "NO_x/PM trade-off" were acknowledged: new combustion strategies and exhaust gas aftertreatment. Because of the additional cost of post-treatment devices, a multitude of alternative combustions strategies based on the use of exhaust-gas recirculation (EGR), multiple, advanced or delayed, high-pressure injections have been proposed [16]. As they became insufficient in the course of time, the introduction of expensive aftertreatment systems became ineluctable. At first, some strategies prioritized the reduction of one contaminant to make proficient after-treatment of the other. Accordingly, De Rudder [17] proposed a strategy with extra-low NO_x assuming DPF would become a standard, avoiding that way the introduction of expensive NO_x trap systems. However, this strategy suffered slightly higher fuel consumption. Conversely, strategies for heavy-duty applications, where fuel consumption is a critical criterion for customers, rather aimed at reducing PM internally whereas NO_x emissions are post-treated with urea injections *via* a SCR system. The issue in that case is to ensure a perfectly stoichiometric and homogeneous mixture of urea and exhaust gas, while maintaining high temperature levels in the exhaust. Otherwise ammonia is released in the atmosphere with other toxic concerns than the proper NO_x. More recently, highly-diluted combustion concepts have been suggested, reducing local temperatures, i.e. enabling lower NO_x emissions, and concurrently skipping fuel-rich regions to impede soot and PM formation [18, 19]. The utmost of these concepts is the homogeneous charge compression ignition (HCCI) which still remains restrained to a status of concept because of its limitation to low-load and prohibitive difficulties of control. More realistic alternatives stand halfway between conventional combustion and this idealistic HCCI. They may get stilted names sometimes, although they are often variants of a same combustion mode with partially-premixed charge (PCCI). However, these low-temperature combustion strategies often entail higher unburned hydrocarbons (UHC), CO emissions, and a fuel consumption penalty with unavoidable repercussion on higher CO_2 emissions [20, 21].

In parallel with emissions requirements for internal combustion engines, environmental agencies have also been imposing pressure over fuel manufacturers to help reducing hazardous engine emissions. A review of the past regulations quickly exudes the important effort made to reduce diesel sulfur content, consistent with the danger of sulfur dioxide previously mentioned. A similar

program was also adopted in Japan, Europe and USA, starting with limitations around 2000 ppm in 93, between 50 and 350 ppm in 2005 and 10 ppm between 2007 and 2009 [7]. Soon after these limitations, minimum levels of cetane number (CN) were introduced and rapidly increased. Motivations were based on several empirical studies acquainting for NO_x reduction when using fuels with higher ignitability while having minor or even no counteracting effect over PM emissions [22]. Although HC and *CO* are only characteristic contaminants of transient engine operating conditions or cold-start, it is to highlight their reduction with higher CN fuels. But in view of all the hardware and different strategies employed to increase the level of premixing (HCCI, PCCI), the constraint of continually refining always more reactive diesel fuels may seem paradoxical. Finally, in order to reduce PM emissions, it was also required to reduce the share of aromatics. Indeed, these unsaturated (poly)cyclic molecules increase the fuel propensity to soot formation, knowing that soot agglomerates constitute the matrix for the condensation of gaseous unburnt hydrocarbons (HC), i.e. to the formation of complex particles (PM). Table 1.1 has been adapted from [4, 22–24] and summarizes the preceding statements.

Table 1.1. *Fuel properties effect on Diesel engine emissions sampled in the exhaust. Sources: [4, 22–24]*
*⇓⇓ / ⇑⇑ = large effect, ⇓ / ⇑ = small effect, ↓ / ↑ = very small effect, 0 = no effect. *= for engines without aftertreatment systems, l = low-emission engine, h = high-emission engine, a = polyaromatics are expected to give a bigger reduction than mono-aromatics, b = reducing sulfur from 3000 ppm to 500 ppm gives relatively large benefits, reducing S from 50 ppm to lower levels has smaller direct benefits [23].*

Fuel modification	HC		*CO*		NO_x	PM	
	l	h	l	h		l	h
Reduction of Sulfur*	0	0	0	0	0	$\Downarrow\Downarrow^b$	$\Downarrow\Downarrow^b$
Increase in CN	0	⇓⇓	0	⇓⇓	⇓	0	0
Reduction in Total Aromatics	0	0	0	0	$\Downarrow^a$	0	0
Reduction in Density	⇑⇑	⇑⇑	⇑	⇑	⇓	0	
Reduction in Polyaromatics	⇓	⇓	0	0	$\Downarrow^a$	0	⇓⇓
Reduction $T_{90\,\%}/T_{95\,\%}$	↑	↑	↑	↑	↓	0	0

Nowadays, considering both the implementation of direct injection on gasoline engines in order to produce stratified combustion, and the drift

towards Diesel more homogeneous combustion strategies, one can observe how Diesel and gasoline engines are likely reaching crossroads. Emissions of both engines reach similar composition, including PM for gasoline engines, or UHC for Diesel engines, steering in consequence emissions standards towards comparable requirements for both technologies (Euro 6). In addition, the EU also regulates engine release of CO_2 since 2009 whose high-emission scales directly with high fuel consumption. Although Figure 1.3 displays a decreasing fuel consumption over the past 20 years, such a trend slowed down after the introduction of emissions standards without which more significant progress would have been achieved [25, 26]. Future trends are definitely challenging to predict, but if air pollution was definitely the main driving force for engine design up to now, the focus could possibly shift towards other issues such as greenhouse gas emissions and fuel depletion as illustrated in Figure 1.4. Thus, the new CO_2 restrictions added to affordable SCR systems seem to lead car constructors towards simpler engine designs, although optimized for lower consumption (and lower CO_2), while using full aftertreatment of NO_x and PM emissions. Priorities will probably have to be reset in the treatment of exhaust gases: Are PM and NO_x still a priority in suburban drives when CO_2 emissions enhance the greenhouse effect and threaten climate stability? Should NO_x and PM restrictions continue to be so severe for heavy-duty transport applications spending most of their lifetime on highways as they are forbidden in city centers? Is ammonia a better substitute to NO_x? These questions deserve to be addressed in the next milestones for future engine emissions.

1.2.3. Energetic dependency, consumption and sustainability

"More than any other time in history, mankind faces a crossroads. One path leads to despair and utter hopelessness. The other, to total extinction. Let us pray we have the wisdom to choose correctly.", Woody Allen

Since the discovery of the first oil wells at the end of the 19^{th} century, our societies' development has been catalyzed by this cheap, powerful and abundant source of energy. Since that time, worldwide oil consumption kept increasing unremittingly, permeating our daily lives and reaching somehow almost every item of our workaday. Its use spread onto most of our modern economical models, passing by industry, agriculture, residential, services and of course transport, which represents by itself 58 % of the overall oil consumption [5]. Nowadays, oil production and consumption have attained almost 90 million barrels a day (14.3 million m^3) [28] and questions about the possibility of increasing this number divides specialists of the sector. In 1956, Hubbert was the first to propose a model accounting for ground limitations of oil resources.

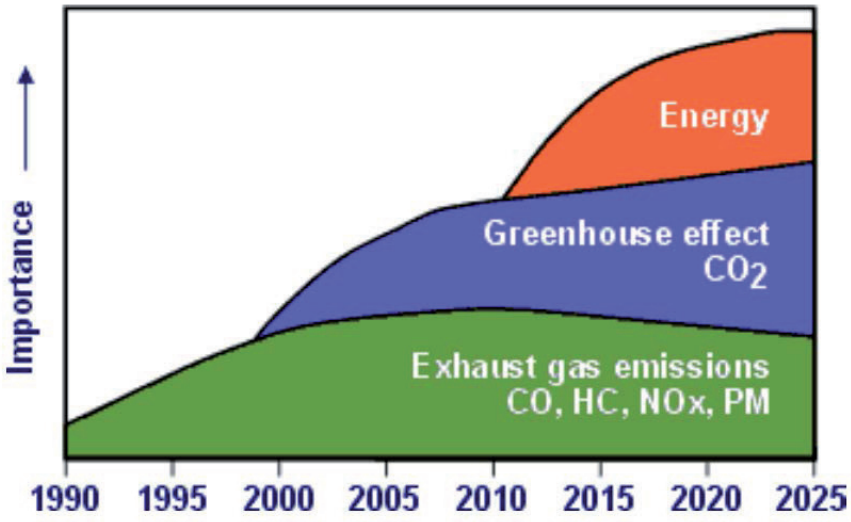

Figure 1.4. *Environmental driving forces. Source: [27].*

He foresaw that oil production would increase up to a maximum called *peak-oil*, and that a long decline would ensue caused by the depletion of oil resources. Originally applied locally, Hubbert bell-shaped curve predicted with quite a good accuracy the US *peak-oil* between 1965 and 1970. But, interrogations remain and opinions vary on its extension to a worldwide scale. A disagreement exists on the timing of such *peak-oil*, whether it passed already or is yet to come, and the precise shape of the depletion [29]. The 2009-Reference Scenario of the International Energy Agency (IEA) still expects an increase up to 100 million barrels in 2030 (time limit of the study) [5]. In addition to the natural uncertainty intrinsic to a prediction model, multiple factors have possibly delayed Hubbert's peak which are as many other factors susceptible to affect the depletion trend. Among them:

- Progress made on the technologies for both oil prospection and extraction: While "easy wells" rarefy, a lot of effort has been concentrated in order to extract oil from unexploited sources. With the development of offshore oil structures for submerged wells, hydraulic fracturing for gas shale, or hydro-treatment of oil sands, oil reserves have virtually increased. However, all these processes significantly increase the cost of extraction and present more risks for the environment. The recent Gulf of Mexico oil spill in 2010 is the most recent example of such issues.

- Decrease of oil consumption in occidental economies: Between 1985 and 2010, oil consumption was maintained almost constant in North America and even decreased slightly in Europe, each of these regions representing around 20 % of the total consumption [28]. Over the same period, both of them more than doubled their consumption of nuclear energy. This is the result of policies aiming at reducing their dependency towards oil after both crisis of 1973 and 79.

- Massive emergence of developing countries: With the economic growth of China, India and other developing countries, the world demand of primary energy is expected to increase by 40 % between 2007 and 2030 [5]. More than 2000 million people will increase their energy needs and modify in consequence the trend of fuel reserves depletion. For instance, nearly 200 million vehicles were circulating on Chinese roads in 2010, among which 85 million cars. But each year, both the number of vehicles in circulation and number of car holders increase by more than 20 million [30].

Therefore, future energetic and economic challenges are crucial and their timing difficult to address. All in all, nobody contest that oil is a non-renewable resource and that the world will soon or later face its depletion. There seems to be quite a wide agreement that a unique response does not exist, and that the solution to all these future energetic issues will pass by the multiplication and the diversification of resources. Besides, history is also the witness of how hazardous it is to base one's entire energetic production on a single resource. As to complicate a little bit more the already complex energetic equation, recent studies evidenced how global warming, engendered by CO_2 emissions of our important industrial activity and energy consumption [31], accelerates the climate change with important repercussions on all ecosystems. These threats have been driving authorities to encourage the implantation of clean and renewable energy in order to develop a sustainable economic and social system.

"Never before has man had such capacity to control his own environment, to end thirst and hunger, to conquer poverty and disease, to banish illiteracy and massive human misery. We have the power to make this the best generation of mankind in the history of the world or to make it the last.", John F. Kennedy

In regard to transport applications, alternative solutions to oil propulsion are essentially of three kinds: electricity, hydrogen and biofuels. In electric applications, the power required to put the vehicle in motion is usually produced thanks to a fuel cell working with hydrogen or *via* energy stocked

within batteries. If the first one has not reached serial production yet, the first 100 % electric passenger vehicles powered with batteries start to penetrate the market significantly. They represent an economically interesting alternative to the internal combustion engines, although currently their capacity still restrains their use mainly to urban purposes. But, it is to highlight that neither electricity nor hydrogen are natural sources of energy; they are so-called "energy vectors" or "energy carriers". Thus, the focus should be brought on the way electricity and hydrogen are generated. If in France 77 % of the electric needs are produced thanks to nuclear plants [28], several other nations still generate most of it through coal, gas and fuel plants, which makes the strategy as unsustainable as burning fuel directly in a combustion engine. This matter also applies to hydrogen production proceeding from steam reforming of hydrocarbons. Yet their advantage respect to engine combustion is to concentrate air pollution onto one production spot, releasing cities from this issue and making contaminants treatment easier. Extending the conventional nuclear solution (by fission) suffers similar concerns as oil, in that nuclear fuel is a non-renewable source also subject to future depletion. Besides, following the nuclear accidents of Tchernobyl and more recently of Fukushima, nuclear security raised concerns and several countries, such as Japan and Germany, already announced the future and progressive retirement of this type of energy production. Any other way to produce hydrogen, by hydrolysis or by electrolysis, also requires a high amount of thermal or electric energy. In conclusion, any country willing to convert its entire fleet of passenger cars from petrol to electric propulsion would/will require an important increase of its electric power capacity. It is likely that today, any country in the world has the capacity to absorb such a turnaround of energetic strategy. Still, problems would remain for heavy-duty and air transport applications for which electric solution does not exist. But the production of clean electric increases and will certainly represent a viable alternative in a longer term scope.

Therefore, in this complex energetic context, alternative fuels and especially biofuels may be called upon to play a key role on the energetic spectrum, at least at short or middle term. Before entering into deeper considerations, it may be appropriate to remind or agree on the terminology employed in this document. The expression *"alternative fuels"* regroups any fuels other than the conventional diesel and gasoline fuels. It includes liquid fuels obtained by liquefaction of gas or coal, but also fuels derived from organic matter, which are usually referred to as *"biofuels"*. Among the so-called biofuels, different terminology also applies depending on the feedstock and the industrial process employed for their synthesis. Following the definitions provided by the IEA [32], *"first-generation biofuels... include sugar- and*

starch-based ethanol, oil-crop based biodiesel (mono alkyl esters produced by transesterification) and straight vegetable oil, as well as biogas derived through anaerobic digestion. Typical feedstock used in these processes include sugarcane and sugar beet, starch-bearing grains like corn and wheat, oil crops like rape (canola), soybean and oil palm, and in some cases animal fats and used cooking oils. Second- or third-generation biofuels use advanced conversion technologies which are still in the research and development (R&D), pilot or demonstration phase. This category includes hydrotreated vegetable oil (HVO), which is based on animal fat and plant oil, as well as biofuels based on lignocellulosic biomass, such as cellulosic-ethanol, biomass-to-liquids (BtL)-diesel and bio-synthetic gas (bio-SG). The category also includes novel technologies that are mainly in the (R&D) and pilot stage, such as algae-based biofuels and the conversion of sugar into diesel-type biofuels using biological or chemical catalysts". Incidentally, when Rudolf Diesel first presented his invention in the *"Exposition Universelle"* of Paris in 1900, his engine was actually running on peanut oil. Diesel himself was already foreseeing a possible interest for this type of fuels in the future. In essence, unprocessed vegetable oils are technically biofuels indeed. But although they have already been used successfully in the past to replace diesel, their operation requires important modifications of both the fuelling system and the engine to handle its higher viscosity and poor low temperature flow characteristics [33]. In practice, vegetable oils are rather processed into more diesel-like liquids by transesterification. Correspondingly, the Fischer-Tropsch process also enables quite a large fuel flexibility for Diesel engines. This aspect of "imitating" conventional fuels seems essential as the potential success of biofuels probably lies on its capacity to be used, pure or blended with conventional diesel fuel, with no major modification of the engine technology.

Because they consume CO_2 during their full life-cycle (cradle-to-grave), biofuels could help reducing greenhouse gas emissions on a "human-life timescale" and have been raised accordingly to a status of major candidate for fossil fuel substitution in the transport sector. Today, more than 50 countries in the world have been encouraging their production by adopting blending targets or mandates. For instance, the EU fixed their share for transport purposes to 2, 5.75 and 10 % to be met respectively by 2005, 2010 and 2020 [34, 35]. Countries such as India, Colombia or Bolivia adopted even more challenging schedules with a 20 % share by 2020 [32]. As a result, biofuels production has been increasing exponentially during the past twenty years as shown by Figure 1.5. The figure also points out the type of fuels refined in the most productive regions. In America, where cars are mostly powered by spark-ignited engines, ethanol is typically transformed from corn to replace fossil gasoline, whereas

in Europe biodiesel is produced for its extensive market of Diesel cars. Despite such infatuation with biofuels, they still accounted for only 1.5 % of total road-transport fuel in 2007 [5].

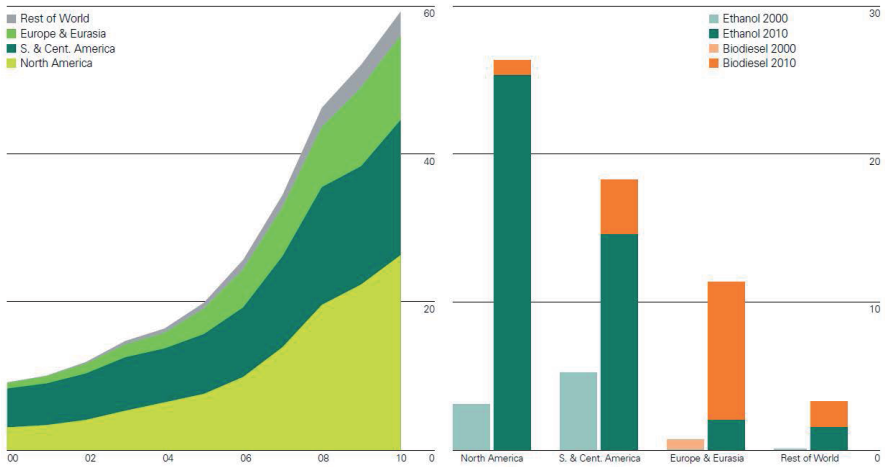

Figure 1.5. *World biofuel production between 1985 and 2010. Quantities are given in million tonnes oil equivalent. Source: [28].*

Today, the biofuel industry is rather going through a hard time. Higher prices of crops -which they provoked in some extent- combined to lower oil prices, struggles producers and cut significantly their profitability respect to conventional fuels. Indeed, biofuels industry is particularly sensitive to lower oil prices. During the 2002-2008 period, WTI price increased gradually from 20$ to almost 150$ in July 2008. In the meantime, biofuels production developed, reaching an impressive growth of +36 % between 2006 and 2007. Six months later, in January 2009, the WTI had dropped back to 40$ with the worldwide crisis, plunging the sector into a critical and uncertain situation. In addition to the economic issues, concerns of ethic and ecologic nature were raised. Ethical first, with the loss of food sovereignty and security after that a world food price crisis occurred in 2007-2008. Ecological then, with ground impoverishment, important water consumption, water and soil contamination (pesticides and fertilizers), deforestation, bio-diversity losses driven by intensive culture. Also, questions were raised about the magnitude of the greenhouse-gas emissions savings associated with switching to biofuels. These doubts have seen several countries rethinking their biofuels blending targets and even lead its most fervent detractors to refer to them as "agrofuels" in order to remove any connotation of an eco-friendly product [36].

Still, IEA predictions of Figure 1.6 for 2050 confirm the extrapolation of the trend observed in Figure 1.5. In order to deal with the ethical and ecological issues associated to biofuels production, authorities incentivised the exploration of other routes. For example, some research focused on the development of genetic transformation of crop plants specific to oil production, optimizing their oleaginous propensity while not competing (at least not directly) with agricultural crops for food [37, 38]. But the approach that draws most attention seems to be the production of second-generation biofuels. By using organic wastes and residues as feedstock, lignocellulosic biofuels exploit the poor part of plants and remove the ethical issues previously commented. Indeed, although investments of first generation biofuels have fallen heavily, the funding to these second-generation biofuels is likely to grow [5]. Although their efficiency from a commercial point of view is still to (im)prove, according to a study by the US Departments of Agriculture and Energy [39], the USA has sufficient resources of unexploited biomass to cover more than one-third of its fuel demand for transportation (diesel and gasoline). In Europe, a similar analysis concluded that the potential exists to produce between 27 and 48 % of the road transport fuel needs by 2030 [40]. Within all predicted scenarios of the IEA, the share of biofuels accounts for 4 to 9 % of the total transport fuel consumption by 2030. It is also mentioned an outstanding increase of this figure to 27 % by 2050, with significant contribution of diesel, kerosene and jet fuel replacement. Such predictions are virtually met in two steps: first, by a sustainable production of first-generation biofuels in the early years of the projection period; followed by the reach to maturity of second-generation biofuels by 2020 and expectations of considerably cheaper production costs than first generation by 2030 [5]. As a final remark, if biofuels can possibly reach a significant portion of the energy supply in the transport sector particularly, it is still subject to massive investments which depend in first instance on the potential profitability respect to oil price, but also to a large extent on the investors' confidence driven by long-term assurance, transparency and determination of authorities' policies.

1.3. Objectives of the study

Today probably more than ever, the surrounding context of this study is challenging to address as it keeps evolving and definitely goes beyond the single transport sector. Institutions and industries involved in this immense framework are numerous, from different horizons, and often engaged in a

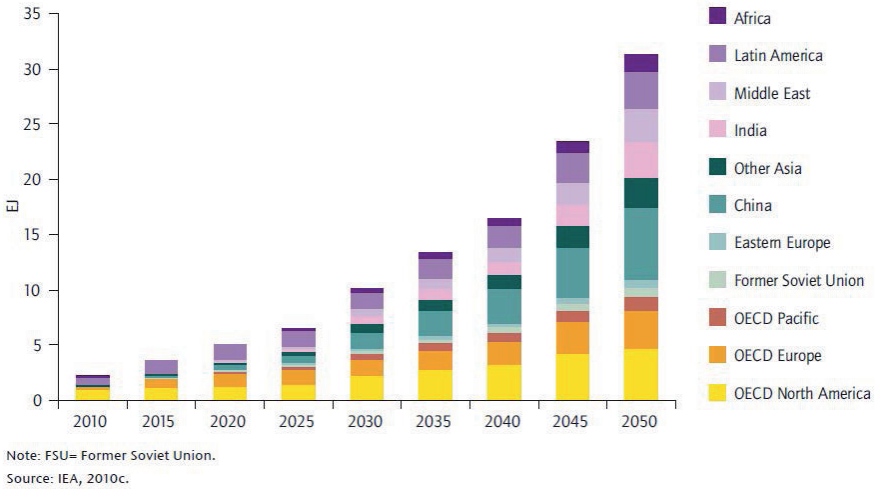

Figure 1.6. *Biofuel demand by region 2010-50. Source: [32].*

passionate debate. In the attempt made above, the take-home message is probably the following:

- Diesel engines are undeniably, by their appropriate conception and technology, a benchmark of efficiency and low-contamination among road transport applications. Still, they have been the focus of environmental issues with their emissions of $NO_x$and PM, whose understanding remains incomplete. In addition to these local emissions, it may be added the future challenges which include both larger-scale pollution issues with CO_2 and other greenhouse gases emissions, and a successful insertion among new policies of energy management.
- Biofuels have already begun to penetrate the fuel market in the whole world. Among the large energetic spectrum before us, they can potentially represent, in a near future and in the transport sector in particular, a viable alternative to face fuel depletion while maintaining energy security and keeping greenhouse gas emissions low.

Therefore, whether or not biofuels are factually included in the future scenarios for engine technology, it is necessary to investigate from today their effect when injected in a Diesel engine, and fundamental to obtain a detailed understanding of their spray and combustion characteristics in order to extract the maximum benefits from them in the optimization of engine design and

calibration [41].
Thus, the main objective of this study will be to: **Improve the understanding and assess the effect of fuel properties over the physical and chemical mechanisms associated to the processes of combustion and emissions formation of a Diesel spray**.
Accordingly, the questions this document aims at answering are: *How and how much do fuel physical and chemical properties affect combustion in its different phases? What physical or chemical properties dominate in each case? Is the knowledge of the conventional diesel spray extendable when using alternative fuels?*
In this regard, the use of alternative fuels, beyond the discussion about feasibility, is rather the opportunity to add new variables for the study of Diesel sprays, in order to dig a little bit more into the mechanisms involved and to improve the understanding of their combustion in a Diesel-like environment.

1.4. Approach and content of the study

The challenge in Diesel combustion stands in converting a high amount of energy contained within a fuel into a pressure increase in a millisecond order of magnitude. The fuel is injected in liquid-phase through a nozzle at very high-pressure in a high-density and high-temperature environment. A spray forms, atomizes and fuel droplets vaporize. In presence of oxygen, fuel vapor ignites, and a lifted turbulent diffusion flame develops. While it progresses within the chamber, the flame is likely deflected by the air swirl motion before it hits the piston wall. In every cylinder of a Diesel engine, 5 to 12 burning sprays of this kind develop simultaneously within a small volume. An important amount of heat is released which, in combination with the relatively high-speed motion of the piston, modifies drastically ambient conditions in terms of temperature, density and oxygen concentration, and causes subsequent effect on the combustion process. Therefore, the combustion event in a Diesel engine results in a very complex equation in which a multitude of intertwining chemical and physical processes occur simultaneously and possibly inter-react. This makes its understanding delicate and challenging. *Chapter 2* proposes a detailed description of the state of knowledge relative to the process of combustion in direct injection Diesel engines. In view of the extensive amount of information and knowledge existing about each one of the processes mentioned above, the objective of this chapter is obviously not to make an exhaustive review, but rather to present an updated synthesis of the most important mechanisms involved in the combustion phenomenology. This

chapter is also essential as it defines most of the terminology used thereafter, addresses both past knowledge and actual effort of research and emphasizes the lack of understanding which this study intends to overcome.

In view of this complex environment, the field of study must be reduced, leaving some of the real-engine aspects mentioned above out of our framework. Accordingly, this work focuses on the study of free single sprays under quasi-steady conditions, with the purpose of isolating the spray from possible interactions with the wall and other sprays while avoiding the potential effect of flame heat release. *Chapter 3* presents an experimental methodology able to extract the effect of fuel properties from the rest of parameters inherent to engine operation. For the purpose of the study, it is first proposed to define each term of an "equation of combustion" that would include on one hand the physical and chemical parameters relative to the fuel, and on the other hand those inherent to the engine operation. An incremental approach based on three groups of experiments is proposed:

1. The first step consists in assessing each of these terms separately by measuring the fuel properties, and by providing a precise characterization of both injection and thermodynamic conditions of the chamber. In this respect, this first group of experiments is also the definition of the boundary conditions for the following two groups of experiments.

2. In the second group of experiments, a single spray is now placed in a steady-state Diesel environment, but without oxygen, removing consequently the possibility of any chemical reaction of combustion. Thus, this experience permits to measure the importance of fuel physical properties compared to those of the engine. Optical diagnostics enabling this assessment are also presented in *Chapter 3* as well as their corresponding post-computing. They aim at characterizing both fuel atomization and evaporation characteristics in order to assess their differences respect to changes of thermodynamic and injection conditions representative of those met in a Diesel engine. The analysis and presentation of the results is presented in *Chapter 4*.

3. Finally, in the last group of experiments, the previous parametrical study is repeated by replacing this time the nitrogen by air at 21 % oxygen. In this case, all terms of our complex equation of combustion thus express. A new set of optical diagnostic is carried out simultaneously, to assess the level of flame premixing, the amount of soot it forms and its temperature. The details and the development required for these techniques, as well as their computer post-processing are also presented in *Chapter 3*. Analysis

and presentation of the results is made in *Chapter 5*, accounting also for those of the two preceding groups, to assess the importance of each of the terms of our equation of combustion.

4. In conclusion, *Chapter 6* summarizes and contrasts the contribution brought by this incremental succession of experiments with the objectives initially defined. It highlights the most relevant results obtained in this study and emits a list of future possible works, issued from the doubts met in this study, and which could allow the improvement of both these results and the knowledge of combustion in a Diesel engine in general.

References

[1] Diesel R., *Arbeitsverfahren und Ausführungsart für Verbrennungskraftmaschinen*, Deutsches Reichspatent Nr. 67207, 1892.

[2] Diesel R., *Die Entstehung des Dieselmotors*. Springer, 1913.

[3] Diesel R., *Theorie und Konstruktion eines rationellen Wärmemotors zum Ersatz der Dampfmaschinen und der heute bekannten Verbrennungsmotoren*. Springer, 1893. Reprint: VDI-Verlag, 1986.

[4] Mollenhauer K., Tschöke H., *Handbook of Diesel Engines*. Springer-Verlag, 2010.

[5] International Energy Agency. *World Energy Outlook 2009*. OECD Publications, 2009.

[6] García A., *Estudio de los Efectos de la Post-Inyección Sobre el Proceso de Combustión y la Formación de Hollín en Motores Diesel*. Tesis Doctoral, Universidad Politécnica de Valencia, Departamento de Máquinas y Motores Térmicos, 2009.

[7] DieselNet: Diesel Emissions Online, *Information available at http://www.dieselnet.com/standards*.

[8] Stieb D.M., Judek S., Burnett R.T., "Meta-Analysis of Time-Series Studies of Air Pollution and Mortality: Effects of Gases and Particles and the Influence of Cause of Death, Age, and Season". *Journal of the Air & Waste Management Association*, Vol. 52, pp. 470-484, 2002.

[9] Jerrett, M., Finkelstein, M.M., Brook, J.R., Arain, M.A., Kanaroglou, P., Stieb, D.M., Gilbert, N.L., Verma, D., Finkelstein, N., Chapman, K.R., Sears, M.R., "A Cohort Study of Traffic-Related Air Pollution and Mortality in Toronto, Ontario, Canada". *Environmental Health Perspectives*, Vol. 117, pp. 772-777, 2009.

[10] Turns S.R., *An introduction to combustion*, 2^{nd} Ed., McGraw-Hill Publishing, 2000.

[11] Stieb D.M., Szyszkowicz M., Rowe B.H., Leech J.A., "Air pollution and emergency department visits for cardiac and respiratory conditions: a multi-city time-series analysis". *Environmental Health*, pp. 8:25, 2009.

[12] Maestrelli P., Canova C., Scapellato M.L., Visentin A., Tessari R., Bartolucci G.B., Simonato L., Lotti M., "Personal exposure to particulate matter is associated with worse health perception in adult asthma". *Journal of Investigational Allergology and Clinical Immunology*, Vol. 21, pp. 120-128, 2011.

[13] Grondin O., Stobart R., Chafouk H., Maquet J., "Modelling the Compression Ignition Engine for Control: Review and Future Trends". *SAE Paper 2004-01-0423*, 2004.

[14] Payri F., Desantes J.M., *Motores de combustión interna alternativos*, 1^{era} Ed., Editorial Reverté, 2011.

[15] Heywood J.B., *Internal combustion engine fundamentals*. McGraw-Hill Publishing, 1988.

[16] Molina S.A., *Estudio De La Influencia De Los Parámetros De Inyección Y La Recirculación De Gases De Escape Sobre El Proceso De Combustión, Las Prestaciones Y Las Emisiones De Un Motor Diesel De 1.8 Litros De Cilindrada*. Tesis Doctoral, Universidad Politécnica de Valencia, Departamento de Máquinas y Motores Térmicos, 2003.

[17] De Rudder K., *An Approach To Low Temperature Combustion In A Small HSDI Diesel Engine*. Tesis Doctoral, Universidad Politécnica de Valencia, Departamento de Máquinas y Motores Térmicos, 2007.

[18] Kimura S., Aoki O., Kitahura Y., Aiyoshizawa E., "Ultra-Clean Combustion Technology Combining a Low-Temperature and Premixed Combustion Concept for Meeting Future Emissions Standards". *SAE Paper 2001-01-0200*, 2001.

[19] Pickett L.M., Siebers D.L., "Non-Sooting, Low Flame Temperature Mixing-Controlled DI Diesel Combustion", *SAE Paper 2004-01-1399*, 2004.

[20] Amorim R., *Combustión Por Difusión De Baja Temperatura En Motores Diesel De Pequeña Cilindrada*. Tesis Doctoral, Universidad Politécnica de Valencia, Departamento de Máquinas y Motores Térmicos, 2007.

[21] Arthozoul S., *Association of premixed and diffusive combustion modes in a Heavy-Duty Diesel engine*. Tesis Doctoral, Universidad Politécnica de Valencia, Departamento de Máquinas y Motores Térmicos, Document under preparation.

[22] Owen K., Coley T., *Automotive Fuels Reference Book*. SAE International, 1995.

[23] Maly R., Schaefer V., Hass H., Cahill G., Rouveirolles P., Röj A., Wegener R., Montagne X., Di Pancrazio A., Kashdan J., "Optimum Diesel Fuel for Future Clean Diesel Engines". *SAE Paper 2007-01-0035*, 2007.

[24] Arcoumanis C., Kamimoto T., *Flow and Combustion in Reciprocating Engines*. Springer-Verlag, 2010.

[25] Baert R., *Advanced topics in engine combustion*. CMT Internal Seminar Program, 6-9th September, 2010.

[26] Andersson Ö, *Advanced topics in Diesel engine combustion: techniques and concepts*. CMT Internal Seminar Program, 18-22nd July, 2011.

[27] Leohold J., *Vision for future mobility - Volkswagen fuel and powertrain strategy*, SYNBIOS II Conference, Stockholm, Sweden, May 23-24, 2007.

[28] BP, *Statistical Review of World Energy*, 2011.

[29] Murray J., King D., "Climate policy: Oil's tipping point has passed". *Nature*, Vol. 481, pp. 433-435, 2012.

[30] Comité des Constructeurs Français d'automobile. Press bulletin of 12/10/2010. On behalf of China Daily of 7/10/10.

[31] Sawyer R.F., "Science based policy for addressing energy and environmental problems". *Proceeding of the Combustion Institute*, Vol. 32, pp. 45-56, 2009.

[32] International Energy Agency, *Technology Roadmap. Biofuels for Transport*, OECD Publications, 2011.

[33] DieselNet Technology Guide, "www.dieselnet.com/tech".

[34] Directive 2003/30/EC of the European Parliament and of the Council of 8 May 2003. Official Journal L123, 42-46, 2003.

[35] Directive 2009/28/EC of the European Parliament and of the Council of 23 April 2009. Official Journal L140, 16-62, 2009.

[36] Bolis A.,"Agrocarburants : un cocktail qui coûte très cher à la pompe". Le Monde, 25th January, 2012.

[37] Taylor D.C., Katavic V., Zou J., MacKenzie S.L., Keller W.A., An J., Friesen W., Barton D.L., Gossen K.K., Giblin E.M., Ge Y., Dauk M., Luciw T., Males D., "Field-testing of transgenic rapeseed cv. Hero transformed with a yeast sn-2 acyltransferase results in increased oil content, erucic acid content and seed yield". *Molecular Breeding*, Vol. 8, pp. 317-322, 2002.

[38] Vigeolas H., Waldeck P., Zank T., Geigenberger P., "Increasing seed oil content in oil-seed rape (Brassica napus L.) by over expression of a yeast glycerol-3-phosphate dehydrogenase under the control of a seed-specific promoter". *Plant Biotechnology Journal*, Vol. 5, pp. 431-441, 2007.

[39] Perlack R.D., Wright L.L., Turhollow A., Graham R.L., Stokes B., Erbach D.C., *Biomass as feedstock for a bioenergy and bioproducts industry: the technical feasibility of a billion-ton annual supply*. U.S. Department of Energy and U. S. Department of Agriculture, 2005.

[40] EU, 2006. "Biofuels in the European Union - A vision for 2030 and Beyond", European Union, *Final report of the Biofuels Research Advisory Council*, EUR 22066, 2006.

[41] Kook S., Pickett L.M., "Liquid length and vapor penetration of conventional, Fischer-Tropsch, coal-derived, and surrogate fuel sprays at high-temperature and high-pressure ambient conditions". *Fuel*, Vol. 93, pp. 539-48, 2012.

Chapter 2

Combustion processes in a direct injection Diesel engine

Contents

2.1. Introduction

This chapter provides an updated description of the main physical and chemical processes occurring inside the combustion chamber of a direct injection Diesel engine whose purpose is the transformation of the fuel energy content into an increase of pressure producing work. This review is essential in order to both place the objectives expressed in *Chapter 1* into their technical context, and to establish the foundations of this study. The approach is rather conceptual, intending to describe such processes in a qualitative way, without necessarily clipping their details. It calls upon conceptual models which researchers of the engine community have contrived on behalf of the experiments they performed and the phenomena they observed. Such as Dec suggests, himself author of a reference conceptual model for Diesel combustion: *"An accurate conceptual model would provide a framework for interpreting experimental measurements, guide the development of numerical modeling, and furnish engine designers with a mental image to guide their thinking"*.

Precisely while mentioning mental imaging, a remarkable example of such exercise is provided in the *Appendix* of this chapter. In a quite apocalyptical description of the combustion event, although not without a touch of humor, Sir Ricardo sets his vision of the combustion event at a time where optical techniques permitting its visualization did not exist yet. Thus, one can understand how Dec [1], as an introduction to his conceptual model, presents Diesel combustion as *"a complex, turbulent, three-dimensional, multiphase process that occurs in a high-temperature and high-pressure environment"*. More recently, Novella [2] rightly pointed out that *"the main characteristic of the Diesel combustion process is its structure essentially heterogeneous, which for the most part determines its properties. [...] The heterogeneous nature of diesel combustion involves the existence of different gradients inside the cylinder during the whole process. Three gradients are particularly important for their relationship with the control of both combustion process and pollutants formation: the gradients of composition, the gradient of temperature and the gradient of density, while the pressure inside the cylinder can be considered homogeneous at each instant"*. In a Diesel engine, a liquid fuel is injected at very high pressure in a high density and high temperature environment. The liquid phase atomizes and penetrates up to a point where enough energy is entrained to heat up and evaporate the fuel. The vapor-phase continues its progression downstream the chamber. If oxygen is available, the rich vapor region auto-ignites, the flame tip spreads and continues to develop downstream, possibly gets deflected by the walls of the piston bowl, and results in what Siebers and Higgins [3] describe as a *"lifted, turbulent diffusion*

flame [...] during the mixing-controlled phase of heat release". This event, while occurring in a millisecond order of magnitude, involves a complex interaction between numerous physical and chemical processes, including important temporal and spatial considerations, and for which understanding is still needed nowadays.

With regard to offer a complete description of the combustion process in a Diesel engine, this chapter follows a structure similar to the works of García [4], Novella [2] and García [5]. To a lesser extent, some contents may coincide, although the emphasis given towards the assessment of fuel effect is likely different, which unavoidably involves and requires both a different scope and a different substance. Accordingly, this chapter breaks down as follows: a first section presents the historical definition of the different stages composing the Diesel combustion process issued from the laws of injection and heat release. The next sections address the description of this process from the point of view of a spray through all its phases, starting with the liquid fuel injection, continuing with the formation of a mixture of fuel and air, and ending with its autoignition and the establishment of a diffusion flame. In each of these stages, continual intent will be made to connect information about the fuel effect with the common thread. Finally, as a conclusion, specific objectives will be released, aiming at both understanding the fuel effect over Diesel combustion processes, but also at completing some of the missing lines remaining in the general picture of Diesel combustion drawn by the whole past research effort.

2.2. Phases of the combustion process

The most appropriate way to start with the review of Diesel combustion processes is probably to begin with the presentation of the historical, and still the most conventional tool today for combustion diagnostic: the analysis of the rate of heat release (RoHR). The RoHR is obtained from the analysis of the cylinder pressure trace based on the application of the first law of thermodynamics [6, 7]. This parameter accounts for the intensity with which the chemical energy contained within the fuel is released. By comparing its phasing with the fuel mass rate of injection, it is possible to define the different phases of the combustion process. Figure 2.1 shows the comparison between both angular-based evolutions. The main phases are conventionally defined as follows [6, 8]:

- Ignition Delay: This first stage covers the period between the start of injection (SoI) and the start of combustion (SoC); or more explicitly

between the time at which the first fuel droplet penetrates within the chamber and the time of significant heat release growth. During this lapse, the fuel is injected with apparently no heat release activity as shown in Figure 2.1, although further details about this statement will be discussed in Section 2.4. Fuel mixes with air at a rate controlled by the momentum flux created by the pressure drop between the injector nozzle and the chamber. A spray forms and goes through a succession of purely physical processes which breaks down into liquid fuel atomization, air entrainment and fuel vaporization. A detailed description of each of these processes is provided in Section 2.3. Due to the presence of oxygen inside the combustion chamber, the forming air/fuel mixture is very unstable as such chemical pre-reactions of low intensity ensue in its core. They cause the rupture of fuel molecules into shorter hydrocarbon chains and free radicals *via* a process called fuel pyrolysis. These small reactions lead to the spontaneous self-ignition of the mixture unleashing highly exothermic reactions (Section 2.4) and a measurable pressure increase defining the SoC.

- Premixed combustion: Immediately after the first stages of ignition, combustion propagates to all the vaporized fuel that mixed during the lag before ignition, but that had not reach the chemical conditions required to trigger ignition itself. The burning of this accumulated mixture is rather fast so that energy is released at fairly high rate, producing a characteristic peak on the RoHR trace. Afterwards, the RoHR drops to a relative minimum (time derivative of RoHR equal to 0), which tags the end of the premixed combustion phase. Further details of the physicochemical phenomena associated to this phase are approached in Section 2.4.

- Fast mixing-controlled combustion: This phase starts with the end of the aforementioned premixed burn, namely once the entire mixture amassed prior to the ignition onset burns completely. Throughout this phase, heat is assumed to be released at the same rate as fuel mixes with air, hence its name [6, 9]. A reaction surface develops at the stoichiometric location on the jet edges and forms a diffusion flame [6, 10, 11]. If the injection duration is long enough, the flame reaches its natural length and thus stationary conditions. This partially-premixed diffusion structure maintains until the end of the injection process (EoI).

- Slow mixing-controlled combustion: Once the injection process stops, the introduction of mass and momentum disappears. The amount of mixture remaining in the chamber burns slowly as illustrated by the

progressive decrease of RoHR displayed by Figure 2.1. Combustion looses intensity until flame quenches and puts an end to the whole combustion process. The withdrawal of spray momentum modifies expectedly the mixing process and the flame structure looses its quasi-stationarity. In this respect, recent studies report the development of an entrainment wave increasing mixing and soot oxidation during this phase [5, 12, 13].

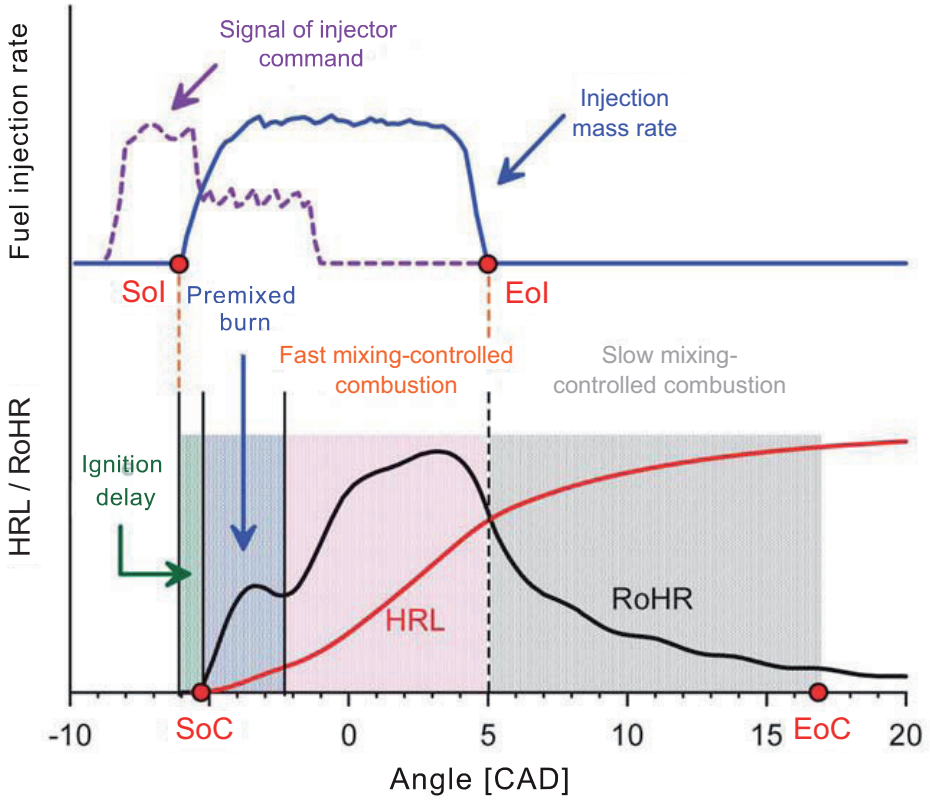

Figure 2.1. *Definition of the combustion phases by comparison of the fuel rate of injection with the RoHR trace. Source: [2].*

This description considers the engine and the associated combustion process as a "black box", thus limiting its understanding. The following sections seek to examine each of these phases in more detail, mostly enabled by the use of optical engines and techniques. Although a more accurate description of the temporal sequence is obtained, most of the contribution actually concerns the spatial resolution of these processes.

2.3. Fuel injection & formation of the air/fuel mixture in a Diesel spray

Prior to the onset of ignition, the processes involved in spray formation are entirely driven by physical phenomena until the oxygen content of the mixture triggers the first chemical reactions and modifies both its physical and chemical environment. In response to the interest of analyzing separately spray physical and chemical basic aspects, different types of experiments and studies investigated injection and spray development under non-reactive atmospheres. They include the internal-flow characterization of the injector, which has been widely studied by Gimeno [14, 15] and Hermens [16] in terms of efficiency respect to Bernoulli's law of discharge. Regarding the causes of such efficiency loss, they are credited for the major part to liquid friction but also to nozzle cavitation which is extensively detailed in the works of Salvador [17, 18]. Once injected within the chamber, liquid fuel atomizes into small droplets which possibly reform by coalescence before their vaporization. Such processes are very similar to those when injecting the same spray into an atmosphere of inert gases. Therefore, on the way to further simplification of the spray physical context, a step forward has been frequently considered, consisting in injecting fuel in an ambient of inert dense gases such as sulfur hexafluoride (SF_6) at temperatures close to Standard Temperature and Pressure (STP). Because of similar density conditions but much lower temperature than conventional Diesel-like conditions, the so-called isothermal spray enables fuel atomization and coalescence while avoiding its vaporization. The works of Correas [19], Arrègle [20], Ruiz [21] and López [22] provide in-depth discussions about the physical processes leading to liquid jet atomization and their modeling. García [4] completed the description of the physical framework investigating fuel evaporation and the subsequent mixing. The information contained within all these works is fairly extensive as such this review only summarizes the main concepts required for the accomplishment of this study and its objectives. The section closes with the presentation of spray morphological characteristics of interest accounting for the processes mentioned above.

2.3.1. Injector internal flow

Before it actually starts to penetrate the chamber, fuel is pressurized at several hundred bars typically in a common-rail system. As the needle lifts, it flows across the complex geometry of the injector body, goes through micro-orifices, before being finally released within the combustion chamber in which ambient pressure is much lower in comparison. For reference, current

technology enables customized shape nozzle holes (cylindrical, convergent or divergent) with diameters down to 50 μm, and injection pressure over 200 MPa. As a result of the pressure drop between the orifice extremities, fuel pressure is converted into velocity following Bernouilli's law (Eq. 2.1). The understanding of the phenomena occurring in this critical region is essential for engine design as it fixes both the fuel mass flow rate ($\dot{m}_f$) and its momentum flux ($\dot{M}_f$), i.e. its mixing capacity, at the exit of the injector. In [14], the experimental protocol to measure both variables is provided as well as their algebraic association in order to distribute the discharge coefficient (C_d) (i.e. the efficiency respect to an ideal nozzle) in terms of velocity (C_v) and area efficiencies (C_a). While C_v compares the effective velocity (u_0) respect to Bernouilli's (u_{th}), which accounts mostly for internal friction, C_a characterizes the contraction of the orifice exit produced by nozzle cavitation. As commented above, the fuel is exposed to extremely strong pressure gradients along the orifice, increasing its velocity while decreasing its pressure locally, so that it may reach values below the fuel vapor pressure in some point, typically at the entrance of the orifice. Kernels of fuel vapor form and are likely dragged by the fuel stream towards the nozzle exit. In consequence, these vapor "bubbles" virtually reduce the exit section as they consist of low density fuel vapor. With different experimental approaches, the works of Sou [23], Badock [24], and Chaves [25] permitted to observe their occurrence within transparent conducts, while Desantes [26] showed how they were surviving into the spray, right at the orifice exit. In practice, factors encouraging cavitation are smaller orifice diameters, higher injection pressure, but also important changes in the flux direction. For example, conventional multi-hole nozzles drive the stream orthogonally in order to inject the fuel in the radial direction of the piston bowl, and are more prone to cavitation compared to axially drilled single-hole nozzles. Correspondingly, convergent[1] orifices typically smooth the "elbowed-shape" of the flux at the orifice entrance and avoid cavitation at a given injection pressure where cylindrical or divergent nozzle would cavitate. In terms of effects, there is actually no clear agreement on the beneficial or disadvantageous character of cavitation. Although it defines the point of mass flow collapsing, i.e., the level of injection pressure from which any further increase does not rise the fuel mass rate, discussions still exist on its benefits to enhance air-fuel mixing. The point thus far, rather than taking advantage from it, is to be able to measure, understand and predict the processes associated in order to better control its appearance and improve injector design.

[1]To quantify nozzle convergence, it is often made reference to the $K - factor$ defined as (d_{inlet} - d_{outlet})/10. A nozzle is then convergent when $K > 0$.

$$u_{th} = \sqrt{\frac{2 \cdot (P_{inj} - P_{back})}{\rho_f}} \tag{2.1}$$

In regard to fuel considerations, literature is rather poor on the subject, being probably the consequence of the recent interest for this field. Still, several studies have approached these issues along with others using conventional diesel in particular conditions such as cold start, and whose knowledge may be extended to a fuel change context. Kegl *et al.* [27] evidenced, by using a numerical method of mechanical optimization, that improvements in nozzle geometry and control is needed when using rapeseed-based biodiesel. Starting with the effect on fluid dynamic internal to the injector, biodiesel appears to advance injection [28] due to its higher bulk modulus [29, 30], whose increase respect to conventional diesel or Fischer-Tropsch fuels can be explained by the presence of carboxylic groups, its longer mean carbon alkyl chain, and its higher degree of unsaturation [31]. On the other hand, results of mass flow rate quite vary from one study to another. In theory, Eq. 2.2 shows it should scale with the square-root of fuel density. While the trend is verified in [32–34] by considering up to 7 fuels, Desantes *et al.* [35, 36] report that for their selection of fuels, the fuel has no effect on the mass flow rate. In their quite complete review, Soid and Zaina [37] even report a work from Suh *et al.* [38] where injection pressure of biodiesel was increased to equalize injection rate with that of conventional diesel. Thus, conflicting results exist in the bibliography about this topic. Although it is likely that density differences are very low to be detected in this measurement (typically $\Delta\rho_f < 10\,\%$ so $\Delta\dot{m}_f < 5\,\%$), part of these inconsistencies may be explained by biodiesel higher propensity to reach cavitation [39, 40], or biodiesel higher viscosity which both lead to lower discharge coefficient [40]. This result is also consistent with conventional diesel at cold start and/or winter temperature, since the Reynolds number decreases due to higher viscosity [30]. At these conditions a priori favorable to limit cavitation, the flow may switch from turbulent to laminar regime and increase pressure losses. In addition, complex pressure-waves, bouncing between the common rail and the injector tip and also modified by bulk modulus, could also be another source to such differences.

$$\dot{m}_f = u_{th} \cdot A_0 \cdot \rho_f \tag{2.2}$$

$$\dot{M}_f = C_v^2 \cdot C_a \cdot A_{geo} \cdot 2\Delta P \tag{2.3}$$

To conclude, the processes relative to internal injector dynamics occur prior to those of fuel injection and combustion. The knowledge and derived analysis in this domain is important but mostly empirical, making difficult predictions when changing fuel properties or injector hardware. This upstream position and the lack of understanding in the context of a fuel change should be accounted carefully as they could engender different results in all the processes coming thereafter, and mislead the analysis if they are not properly addressed.

2.3.2. Atomization and coalescence

Atomization is the process that transforms the liquid spray from a continuous media into a cloud of droplets. While liquid fuel penetrates within the chamber, its important velocity relative to surrounding dense air causes droplets to shear off the liquid core initially forming. The increase of exchange surface between air and fuel it provides is essential to facilitate diffusion of heat, mass, momentum and species and in consequence for the processes of vaporization and mixing.

Four regimes of atomization of a liquid jet are defined by Reitz [41, 42], with limits fixed by both Reynolds and Ohnesorge numbers. Other authors rather use the Weber number although these three numbers are linearly combined and functions of fuel viscosity, density, surface tension, orifice diameter and velocity. The experimental work of Arrègle [20] concludes that under conventional conditions of a DI Diesel engine, diesel jets are always under the regime of atomization called "regime of complete atomization". In other terms, it means that downstream a given axial distance from the nozzle exit, the continuous liquid core disappears and only droplets survive, surrounded by the entrained gas. The distance between this point and the injector is commonly referred to as the "break-up length" as shown in Figure 2.2. Although no real agreement exists about its quantitative value, most of the studies agree that under Diesel-like conditions, it is reached at few nozzle diameters from the nozzle exit, according to Smallwood and Gülder's review [44]. Concerning the droplets size, the subject has been widely treated in the literature. It is worth mentioning that several authors refer to an important spatial and temporal variability, as suggested by Figure 2.2. Such observation is partially explained by the complexity of performing measurements in a dense and numerous population such as the one proposed by a Diesel spray environment. But the main contribution is often attributed to the coalescence of droplets in downstream portions of the spray. This effect is particularly significant in the dense spray axis region where the probability of two droplets to collide is higher and when using high injection velocity. Also, some of the research

effort has been driven towards the establishment of empirical correlations of the Sauter Mean Diameter as a function of injection parameters, ambient conditions and fuel properties [45–49]. Recently, Soare [50] confirmed and completed the following trends: the droplets diameter (20-100 μm) decrease with decreasing nozzle diameter, and with increasing both air density and injection pressure. In presence of nozzle cavitation, the expected decrease of droplets size was not verified and results dispersion remains unexplained.

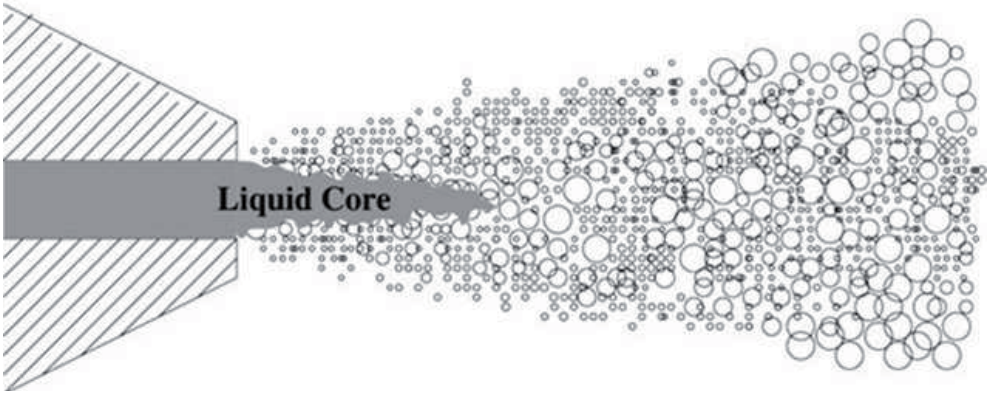

Figure 2.2. *Conceptual representation of the atomization and coalescence processes within a Diesel spray [43].*

Numerous studies have approached the fuel effect and report that both higher viscosity and density lead to increased droplets size [32, 35, 36, 51, 52]. An analytical study performed with seven FAMEs and a large amount of their blends with conventional diesel reports that viscosity accounts for 90 % of the predicted differences while density does only for about 2 % [53]. This result is quite expected for a Newtonian fluid. The study also highlights the higher droplets size expected for the more viscous rapeseed methyl ester respect to coconut, cotton, palm and all the other plant-derived FAMEs treated. The group of Hanyang University, Korea, published an extensive amount of works involving biodiesel, DME, ethanol and their comparison to conventional diesel [33, 38–40, 54–60]. By means of both PDA measurements and calculations performed with either blends or pure substances, biodiesel typically produces droplets 30 % larger compared to conventional diesel while DME smaller by another 30 %. Again, reference to the viscosity and surface tension effects is systematically made to justify these trends. In a quite singular study involving a realistic Fischer-Tropsch fuel, Payri *et al.* [61] showed that it had a similar SMD, consistent with the similar viscosity.

2.3.3. Evaporation

Once they are detached from the intact core of the spray, fuel droplets are in practice surrounded with much warmer air, eventually diluted with combustion products, so that heat transfers through the droplet surface. This exchange produces a continuous increase of the fuel temperature and, accordingly, an increase of its vapor pressure. In a race to equilibrate liquid and vapor phases at the given pressure, the droplet shrinks until its complete evaporation.

Because the liquid fuel impingement on the piston bowl constitutes a major issue, the maximum liquid-phase penetration, often referred as "liquid length", has been widely considered in the literature. As reported in [62], liquid-fuel impingement against cylinder and/or piston bowl surfaces is known to contribute to oil dilution, reduced combustion efficiency, and higher emissions of both unburned hydrocarbons (HC) and carbon monoxide (CO) [63–69]. Impingement also can lead to the formation of fuel films that subsequently can ignite to form pool fires separate from the primary combustion event [66, 70]. Such impingement-induced pool fires are associated with high soot levels and increased NO_X emissions, the former being attributed to hot, fuel-rich regions above the fuel films, and the latter being attributed to poor fuel/charge-gas mixing including stoichiometric regions between the fuel-rich pool fires and the fuel-lean in-cylinder gas. As such, numerous experimental sources establish that liquid-phase reaches its maximum penetration in the very first instants of the injection process and do not overpass a limit fixed by both fuel properties and thermodynamic conditions of the chamber [71–79]. From that point, the spray development ensues with fuel in vapor-phase exclusively. Through their observation of the liquid length under realistic conditions of an engine (injection close to TDC), Espey and Dec showed that liquid length reached its maximum far before the combustion onset [75]. Thus, they concluded that mixing with hot ambient air provides enough energy for evaporation completion, in response to older conceptual models suggesting that heat of combustion was required. Although under particular engine operating conditions the entire injection event occurs before the first heat release get to modify the liquid length, fuel injection and combustion can also possibly overlap when performing long injections of a full-load operating condition (negative ignition dwell) or when using multiple injection strategies. Besides, the use of early injections also implies the fuel to be injected during the rapid piston motion. Hence, liquid length is likely subject to significant time and spatial derivatives of ambient boundary conditions, but literature is missing about how it would adapt to such a variable environment.

According to the experimental results previously mentioned, the liquid length is highly influenced by the spray boundary conditions, in particular by nozzle diameter [71, 76, 79], by both the ambient temperature and density within the chamber [71, 72, 75–77, 79] and by fuel properties [71, 75, 76, 80–82]. Thus, the equivalent diameter defined by Thring and Newby [83] (Eq. 2.4) is often referred as the scaling parameter of liquid length. On the opposite, the fuel injection pressure appears not to play any significant role on the liquid length establishment [72, 76, 77, 79, 84]. As such, when the rate of fuel mass increases, the rate of air entrainment increases in the same proportion, maintaining the mixing rate constant accordingly. This observation led Siebers [76] to conclude that the evaporation process in conventional conditions of a Diesel engine is mostly controlled by turbulent mixing. This, in other terms, means that fuel droplets evaporate whenever the gas proceeding from the surrounding ambient provides enough enthalpy to the mixture. Under this assumption, the liquid contour establishes where the mixture reaches an air-fuel ratio specific of each fuel and ambient condition, whereas the local transfer rates of momentum, mass and energy between the liquid and gas phases at the droplet surface are considered to be fast in comparison to the rate of flow field development as a whole. With a scaling law based on this so-called "mixing-limited" hypothesis [77], Siebers could predict the experimental trends of liquid length he had previously obtained in [76]. Such hypothesis which ultimately assimilates the Diesel spray to a gaseous jet was later implemented in the 1D-models of García, Pastor and Musculus [4, 12, 85, 86] while including time-resolution and a more elaborated radial distribution of the fuel mass. These models represent a good alternative to 3D-CFD codes based on the discretized resolution of Navier-Stokes equations whose high computational cost used to be prohibitive in the past. Although with harder hypotheses, they can reasonably predict spray morphology and give a quantitative assessment of the spray mixture fraction field, especially at high density levels [87]. Today, the computational cost of 3D-CFD models may not be such an issue anymore, but the development of these 1D-codes is still of interest as they represent a valuable tool for the spray analysis and may potentially be included in future online algorithms of onboard ECU systems. But the introduction of alternative fuels as well as their use in blended formulations with conventional diesel could lead to different mechanisms priority, such as increasing atomization and evaporation timescales, or having the less volatile components controlling the liquid length. Therefore, the validity of Siebers' hypothesis must be checked when extended to different type of combustible.

$$d_{eq} = d_0 \cdot \sqrt{\frac{\rho_f}{\rho_a}} \tag{2.4}$$

In addition to the hypothesis validity, another difficulty for the use of these models is the important amount of input data needed to start the calculations. So far, they have shown a good agreement with parametrical variations of ambient and injection conditions using diesel surrogates (usually heptane or heptadecane). But in order to get all the fuel properties required, the first step is the selection of an adequate surrogate, namely a fuel composed of one or a small number of pure compounds, whose behavior matches certain injection and combustion characteristics of the realistic target fuel, typically composed of hundreds of species varying from one lot to another. By way of example, relevant convergence points include ignition behavior, molecular structures, adiabatic flame temperature, $C/H/O$ content, sooting propensity, in terms of chemistry, while volatility, density, viscosity, surface tension, diffusion coefficients may be considered in terms of physics [88]. But even with a surrogate matching well the target fuel, it remains difficult to find data of density, heat capacities and heat of vaporization covering its behavior throughout such a wide range of temperature and high levels of pressure handled in diesel-like conditions. To overcome this difficulty, the use of empirical correlations is of interest for liquid length predictions. This approach represents an interesting alternative for engineering of the combustion chamber by using conventional and cheap off-engine measurements. In that sense, Higgins *et al.* provided a liquid length model accounting for the fuel effect with properties obtained at STP [80]. Numerous realistic fuels including biodiesel and Fischer-Tropsch were evaluated under a large set of Diesel-like conditions. Their correlation (Eq. 2.5) based on two terms, being A the "fuel/air density ratio", and B the "specific energy ratio" quite confirms the square root dependency of the equivalent diameter and the significance of fuel volatility. Although rigorous, this correlation may be missing the relevance of fuel properties compared to engine thermodynamic conditions. In addition, c_p and L_v, even if they are fixed and obtained at STP, are not among the conventional fuel measurements and had to be assimilated to that of pure compounds in this study as well. For instance, no information exists in the literature of how much a 10 % increase of fuel density affects evaporation respect to a 10 % increase of air temperature. Therefore, a direct assessment of the importance of fuel physical properties compared to other physical variables intrinsic to engine operating conditions would be useful to understand better the fuel effect on the evaporation process.

$$\frac{x_{liq}}{d_0} = 10.5 \cdot A^{0.58} \cdot B^{0.59} \tag{2.5}$$

with $A = \frac{\rho_f}{\rho_a}$ and $B = \frac{c_{p,fl} \cdot (T_b - T_f) + L_v}{c_{p,air} \cdot (T_{air} - T_b)}$

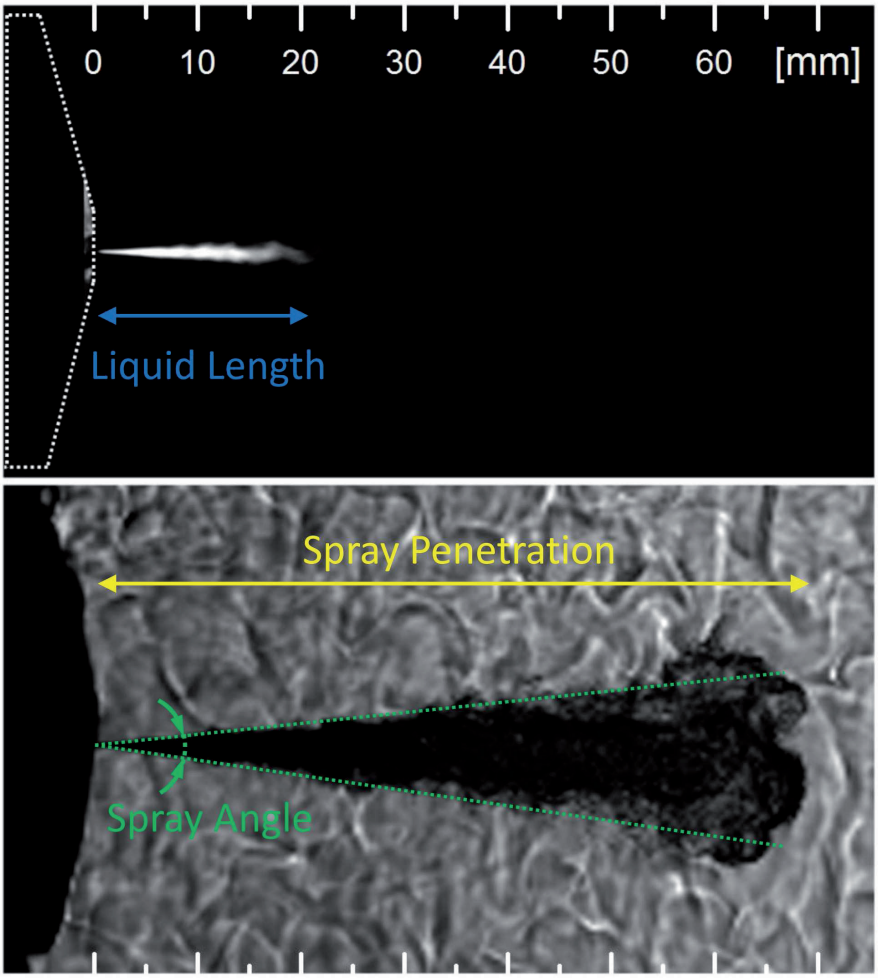

Figure 2.3. *Free n-heptane spray at ρ_a= 17.2 $kg.m^{-3}$, T_a=822 K, 150 MPa under inert conditions. Mie scattering (top) and Schlieren (bottom).*

2.3.4. Morphological characterization of spray mixing

The spray volume is directly related to air entrainment and its quantification enables to address the mixing process quality. In consequence, spray penetration and angle are morphological parameters of interest and have been largely considered both experimentally and numerically in the literature.

The spray penetration is defined as the distance between the nozzle exit and the spray tip as shown in Figure 2.3. Numerous works have been studying the penetration of free sprays as a function of time although mostly under isothermal environments [47, 89]. They produced empirical correlations -useful to predict the instant when the spray hits the piston wall- in which parameters such as pressure drop (difference between injection pressure and chamber backpressure), nozzle permeability (diameter and orifice discharge coefficient), ambient density, and spray angle reveal their controlling character. In [47], Hiroyasu suggests that two stages exist: during a short period, the penetration is faster and linear with time, up to a "transition time" from which penetration scales with the square root of time. In [85, 90], Desantes and Pastor propose an analytical solution based on the momentum conservation along the spray axis and validate it with experimental measurements. In the resulting Eq. 2.6, the information of pressure drop, nozzle diameter and discharge characteristics is included within the momentum flux factor. The larger entrained mass caused by higher air density leads reasonably to slower penetration. Under this assumption, the temperature does not have any straight influence on mixing rate but does have an indirect "binary effect" when it is sufficient to switch to vaporizing conditions. In [91] the difference between vaporized and non-vaporized sprays reaches 20 % at low density conditions. The authors hypothesize that this reduction is the result of a local increase of mixture density as it cools while evaporating fuel.

$$S(t) = 1.26 \cdot \dot{M}_f^{0.25} \cdot \rho_a^{-0.25} \cdot \tan^{-0.5}(\frac{\theta}{2}) \cdot t^{0.5} \tag{2.6}$$

Regarding a possible fuel effect, it may be useful to first remind that fuel density does not affect spray momentum theoretically (Cf. Eq. 2.3). Although a different nozzle discharge could lead to a different coefficient of momentum C_m (Cf. Eq. 2.7), it is rather expected for the spray angle to be the main responsible parameter for a potential change of penetration when switching from one fuel to another. Several studies do observe a smaller spray angle when using biodiesel [92, 93] although only leading to small or insignificant differences in penetration [54, 58, 94]. This result of biodiesel smaller angle is consistent with other studies focusing on this specific subject. Naber and

Siebers [91] made an extensive review on the relationship between the spray angle and the operating conditions in the case of non-evaporative jets. The authors agree that spray angle depends primarily on the geometric parameters of the nozzle hole and the density ratio between ambient gas and fuel. The correlations exposed show that the tangent of the spray semi-angle scales with the air/fuel densities ratio powered to an exponent between 0.18 and 0.5 [47, 48, 91, 95–97]. All in all, unless drastic differences in density exist among fuels, there should not be any significant effect over the spreading angle, and even less over spray penetration.

$$C_m = C_v^2 \cdot C_a \tag{2.7}$$

2.4. Autoignition of a Diesel spray

Now that processes associated to injection, spray formation and mixing have been described, let us approach their purpose and what an engine is fundamentally made for: burning fuel to produce work. While the studies presented so far were performed in inert conditions, the oxygen now present in the ambient results in a highly unstable mixture which reacts and self-ignites after some time along the spray development described above. In practice, comprehension of this stage is essential in terms of noise and chemical emissions. Autoignition appears when local conditions of mixture and temperature are appropriate to trigger the first chemical reaction of fuel oxidation. It manifests by the development of intermediate short-lived species and the release of energy. But these exothermic reactions also influence locally the thermodynamic state of the spray, modifying its development sequence and the mixing process associated. Therefore, physical and chemical processes are intimately intertwined from that instant until the end of the combustion process. This section describes the transition phase occurring between the start of combustion until the establishment of a stabilized diffusion flame front.

2.4.1. Stages of the process

Numerous are the experimental works having described Diesel autoignition as a two-stage ignition process similar to those observed in self-ignition of homogeneous mixtures [98–102]. Thus, these studies suggest that a phase of low-intensity and low temperature reactions actually exists prior to the start of the premixed-burn heat release as defined in Section 2.2. Although this effect is not appreciable on the RoHR trace of an engine as displayed in Figure 2.1 or

in [100], such low-intensity reactions can produce a detectable pressure activity [101] and challenge somehow the corresponding limits defined to separate the different phases of the combustion event.

Long hydrocarbon chains injected in hot air break down due to a complex association of pyrolysis and oxidation mechanisms until converting into water and carbon dioxide. In the meantime, they release free radicals which, for a part, are raised to a short-lived excited electronic state by the exothermic reactions. The decay from such excited state down to equilibrium groundstate produces their chemiluminescence. Because the pattern of chemiluminescence wavelengths is specific of each species, the acquisition of the flame spectrum enables their identification and provides information on both the reaction nature and the air/fuel mixture state. Spectroscopic studies of atmospheric hydrocarbon flames indicate that the methylidyne- (CH^*, 432 nm), hydroxyl- (OH^*, 306 nm), carbon- ($C_2{}^*$, 470-516-560 nm) and formaldehyde- (CH_2O^*, 368-470 nm) radicals are the main excited species involved in fuel combustion [103]. Although it is likely that most of these chemiluminescences coexist all along the combustion process, their prominence and spatial location are expected to evolve in time as a function of the combustion regime.

By visualizing the combustion process in an optical engine with an intensified camera system, and by sharply shifting its synchronization respect to the start of injection, Dec, Coy and Espey [100, 104] studied in detail the phasing of the flame development respect to the cylinder pressure signal. Thus, it was indeed observed the yield of low-intensity chemiluminescence in the rich vapor region of the spray prior to the main heat release. Some isolated spots were first detected until developing uniformly in the rich leading portion of the jet. This latter instant appeared to match the very first heat release (negative minimum of RoHR), before it could even recover from the heat absorption due to fuel evaporation. Further spectroscopic analysis revealed that such chemiluminescence was virtually arising from CH_2O^* but also, and above all from CH^*, conferring on the latter the status of autoignition marker. As the combustion process was ensuing, the luminous intensity was rapidly growing by several orders of magnitude due to important radiation proceeding from soot incandescence. Such radiation was rather broadband and dominated throughout the whole reaction region, preventing any distinction between the initial chemiluminescence and the rest of the combustion process if no specific filtering was applied.

Seeking further insight into this previous description, Higgins *et al.* [101] performed similar measurements under steady-state conditions enabled by the use of a constant-volume combustion chamber. They confirm that the

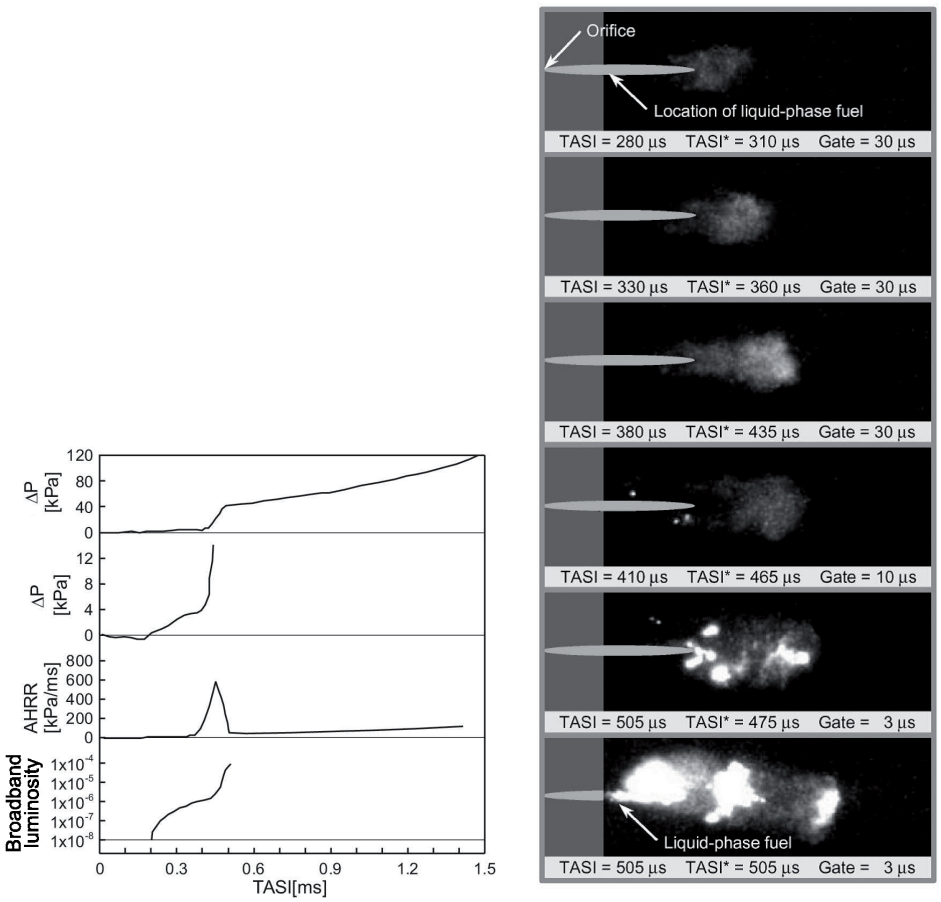

Figure 2.4. *(a) Evolution of the pressure increase (ΔP), apparent heat release rate (AHRR) and relative luminosity during the self-ignition of a Diesel spray in a constant volume chamber.*
(b) Corresponding broadband images (no filtering) of the spray autoignition sequence. TASI stands for time after the start of injection. TASI corresponds to TASI after a time-correction is applied, accounting for cycle-to-cycle dispersion. Gate is the energizing time of the intensifier, namely the effective exposure time of each image. Air conditions: 1000 K, 14.8 kg/m^3, 21 % O_2.*
Source: Higgins et al. *[101] .*

autoignition process breaks down in three successive phases detailed next. Figure 2.4 collected from their study will serve as the support of the following description. The figure is the result of tests conducted with fuel injected at

a pressure of 1400 *bar* through a single-hole nozzle of 0.246 *mm* diameter, in conditions of temperature and density of 1000 K and 14.8 kg/m^3, respectively. In (a), the first two plots represent the same variable (ΔP) with different scales of the same axis, in order to appreciate better the growth of the pressure signal during the start of combustion. The last two plots represent the apparent heat release obtained from a first-law analysis of ΔP (AHRR) and the relative luminosity measured with a photodiode, respectively. All the four plots are represented as a function of time after the start of injection (TASI). In (b), the image sequence of the autoignition process under the same conditions is shown. The camera system only permitted the acquisition of one image per injection so the event is reconstructed from several cycles by shifting the camera phasing. Accordingly, the three defined stages are the following:

- **Physical induction stage:** this phase extends from the start of injection (0 *ms* ASI) until the very first heat release, which is, as depicted above, coincident with the emission of low-intensity and low-temperature chemiluminescence (0.2 *ms* ASI). During this period, mixture formation occurs as described in the precedent section, i.e. dominated exclusively by the physical processes of atomization, air entrainment, mixing, and evaporation. Fuel heating and vaporization consume energy so that heat release goes negative. As fuel molecules keep diluting with hot air, the mixture temperature increases up to a value called "temperature of crossover". This defines the temperature level from which the mixture heat release becomes superior to its heat absorption [105]. From that point, the mixture switches to unstable state and chemical reactions of oxidation propagate to the surrounding. The onset of this chain reaction technically marks the end of this physical induction phase. Still, it does not mean that physics no longer matters. Spray mixing induced by the velocity field and shear stress continues to prepare the mixture prior to its burn while modifying strongly the local composition and the temperature field afterwards.

- **First-stage ignition period:** this phase begins with the first detectable chemical activity in terms of chemiluminescence or pressure, and progresses until a significant heat release attests for the premixed burn commencement. It is to note the uncertainty of this period duration as the first limit quite depends on the resolution of the hardware employed for the measurement, and the second on the subjective criteria used to consider the RoHR as "significant". In Figure 2.4, this period corresponds to the positive low-intensity heat release occurring between 0.2 and 0.4 *ms* ASI. This period is also usually referred to in the literature

as "low-temperature autoignition" [106] or "cool-flame" [100, 107, 108]. As observed in the first images, Higgins *et al.* [101] suggest that the first-stage ignition chemistry grows broadly in the region of the spray comprised between the liquid length and the penetrating tip of the spray, in agreement with Dec and Espey's observations [100]. Because of the relatively uniform distribution of chemiluminescence in this zone, it is likely that the first-stage chemistry develops uniformly throughout the region. Kosaka *et al.* [102, 109] provide deeper insight into the species involved, by imaging the whole formaldehyde population (not only under excited state) after inducing their fluorescence *via* laser techniques (LIF). This accurate 2D-analysis yet confirms the presence of formaldehyde during autoignition as was suggesting the spectra analysis performed by Dec and Espey [100]. But in addition, if formaldehyde first appeared homogeneously at recovery time (when cool-flame heat release equals the heat absorption of fuel vaporization), it was also observed that it only survived until the onset of the second-stage chemistry. Therefore, the authors suggest that this species acts as a stable intermediate compound that arises exclusively in the phase of low-temperature autoignition. Note that this statement will be further discussed in Section 2.5 as formaldehyde also coexists in the steady-state mixing-controlled flame. Higgins *et al.* [101] estimate that the average air/fuel mixture in the cool-flame region is rich, with an equivalence ratio comprised between three and four. Also, as they observe how both heat release and chemiluminescence dampen prior to high-temperature ignition (between 0.3 and 0.45 ms ASI), they suggest that "chain-branching reactions" dominate early in the first-stage. Such reactions produce an important amount of radicals while releasing small but significant enough quantities of energy to cause a rapid pressure-rise. However, as the temperature further increases due to both mixing and first-stage chemistry, it reaches levels ($\sim$750-900 K) where the "dissociation" of intermediate products begins to occur, while reducing the chain-branching process. This effect is commonly referred to as the negative temperature coefficient (NTC) regime. Szybist *et al.* [110] complete this statement by indicating that formation of alkylperoxy radicals [111] is no longer favored, slowing down the overall rate of reaction. Even if the mixture temperature continues to increase, this process effectively decreases the rate of fuel consumption, and most likely explains the decrease in the rate of pressure and chemiluminescence rise in the later part of the first-stage ignition. In other operating conditions [101], chemiluminescence and heat release even get to decrease prior to the premixed burn. The temperature

increase during the whole low-temperature ignition phase is estimated to be between 200 and 300 K, although only two-thirds are attributed to the cool-flame heat release, while the rest would proceed from hot air entrainment. Therefore, the injection process still plays an important role in the heating of the air/fuel mixture. Such increase raises the mixture to the conditions necessary to trigger the second-stage chemistry at high temperature and start the final phase of autoignition.

Before detailing the processes relative to second-stage ignition, a point should be made about the imaging techniques applied to the study of first-stage ignition. In practice, the implementation of LIF to visualize CH_2O (or any other species) is rather laborious and requires both particular care and abundant hardware. On the other hand, spectroscopy analysis usually limits the spatial resolution. Thus, line-of-sight visualization of CH^* is widely employed as an alternative to trace autoignition. Its ample peak at 432 nm makes it is easy to perform interferential filtered imaging. However, none of the three techniques is time-resolved. In consequence, they all require a set of injections to reconstruct the sequence with, of course, problems associated to cycle-to-cycle dispersion. Recently, schlieren imaging showed a good sensitivity to the early, cool-flame stages of ignition by displaying a "disappearance" of the vaporized fuel jet head [112]. Such "disappearance" appeared simultaneously with chemiluminescence, and is believed to be the result of fuel breakdown and mild heat release that makes the refractive index of the cool-flame region matching that of the ambient gases. The improvement in imaging cool-flame transients with this technique is significant because it can be operated with high-speed cameras and is consequently time-resolved. Still, it is to highlight the very recent improvements in both the sensitivity and the frequency of high-speed CCD sensors which will certainly soon enable CH^* imaging without intensification. This in consequence removes the limits of acquisition frequency and enables the collection of the complete sequence of ignition at once.

- **Second-stage ignition/premixed burn period:** this phase corresponds to the sudden heat release according to the description given in Section 2.2. As commented above, it starts once the energy transferred to the mixture by both hot air entrainment and cool-flame heat release meet the threshold condition required to enter the phase of high temperature ignition. Higgins *et al.* [101] comment that this transition is caused by the trigger of hydrogen peroxide dissociation reactions which turn out to dominate the chemistry ($\sim$900 K) and produce a significant heat release.

In Figure 2.4, this phase is delimited by each ridge of the AHRR peak, between 0.4 and 0.5 *ms* ASI. In the meantime, combustion propagates to the regions of vaporized mixture accumulated during ignition delay and which had not had the capacity to trigger ignition themselves. With the local temperature increase in their neighborhood, they now turn to reach the limit of flammability and an important heat release follows. As ignition delay increases, charge-gas mixtures raise while getting closer to stoichiometric conditions, therefore creating higher local temperatures, and both higher pressure gradients and time-derivatives. Minimizing this phase is then a critical point for studies which aims at noise and NO_X reductions. As indicated in *Chapter 1*, this issue motivated in part the increase of fuel ignitability (higher CN) required in the standards of homologation for diesel-type fuels.

Another indicator of the local temperature increase driving autoignition towards high temperature autoignition is the apparition of incandescent soot. As shown by the forth image of Figure 2.4, soot radiation causes the image saturation on several points because the intensity is about 3 to 5 orders of magnitude higher [99, 100] than the first chemiluminescence detected. Indeed, soot requires rich mixture, time, but also temperatures above 1300 K to reach formation, which is way more than the levels achieved in the cool-flame. Soot radiation extends rapidly from the instant it first appears, and dominates the broadband luminosity produced by the flame. In practice, when operating intensified imaging of chemiluminescence, the difference of intensity is so important and the occurrence so fast, that a special care has to be taken not to saturate the image and provoke damage to the intensifier. This difference also explains why the first studies using film cameras were suggesting that combustion began precisely with the first appearance of soot and that the first stages of ignition were not luminous (e.g. [113]). The hardware employed was just not sensitive enough to detect the lowest levels of light intensity. In previous but comparable images obtained by Dec and Espey [99, 100], soot appeared quite randomly in the form of bright spots, first on the jet sides and upstream the chemiluminescence region, before extending similarly to the central area initially occupied by the cool-flame. In this work, the authors also argue against the role of soot in spreading autoignition to other jet locations -an idea initially suggested by Edwards *et al.* [114]- and rather present its occurrence as an auxiliary effect. This observation is relevant for studies involving combustion strategies which aim at reducing soot formation since its eradication therefore does not slow down the combustion development.

The phasing of soot onset respect to the start of combustion obtained from the pressure signal has been approached in several occasions and by different authors [114, 115]. Expectedly, a delay was always observed although only Dec, Espey [99, 100] and Higgins *et al.* [101] present explicit results in this regard, situating soot onset after the start of premixed combustion. While Dec and Espey [99, 100] state that soot appears midway between the start of premixed combustion and the peak of heat release, Higgins *et al.* [101] first observation occurs on the latter peak. However, the author's justification for such difference rather seems to proceed from a different pressure signal analysis. Finally, Higgins *et al.* [101] conclude that the time required for the first soot occurrence corresponds to the time needed to both consume all the entrained oxygen during ignition delay, and to reach the temperature levels required to form soot. From that time, soot formation has represented a major topic of study. Several studies do provide deeper details on these processes and will be approached in Section 2.5.

2.4.2. Influence of engine operation conditions and fuel characteristics

The previous description of self-ignition on a three stages basis corresponds to a generic process, with given fuel and engine operating conditions. But details of this mechanism in terms of spatial distributions and characteristic time-scales depend strongly on both these factors.

Considering ambient conditions first, variations of temperature, density and oxygen concentration have a significant contribution. Their increase almost systematically leads to faster ignition in all its phases. First, ambient temperature variations do not modify air/fuel mixing, but an increase helps the evaporation process by increasing the mixture-fraction of evaporation ($Y_{f,evap}$) and therefore produces faster vapor release. Above all, it accelerates the reaction rate of any chemical reactions involved, although on the broad outlines only since the response of ignition-delay to temperature variations is not monotonic. As suggested in the previous analysis of the cool-flame transient state, observations and measurements of fully premixed flames in jet-stirred reactor, flow reactors, and shock tubes conclude to the existence of a negative temperature coefficient (NTC). Over a limited range of ambient temperature, the strength and the priority of chemical paths are modified while increasing temperature. As a consequence, the rate of reaction decreases, resulting into the increase of ignition delay [116]. The effect of ambient density is more direct. Increasing density enhances the entrainment rate of hot air. More enthalpy

and more oxygen are then available locally, helping both fuel evaporation and possibly chemical kinetics with similar reservations concerning NTC. Finally, the oxygen concentration has both direct and indirect effects. Firstly, increasing oxygen has a direct chemical effect similar to that observed for homogeneous mixtures, by catalyzing the reactions of ignition at both stages. Secondly, given a fixed entrainment rate as in a spray context, more oxygen is physically available. Thus, increasing air oxygen content at given conditions of temperature and density reduces the equivalence ratio (or increases the mixture fraction) required to activate the first chemical reactions.

Now considering the preponderance of thermodynamic variables over either the physical or chemical aspects of autoignition, Higgins *et al.* [101] observed the cool-flame development for different temperature conditions from that of Figure 2.4. While increasing temperature, the cool-flame kept shifting significantly towards the injection orifice compared to the liquid length, until reaching regions even situated upstream of the liquid length. The authors therefore suggest that the effect of temperature is more significant on the chemical reactions of autoignition than it is for the evaporation process. Dec and Espey [99, 100] got to the same conclusion, but adding that density and temperature have a greater effect on both the onset and duration of the high temperature autoignition phase than on the cool-flame mechanisms.

Fuel injection pressure (i.e. spray velocity) is the last parameter belonging to the group of variables associated to engine operating conditions, but only few references connect its effect with autoignition. Heywood [6] reports that injection pressure reduces ignition delay, although with very moderate influence. In the analysis of single-cylinder pressure traces, Molina [8] quantified its effect through a statistical analysis and obtained a dependence of ignition delay from injection pressure to a power of -0.2, consistent with Heywood's statement. Kosaka *et al.* [102] observed that increasing injection pressure advanced both appearance and disappearance of formaldehyde. The consequences for autoignition being barely modified by injection pressure may be important if they are confirmed over the whole range of operation of a Diesel engine. In order to seek into further analysis, let us consider two sprays each injected at a different level of pressure. Reminding Section 2.3, it is quite expected that injection pressure does not modify the mixture fraction field quantitatively, if not the velocity at which it establishes. Under these circumstances, their respective development would only differ in the fact that one spray is significantly more advanced in the mixing process than the other. If both sprays now ignite simultaneously, a first observation is that autoignition seem to be less depending on characteristic time-scales associated to spray mixing than to those fixed by chemical kinetics. In appearance

then, the spray tends asymptotically to behave like a homogeneous mixture as kinetics keeps going slower, when for instance further decreasing ambient temperature conditions. Under the conventional expressions relating chemical reaction timescale to physical ones, this first statement would translate into a low Damköhler number ($Da << 1$) or a high Karlovitz number ($Ka >> 1$). In addition, at the time of autoignition, each spray would disclose very different fields of both temperature and mixture fraction, especially at the jet heat where ignition occurs as stated at the beginning of this section. Accordingly, mixture ignition would still be sensitive to ambient temperature, density and oxygen concentration but rather in average terms and so quite in a "zero-dimensional way", clipping the local effects among the wide range of "temperature/stoichiometric dosage couples" enabled by each spray. This observation proceeding from a fundamentally local process is rather surprising and should be further investigated.

In this context apparently dominated by chemistry, fuel characteristics are definitely essential with regard to ignition processes. Hydrocarbon fuel ignitability depends typically and fundamentally on the components' chemical structure it is made up. Although detailed kinetic mechanisms are known for paraffinic fuels up to 10 carbons for homogeneous mixtures, combustion chemistry remains unresolved when considered mixtures of hundreds of long hydrocarbons chains (up to 20-30 carbons in fossil fuels), including cyclic, polycyclic and aromatic molecules, burning in a millisecond second order of magnitude while involving important time-derivatives and drastic gradients of thermodynamic conditions, velocity and mixture composition.

Hence, the assessment of fuel ignition qualities is rather empirical in practice through global indicators such as cetane number (CN) and octane number (ON). However, overall trends exist if information on fuel chemical composition is available. For instance, the capacity for a hydrocarbon molecule to ignite easily resides in its facility to first break one of its bonds. Bonds' strength varies respect to numerous parameters. In particular, carbon-oxygen bonds ($C-O$) and carbon-hydrogen double-bonds ($C=H$) are expensive to gap, so that fuel molecules rather break onto a $C-H$ single-bond first in a process called H-atom abstraction [111]. That is, the strength of $C-H$ bonds also varies with their position in the molecule, and with the kind of radicals connected to the other branches of the same carbon atom. These associations modify the overall electronic state of the molecule and the related strengths (Van der Waals interaction). For instance, $C-H$ bond of a primary carbon (CH_3) is stronger than that of a secondary carbon (CH_2) which in turn is stronger than a $C-H$ bond adjacent to either an ether linkage ($R-O-R'$)

or a carboxyl group ($R-COOH$) [117]. General rules, partially derived from the previous statements, are renowned:

- Linear alkanes (n-alkanes) have natural predisposition for ignition. They typically have the highest ignitability among their corresponding isomers. By way of example, the selected fuels to embody the upper limits of ignitability for the empirical scales of ON and CN are respectively n-heptane and n-hexadecane. Also, when the number of carbon atoms of n-alkanes increases, their ignitability increases as well.
- As fuel molecules get more ramified and/or become unsaturated with the occurrence of cycles or $C = H$ double bounds, or both (aromatics), their ignitability decreases. By way of example, the lower limits of ignitability for ON and CN scales are represented by isooctane and isohexadecane for ON and CN respectively. Both these fuels have methyl groups (CH_3) distributed along the core of the molecule, multiplying strong bonds. Note that hexadecane and isohexadecane are isomers and define the limits of the CN scale just by having a different molecule skeleton.
- In a mixture of fuels, the easiest fuel to ignite commands the first ignition reaction. This observation is best exemplified by the frequent recourse to cetane improvers, typically nitrates and peroxides, to enhance fuel ignition qualities. Cetane improvers are fuel additives which are added to diesel fuel at concentrations commonly less than 1 % (typically 0.1-0.25 %). Treatment at 0.1-0.25 % typically increases the CN of conventional diesel fuels by an average of 6 cetane numbers [118].

Only few pieces of information exist about fuel behavior respect to the three phases of ignition presented. In a selection of alternative fuels, including biodiesel and Fischer-Tropsch, Szybist *et al.* [110] observed two-stage ignition in all cases. Biodiesel also appeared to be subject to NTC effects. By time-resolving the visualization of CH-chemiluminescence, Pastor *et al.* [119] observed that biodiesel ignition was first emerging from eddy structures situated at the jet sides, although a more conventional homogeneous development in the jet head vortex was ensuing thereafter. This effect was interpreted as the result of both biodiesel lower volatility and higher ignitability. Under these relatively low temperature conditions, biodiesel would last longer in reaching its natural liquid length. His more heat-consuming evaporation should also further reduce the temperature in the head vortex region, favoring ignition kernels to first occur on the jet sides.

Therefore, as suggested in the above paragraphs, quantification of fuel ignitability is in practice often estimated empirically, by obtaining a blend

of both a sensitive and a resisting fuel to self-ignition matching the ignition delay of the sample fuel [120, 121]. ASTM standards define precisely the experimental protocol and the boundary conditions of a purposely-modified engine [120] and a combustion bomb [121] operated to simulate Diesel-like engine conditions. However, the resulting cetane number (CN) has been widely criticized in the past for failing in being representative of fuel ignition quality when considering alternative fuels or particular engine operating conditions such as cold-start. In [122], Siebers first remarks that all fuels do not have the same sensitivity to temperature variations. Also, they seem to behave quite differently with respect to first and second stages of ignition. Due to intense first-stage, some fuels may exceed the fixed heat release threshold used to determine ignition delay prior to the second-stage implicitly targeted by the standard. However, most of the criticism stems from the use of a specific engine setup with its own derived variables such as internal geometry and turbulence, but also and above all, built with quite a different hardware compared to modern engines. Motivated by numerous studies [123], part of these issues were accounted by using a combustion bomb instead [121], but the use of large nozzle holes (0.5 mm) and low injection pressure (10-20 MPa) are still fairly obsolete in comparison to the actual diesel technology. Bogin *et al.* [124] imaged the IQT spray for a comparison with modeling results. Figure 2.5 displays clearly the differences with the description of a Diesel spray made so far in terms of atomization, evaporation, angle and scale. In addition, operating conditions (818 K, 9.1 kg/m^3) may not be representative of the average conventional Diesel thermodynamic environment [120, 121]. Despite these inconsistencies, results from both experimental methods led the ASTM organization to the production of empirical correlations for fuel ignitability prediction. Their output is referred to as the cetane index (CI) and aims at simulating CN using fuel physical properties as inputs [125–127]. Based on a regression using around 1000 diesel-like fuels, the resulting algorithm identify fuel density and volatility as the physical variables controlling ignition qualities. However, as mentioned in the standards, these correlations do not extend to alternative fuels and the relevance of both physical properties is not demonstrated out of the limited range analyzed. Recent initiatives from Lapuerta *et al.* [128, 129] aim at proposing a new cetane index for alternative fuels. It accounts for some of the additional effects mentioned above, including a correction of the fuel density effect [129] and the addition of the iodine number, namely the level of insaturation of the molecule [128].

To summarize this section, autoignition of a Diesel spray first requires the fuel to be evaporated. Eventually, fuel vapor mixes with the ambient gas (usually air), until creating the conditions propitious for the activation

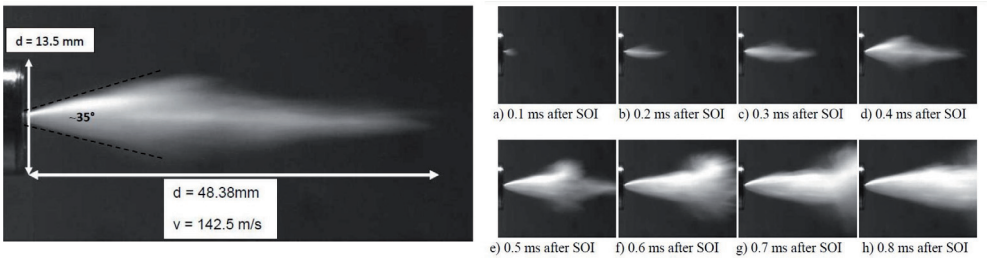

Figure 2.5. *High-speed images of an n-heptane spray during the injection process at IQT operating conditions. Source: Bogin Jr. G.E. et. al [124].*

of chemical reactions of hydrocarbon oxidation. Such reactions develop in parallel with the mixing process between air and fuel and break down in three stages. Prior to any chemical activity, a stage of "physical induction" vaporizes the liquid fuel and prepares the mixture to generate favorable conditions for ignition. This phase seems to be depending on chemical kinetics rather than on mixing time-scales. Chemical kinetics itself is controlled by fuel molecule structure, oxygen content and temperature. Subsequently, two stages of chemical reactions ensue, similar to those observed in shock-tubes with homogeneous mixtures of pure hydrocarbons and air. The first-stage ignition, also known as low-temperature heat release or cool flame, conducts to a small heat release, formation of formaldehyde and emission of chemiluminescence. This phase ends with the onset of the third and final stage also known as high-temperature autoignition or premixed burn and defines what is traditionally known as the ignition delay. The sudden burn of all the vaporized fuel accumulated during the two previous phases leads to a rapid growth of the heat release. Following this phase, transitory as the two others, a lifted, partially-premixed turbulent diffusion-flame establishes and will be the subject of the next section.

2.5. The lifted, turbulent, mixing-controlled, diffusion flame

Subsequent to the premixed combustion detailed earlier, a partially-premixed turbulent flame develops, marking the beginning of a phase of combustion by diffusion. In opposition to autoignition, this process is self-sustained, in the sense that its own heat release permits to sustain the reaction rate.

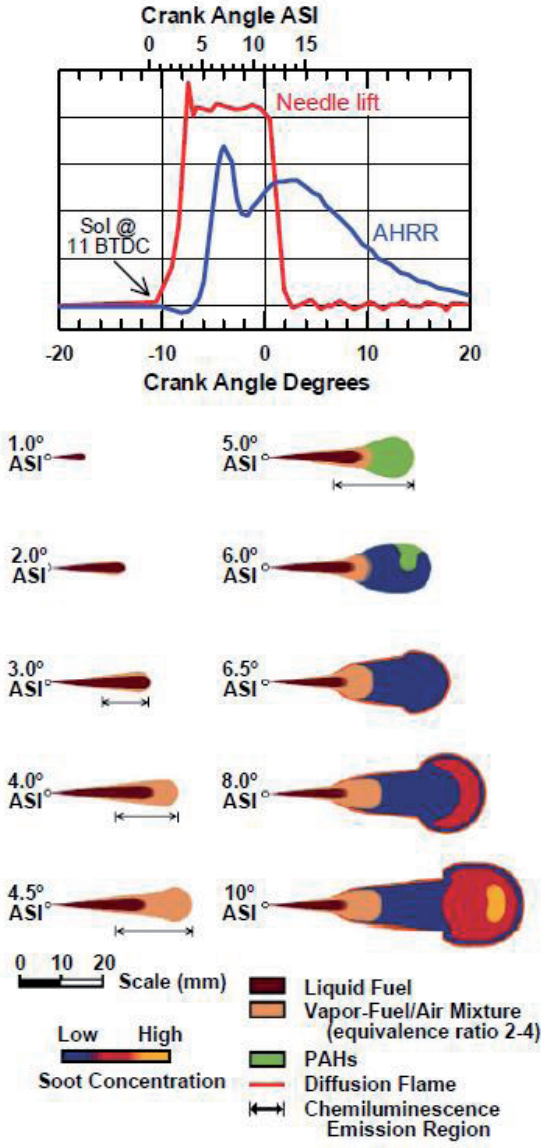

Figure 2.6. *Temporal sequence of schematics showing how DI diesel combustion evolves from the start of injection up through the early part of the mixing-controlled burn. The temporal and spatial scales depict combustion for the base operating with an injection duration extending beyond the sequence shown. The crank angle degree ASI is given at the side of each schematic (1 CAD = 139 μs). Source: Dec [1], Flynn [106].*

The transition between these two phases has been studied by Dec and Coy [104] and more recently by Bruneaux [130] while visualizing the fluorescence of OH radicals induced by a laser sheet. As stated by Curran, OH radicals form at several levels of the kinetics mechanism for hydrocarbons oxidation, and survive well away from the flame front under atmospheric conditions [131, 132]. But under higher pressure such as in Diesel-like conditions, the "super-equilibrium OH" or "groundstate-OH" contained within post-combustion gases recombines and disappears at a much higher rate than in conventional flames [133]. Accordingly, OH radicals represent a good tracer of the high-temperature reaction region for Diesel diffusion flames. In his conceptual model of a DI Diesel flame shown in Figure 2.6, Dec collects data from [104] to depict the temporal sequence witnessing this transition. As displayed by the sketch at 6.5 CAD ASI, the authors observed that OH first establishes as a thin layer surrounding the flame head vortex, and then extends back toward the injector to a point just upstream of the liquid length where it stabilizes. Under this assumption, diffusion flame starts during the premixed burn, near the maximum rate of heat release. Bruneaux recently obtained similar results to Dec's by observing OH release slightly prior to the premixed burn peak of heat release. Figure 2.7 shows his conceptual model, along with original images and the corresponding RoHR trace. In part because of the lower ambient temperature (800 K), the longer premixed burn enabled a more accurate time-resolution of the sequence. In addition to OH fluorescence, PLIF at 355 nm was applied simultaneously and allowed OH localization relative to formaldehyde (low temperature ignition tracers), PAH (soot precursors) and soot subsequently. The transition from autoignition (1) to diffusion flame (2) is described precisely in a succession of six stages, from the first appearance of formaldehydes (1-) until the establishment of a stabilized diffusion-limited flame (2+). In between, the switch from the last stage of autoignition (1+) to the first diffusion one (2-) is marked by the development of the high temperature reaction region (OH) consuming most of the cool flame formaldehyde, while the diffusion flame establishes at its periphery. In parallel, OH from the flame core is consumed and replaced by PAH, as a result of fuel-rich pockets mixing with the hot diffusion flame products. Remaining formaldehyde concentrate at the periphery of the diffusion flame suggesting the existence of a fuel-lean region. This occurrence attests that the flame is not yet fully controlled by mixing. In summary, the first stage of diffusion flame is characterized by the presence of an interface between low- and high-temperature zones. This stage results from the successive occurrence of formaldehyde, OH and PAH respectively. The three species coexist, growing from the flame core and pushing the preceding species towards the edge.

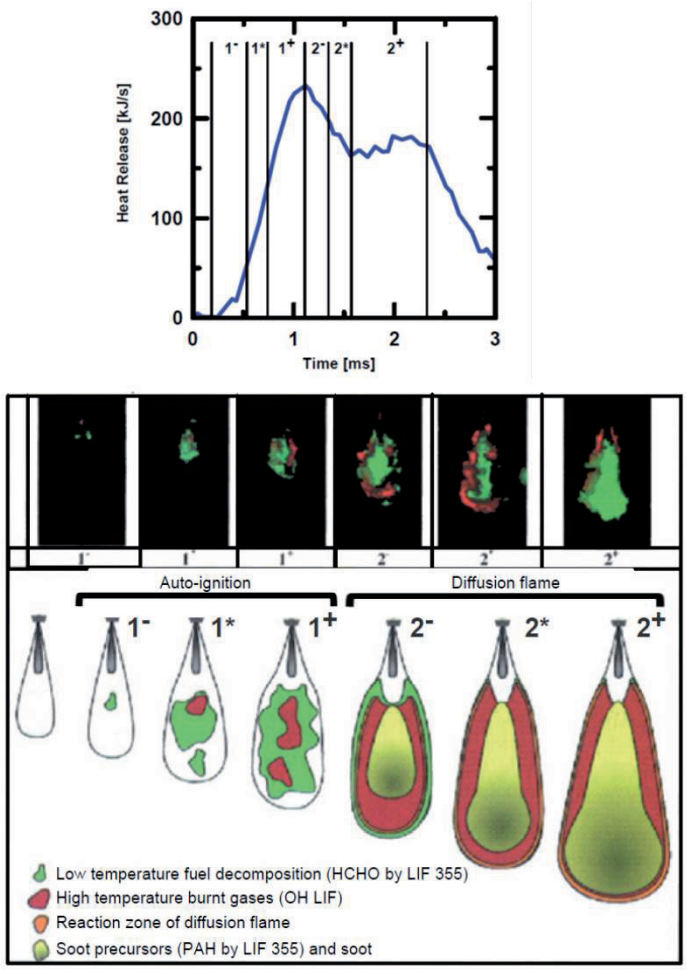

Figure 2.7. *Schematic diagram of the improved time-resolved conceptual model proposed by Bruneaux for the DI Diesel combustion process. It depicts the transition between the cool flame (1-) and the establishment of the mixing-controlled diffusion flame (2*). Source: Bruneaux [130].*

During the phase of diffusive combustion, the flame front establishes and progresses until reaching its natural maximum length, while being maintained by the convective and diffusive contribution of fuel and oxygen. Contribution of fuel convection is fundamental, as it enables the mixing process in virtue of spray momentum. When fuel injection stops, the combustion process turns out to be dominated by the diffusion of both fuel and oxygen, prompting a substantial change of the flame structure until the flame quenches in a

process often referred as a major issue in soot exhaust emissions [134–136]. As presented in the introduction of this section, some authors [6, 113] consider such phase as another independent process referred to as the "late diffusion-controlled combustion". It will not be approached in the following section, whereas the self-maintained diffusion flame will be described exhaustively, that is, from the onset of the diffusion flame until the end of the injection process.

The structure of the Diesel diffusion flame has been the subject of multiple studies in the past [137–139]. Currently, the most widespread and accepted vision is probably the conceptual model proposed by Dec [1] and later extended by Flynn *et al.* [106]. Figure 2.8 shows a schematic of this approach derived from laser-sheet imaging for a typical instant during the first part of the mixing-controlled burn (i.e. prior to the end of injection):

- A first region exists, located between the nozzle exit and the onset of heat release, in which the conditions are similar to those observed for the non-reactive spray (*zone I*). Chemical reactions do not propagate to this zone because of the high local speeds, low temperature, poor mixing, high scalar dissipation rates, and more generally important gradients of numerous kinds that would lead to flame quenching [2, 140]. Therefore, this region behaves like a non-reactive and evaporative spray in terms of atomization, air entrainment and evaporation although such processes could be altered to some extent by the presence of the diffusive flame downstream. The length of this first zone is commonly referred to as the "lift-off length" (LOL).

- Downstream the lift-off length, the flame gets the typical structure of a diffusion flame (*zone II*), consisting of an internal volume occupied by intermediate combustion products and surrounded by a surface of reaction which impedes the oxygen to flow in. These substances, including unburned hydrocarbons possibly mixed with soot, complete their oxidation into carbon dioxide and water when finding the adequate amount of oxygen on the flame surface. More precisely, oxygen along with other air components are naturally convected towards the spray central axis through the mixing process described in previous sections. But once reaching local stoichiometric conditions, oxygen is stopped to be consumed in the reaction with fuel hydrocarbons to form the surface of reaction, while air nitrogen pursues its way inside the flame. Therefore, the flame is considered as mixing-controlled since the front establishes subsequent to the formation of a stoichiometric layer driven by spray mixing. Previous experiments conducted by Dec and Coy [104] showed that the thickness of such reactive surface was inferior to 120

μm while LIF measurements revealed it was the location of nitrogen oxides formation, consistent with conditions of high temperature ($\sim$2700 K when T_{air}=950 K) and oxygen excess necessary for the appearance of this species [141]. Dec represents the shape of the reactive surface including a head vortex on the leading portion of the flame. This vortex is created during the transient development before the flame reaches its natural length. In this region, soot peaks as its formation and growth are particularly favored by the high temperature levels and the high residence time required by "rich premixed combustion products" to reach the flame surface.

- Such rich premixed combustion products proceed from a third region situated immediately downstream the lift-off length. Dec hypothesizes the existence of a rich combustion in which premixed reactions would consume all the oxygen entrained in the first non-reactive region (*zone I*). Flynn *et al.* estimate that, for a fuel initially injected at 350 K within an ambient at 950 K, the temperature of this region increases from 825 K to 1600 K thanks to this rich combustion although only 10 to 15 % of the fuel energy content is released. Combustion products, mostly composed of carbon monoxide and partially oxidized hydrocarbons (mainly PAH), are often referred to as soot precursors and would provide the basis for soot formation within the diffusion flame.

Dec's model was published in 1997 and inspired numerous studies from then on. It has been the basement of several approaches aiming at its improvement in both time- (Cf. previous section) and space-basis. Hence, it has been tried to obtain more quantitative data in terms of species and flame morphology, while varying operating conditions and fuel type. A more detailed description of the species involved was obtained as well as their possible interaction. Also, while Dec's experiments were conducted in an optical engine, with limitations of injection duration and space available for flame development, the arrival of new-generation optical facilities allowed performing longer injections in order to reach steady-state of the flame diffusion portion prior to the end of injection. Their easier optical access enabled both to set up new optical techniques and their simultaneous use, while their large and constant volume permitted to maintain precise and constant ambient conditions (temperature, density, oxygen concentration) all along the combustion process of free sprays. Accordingly, numerous works have contributed directly or indirectly to the improvement of Dec's model, providing deeper insight into Diesel combustion phenomenology. While several of them, either with a specific or quantitative approach, will be discussed later in the

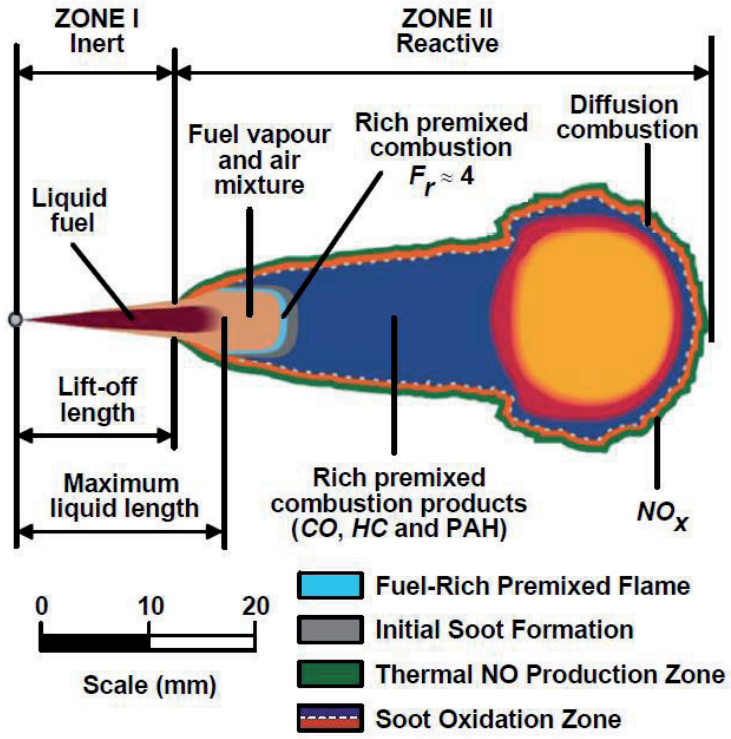

Figure 2.8. *Structure of the free Diesel diffusive mixing-controlled flame in quasi-steady state according to the conceptual model proposed by Dec. Source: Dec [1].*

document, those providing a major conceptual contribution are reviewed in the following paragraphs [107, 109, 142].

Quite in agreement with Bruneaux's recent update [130], Kosaka *et al.* [109] had first observed a rapid release of soot precursors forming after autoignition within the whole leading portion of the spray. Additional visualization of laser induced incandescence indicates that those located at the periphery of the flame head vortex are the first to be converted into soot particles, being referred to as "young soot". Because the factors necessary to soot formation are high temperature and rich mixture throughout a high residence time [135], this region, corresponding to the peripheral OH observed by Bruneaux (2-), suggests that high temperature is the first factor to trigger soot formation. However, once reaching the quasi-steady diffusion combustion period depicted in Figure 2.9, mechanisms become quite different. The figure shows that

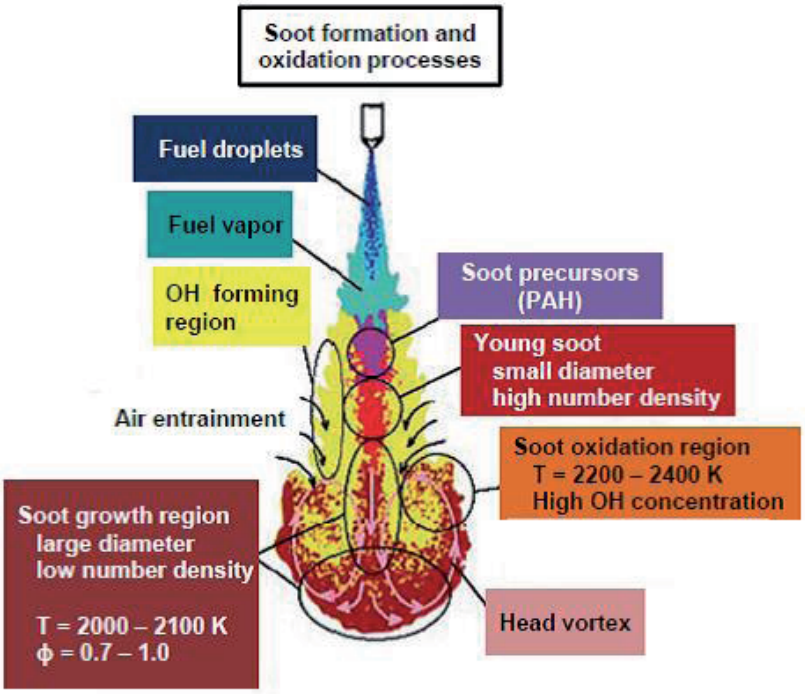

Figure 2.9. *Conceptual model of soot formation, and oxidation processes in a Diesel spray flame. Source: Kosaka [109].*

soot precursors keep forming within the central fuel-rich region, while being surrounded by a thick leaner region of OH radicals. This thick region is the result of peripheral OH, flowing inside the flame and consumed before it can even reach the spray axis. Indeed, if intuitively the OH formed at the lean peripheral regions diffuses on both sides of the flame front, an important share is naturally convected towards the flame axis. However, as a very active carbon oxidizer, OH is rapidly consumed as it meets PAH and soot, letting only those from the center survive. OH is effectively very proficient in that process as Haynes and Wagner [143] state that 10 to 20 % of all OH collisions with soot are effective at gasifying a carbon atom. According to Bartok and Sarofim [144], OH is most likely to dominate soot oxidation under fuel-rich and stoichiometric conditions while under lean conditions, soot is oxidized by both OH and O_2. Next, the figure shows that the surviving PAH from the spray center converts into young soot particles. Mostly composed of isolated primary particles, such young soot is formed by surface growth upon nuclei,

and coagulates because of molecule collisions induced by the spray convection while progressing downstream the central fuel-rich region. This description, illustrated in Figure 2.10, is consistent with the recent work from Tree and Svensson [135] in which soot formation mechanisms in the context of a Diesel engine are outstandingly reviewed. The authors specify that nucleation (also called soot particle inception) is the formation of particles from gas-phase reactants where two C_3H_3 radicals are likely to form the first ring. After growing and turning into PAH until reaching the size of nuclei (1.5 to 2 nm), particles dehydrogenate yielding a graphite-like structure of carbon atoms. This process occurs in radical-rich regions while requiring temperatures between 1300 and 1600 K. Yet, the majority of the soot mass is added during the time-consuming following stage called "surface growth". Spherical primary particles (15-20 nm) of soot proceed from the coalescence (also called coagulation) of nuclei colliding, thereby decreasing the number of particles but holding the combined mass of soot particles constant. This phase corroborates that residence time has a large influence on the total soot mass or soot volume fraction. Relevance of residence time in soot formation processes was confirmed by Pickett *et al.* when they observed the lack of a unique equivalence ratio-temperature region for soot precursor formation. Accordingly, this implies that the soot formation process rather depends upon the equivalence ratio-temperature path followed during jet mixing, and the residence time along the path [145]. In regard to the specific objectives of this study, it should be noted that soot nucleation and growth are apparently very similar for all type of fuels [135]. Although primary particles maintain their shape, particles lose their spherical pattern in the next process of agglomeration through which primary particles stick together to form larger groups called "agglomerates". When these aggregates reach the leading portion of the jet, Kosaka *et al.* indicate that they are pushed aside, convected upstream by the motion of head vortices and finally re-entrained into the lean side of the flame, where the high concentration of OH expectedly initiates their oxidation. Therefore, the transient nature given by this head vortex dynamics also seems to be helpful in the oxidation of soot particles. To conclude, OH oxidation occurs at both the steady region and the transient head vortex of the flame. This observation goes against the mainstream idea that soot oxidation does not happen within the diffusion flame and exclusively occurs when crossing the diffusive oxidation layer. Still, no concrete experimental evidences exist to support these statements. For instance, extraction of soot samples from the inside of the flame could provide deeper information.

Whenever the injection lasts enough so the flame can reach its natural length, the head vortex "detaches" from the tip and the flame rather gets

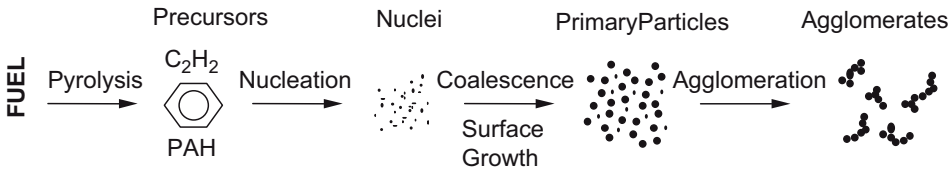

Figure 2.10. *Schematic diagram of the steps in the soot formation process from gas phase to solid agglomerated particles. Source: Tree [135].*

the natural "plume-shape" of a steady-state flame. This phase may require more than 3 ms to establish and depends mostly on injection pressure (spray velocity). Therefore, this state is not that realistic of real Diesel engine conditions where injection barely exceeds 1 ms at full-load; but again, it represents an interesting and necessary simplification on the way to match modeling and experimental results. Under these conditions, Pickett *et al.* released two updates of Dec's conceptual model, using multiple diagnostics in order to identify the maximum number of species. In order to support the analysis, the two-stage Lagrangian model (TSL) from Broadwell and Lutz [146] was employed jointly to predict roughly the mixture fraction field and the temperature stratification. Figures 2.11 (a) and (b) represent these two models collected respectively from [107] and [142]. As it can be observed, their focus is driven towards the processes occurring at the lift-off length. This effort was motivated by several studies highlighting the importance of increasing the level of premixing in the lift-off region to reduce flame sooting propensity [3, 147–155]. Although lift-off length is a classical and relatively easy measurement, which is nowadays considered as essential in the analysis of combustion and emission formation [2], the processes determining the position of its establishment are still undetermined. In their review, Venugopal and Abraham [140] propose three potential mechanisms of stabilization, including (i) quenching at the flame base, (ii) equalization of spray convection with velocity of flame propagation, and (iii) connection with ignition location and heat release. But still, the lift-off length is not enough to explain the soot formation within the flame and further investigation is needed to understand it relationship with soot formation [145, 156]. Both models seek answers to these discussions by studying the relative positions of formaldehyde, polyaromatics and soot respect to the diffusion flame. Results are obtained through two different experimental approaches: in (a), n-heptane is injected and different sooting grades are obtained by varying both ambient temperature and oxygen concentration, while (b) is achieved under a unique baseline condition using

three different fuels with distinct concentrations of aromatics and oxygen. Still, both test matrices are common in some extent, using for instance similar injection pressure (138 MPa), nozzle diameter (180 μm) or ambient density (14.8 kg/m^3).

Starting with the variation of ambient conditions carried on in (a), three levels of soot, labeled "no-", "low-" and "moderate-soot" are achieved by lowering their propensity through reducing both ambient temperature and oxygen concentration. The effect of temperature on soot processes is twofold: First, it naturally promotes chemical kinetics of soot formation. Then, it shortens the lift-off length, and thus establishes a richer premixed combustion in the lift-off region, therefore more prone to soot precursors formation. Regarding the decrease of ambient oxygen concentration, offsetting effects come into play. First, with more difficulties to hook oxygen molecules, the flame lengthens which implicitly increases soot residence time. Also, oxygen reduction participates to the overall enrichment of the spray mixture. Therefore, at a given axial distance (or given lift-off length), the equivalence ratio is expected to be higher. But on the other hand, oxygen reduction also causes the lift-off length to increase (inversely proportional [147]). The three hypotheses mentioned above for lift-off stabilization can explain this shift downstream: (i) it deteriorates the velocity of turbulent-flame propagation, (ii) it promotes flame quenching, and (iii) it delays and shifts downstream the first exothermic reactions of ignition. As a result, Pickett *et al.* [153, 154] conclude that such longer lift-off length balances the lower air oxygen content in a way that equivalence ratio is maintained in the lift-off region. Consequently, the lower sooting propensity under reduced-oxygen ambient is likely driven by the lower averaged temperature of the flame, being soot formation rates more sensitive to chemical reactions freezing than to the prolonged residence time. Now considering the flame structure reconstructed in Figure 2.11 (a), it is first to underline that the collection of techniques employed and the accuracy achieved are such that it could be likely defined as a novel two-dimensional chromatography technique. For the no-soot condition, formaldehyde ($HCHO$) appear to be formed upstream of the lift-off location and is consumed downstream within the fuel-rich premixed reaction zone at the spray center. This represents an important contribution as it sets that a first region of heat release, quite similar to the cool-flame of ignition, exists at the flame base. Despite such fuel-rich combustion, and a fuel-rich core enclosed downstream within the high-temperature diffusion flame, there is no detectable PAH formation in this no-soot condition. This result is consistent with the mechanism presented above where PAH was required as a matrix for further soot development. For the low-soot condition, $HCHO$ is formed upstream of

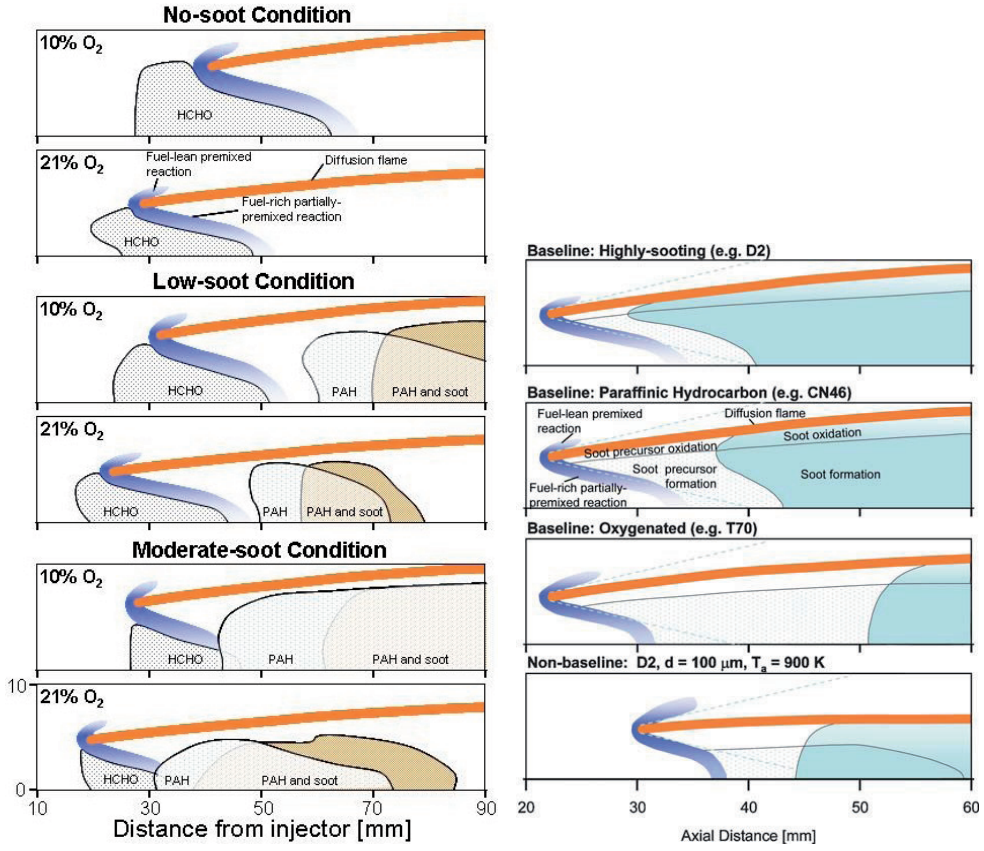

Figure 2.11. *(a) Conceptual model of HCHO, PAH and soot formation for the no-soot (900 K and 850 K), low-soot (1000 K and 900 K) and moderate-soot conditions (1100 K and 1000 K) at respectively 10 % and 21 % O_2 conditions.*
(b) Schematics illustrating the fuel effect on soot processes near the lift-off length in mixing-controlled diesel fuel jets. The upper three schematics show the average location of various processes that are expected for fuel jets at baseline operating conditions: 1000 K, 14.8 kg/m^3, 138 MPa pressure drop, and 180 μm orifice. The class of fuel considered is given at the top of the schematic. The bottom schematic is for D2 fuel at a non-baseline condition: 900 K, 14.8 kg/m^3, 138 MPa pressure drop, and 100 μm orifice.
Source: Pickett et al. *[107, 142] .*

the lift-off length as well, and consumed downstream of the lift-off length at the jet center, followed by PAH and soot formation. However, there is a distinct separation between the region of *HCHO* consumption and PAH formation.

As ambient temperature is increased further to produce the moderate-soot condition, the axial location of $HCHO$ formation is essentially coincident with the lift-off length and it becomes harder to distinguish between $HCHO$ and PAH downstream.

Continuing with analogous experiments and analysis, three fuels with significant differences in physical and chemical characteristics are injected under the 21 % oxygen-moderate-soot condition (1000 K, 14.8 kg/m^3, 138 MPa, 180 μm). The US conventional fossil diesel ♯2 (D2), containing a substantial amount of aromatics (34 %) and olefins, is contrasted with two of its surrogates, namely CN80 and T70, resulting from the mixture of pure compounds. This is unfortunately not the place to discuss in depth the surrogate subject, but the reader is referred to the excellent review from Pitz and Mueller [88] to find more information on this topic. Thus, CN80 is a surrogate for D2 aiming at reproducing conventional properties such as density, volatility, stoichiometry and lower-heating value. The main difference lies in the absence of aromatics, known for their sooting propensity when intrinsically present in the fuel. As a paraffinic fuel, it also has a much higher ignitability (CN=80 against CN=42 of D2). This surrogate offers the opportunity to compare a fuel with shorter lift-off length and consequently a more propitious trend to condense aromatics after the premixed combustion, with the conventional D2 allowing more mixing prior to the lift-off length but already containing aromatics intrinsically. Yet in its historical use, the second surrogate T70 precisely had as a target to match D2 ignition delay under a baseline condition, although with different stoichiometry and physical properties. Already employed by Dec in [1] as well as in several other works of Sandia's group involving optical engines, the objective of injecting T70 instead of D2 was uppermost to reduce the soot concentrations within the jet in order to permit an easier application of optical diagnostics and minimize depositions of soot when the jet impinges on the windows surface. As T70 results from a blend between 70 % of tetraethoxy-propane ($C_{11}H_{24}O_4$) and 30 % of heptamethyl-nonane ($C_{16}H_{34}$), the interest here is to observe the effect of the oxygen content in a fuel, such as biodiesel or oxygenated fuels could contain, and seek deeper knowledge in their impact on soot processes within a Diesel flame. Results show that fuel sooting propensity decreases in the order D2<CN80<T70. Thus, the richer premixed combustion of CN80 does not offset D2's aromatics content. Expectedly, T70 has the lowest soot propensity. Its important oxygen content both leans the premixed combustion and shortens the flame length (smaller residence time) while not having significant effect on the adiabatic flame temperature. For all the three fuels, soot formation starts at a finite distance downstream of the lift-off length

but the location vary depending on the fuel type. In Figure 2.11 (b), the baseline schematics are generated for classes of fuels that have similar fuel characteristics, flame temperature, cetane number, and the same lift-off length. Thus, CN80 is assimilated to a fictitious CN46 without aromatics like CN80 but with a lift-off length similar to D2. It can be observed how the distance from the lift-off length to the location of the first soot formation increases as the fuel sooting propensity decreases. The most upstream soot formation occurs at the edges of the jet for D2 and CN80, while for T70 the soot formation is confined to the jet central region. The authors believe it is due to the low temperature level insufficient to trigger soot formation in the axis, while on the sides, the contribution of diffusive combustion products is important. In agreement, they also observe that the initial soot formation with D2 fuel jets returns back towards the jet centre when conditions are varied to increase A/F mixing upstream the lift-off length. Finally, the authors also suggest that the rates of soot precursor formation depend strongly on fuel type in the region between the lift-off length and the first soot formation.

To close this review of the combustion phenomenology, a last reference may get a significant importance especially in the context of fuel effect assessment. Although performed with conventional diesel, Musculus [157] studied soot radiation and its possible effect on both combustion efficiency and NO_x emissions. Though soot radiation is leveraged in certain combustion applications (water heaters, etc.), it clearly represents a weak point in a Diesel engine where the purpose is to transform the fuel energy content into pressure. Soot radiation contributes into heating the walls and thus participates to the typical 30 % of fuel energy content lost in engine cooling [6, 7]. By sweeping the phasing of fuel injection between -12 and 15.5 CAD ASOI in an optical engine, Musculus [157] modified the history of ambient conditions met by the mixture and created different sooting conditions subsequently. As a first result, the fraction of the chemical energy release lost to soot radiation was evaluated between 0.31 % for the latest SOI and 1.87 % at 3 CAD ASOI based on the pressure signal analysis. As a reference, other authors had previously found values between 5 and 10 % [158, 159] although under higher-sooting and higher-load conditions. Still, it should be noted that this type of estimations is rare in the literature. The second important contribution of [157] is the effect of soot radiation observed on flame temperature. Variations of the SoI revealed the appearance of the so-called "NO_x bump", namely a punctual increase of NO_x emissions in the exhaust corresponding to a simultaneous and important decrease of soot luminosity. This observation suggested the vanishing of soot radiation losses due to the flame conversion from a sooting to a non-sooting regime, causing an increase of the flame temperature and the

subsequent enhanced formation of thermal NO_x *via* the Zeldovich mechanism. Precisely, further soot thermometry confirmed that radiative cooling could reduce flame temperatures by up to 25-50 K, which had as an effect to reduce exhaust NO_x by 12-25 %. Therefore, the NO_x/PM trade-off observed in exhaust measurements as introduced in the previous chapter could actually proceed from very local effects although no experimental evidences of that statement exist.

2.6. Alternative fuel effect

As an introduction to this work, it was made reference and demonstrated the potential of alternative fuels, including biodiesel and Fischer-Tropsch for the future substitution of standard diesel derived from fossil sources. It was also reminded the issues that Diesel engine has had to face so far in terms of local contamination through the reduction of both NO_x and particulate matter (PM) emissions, and the future challenges it will have to consider with CO_2 limitations. As mentioned in the two excellent reviews from Lapuerta *et al.* [160] and Gill *et al.* [161], the interest of the Diesel engine scientific community on alternative fuels is only recent but has been growing exponentially since the late 90's for biodiesel to reach more than 200 publications in 2005, and since 2004 for Fischer-Tropsch fuels, reaching more than 40 publications in 2009. Note that such figures include highly rated journals in scientific indexes, but also other non-indexed publications such as SAE technical papers, according to their high impact in the engine scientific community as reported in [162]. Naturally, the research effort has been driven towards both combustion and emissions performances when using these fuels directly in modern Diesel engines. In this regard, Table 2.1 has been adapted from these two reviews and estimates the percentage of publications reporting an increase or a decrease in respect to a selection of parameters of interest. Accordingly, the actual picture presents alternative fuels as a way to reduce all type of exhaust pollutants compared to the conventional diesel, except for biodiesel which imposes a penalty on NO_x emissions. Fischer-Tropsch diesel fuels also seem to increase engine performance, whereas biodiesel deteriorates the effective power and specific consumption of the engine.

Looking in more detail into these reviews, several benefits of Fischer-Tropsch are suggested to derive from differences in the fuel composition. Typically, their lower distillation characteristics improve atomization and dispersion of the fuel spray, which enables faster evaporation and accelerates the fuel mixing with air. Its paraffinic nature (no aromatics), reduces soot

formation while also engendering higher ignitability. The latter affects in consequence the combustion process by reducing for example the fraction of fuel burnt under premixed combustion. Fischer-Tropsch also seems to have a better response to lower oxygen concentrations induced by high EGR levels. Aizawa *et al.* [163] observed that PAHs appear delayed and shifted downstream compared to conventional diesel but this type of optical studies involving Fisher-Tropsch fuels is rather rare. Regarding biodiesel, most of the studies agree that biodiesel lower performance in terms of effective power and BSFC is due to its oxygen content inducing a lower heating value (LHV). Lapuerta *et al.* [160] report a decrease of the energy content of 14 % in mass- and 9 % in volume-basis, the latter being balanced by its higher density. On the other hand, the authors observe quite a wide disparity of results with exhaust emissions that they attribute to the large number of different engine technologies tested, the varying operating conditions or driving cycles followed, the different biodiesel fuels used (different feedstock and different quality), and the various measurement techniques and procedures applied. Still, dominant trends were extracted starting with the reduction of the PM, and more particularly a decrease of the mean diameter of the particles sampled in the exhaust. This diminution is the consequence of the largest particles vanishing, although some studies reveal an increase in the number of the smallest ones in return. Most of the studies connect this effect with a reduction of soot formation, a better soot oxidation stirred by the fuel oxygen content, and the absence of aromatics. Such "more complete" combustion would also help to decrease significantly other regulated emissions such as THCs and CO. In order to seek further into all these considerations, several studies have investigated biodiesel effects using optical research engines similar to Dec's facility [164–171]. These studies typically associate simultaneous measurements of high-speed spatially-integrated natural luminosity (SINL) (usually through a transparent piston), in-cylinder pressure and tail-pipe emissions. All report a consistent reduction of PM exhaust emissions when biodiesel is injected instead of conventional diesel, but also a coincident decrease of the SINL which is frequently interpreted as a decrease of soot formation within the flame. Though SINL measurement can provide a qualitative measure of in-cylinder soot formation, this technique is not quantitative and may even be tricky. This is primarily due to the high dependence of this diagnostic to the soot temperature (exponent 5 to 11) while it is merely linear with the soot volume fraction [172]. In all cases, such result is quite expected as several other studies report that a lean mixture equivalence ratio at the lift-off length can reduce sooting propensity [3, 147–155]. The oxygenated nature of biodiesel then offers a mechanism with which to accomplish these leaner equivalence

ratios. Concerning the mechanisms leading to higher NO_x, the origin is much more uncertain since, as Mueller *et al.* [165] suggest, no major differences are to expect on the adiabatic flame temperature. Although Lapuerta´s review [160] indicates that the reason most frequently pointed out is that the injection process with biodiesel is slightly advanced compared to diesel due to its higher bulk modulus (Cf. Section 2.3.1), Mueller *et al.* [165] raises several other hypotheses that could explain biodiesel NO_x increase. First, a potential faster ignition delay could reduce the fuel fraction burnt under premixed mode. Then, the shorter combustion duration caused by its oxygen content could also make the whole process to occur closer to TDC and thus at higher temperature levels where Zeldovich mechanism of thermal NO_x is enhanced. Finally, as suggested by Musculus [157], soot radiation can potentially reduce the flame temperature and also reduce the formation of thermal NO_x. Various intents have been made to isolate the soot radiation effects from other factors susceptible to affect NO_x formation. By matching the phasing of combustion instead that of injection between diesel and biodiesel, Mueller *et al.* [165] and Armas *et al.* [173] first ruled out the hypothesis of an anticipated fuel injection. Further intents to isolate the rest of hypotheses appeared to be difficult in such a facility as all these effects are constantly intertwining, making the connections and assessment difficult to establish [174].

2.7. Research questions and specific objectives of this work

Now that the processes involved in Diesel combustion have been detailed and the issues relative to alternative fuels reviewed, time comes to reconsider the initial goal of this study and release more specific objectives in agreement with the knowledge presented so far. The previous review has provided a better understanding of all the aspects related with the different phases involved in Diesel combustion and capture the missing comprehension when conventional diesel is replaced by another type of fuel.

The last section provides a qualitative description of the effects observed when introducing alternative fuels instead of conventional diesel into a Diesel engine, but above all, it highlights the research questions of the present study. Although more complete for biodiesel thanks to the most recent optical studies performed, the state of the art evidences the lack of understanding and the uncertainty associated to the replacement of fossil diesel with fuels proceeding from other sources. As a first step, most of the experimental work has been naturally focused towards studies aiming at injecting the

Table 2.1. *Estimated percentage number of publications which have reported increases, similarities or decreases in engine performance and emissions with biodiesel and Fischer-Tropsch fuels in comparison to conventional diesel fuel. The statistics is made over 158 publications for biodiesel and 68 for Fischer-Tropsch. The dominating trend for each field is highlighted: in green (or with a) when advantageous, in red (or with d) when disadvantageous and in grey (or with n) when neutral. Source: Lapuerta* et al. *[160], Gill* et al. *[161].*

	Biodiesel			Fischer-Tropsch		
	Increase	*Same**	*Decrease*	*Increase*	*Same**	*Decrease*
Effective power	-	2	96^d	-	75^n	25
BSFC	98^d	2	-	17	-	83^a
Thermal efficiency	8	80^n	4	58^a	33	8
NO_x emissions	85^d	10	5	-	21	79^a
PM emissions	3	2	95^a	5	16	79^a
THC emissions	1	3	95^a	-	-	100^a
CO emissions	2	7	90^a	-	6	94^a
CO_2 emissions	-	-	-	11	22	67^a

fuel directly in multi-cylinder engines. But under this approach, most of the details relative to internal processes are clipped and resumed to a "black box" status. The extreme complexity of the derived "transfer function" and the large distance between its inputs and outputs expectedly leads to confounding observations and limits its comprehension. As Lapuerta *et al.* [160] warn when referring to their literature review on combustion and emissions performance: *"although a dominant trend could be found in most cases, there have always been opposing trends proposed elsewhere by contrast"*. In addition, it is to note that most of the descriptions furnished are rather qualitative, especially regarding fuel properties. Therefore, further insights and quantification into spray and combustion characteristics are fundamental in order to extract the maximum benefits from these fuels in the optimization of engine design and calibration, and possibly provide some light to improve their own design and fabrication. In this regard, Sections 2.1 to 2.5 detailing the combustion process permitted to identify the relevant stages and key points where an assessment of the fuel effect is required to better understand both its consequences on the combustion phenomenology and the resulting engine performance in terms

of combustion efficiency and emissions. Prior to a detailed break-down of further specific objectives, our main objective should be first reminded as it has been initially enunciated in the introduction to this document: **Improve the understanding and assess the effect of fuel properties over the physical and chemical mechanisms associated to the processes of combustion and emissions formation of a diesel spray.** In agreement with the phase analysis performed in the combustion review, some other more specific objectives can be considered for the different stages of the combustion process:

- Injector internal flow: Its upstream position respect to both fuel injection and combustion confers to the internal injector processes a major importance. Beyond varying mass rate and energy rate of injection, a different nozzle behavior in terms of hydraulic delay and discharge efficiency could engender different results downstream and mislead the spray injection and combustion analysis if they are not properly addressed. Therefore, although the analysis of the fuel injection system itself is not an objective since it has been treated in depth in [30], it is necessary to determine how the fuel affects its mechanisms as a boundary condition of this study.

- Atomization/Evaporation: According to the review, the Diesel spray reaches complete atomization very close to the nozzle exit which strongly helps heat exchanges between air and fuel. Despite the wide distribution of droplet sizes, their evaporation is controlled by mixing, namely by the amount of entrained heat rather than by the exchange processes occurring at the droplet surface. However, as for any other Newtonian fluid, droplet size may increase significantly with viscosity perhaps in such a way that droplets surface effects become significant. Therefore, it should be verified that such mixing-controlled hypothesis is not called into question by a fuel replacement. Several paths enable the check: (i) The liquid length should remain constant when varying injection pressure. (ii) While using biofuels in blended formulations with conventional diesel, the liquid length should scale with the blending ratio and not having the less volatile components controlling the liquid length. (iii) Under time and spatial derivatives of ambient boundary conditions, liquid length should adapt instantaneously to its environment. The validity of Siebers' mixing-limited hypothesis is not essential but considerably time-saving for the computing of spray calculations. Its extension to alternative fuels would enable their application into both 1D spray models and scaling laws using this assumption.

Finally, regarding the quantification of fuel effects, it would be contributive to determine in a first instance if the sensitivity of each fuel respect to variations of ambient conditions is similar to that of diesel. Then, the fuel properties that alter the liquid length should be identified and their relevance compared to the thermodynamic environment in the combustion chamber should be assessed.

- Air/Fuel mixing: According to the review, no significant effect is actually expected under non-evaporative conditions on both the spreading angle and the spray penetration although differences in density may exist among fuels. This expectation states for an equivalent mixing rate independently from the fuel origin. However, under evaporative conditions, the local cool down could lead to differences in penetration between evaporative and non-evaporative spray. Since such cool down likely vary from one fuel to another because of different latent heat, spray penetration (and consequently mixing) under evaporative conditions should be established when changing the fuel.

- Autoignition: This triple-stage process appeared to be the result of a complex interaction between physical and chemical processes. Ignition delay appeared to be strongly affected by both the fuel molecular structure and ambient conditions, in particular by temperature. However, the assessment of each factor in a Diesel spray context is missing. As an indication of the fuel property effects, ASTM standards suggest that fuel ignitability is somehow related with its density and volatility properties although for conventional diesel exclusively. The contribution that would bring an extension of this type of empirical correlations to alternative fuels is interesting from an engineering point of view as they are relatively easy and avoid engine testing. In addition, a direct comparison between ignition delays from different fuel sources could give a hint of the fraction burnt under premixed mode and could partially explain results of exhaust emissions. Finally, the confirmation of the non-effect of injection pressure would indicate that the time of establishment of the mixture fraction field, namely the characteristic time-scales of mixing are not relevant in comparison to chemical kinetics.

- Flame lift-off: This morphological parameter acquaints for the amount of air/fuel mixing achieved upstream the diffusion flame. At the flame base, a rich premixed combustion develops consuming all the oxygen entrained and possibly forming polycyclic aromatic hydrocarbons (PAH) which serve as soot precursors inside the diffusion flame. Therefore, the indication given by the lift-off length turns out to be essential in

the understanding of soot formation. However, the literature review indicates that processes governing the lift-off stabilization are not clearly established yet although several hypotheses actually exist. The most recent one suggest a connection with the ignition location though without any cause-to-effect relationship being demonstrated. Under this assumption, an interesting trade-off emerges between aromatic and paraffinic fuels: while aromatic fuels intrinsically contain those aromatic precursors, their lower ignitability enable a longer lift-off, thus more premixing upstream the diffusion flame, and less soot precursor formation. In addition, oxygenated fuels participate in leaning the mixture at the lift-off length with potentially similar effects than a longer lift-off length. Therefore, beyond the interest of obtaining quantitative values for alternative fuels, the context of fuel properties assessment also gives the opportunity to investigate further the mechanisms governing the lift-off establishment and the connection with soot formation processes.

- Soot formation/radiation: Sometimes presented in the past as an assistance to the combustion process, soot is now clearly established as an auxiliary effect whose emissions from Diesel engine are dangerous for human health and limited by air pollution standards. Moreover, it acts as a support matrix to the condensation to other contaminants such as unburnt hydrocarbons. In order to reduce or erase its formation, a deeper investigation on the relationship between the fuel molecular structure, the mixture stoichiometry at the lift-off length, the residence time and ambient conditions is needed. A quantitative assessment of in-cylinder soot formation is desirable to help understanding the mechanisms behind the reduction of exhaust soot (PM) when using alternative fuels. Historically, soot radiation is known to play a significant role in the overall heat transfer to the engine walls, though its effect is only hardly quantified in the literature. Beyond the latter loss of efficiency, the literature points out its potential effect on the flame temperature reduction. Therefore, the absence of soot radiation is listed among the potential effects responsible for exhaust NO_x increase when using biodiesel although experimental limitations impede its detachment from the rest of effects. Therefore, a better understanding of the relationship between soot, flame temperature and NO_x inside the combustion chamber is required in order to contribute to the understanding of the "soot/NO_x trade-off" usually mentioned when describing the complexity for reducing both contaminants in Diesel exhaust.

In order to fulfill these objectives, an incremental methodology has been designed purposely. It is based on a succession of selected experiments which complexity increases until reaching the combinations of processes involved in Diesel combustion. This methodology as well as the boundary conditions of the study are both detailed in the following chapter.

Appendix

In a quite impressive mental exercise, Sir Harry Ricardo (1885-1974) invites his students into his conception of the combustion processes occurring in an engine: *"Before concluding, I am going to take a rather unconventional course, in a technical lecture, of asking you to accompany me, in imagination, inside the cylinder of a Diesel engine. Let us imagine ourselves seated comfortably on the top of the piston, at or about the end of the compression stroke. We are in complete darkness, the atmosphere is a trifle oppressive, for the shade temperature is well over 500C-almost a dull red heat-and the density of the air is such that the contents of an average sitting-room would weigh about a ton: also it is very draughty, in fact, the draught is such that in reality we should be blown off our perch and hurled about like autumn leaves in a gale. Suddenly, above our heads a valve is opened and a rainstorm of fuel begins to descend. I have called it a rainstorm, but the velocity of droplets approaches much more nearly that of rifle bullets than of raindrops. For a while nothing startling happens, the rain continues to fall, the darkness remains intense. Then suddenly, away to our right perhaps, a brilliant gleam of light appears moving swiftly and purposefully; in an instant this is followed by a myriad others all around us, some large and some small, until on all sides of us the space is filled with a merry blaze of moving lights; from time to time the smaller lights wink and go out, while the larger ones develop fiery tails like comets; occasionally these strike the walls, but being surrounded with an envelope of burning vapour they merely bounce off like drops of water spilt on a red-hot plate. Right overhead all is darkness still, the rainstorm continues, and the heat is and now we shall notice that a change is taking place. Many of the smaller lights around us have gone out, but new ones are beginning to appear, more overhead, and to form themselves into definite streams shooting rapidly downwards or outwards from the direction of the injector nozzles. Looking round again we see that the lights around are growing yellower; they no longer move in definite directions, but appear to be drifting listlessly hither and thither; here and there they are crowding together in dense nebulae, and these are burning now with a sickly smoky flame, half suffocated for want of oxygen. Now we are attracted by a dazzle overhead, and, looking up, we see that what at first was cold rain falling through utter darkness, has given place to a cascade of fire, as from a rocket. For a little while this continues, then ceases abruptly as the fuel valve closes. Above and all around us are still some lingering fireballs, now trailing long tails of sparks and smoke and wandering aimlessly in*

search of the last dregs of oxygen which will consume them finally and set their souls at rest. If so, well and good; if not, some unromantic engineer outside will merely grumble that the exhaust is dirty and will set the fuel valve to close a trifle earlier. So ends the scene, or rather my conception of the scene, and I will ask you to realize that what has taken me nearly five minutes to describe may all be enacted in one five-hundredth of a second or even less."

References

[1] Dec J.E., "A Conceptual Model of DI Diesel Combustion Based on Laser Sheet Imaging". *SAE Paper 970873*, 1997.

[2] Novella R., *Estudio De La Influencia De Los Ciclos Atkinson Y Miller Sobre El Proceso De Combustion Y Las Emisiones Contaminantes En Un Motor Diesel*. Tesis Doctoral, Universidad Politécnica de Valencia, Departamento de Máquinas y Motores Térmicos, 2009.

[3] Siebers D.L., Higgins B.S., "Flame lift-off on direct-injection diesel sprays under quiescent conditions". *SAE Paper 2001-01-0530*, 2001.

[4] García-Oliver J.M., *Aportaciones Al Estudio Del Proceso De Combustión Turbulenta De Chorros En Motores Diesel De Inyección Directa*. Tesis Doctoral, Universidad Politécnica de Valencia, Departamento de Máquinas y Motores Térmicos, 2004.

[5] García A., *Estudio De Los Efectos De La Post-Inyección Sobre El Proceso De Combustión Y La Formación De Hollín En Motores Diesel*. Tesis Doctoral, Universidad Politécnica de Valencia, Departamento de Máquinas y Motores Térmicos, 2009.

[6] Heywood J.B., *Internal Combustion Engine Fundamentals*. McGraw-Hill Publishing, 1988.

[7] Payri F., Desantes J.M., *Motores de combustión interna alternativos*, 1^{era} Ed., Editorial Reverté, 2011.

[8] Molina S.A., *Estudio De La Influencia De Los Parametros De Inyeccion Y La Recirculacion De Gases De Escape Sobre El Proceso De Combustion, Las Prestaciones Y Las Emisiones De Un Motor Diesel De 1.8 Litros De Cilindrada*. Tesis Doctoral, Universidad Politécnica de Valencia, Departamento de Máquinas y Motores Térmicos, 2003.

[9] Plee S.l., Ahmad T., "Relative Roles of Premixed and Diffusion Burning in Diesel Combustion". *SAE Paper 831733*, 1983.

[10] Glassman I., Yetter R., *Combustion*, 4^{th} Ed., Academic Press, 2008.

[11] Turns S.R., *An introduction to combustion*, 2^{nd} Ed., McGraw-Hill Publishing, 2000.

[12] Musculus M.P.B., Kattke K., "Entrainment Waves in Diesel Jets". *SAE Paper 2009-01-1355*, 2009.

[13] Musculus M.P.B., Lachaux T., Pickett L.M., Idicheria C., "End-of-Injection Over-Mixing and Unburned Hydrocarbon Emissions in Low-Temperature-Combustion Diesel Engines". *SAE Paper 2007-01-0907*, 2007.

[14] Gimeno J., *Desarrollo y Aplicación De La Medida Del Flujo De Cantidad De Movimiento De Un Chorro Diesel*. Tesis Doctoral, Universidad Politécnica de Valencia, Departamento de Máquinas y Motores Térmicos, 2008.

[15] Payri R., García J.M., Salvador F.J., Gimeno J., "Using spray momentum flux measurements to understand the influence of diesel nozzle geometry on spray characteristics". *Fuel*, Vol. 84, pp. 551-61, 2005.

[16] Hermens S., *Influence Of Diesel Injector Nozzle Geometry On The Injection And Combustion Process*. Tesis Doctoral, Universidad Politécnica de Valencia, Departamento de Máquinas y Motores Térmicos, 2008.

[17] Salvador F.J., *Estudio Teorico Experimental De La Influencia De La Geometria De Toberas De Inyección Diesel Sobre Las Carateristicas Del Flujo Interno Y Del Chorro*. Tesis Doctoral, Universidad Politécnica de Valencia, Departamento de Máquinas y Motores Térmicos, 2003.

[18] Payri F., Bermúdez V., Payri R., Salvador F.J., "The influence of cavitation on the internal flow and the spray characteristics in diesel injection nozzles". *Fuel*, Vol. 83, pp. 419-31, 2004.

[19] Correas D., *Estudio Teórico-Experimental Del Chorro Libre Diesel Isotermo*. Tesis Doctoral, Universidad Politécnica de Valencia, Departamento de Máquinas y Motores Térmicos, 1998.

[20] Arrègle J., *Análisis De La Estructura Y Dinámica Interna De Chorros Diesel*. Tesis Doctoral, Universidad Politécnica de Valencia, Departamento de Máquinas y Motores Térmicos, 1997.

[21] Ruiz S., *Estudio Teórico-Experimental De Los Procesos De Atomización Y De Mezcla En Los Chorros Diesel D.I.*. Tesis Doctoral, Universidad Politécnica de Valencia, Departamento de Máquinas y Motores Térmicos, 2003.

[22] López J.J., *Estudio teórico-experimental del chorro libre Diesel no evaporativo y de su interacción con el movimiento del aire*. Tesis Doctoral, Universidad Politécnica de Valencia, Departamento de Máquinas y Motores Térmicos, 2003.

[23] Sou A., Hosokawa S., Tomiyama A., "Effects of cavitation in a nozzle on liquid jet atomization". *International Journal of Heat and Mass Transfer*, Vol. 50, pp. 3575-82, 2007.

[24] Badock C., Wirth R., Fath A., Leipertz A., "Investigation of cavitation in real size diesel injection nozzles". *Int. J. of Heat and Fluid Flow*, Vol. 20, pp. 538-44, 1999.

[25] Chaves H., Knapp M., Kubitzek A., Obermeier F., Schneider T., "Experimental Study of Cavitation in the Nozzle Hole of Diesel Injectors Using Transparent Nozzles". *SAE Paper 950290*, 1995.

[26] Desantes J.M., Payri R., Salvador F.J., De la Morena J., "Influence of cavitation phenomenon on primary break-up and spray behaviour at stationary conditions". *Fuel*, Vol. 89, pp. 3033-41, 2010.

[27] Kegl B., Kegl M., Pehan S., "Optimization of an injection system for diesel and biodiesel usage". *Energy Fuels*, Vol. 22, pp. 1046-54, 2008.

[28] Szybist J.P., Boehman A.L., "Behavior of a diesel injection system with biodiesel fuel". *SAE Paper 2003-01-1039*, 2003.

[29] Boehman A.L., Morris D., Szybist J.P., Esen E., "The Impact of the Bulk Modulus of Diesel Fuels on Fuel Injection Timing". *Energy Fuels*, Vol. 18, pp. 1877-82, 2004.

[30] Bracho G., *Experimental And Theoretical Study Of The Direct Diesel Injection Process At Low Temperatures*. Tesis Doctoral, Universidad Politécnica de Valencia, Departamento de Máquinas y Motores Térmicos, 2011.

[31] Lapuerta M., Agudelo J.R., Prorok M., Boehman A.L., "Bulk Modulus of Compressibility of Diesel/Biodiesel/HVO Blends". *Energy Fuels*, Vol. 26, pp. 1336-43, 2012.

[32] Desantes J.M., Arrègle J., Pastor J.V., Delage A., "Influence of the Fuel Characteristics on the Injection Process in a D.I. Diesel Engine". *SAE Paper 980802*, 1998.

[33] Park S.H., Kim H.J., Suh H.K., Lee C.S., "A study on the fuel injection and atomization characteristics of soybean oil methyl ester (SME)". *Int. J. Heat Fluid*, Vol. 30, pp. 108-16, 2009.

[34] Boudy F., Seers P., "Impact of physical properties of biodiesel on the injection process in a common-rail direct injection system". *Energy Convers. Manage.*, Vol. 50, pp. 2905-12, 2009.

[35] Desantes J.M., Arrègle J., Ruiz S., "Characterisation Of The Injection-Combustion Process In A D.I. Diesel Engine Running With Rape Oil Methyl Ester". *SAE Paper 1999-01-1497*, 1999.

[36] Desantes J.M., Benajes J., Arrègle J., Delage A., *Effect of the properties of several fuels on the injection and combustion in HSDI Diesel engine*. Thermofluidynamic processes in Diesel engines, Valencia, Sept. 13-15, 2000.

[37] Soid S.N., Zainal Z.A., "Spray and combustion characterization for internal combustion engines using optical measuring techniques - A review". *Energy*, Vol. 36, pp. 724-41, 2011.

[38] Suh H.K., Roh G.H., Lee C.S., "Spray and combustion characteristics of biodiesel/diesel blended fuel in a direct injection common-rail diesel engine". *Trans. ASME J. Eng. Gas. Turbines Power*, Vol. 130, pp. 2807-15, 2008.

[39] Park S.H., Suh H.K., Lee C.S., "Effect of cavitating flow on the flow and fuel atomization characteristics of biodiesel and diesel fuels". *Energy Fuels*, Vol. 22, pp. 605-13, 2008.

[40] Suh H.K., Park S.H., Lee C.S., "Experimental investigation of nozzle cavitating flow characteristics for diesel and biodiesel fuels". *Int. J. Automot. Techn.*, Vol. 9, pp. 217-24, 2008.

[41] Reitz R.D., Bracco F.V., "Mechanism of atomization of a liquid jet". *Phys. Fluids*, Vol.25, pp. 1730-42, 1982.

[42] Reitz R.D., Bracco F.V., "Mechanisms of Breakup of Round Liquid Jets". *The Encyclopedia of Fluid Mechanics*, Vol. 3, Chapter 10, pp. 233-49, 1986.

[43] Ashgriz N., *Handbook of atomization and sprays: theory and applications*, Springer, 2011.

[44] Smallwood G.J., Gülder Ö.L., "Views on the Structure of Transient Diesel Sprays". *Atomization and Sprays*, Vol. 10, pp. 355-86, 2000.

[45] Hiroyasu H., Kadota T., "Fuel droplet size distribution in Diesel combustion chamber". *SAE Paper 740715*, 1974.

[46] Hiroyasu H., Arai M., Tabata M., "Empirical equations for the Sauter mean diameter of diesel spray". *SAE Paper 890464*, 1989.

[47] Hiroyasu H., Arai M., "Structures of Fuel Sprays in Diesel Engines". *SAE Paper 900475*, 1990.

[48] Arrègle J., Pastor J.V., Ruiz S., "The Influence of Injection Parameters on Diesel Spray Characteristics". *SAE Paper 1999-01-0200*, 1999.

[49] Levy N., Amara S., Campoussin J.-C., Guerrassi N., "Non-Reactive Diesel Spray Computations Supported by PDA Measurements". *SAE Paper 970049*, 1997.

[50] Soare V.T., *Phase Doppler Measurements In Diesel Dense Sprays: Optimization Of Measurements And Study Of The Orifice Geometry Influence Over The Spray At Microscopic Level*. Tesis Doctoral, Universidad Politécnica de Valencia, Departamento de Máquinas y Motores Térmicos, 2007.

[51] Wang X., Huang Z., Kuti O.A., Zhang W., Nishida K., "Experimental and analytical study of biodiesel and diesel spray characteristics under ultra-high injection pressure". *Int. J. Heat Fluid Fl.*, Vol. 31, pp.656-66, 2010.

[52] Choi S., Oh Y., "The spray characteristics of unrefined biodiesel". *Renewable Energy*, Vol. 42, pp. 136-39, 2012.

[53] Ejim C.E., Fleck B.A., Amarfazli A., "Analytical study for atomization of biodiesels and their blends in a typical injector: Surface tension and viscosity effects". *Fuel*, Vol. 86, pp. 1534-44, 2007.

[54] Lee C.S., Park S.W., Kwon S.I., "An Experimental Study on the Atomization and Combustion Characteristics of Biodiesel-Blended Fuels". *Energy Fuels*, Vol. 19, pp. 2201-08, 2005.

[55] Suh H.K., Park S.H., Lee C.S., "Atomization Characteristics of Dimethyl Ether Fuel as an Alternative Fuel Injected through a Common-Rail Injection System". *Energy Fuels*, Vol. 20, pp. 1471-1481, 2006.

[56] Park S.W., Kim S., Lee C.S., "Effect of Mixing Ratio of Biodiesel on Breakup Mechanisms of Monodispersed Droplets". *Energy Fuels*, Vol. 20, pp. 1709-15, 2006.

[57] Kim H.J., Suh H.K., Park S.H., Lee C.S., "An Experimental and Numerical Investigation of Atomization Characteristics of Biodiesel, Dimethyl Ether, and Biodiesel-Ethanol Blended Fuel". *Energy Fuels*, Vol. 22, pp. 2091-98, 2008.

[58] Park S.H., Suh H.K., Lee C.S., "Effect of Bioethanol-Biodiesel Blending Ratio on Fuel Spray Behavior and Atomization Characteristics". *Energy Fuels*, Vol. 23, pp. 4092-98, 2009.

[59] Kim H.J., Park S.H., Suh H.K., Lee C.S., "Atomization and Evaporation Characteristics of Biodiesel and Dimethyl Ether Compared to Diesel Fuel in a High-Pressure Injection System". *Energy Fuels*, Vol. 23, pp. 1734-42, 2009.

[60] Park S.H., Suh H.K., Lee C.S., "Nozzle flow and atomization characteristics of ethanol blended biodiesel fuel". *Renewable Energy*, Vol. 35, pp. 144-50, 2010.

[61] Payri F., Arrègle J., Fenollosa C., Belot G., Delage A., Schaberg P., Myburgh I., Botha J., "Characterisation Of The Injection-Combustion Process In A Common Rail D.I. Diesel Engine Running With Sasol Fischer-Tropsch Fuel". *SAE Paper 2000-01-1803*, 2000.

[62] Fisher B.T., Mueller C.J., "Liquid penetration length of heptamethylnonane and trimethylpentane under unsteady in-cylinder conditions". *Fuel*, Vol. 89, pp. 2673-96, 2010.

[63] Mueller C.J., Martin G.C., Briggs T.E., Duffy K.P., "An experimental investigation of in-cylinder processes under dual-injection conditions in a DI diesel engine". *SAE Paper 2004-01-1843*, 2004.

[64] Kashdan J.T., Mendez S., Bruneaux G., "On the origin of unburned hydrocarbon emissions in a wall-guided, low NOx diesel combustion system". *SAE Paper 2007-01-1836*, 2007.

[65] Opat R., Ra Y., Gonzalez M.A., Krieger R., Reitz R.D., Foster D.E., Durrett R.P., Siewert R.M., "Investigation of mixing and temperature effects on HC/CO emissions for highly dilute low temperature combustion in a light-duty diesel engine". *SAE Paper 2007-01-0193*, 2007.

[66] Martin G.C., Mueller C.J., Milam D.M., Radovanovic M.S., Gehrke C.R., "Early direct-injection, low-temperature combustion of diesel fuel in an optical engine utilizing a 15-hole, dual-row, narrow-included-angle nozzle". *SAE Paper 2008-01-2400*, 2008.

[67] Takeda Y., Keiichi N., Keiichi N., "Emission characteristics of premixed lean diesel combustion with extremely early staged fuel injection". *SAE Paper 961163*, 1996.

[68] Drake M.C., Fansler T.D., Solomon A.S., Szekely G.A., "Piston fuel films as a source of smoke and hydrocarbon emissions from a wall-controlled spark-ignited direct-injection engine". *SAE Paper 2003-01-0547*, 2003.

[69] Hardy W.L., Reitz R.D., "A study of the effect of high EGR, high equivalence ratio, and mixing time on emissions levels in a heavy-duty diesel engine for PCCI combustion". *SAE Paper 2006-01-0026*, 2006.

[70] Fang T., Coverdill R.E., Lee C.F., White R.A., "Smokeless combustion within a small-bore HSDI diesel engine using a narrow angle injector". *SAE Paper 2007-01-0203*, 2007.

[71] Browne K.R., Partridge I.M., Greeves G., "Fuel property effects on fuel/air mixing in an experimental Diesel engine". *SAE Paper 860223*, 1986.

[72] Kamimoto T., Yokota H., Kobayashi H., "Effect of high pressure injection on soot formation processes in a rapid compression machine to simulate Diesel flames". *SAE Paper 871610*, 1987.

[73] Hodges J.T., Baritaud T.A., Heinze T.A., "Planar liquid and gas fuel and droplet size visualization in a DI Diesel engine". *SAE Paper 910726*, 1991.

[74] Bower G.R., Foster D.E., "The effect of split injection on fuel distribution in an engine-fed combustion chamber". *SAE Paper 930864*, 1993.

[75] Espey C., Dec J.E., "The effect of TDC temperature and density on the liquid-phase fuel penetration in a DI Diesel engine". *SAE Paper 952456*, 1995.

[76] Siebers D., "Liquid-phase fuel penetration in Diesel sprays". *SAE Paper 980809*, 1998.

[77] Siebers D., "Scaling Liquid-Phase Fuel Penetration in Diesel Sprays Based on Mixing-Limited Vaporization". *SAE Paper 1999-01-0528*, 1999.

[78] Juliá J.E., *Medida De Concentraciones De Combustible En Chorros Diesel Mediante Tecnicas De Fluorescencia Inducida Por Laser*. Tesis Doctoral, Universidad Politécnica de Valencia, Departamento de Máquinas y Motores Térmicos, 2003.

[79] Martínez S., *Desarrollo de una instalación experimental para el estudio de chorros diesel evaporativos en atmósfera inerte y reactiva*. Tesis Doctoral, Universidad Politécnica de Valencia, Departamento de Máquinas y Motores Térmicos, 2003.

[80] Higgins B.S., Mueller C.J., Siebers D., "Measurements of fuel effects on liquid-phase penetration in DI sprays". *SAE Paper 1999-01-0519*, 1999.

[81] Verhoeven D., Vanhemelryck J.L., Baritaud T., "Macroscopic and ignition characteristics of high-pressures sprays of single-component fuels". *SAE Paper 981069*, 1998.

[82] Canaan R.E., Dec J.E., Green R.M., Daly D.T., "The influence of fuel volatility on the liquid-phase fuel penetration in a heavy-duty D.I. diesel engine". *SAE Paper 980510*, 1998.

[83] Thring M.W., Newby M.P., *Combustion length of enclosed turbulent jet flames*. 4^{th} Symposium International on Combustion, pp. 789-96, 1952.

[84] Yeh C., Kamimoto T., Kobori S., Kosaka H., "2-D imaging of fuel vapor concentration in a Diesel spray via Exciplex-based fluorescence technique". *SAE Paper 932652*, 1993.

[85] Pastor J.V., López J.J., García J.M., Pastor J.M., "A 1D model for the description of mixing-controlled inert diesel sprays". *Fuel*, Vol. 87, pp. 2871-85, 2008.

[86] Musculus M.P.B., "Entrainment waves in decelerating transient turbulent jets". *J. Fluid Mech.*, Vol. 638, pp. 117-40, 2009.

[87] Iyer V.A., Post S.L., Abraham J., "Is the liquid penetration in diesel sprays mixing controlled?". *Proc. Combust. Inst.*, Vol. 28, pp. 1111-18, 2000.

[88] Pitz W.J., Mueller C.J., "Recent progress in the development of diesel surrogate fuels". *Prog. Energ. Combust.*, Vol. 37, pp 330-50, 2011.

[89] Wakuri Y., Fujii M., Amitani T., Tsuneya R., "Studies on the penetration of fuel spray in a diesel engine". *Bulletin of Japan Society of Mechanical Engineers*, Vol. 3, pp. 123-30, 1960.

[90] Desantes J.M., Payri R., Salvador F.J., Gil A., "Development and validation of a theoretical model for diesel spray penetration". *Fuel*, Vol. 85, pp. 910-17, 2006.

[91] Naber J.D., Siebers D.L., "Effects of Gas Density and Vaporization on Penetration and Dispersion of Diesel Sprays". *SAE Paper 960034*, 1996.

[92] Allocca L., Mancaruso E., Montanaro A., Vaglieco B.M., Vassallo A., "Renewable biodiesel/reference diesel fuel mixtures distribution in non-evaporating and evaporating conditions for diesel engines". *SAE Paper 2009-24-0054*, 2009.

[93] No S.-Y., "How vegetable oils and their derivatives affect spray characteristics in CI engines - A review". *Atomization Sprays*, Vol. 21, pp. 87-105, 2011.

[94] Faria M.D.C., Valle M.L.M., Pinto R.R.C., "The influence of physic-chemical properties of diesel/biodiesel mixtures on atomization quality in diesel direct injection engines". *SAE Paper 2005-01-4154*, 2005.

[95] Reitz R.D, Bracco F.V., "On the Dependence of the Spray Angle and Other Spray Parameters on Nozzle Design and Operating Conditions". *SAE Paper 790494*, 1979.

[96] Varde K., Popa D., "Diesel Fuel Spray Penetration at High Injection Pressures". *SAE Paper 830448*, 1983.

[97] Payri F., Desantes J.M., Arrègle J., "Characterization of D.I. Diesel Sprays in High Density Conditions". *SAE Paper 960774*, 1996.

[98] Hurn R.K., Hughes K.J., "Combustion Characteristics of Diesel Fuels as Measured in a Constant Volume Bomb". *SAE Paper 520210*, 1952.

[99] Dec J.E., Espey C., "Ignition and Early Soot Formation in for D.I. Diesel Engine Using Multiple 2-D Imaging Diagnostics". *SAE Paper 950456*, 1995.

[100] Dec J.E., Espey C., "Chemiluminescence Imaging of Autoignition in for DI Diesel Engine". *SAE Paper 982685*, 1998.

[101] Higgins B., Siebers D., Aradi A., "Diesel-Spray Ignition and PremixedBurn Behaviour". *SAE Paper 2000-01-0940*, 2000.

[102] Kosaka H., Drewes V.H., Catalfamo L., Aradi A.A., Iida N., Kamimoto T., "Two-Dimensional Imaging of Formaldehyde Formed During the Ignition Process of Diesel Fuel Spray". *SAE Paper 2000-01-0236*, 2000.

[103] Gaydon A.G., "The Spectroscopy of Flames". *Chapman and Hall Ltd.*, 1974.

[104] Dec J.E., Coy E.B., "Radical OH Imaging in for DI Diesel Engine and the Structure of the Early Diffusion Flame". *SAE Paper 960831*, 1996.

[105] Poinsot T., Veynante D., *Theoretical and Numerical Combustion*, 3^{rd} Ed., R.T. Edwards, 2012.

[106] Flynn P.F., Durret R.P., Hunter G.L., zur Loye A.O., Akinyemi O.C., Dec J.E., Westbrook C.K., "Diesel Combustion: An Integrated View Combining Laser Diagnostics, Chemical Kinetics and Empirical Validation". *SAE Paper 1999-01-0509*, 1999.

[107] Idicheria C., Pickett L., "Formaldehyde Visualization Near Lift-off Location in a Diesel Jet". *SAE Paper 2006-01-3434*, 2006.

[108] Idicheria C.A., Pickett L.M., "Ignition, soot formation, and end-of-combustion transients in diesel combustion under high-EGR conditions". *Int. J. Engine Res.*, Vol. 12, pp. 376-92, 2011.

[109] Kosaka H., Aizawa T., Kamimoto T., "Two-dimensional imaging of ignition and soot formation processes in a diesel flame". *Int. J. Engine Res.*, Vol. 6, pp. 21-42, 2005.

[110] Szybist J.P., Boehman A.L., Haworth D.C., Koga H., "Premixed ignition behavior of alternative diesel fuel-relevant compounds in a motored engine experiment". *Combust. Flame*, Vol. 149, 112-28, 2007.

[111] Curran H.J., Gaffuri P., Pitz W.J., Westbrook C.K., "A Comprehensive Modeling Study of n-Heptane Oxidation". *Combust. Flame*, Vol. 114, pp. 149-77, 1998.

[112] Pickett L.M., Kook S., Williams T., "Visualization of Diesel Spray Penetration, Cool-Flame, Ignition, High-Temperature Combustion, and Soot Formation Using High-Speed Imaging". *SAE Paper 2009-01-0658*, 2009.

[113] Lyn W.T., *Study of Burning Rate and Nature of Combustion in Diesel Engines*. 9^{th} Symposium (International) on Combustion, pp. 1069-82, 1963.

[114] Edwards C.F., Siebers D., Hoskin D.H., "A Study of the Autoignition Process of diesel Spray via High Speed Visualization". *SAE Paper 920108*, 1992.

[115] Solbrig C.E., Litzinger T.A., "The Effect of Intake Charge Temperature on Combustion and Emissions in an Optically Accessible DI Diesel Engine with and without Swirl". *SAE Paper 902060*, 1990.

[116] Novella R., García A., Pastor J.M., Domenech V., "The role of detailed chemical kinetics on CFD diesel spray ignition and combustion modelling". *Math. Comput. Model.*, Vol. 54, pp. 1706-19, 2011.

[117] Taylor J., McCormick R., Clark W., *Report on the relationship between molecular structure and compression ignition fuels, both conventional and HCCI*. Prepared for U.S. Department of Energy, *available online*, 2004.

[118] Suppes G.J., Rui Y., Rome A.C., Chen Z., "Cetane-Improver Analysis and Impact of Activation Energy on the Relative Performance of 2-Ethylhexyl Nitrate and Tetraethylene Glycol Dinitrate". *Ind. Eng. Chem. Res.*, Vol. 36, pp. 4397-404, 1997.

[119] Pastor J.V., Payri R., Gimeno J., Nerva J.-G., "Experimental Study on RME Blends: Liquid-Phase Fuel Penetration, Chemiluminescence, and Soot Luminosity in Diesel-Like Conditions". *Energy Fuels*, Vol. 23, pp. 5899-915, 2009.

[120] ASTM standard D-613-01, *Standard Test Method for Cetane Number of Diesel Fuel Oil*. West Conshohocken, PA: ASTM-International, 2001.

[121] ASTM standard D-6890-04, *Standard Test Method for Determination of Ignition Delay and Derived Cetane Number (DCN) of Diesel Fuel Oils by Combustion in a Constant Volume Chamber*. West Conshohocken, PA: ASTM-International, 2004.

[122] Siebers D., "Ignition Delay Characteristics of Alternative Diesel Fuels: Implications on Cetane Number". *SAE Paper 852102*, 1985.

[123] Ryan III T.W., "Correlation of Physical and Chemical lgnition Delay to Cetane Number". *SAE Paper 852103*, 1985.

[124] Bogin Jr. G.E, DeFilippo A., Chen J.Y., Chin G, Luecke J., Ratcliff M.A., Zigler B.T., Dean A.M., *Modeling the Fuel Spray and Combustion Process of the Ignition Quality Tester with KIVA-3V*. Fall Meeting of the Western States Section of the Combustion Institute, Irvine, Oct. 26-27, 2009.

[125] ASTM standard D-976-91, *Standard Test Methods for Calculated Cetane Index of Distillate Fuels*. West Conshohocken, PA: ASTM-International, 2000.

[126] ASTM standard D-4737-03, *Standard Test Method for Calculated Cetane Index by Four Variable Equation*. West Conshohocken, PA: ASTM-International, 2003.

[127] EN ISO standards 4264:2007, *Petroleum products - Calculation of cetane index of middle-distillate fuels by the four-variable equation*, Geneva, Switzerland: International Organization for Standardization, 2007.

[128] Lapuerta M., Rodríguez-Fernández J., Armas O., "Correlation for the estimation of the density of fatty acid esters fuels and its implications. A proposed biodiesel cetane index". *Chem. Phys. Lipids*, Vol. 163, pp. 720-27, 2010.

[129] Lapuerta M., Rodríguez-Fernández J., Font de Mora E., "Correlation for the estimation of the cetane number of biodiesel fuels and implications on the iodine number". *Energy Policy*, Vol. 37, pp. 4337-44, 2009.

[130] Bruneaux G., "Combustion structure of free and wall-impinging diesel jets by simultaneous laser-induced fluorescence of formaldehyde, poly-aromatic hydrocarbons, and hydroxides". *Int. J. Engine Res.*, Vol. 9, pp. 249-65, 2008.

[131] Sietzman J.M., Üngüt A., Paul P.H., Hanson R.K., *Imaging and Characterization of OH Structures in a Turbulent Nonpremixed Flame.* 23^{rd} Symposium (International) on Combustion, The Combustion Institute, pp. 637-44, 1990.

[132] Schefer R.W., Namazian M., Kelley J., *CH, OH and CH4 Concentration Measurements in a Lifted Turbulent-Jet Diffusion Flame.* 23^{rd} Symposium (International) on Combustion, The Combustion Institute, pp. 669-76, 1990.

[133] Barlow R.S., Dibble R.W., Chen J.-Y., Lucht R.P., "Effect of Damköler Number on Superequilibrium OH Concentration in Turbulent Nonpremixed Jet Flames". *Combust. Flame*, Vol. 82, pp. 235-51, 1990.

[134] Dec J.E., Kelly-Zion P.L., "The effects of injection timing and diluent addition on late-combustion soot burnout in a DI diesel engine based on simultaneous 2-D imaging of OH and soot". *SAE Paper 2000-01-0238*, 2000.

[135] Tree D.R., Svensson K.I., "Soot processes in compression ignition engines". *Prog. Energy Combust. Sci.*, Vol. 33, pp. 272-309, 2007.

[136] Arrègle J., Pastor J.V., López J.J., García A., "Insights on postinjection-associated soot emissions in direct injection diesel engines". *Combust. Flame*, Vol. 154, pp. 448-61, 2008.

[137] Faeth G.M., "Current Status of Droplet and Liquid Combustion". *Prog. Energy Combust. Sci.*, Vol. 3, pp. 191-224, 1977.

[138] Kuo K.K., *Principles of Combustion.* Wiley & Sons, pp. 589-94, 1986.

[139] Chiu W.S., Shahed S.M., Lyn, W.T., "A Transient Spray Mixing Model for Diesel Combustion". *SAE Paper 760128*, 1976.

[140] Venugopal R., Abraham J., "A Review of Fundamental Studies Relevant to Flame Lift-off in Diesel Jets". *SAE Paper 2007-01-0134*, 2007.

[141] Dec J.E., Canaan R.E., "PLIF Imaging of NO Formation in for DI Diesel Engine". *SAE Paper 980147*, 1998.

[142] Pickett L.M., Siebers D.L., "Soot formation in diesel fuel jets near the lift-off length". *Int. J. Engine Res.*, Vol. 7, pp. 103-30, 2006.

[143] Haynes B.S., Wagner H.G., "Soot formation". *Prog. Energy Combust. Sci.*, Vol. 7, pp. 229-73, 1981.

[144] Bartok W., Sarofim A.F., *Fossil fuel combustion: a source book.* Wiley, 1991.

[145] Pickett L.M., Caton J.A., Musculus M.P.B., Lutz A.E., "Evaluation of the equivalence ratio-temperature region of diesel soot precursor formation using a two-stage Lagrangian model". *Int. J. Engine Res.*, Vol. 7, pp. 349-70, 2006.

[146] Broadwell J.E., Lutz A.E., "A turbulent jet chemical reaction model: NOx production in jet flames". *Combust. Flame*, Vol. 114, pp. 319-35, 1998.

[147] Siebers D.L., Higgins B.S., Pickett L.M., "Flame Lift-Off on Direct-Injection Diesel Fuel Jets: Oxygen Concentration Effects". *SAE Paper 2002-01-0890*, 2002.

[148] Siebers D.L., Pickett L.M., "Injection Pressure and Orifice Diameter effects on soot in DI diesel fuel jets". *Thermo and fluid-dynamic processes in Diesel engines 2*, Springer-Velag, pp. 253-77, 2004.

[149] Musculus M.P., Dec J.E., Tree D.R., "Effects of fuel parameters and diffusion flame lift-off on soot formation in a heavy duty DI Diesel engine". *SAE Paper 2002-01-0889*, 2002.

[150] Pickett L.M., Siebers D.L., "An investigation of diesel soot formation processes using micro-orifices". *Proc. Combust. Inst.*, Vol. 29, pp. 655-62, 2002.

[151] Pickett L.M., Siebers D.L., "Non-Sooting, Low Flame Temperature Mixing-Controlled DI Diesel Combustion". *SAE Paper 2004-01-1399*, 2004.

[152] Pickett L.M., Siebers D.L., "Soot in diesel fuel jets: effects of ambient temperature, ambient density, and injection pressure". *Combust. Flame*, Vol. 138, pp. 114-35, 2004.

[153] Idicheria C.A., Pickett L.M., "Soot Formation in Diesel Combustion under High-EGR Conditions". *SAE Paper 2005-01-3834*, 2005.

[154] Pickett L.M., Idicheria C.A., *Effects of ambient temperature and density on soot formation under high-EGR conditions*. Thermofluidynamic processes in Diesel engines, Valencia, Sept. 13-15, 2006.

[155] Benajes J., Molina S., De Rudder K., Amorim R.J., "Optimization Towards Low-temperature Combustion in a HSDI Diesel Engine, Using Consecutive Screenings". *SAE Paper 2007-01-0911*, 2007.

[156] Svensson K.I., Richards M.J., Mackrory A.J., Tree, D.R., "Fuel Composition and Molecular Structure Effects on Soot Formation in Direct-Injection Flames Under Diesel Engine Conditions". *SAE Paper 2005-01-0381*, 2005.

[157] Musculus M., "Measurements of the Influence of Soot Radiation on In-Cylinder Temperatures and Exhaust NOx in a Heavy-Duty DI Diesel Engine". *SAE Paper 2005-01-0925*, 2005.

[158] Struwe F.J., Foster D.E., "In Cylinder Measurement of Particulate Radiant Heat Transfer in a Direct Injection Diesel Engine". *SAE Paper 2003-01-0072*, 2003.

[159] Flynn P.F., Mizusawa M., Uyehara O.A., Myers P.S., "An Experimental Determination of the Instantaneous Potential Radiant Heat Transfer Within an Operating Diesel Engine". *SAE Paper 720022*, 1972.

[160] Lapuerta M., Armas O., Rodríguez-Fernández J., "Effect of biodiesel fuels on diesel engine emissions". *Prog. Energy Combust Sci.*, Vol. 34, pp. 198-223, 2008.

[161] Gill S.S., Tsolakis A., Dearn K.D., Rodríguez-Fernández J., "Combustion characteristics and emissions of Fischer-Tropsch diesel fuels in IC engines". *Prog. Energy Combust Sci.*, Vol. 37, pp. 503-23, 2011.

[162] Aleixandre R., Valderrama J.C., Desantes J.M., Torregrosa A.J., "Identification of information sources and citation patterns in the field of reciprocating internal combustion engines". *Scientometrics*. Vol. 59, pp 321-36, 2004.

[163] Aizawa T., Kosaka H., "Investigation of early soot formation process in a diesel spray flame via excitation-emission matrix using a multi-wavelength laser source". *Int. J. of Engine Res.*, Vol. 9, pp. 79-97, 2008.

[164] Fang T., Lin Y.-C., Foong T.M., Lee C.-F., "Biodiesel combustion in an optical HSDI diesel engine under low load premixed combustion conditions". *Fuel*, Vol. 88, pp. 2154-62, 2009.

[165] Mueller C.J., Boehman A.L., Martin G.C., "An experimental investigation of the origin of increased NOx emissions when fueling a heavy-duty compression-ignition engine with soy biodiesel". *SAE Paper 2009-01-1792*, 2009.

[166] Beatrice C., Bertoli C., Del Giacomo N., Guido C., Migliaccio M., "In-cylinder Soot Evolution Analysis in a Transparent Research DI Diesel Engine Fed by Oxygenated Fuels". *SAE Paper 2002-01-2851*, 2002.

[167] Cheng A.S., Upatnieks A., Mueller C.J., "Investigation of the impact of biodiesel fuelling on NOx emissions using an optical direct injection diesel engine". *Int. J. Engine Res.*, Vol.7, pp. 297-318, 2006.

[168] Cheng A.S., Upatnieks A., Mueller C.J., "Investigation of Fuel Effects on Dilute, Mixing-Controlled Combustion in an Optical Direct-Injection Diesel Engine". *Energy Fuels*, Vol. 21, pp. 1989-2002, 2007.

[169] Beatrice C., Capaldi P., Del Giacomo N., Guido C., Mancaruso E., Vaglieco B.M., "Analysis of Impact of Diesel Fuel/Biodiesel Blends on a Modern Diesel Combustion System Performance by Means of Injection Test Rig, Optical and Real SC Engine Experiments". *SAE Paper 2009-01-0484*, 2009.

[170] Klein-Douwel R.J.H., Donkerbroek A.J., Van Vliet A.P., Boot M.D., Somers L.M.T., Baert R.S.G., Dam N.J., Ter Meulen J.J., "Soot and chemiluminescence in diesel combustion of bio-derived, oxygenated and reference fuels". *Proc. Combust. Inst.*, Vol. 32, pp. 2817-25, 2009.

[171] Fang T., Lee C.F., "Bio-Diesel Effects on Combustion Processes in an HSDI Diesel using Advanced Injection Strategies". *Proc. Combust. Inst.*, Vol. 32, pp. 2785-92, 2009.

[172] Mueller C.J., Martin G.C., "Effects of oxygenated compounds on combustion and soot evolution in a DI diesel engine: Broadband natural luminosity imaging". *SAE Paper 2002-01-1631*, 2002.

[173] Armas O., Yehliu K., Boehman A.L., "Effect of alternative fuels on exhaust emissions during diesel engine operation with matched combustion phasing". *Fuel*, Vol. 89, pp. 438-56, 2010.

[174] Szybist J.P., Song J., Alam M., Boehman A.L., "Biodiesel combustion, emissions and emission control". *Fuel. Process. Technol.*, Vol. 88, pp. 679-91, 2007.

Chapter 3

Approach of the experimental study

Contents

3.1. Introduction

Numerous issues relative to the use of alternative fuels in a Diesel engine have been pointed out in the previous chapters. Often considered with a "black box" approach, the mechanisms affecting their combustion and leading to different results of exhaust emissions are still uncertain. Thus, a list of selected objectives has been released in order to understand with more detail how and how much fuel properties influence the combustion process at several key stages identified throughout a detailed review of the conventional Diesel combustion.

The attainment of these objectives of investigation requires the implementation of a proper methodology. This chapter defines and details such experimental methodology based on an incremental strategy. It aims at assessing the impact of fuel properties in order to isolate their effect as far as possible from the rest of engine parameters actuating on the combustion process. In this respect, three groups of experiments have been defined: (i) fuels under atmospheric conditions, (ii) fuels under Diesel inert conditions and (iii) fuels under Diesel reactive conditions. Results and conclusions of the first group of experiments are also presented herein, since fuel properties under atmospheric conditions are considered as boundary conditions of the two following groups of experiments. Then, the facility permitting to reproduce high temperature and high pressure Diesel-like conditions is described and the experimental techniques to be used are presented, but the results and the analysis of the two last groups of experiments will be the object of the two next chapters. This choice of outline is motivated by the complexity of such two groups of experiments, involving the set-up and the computational processing of optical diagnostics, as well as the complexity of the physical processes themselves.

3.2. Experimental methodology

3.2.1. Terminology

The starting point of our analysis sits on a trivial postulate enunciated as follows: *The result of the combustion reaction is a function of physical and chemical properties of both a fuel and an oxidant.*

This approach, although probably the most rigorous under a combustion point of view, may be a bit away from the variables concretely manipulated with an approach of the problem oriented to engine development and optimization. Indeed, the objective of this work is rather to separate the fuel

effects from the all the parameters inherent to the engine functioning, more than just a single oxidant. Therefore, in our approach of the study the physics of the oxidant (P_O) is extended and replaced by a term called "the physics of the engine" (P_E). In the rest of the document, the following terms will be used to refer to these different aspects:

- The **physics of the engine** (P_E) includes the thermodynamic conditions of the gas surrounding the fuel spray, the fuel injection pressure, and could include the nozzle-hole diameter as well, although this parameter has not been varied in this work. This term can actually be seen as an extension of the P_O term including for example the fuel velocity which could be considered in another approach as a parameter relevant from the fuel physics.

- The **physics relative to the fuel** (P_F) includes only its thermodynamic properties such as density, viscosity and volatility. They are mostly variables of the fuel measured at ambient pressure.

- The **fuel chemistry** (C_F) includes its equivalent formula and energy content or Low Heating Value (LHV). The fuel aromatic content and more generally a deeper analysis of the molecular organization could complete the fuel chemical term but this information was not available for our study.

- Finally, the **chemistry relative to the engine** would correspond to the oxidant composition. In this work, air has been used and maintained with a constant composition during combustion. Therefore, the term responding for the engine chemistry has been removed from our study. However, a study including a variation of the oxygen percentage to imitate the use of EGR should include this term.

As a result of all these arguments, the first sentence of this section could be rewritten as: *The result of the combustion reaction is a function of the physics of the fuel interacting with the physics of the engine, and the chemical properties of fuel and oxidant.*

It is always a delicate exercise to make a classification between physical and chemical processes and their origin. The frontiers here established may be permeable and subject to discussion. This is why an effort has been made in defining them carefully. The reader should note that this classification is mostly about definition and terminology, and that such approach will not radically modify the results and their interpretation.

3.2.2. Approach of the experimental study

Now that nomenclature is defined, the objectives require establishing an experimental methodology able to isolate as far as possible the physical and chemical properties of the fuel (P_F+C_F) from those induced by the engine operating conditions (P_E). In this respect, the study has been divided into three major stages with a gradual increase of the complexity and of the number of variables involved. When moving to a more complex experiment, the conclusions established in the previous one are accounted in order to detach the effect of the new variables added. These three stages are described in Figure 3.1 and can be detailed as follows:

- *Stage 1:* The objective of this group of experiments is to characterize the fundamental differences in physical and chemical properties among the fuels tested. To complete this task, a set of ASTM measurements has been selected to measure the fuel density, viscosity, distillation curves, equivalent formula and lower heating value. The choice of ASTM standards was motivated by the wide extension of their use in both engine research and industry.

- *Stage 2:* This stage is a step forward towards more realistic Diesel engine conditions, though combustion is avoided in order to focus on physical processes exclusively. First, a hydraulic injector characterization, *via* measurement of the mass flow rate and momentum flux at the nozzle exit, accounts for fuel effects on the injector performance. Next, the fuel is injected in a large-volume facility fed with pure nitrogen creating the high-temperature and high-pressure conditions of a Diesel engine. Thus, the spray is placed in a free field under evaporative but non-reacting conditions. This latter environment enables the analysis of the physical processes related to spray atomization, evaporation and mixture fraction field establishment without any interaction of combustion chemical reactions.

- *Stage 3:* This last group of experiments repeats the previous evaporative Diesel-like environment while replacing nitrogen by air in order to enable combustion reactions. This stage aims at studying the free reacting spray including the processes of ignition, diffusion flame establishment and soot formation while conserving the purely physical processes of the previous stage.

In the image of Russian dolls nesting into each other, such incremental methodology should first permit an assessment of fuel physical properties with

respect to physical parameters relative to the engine operating conditions. Thereafter, in the last group of experiments where all the effects are intertwined, the knowledge acquired during the first two stages should enable an assessment of the fuel chemical properties with respect to the rest of physical processes.

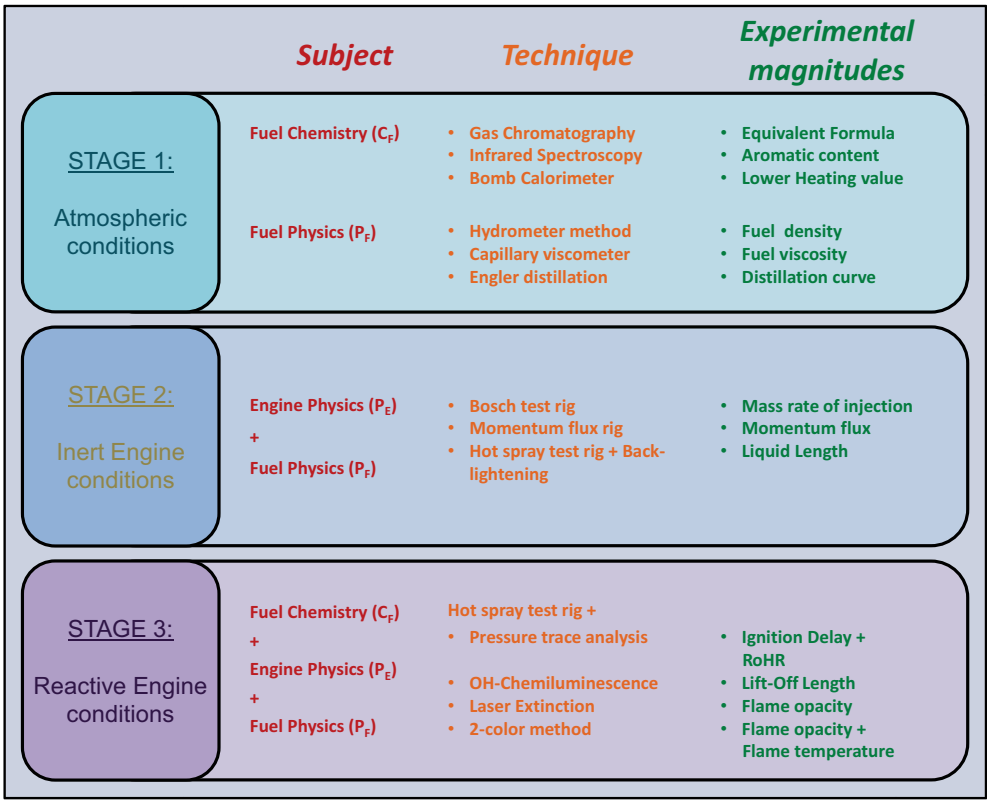

Figure 3.1. *Schematics of the experimental methodology.*

3.3. Fuels

3.3.1. Fuels origin and definition

Five fuels have been selected for the purpose of the study. The first three fuels are partially or entirely derived from a first-generation biodiesel issued from the transesterification of rapeseed oil with methanol. The resulting rapeseed methyl-ester was conserved and used as a pure cut (RME), but

also employed in the formulation of two blends with fossil diesel. Such fuels labeled B05 and B30 contains respectively 5 and 30 percent in mass of RME. It should be reminded that B05 matches the conventional diesel currently supplied in European gas stations. The last two fuels are produced through the Fischer-Tropsch process. Unfortunately, their feedstock origin, either gas, coal or biomass, is unknown. Thus, it cannot technically be affirmed that they stand for "second-generation biofuels". But as suggested earlier, the versatility of the manufacturing process suggests that we could reasonably obtain similar fuels by means of organic waste. They will be referred to as FT1 and FT2 in the study.

3.3.2. Fuels physical properties (P_F)

In order to characterize fuel physical properties, several measurements have been performed off-engine at atmospheric pressure. In agreement with their corresponding ASTM standards, fuel density and kinematic viscosity were measured respectively at 15 and 40°C. The results are summarized in Table 3.1.

Table 3.1. *Fuel physical properties.*

Fuels Properties	*Unit*	*Standard*	**B05**	**B30**	**RME**	**FT1**	**FT2**
Density at 288 K	$[kg.m^{-3}]$	ASTM D1298	833	849	878	784	773
Kinematic Viscosity at 313 K	$[mm^2.s^{-1}]$	ASTM D445	2.5	3.1	4.4	3.4	1.3

At first glance, the three RME-derived fuels have a higher density than the Fischer-Tropsch's. Both their density and viscosity increase proportionally when increasing the RME rate. Under these considerations, the fossil diesel used for the blending (B00) would have a density of 832.6 $kg.m^{-3}$ and a viscosity of approximately 2.45 $mm^2.s^{-1}$, given that in the range of small biodiesel concentrations, viscosity no longer behaves linearly. FT2 is singular by its very low viscosity. Comparative trends in fluid-mechanical properties were also observed in [1] for a similar selection of fuels.

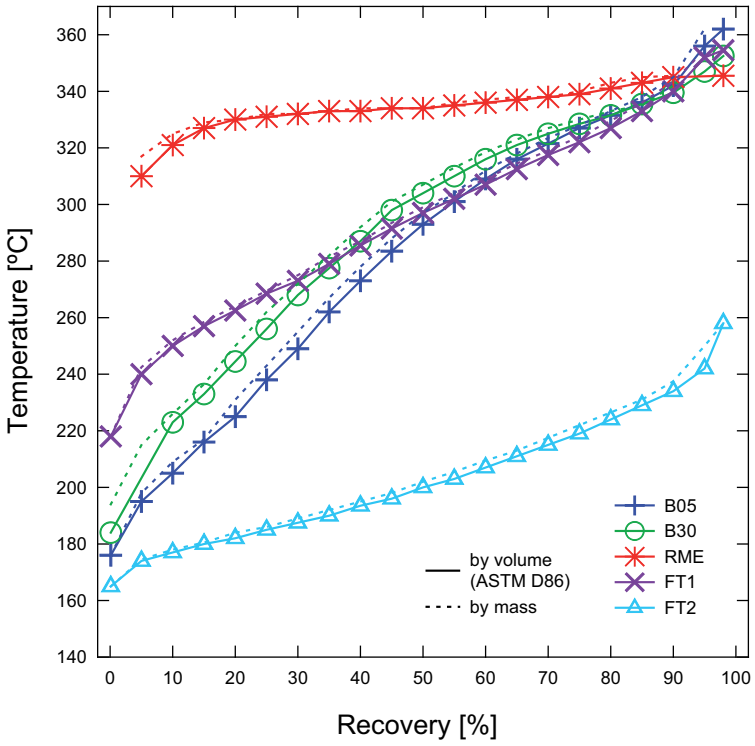

Figure 3.2. *Distillation curves of the five fuels obtained via both ASTM D86 and mass recovery.*

With the objective to characterize fuel volatility, distillation curves have been obtained at atmospheric pressure as specified by the ASTM D86 standard. The curves of Figure 3.2 chart the percentage of the total mixture that has evaporated as the temperature of the fuel was slowly heated. Prior to further description, it may be noted that a vacuumed distillation (ASTM D1160) would rather have been recommended for RME as mentioned by the list of standards to be used with biodiesel (ASTM D6751) [2]. The cracking of fuel molecules due to the higher temperature range expected with biodiesel is usually advanced as the main argument for that choice. By breaking up and converting the largest fuel molecules into lower boiling hydrocarbons, the cracking process can possibly distort the results and lead to an underestimation of the measurements. In his study, Kinast [3] however reports a difference of only 10-20$°C$ between both standards throughout almost the entire range of distillation, for six biodiesels issued

from different feedstocks. In agreement with ASTM D6751, differences become more significant for the final boiling point (FBP), and place the maximum reliable temperature enabled by the ASTM D86 at $350°C$. Thus, given the small temperature offset between ASTM D86 and ASTM D1160 in this report, and the fact that RME measurements remained under $350°C$, the accuracy improvement brought by an ASTM D1160 measurement in our study is believed to be small. In addition, Lapuerta *et al.* [4] recently established the uncertainty associated with the correction to obtain the atmospheric-equivalent-temperature in the ASTM D1160, given that the latter was originally developed for petroleum-derived hydrocarbons but not for oxygenated fuels. Finally, Sadeghbeigi [5] specifies that fuel cracking manifests by a drop in the temperature of the distilled vapor and the presence of brown smoke. None of these effects could actually be observed before reaching the final boiling point (FBP). Based on all these considerations, D86 can be considered for the characterization of RME volatility on 95 % of the distillation range. In addition to the conventional D86 volume measurement, a weighing scale was measuring the collected mass simultaneously, in order to detect a possible shift between mass and volume recovery percentage. Results are also presented in Figure 3.2 by means of dash lines.

Regarding the results, RME and FT2 in a lesser extent, appear to have relatively flat distillation curves. These flat curves are the witness of their molecular homogeneity. For their part, B05, B30 and FT1 observe similar trends, commencing their distillation with temperature values close to those of FT2 and culminating with values close to those of RME. Thus, it can be expected that the lightest fractions of B05, B30 and FT1 are molecules only slightly heavier than FT2 while their heaviest fractions are close to RME in terms of molecular weight. Of course, for both B05 and B30, these heavy fractions are expected to correspond to their RME fraction. No significant differences can be observed on the comparison between mass and volume percentage recovery which supports that no important variations of density exist among the inner components of each fuel.

While the fuel was getting to the temperature of its first boiling point, an important volume expansion has been observed, measured and converted into density as a function of temperature, considering mass conservation. Results plotted in Figure 3.3 show linear trends with high R-squared. Coefficients of linear regressions of the type: $\rho_f = B + A \cdot T_f$ have been summarized in Table 3.2. Hydrometer measurements of fuel density at $15°C$ (ASTM D1298) from Table 3.1 have been added to the plot for illustration, but they have not been used in the linear regressions in order to keep data consistency. A small offset can be observed between the ASTM measurements ($\rho_{ASTM\ D1298}$) and

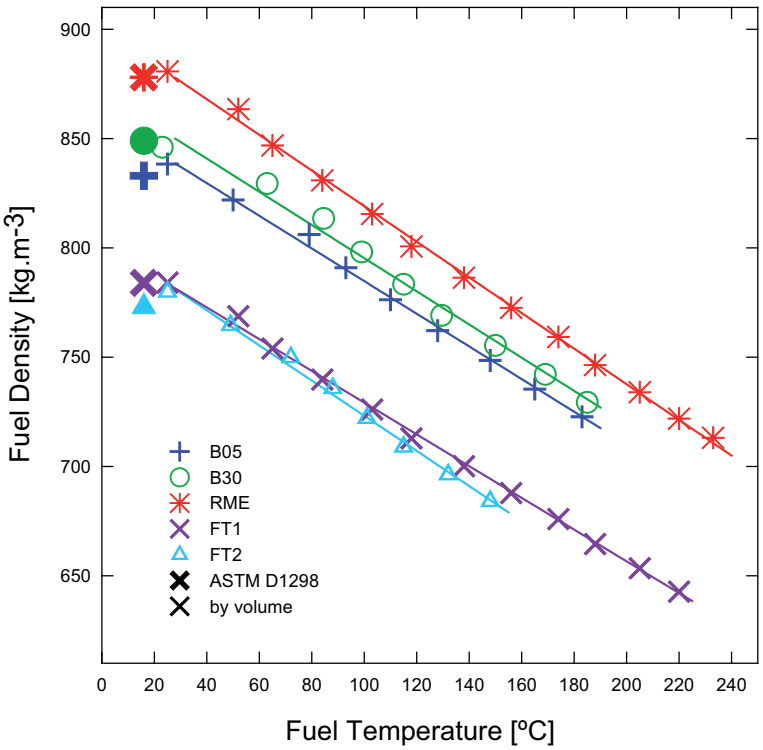

Figure 3.3. *Temperature effect on fuel density under atmospheric pressure. The bold symbols correspond to measurements made at 15°C following the ASTM D1298.*

what would be the corresponding measurement with our "volume method" at 288 K. Naturally, these volume measurements are not as accurate as the ASTM D1298 but the trend itself is probably reliable enough to be used in the equation: $\rho_f = \rho_{ASTM\ D1298} + A \cdot (T_f - 288)$. For reference, Siebers [6] used a similar regression in his scaling-law although the slope for the US diesel ♯2 (D2) was slightly more significant than any of the fuels employed in this study (A_{D2}= -0.9). This characterization of the fuel as a function of temperature is interesting for spray modeling since one issue often reported is the uncertainty related to thermodynamic conditions of the fuel at the nozzle exit. In a real engine, the injector seats in a cylinder-head water-cooled at around 80°C while its nozzle tip faces combustion several tens of times each second. Thus, with almost 1 $kg.m^{-3}$ lost for each degree increase in temperature, fuel density is potentially far from that at STP. Although it would have been interesting to account for these effects, especially in the context of mass rate of injection

approached later in this study, several other effects should have been accounted in parallel. For example, fuel compressibility has a significant counteracting effect at the pressure levels operated. Also, fuel heating may be different depending on the pressure level. In view of all these uncertainties but above all because of the impossibility to measure the fuel temperature inside the nozzle, these results unfortunately could not be totally exploited in this work but they at least have the merit of calling the attention and further research could be performed in that direction.

Table 3.2. *Linear regression coefficients for fuel density dependency to temperature ($\rho_f = B + A \cdot T_f$).*

Coefficients	**B05**	**B30**	**RME**	**FT1**	**FT2**
A	-0.747	-0.759	-0.815	-0.726	-0.804
B	859.5	871.2	900.6	801.8	803.6
R^2	99.8 %	99.4 %	99.8 %	99.8 %	99.4 %

3.3.3. Fuel chemical properties (C_F)

To characterize the chemical properties of the fuel reported in Table 3.3, several parameters of interest have either been collected from the fuel technical sheets or measured in-house. Chemical equivalent formulae of RME, FT1 and FT2 have been measured by means of gas chromatography-FID while those of B05 and B30 were estimated for the purpose of the study by simulating a mixture between RME and heptadecane, commonly used as a surrogate for diesel. It is to note the proximity of Fischer-Tropsch formulae respectively with heptadecane ($C_{17}H_{36}$) and dodecane ($C_{12}H_{26}$) while that of RME is similar to methyl-oleate ($C_{17}H_{36}O_2$). As RME and FT2 previously appeared to be particularly homogeneous in their molecular composition (flat distillation), these similitudes hint that their corresponding alkanes could be good surrogates, although physico-chemical properties such as density, viscosity and saturation level should be further considered.

Measurements of the higher heating values (HHV) have been carried on in a bomb calorimeter following the ASTM D240 standard. The lower heating value (LHV) was obtained, as is common practice, by subtracting the heat of vaporization of the water vapor formed within the calorimeter during combustion. Two methods were used to estimate the mass of water

vapor. Method 1 was rather experimental and although it is not ruled by any standard. It consisted in collecting the water condensed on the walls of the combustion bomb with a tissue and weighting the tissue mass increase. For the three fuels whose equivalent formula had been measured precisely, method 2 consisted in estimating the mass of water formed considering complete combustion. The product of the mass of water by its latent heat of vaporization gave the component of HHV corresponding to water condensation (isothermal process). In view of the result, the two methods show good consistency. As regards comparisons among fuels, both Fischer-Tropsch diesels have a higher energy content while that of RME-derived fuels decreases as the RME rate increases. Energy content of RME is minor because of its oxygen content. Thus for this fuel selection, a density increase is systematically balanced by a lower heating value, making the energy content per liter quite similar among the five fuels. Under a marketing point of view, this data is important since the economical relation maintained with car users generally uses volume units in terms of sales and consumption.

Table 3.3. *Fuel chemical properties (C_F). Data in italic are based on assumptions or derived from regressions.*

Fuels Properties	*Unit*	*Standard ASTM*	**B05**	**B30**	**RME**	**FT1**	**FT2**
Equivalent Chemical Formula	-	D5291	$C_{17.1}H_{36.0}O_{0.1}$	$C_{17.7}H_{35.7}O_{0.7}$	$C_{18.95}H_{35.2}O_2$	$C_{17.0}H_{35.5}$	$C_{12.0}H_{25.0}O_{0.2}$
Aromatics (total)	-	D6591	25.30 %	18 %	*0 %*	-	-
Polyaromatics	-	D6591	4 %	2 to 6 %	*0 %*	-	-
Sulfur	$[mg.kg^{-1}]$	D4294	7	5	*0 %*	<10	<10
Higher Heating Value	$[MJ.kg^{-1}]$	D240	44.27	43.77	40.16	47.2	46.58
Lower Heating Value (Meth. 1/ Meth. 2)	$[MJ.kg^{-1}]$	-	42.11 / -	41.77 / -	38.24 / 37.74	44.76 / 44.20	44.24 / 43.63
Energy content per liter	$[MJ.l^{-1}]$	-	35.08	35.46	33.57	35.09	34.2
A/F_{st} (20.9 % XO_2)	-	-	*14.64*	*13.84*	12.398	14.748	14.388

The review presented in the previous chapter also revealed the importance of the fuel content in aromatics, cyclic compounds and more generally any kind of unsaturated molecules, on combustion processes such as ignition and soot formation. Fuel data sheets provided the aromatic content of B05 and B30. A linear extrapolation to derive that of RME verifies that the latter does not contain any aromatics, in agreement with the literature. In

regard to Fischer-Tropsch fuels, they are equally often referred to as free of aromatics. In fact, their equivalent formula confirms that they tend towards the saturation of an alkane (C_nH_{2n+2}), which even further suggests that they limit any other kind of unsaturation as well. By contrast, biodiesel, although free of aromatics, usually breaks down in numerous unsaturated fatty acid methyl-esters (FAME). In his Ph.D dissertation, Rodriguez-Fernandez [7] reports the composition in methyl-esters of four biodiesels mainly obtained after transformation from cooking wastes of sunflower, olive and palm oils. Methyl-oleate ($C18{:}1$) and methyl-linoleate ($C18{:}2$), respectively with 1 and 2 double-bonds, accounted for over 80 % of the fuel content. This statement is also confirmed by Thomas [8] who reviewed the methyl-ester breakdown of several biodiesels issued from multiple feedstocks. Though coconut or palm-derived biodiesels were mostly composed of saturated methyl-esters, the most common ones issued from rape, soy, sunflower or animal wastes had a similar total of methyl-oleate and methyl-linoleate. Thus, with the aim of estimating and comparing the level of unsaturation of the five fuels, quite independently from the unsaturation origin (aromatics, alkene chains, etc.), a Fourier Transform Infrared Spectroscopy analysis has been completed. Such method based on the absorption of radicals of interest is rather used for bituminous emulsions (ASTM D6805), lubrication oils, and even gasoline-type fuels (ASTM D5986 & D6277), but do not respond to any standard for diesel-type fuels. Unfortunately, such method is not quantitative, but can provide a valuable comparison among fuels or attest for the complete saturation of a fuel if none of these radicals is detected [9]. Figure 3.4 shows the resulting spectra with a focus made on four regions of the spectra. The first three regions are sensitive to the absorption of aromatic rings while the last one is for $C = C$ bonds (alkene chains). Care has been taken to also account for other radicals potentially sensitive in the same range. As such, the high absorption of RME in plots 2 and 3 is rather justified by its high content in $C - O$ and $O - H$ bonds issued from the acid group ($C - O - H$) than by its aromatic content. Several conclusions can be extracted from the observation of the spectra:

(I) In view of plots 2 and 3, FT1 and FT2 absence of aromatics is confirmed. Although inferior to RME-derived fuels, Fischer-Tropsch's small degree of unsaturation is detected in both plots 1 and 4. Therefore, these observations suggest that such unsaturation is due to $= CH_2$ and $C = C$ bonds issued from cyclic or polycyclic molecules. This result is consistent with their equivalent formula of Table 3.3.

(II) The content in aromatics of B05 and B30 is successfully detected in plots 1 and 2 while plot 2 confirms that RME does not contain aromatics.

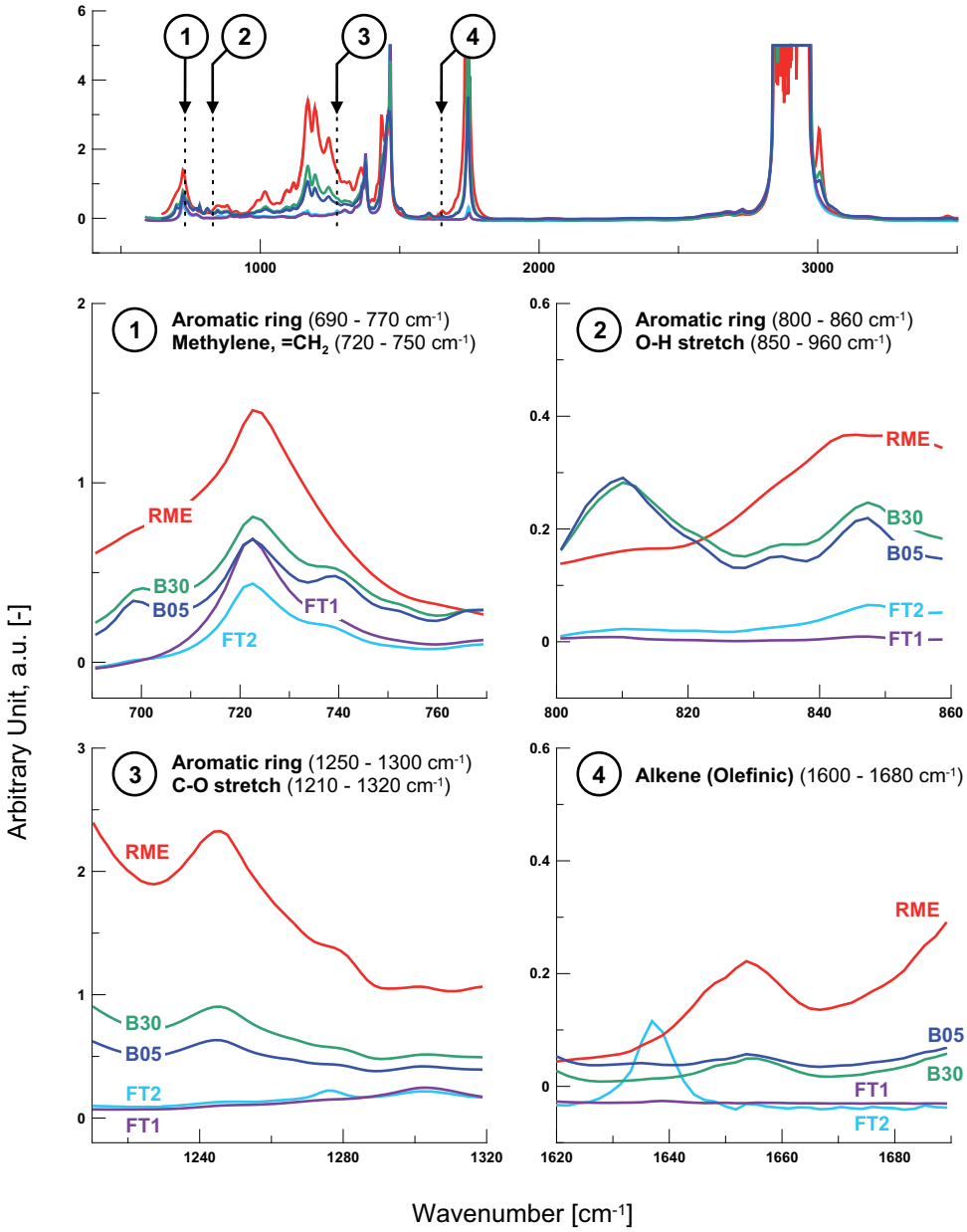

Figure 3.4. *Fourier Transform Infrared Spectroscopy of the five fuels. In 1 to 4, the focus is made on radicals attesting for fuel unsaturation.*

(III) Considering both plots 1 and 4, the overall degree of unsaturation of RME seems superior to that of B05 and B30. The lower but more homogeneous unsaturation of RME *via* $C18{:}1$ and $C18{:}2$ ($= CH_2$), leads to a higher global unsaturation degree than the strong (benzene rings in aromatics) but partial unsaturation of B05 and B30.

3.3.4. Cetane Number/Index

The cetane number (CN) is a long-time established measurement aiming at the quantification of ignition quality for diesel-type fuels. Initially, this number is obtained by equalizing the ignition delay of a sample with that of a blend of two reference fuels in a standardized engine test (ASTM D613/ISO 5165). More recently, a new experimental protocol appeared using a simplified facility (ASTM D6890). Further discussions about the issues associated to this measurement are provided in *Chapter 2*.

Also, the engine community has been looking for empirical correlations reflecting the fuel ignitability using physical properties as tracers of a process mostly controlled by chemical properties. Thus, the object here is to seek insight into the empirical correlations, also proposed by ASTM or ISO standards, aiming at matching those CN measurements while using fuel physical properties. In the context of this study, they permit the connection between the two previous sections and represent a valuable first approach of the relationship between fuel physical and chemical properties. Three correlations have been identified for the establishment of the calculated cetane index (CCI):

(I) $CCI = 454.74 - 1641.416 \cdot \rho_{fuel} + 774.74 \cdot \rho_{fuel}^2 - 0.554 \cdot T_{50\,\%} + 97.803 \cdot log(T_{50\,\%})^2$

(II) $CCI = 45.2 + 0.0892 \cdot (T_{10\,\%} - 215) + [0.131 + 0.901 \cdot (e^{-3.5(\rho_{fuel} - 0.85)} - 1)] \cdot (T_{50\,\%} - 260) + [0.0523 - 0.420 \cdot (e^{-3.5(\rho_{fuel} - 0.85)} - 1)] \cdot (T_{90\,\%} - 310) + 0.00049 \cdot [(T_{10\,\%} - 215)^2 - (T_{90\,\%} - 310)^2] + 107 \cdot (e^{-3.5(\rho_{fuel} - 0.85)} - 1) + 60 \cdot (e^{-3.5(\rho_{fuel} - 0.85)} - 1)^2$

(III) $CCI = -386.26 \cdot \rho_{fuel} + 0.174 \cdot T_{10\,\%} + 0.1215 \cdot T_{50\,\%} + 0.0185 \cdot T_{90\,\%} + 297.42$
with $\rho_{fuel} = \frac{\rho_{ASTM\ D1298}}{1000}$

Equation (i) is the historical model issued from ASTM D976 while (ii) and (iii), each applying for different levels of sulfur, proceeds from the more recent ASTM D4737. Note that Eq. (ii) is also employed in ISO 4264. One can observe that all these models are functions solely of fuel density and specific distillation recovery temperatures of the fuel ($T_{X\,\%}$). Though Eq. (i) is limited to the unique mid-boiling point, the more sophisticated Eqs. (ii) and (iii) include the 0, 50, and 90 % recovery temperatures. Unfortunately, as specified by the standards, these models are strictly restricted to fossil diesel fuels,

moreover without additives and within a very restricted range for both the resulting CCI and the variables involved. Thus rigorously, none of our five fuels fit these requirements, but calculations have been performed anyway to compare the models sensitivity and possibly detect trends in view of the future analysis. Results have been summarized in Table 3.4.

For both B05 and B30, CN measurements (ASTM D613) were actually available from the fuel technical sheets, what constitutes a solid starting point for the analysis. CCI shows quite a good agreement in scalar terms with the experiment. However, none of the three models is able to detect the small CN increase when the RME rate is raised from 5 to 30 %. Accordingly, data becomes fairly uncertain for RME with values oscillating around those of B05 and B30. Both Fischer-Tropsch fuels show higher CCI in comparison with these two, in particular FT1 by reaching values of 80-90. In view of the considerations advanced previously and the variability of the results, caution has to be taken in their interpretation. Nonetheless, the response of these models to such a wide variation of both fuel density and volatility is suggestive. In Section 3.3.2, B05 and FT1 displayed very similar distillation recovery profiles. As such, the significant increase of CCI observed with FT1 is due to the unique contribution of the density drop, from 833 to 784 $kg.m^{-3}$. Now moving from FT1 to FT2, density is nearly conserved whereas fuel volatility increases significantly, with the effect of having CCI returning back to values closer to B05. To summarize, these empirical models suggest that decreasing both fuel density and volatility (higher recovery temperatures) is in favor of better fuel ignitability. When this statement is extended to RME or gasoline, offsetting effects compete. As biodiesel often propose a better ignitability, its lower volatility would outweigh its higher density. In reverse, gasoline higher volatility would prevail over its density decrease to yield a lower CN (higher ON).

Although these observations are fairly empirical and so far only appeared to work for this limited selection of fuels, they may find hypothetical explanations in the review performed in the previous chapter. It was established that saturated and linear hydrocarbons, known for their high ignition qualities, enabled numerous $C-H$ single bonds recognized for their disposition to break easily and trigger ignition. Besides, the density of hydrogen (1 u and 50 pm) atoms is much lower than carbon (12 u and 134 pm) or oxygen (16 u and 96 pm) atoms. Therefore, lower density may be expected for a fuel saturated in hydrogen atoms like an alkane, conferring to such fuel property a status of good estimator for ignitability. Regarding fuel volatility, this property is a function of the molecular weight, being usually the shortest chains the most volatile. But as the chains get shorter, the probability for O_2 to meet a $C-H$ single-bond from a secondary carbon (weaker than those of a primary carbon)

gets lower. Under this assumption, higher volatility could reasonably be in favor of lower ignition.

In conclusion, these ASTM standards propose correlations of fuel ignitability, namely a characteristic fundamentally associated to chemistry, based on the unique variation of physical properties measured at atmospheric pressure. As such, decreasing both fuel density and volatility seem to be in favor of better fuel ignitability. Although it may be a hazardous approach, especially if cetane improvers are used, these physical markers seem to be the image of well-known chemical effects. These correlations cannot permit to conclude over biodiesel-derived fuels but they hint that the two Fischer-Tropsch have a higher ignitability, especially FT1, being this result consistent with the literature and the previous measurements of the fuel saturation degree.

Table 3.4. *Cetane number and cetane index for the five studied fuels. Comparison between the experimental and the empirical modeling approaches.*

	B05	**B30**	**RME**	**FT1**	**FT2**
ASTM D613 / ISO 5165	54	55	-	-	-
(1) ASTM D976	57.9	54.1	48.7	77.5	55.9
(2) ASTM D4737-a / ISO 4264	57.6	53.3	56.7	92.1	59.8
(3) ASTM D4737-b	53.3	51.5	61.1	80.5	58.3

3.4. Injection settings and hydraulic characterization of the injector

Now that the five fuels have been presented and characterized, it must be considered the hardware used to inject these latter inside the combustion chamber and in particular its response to the change of fuel properties. After a rapid presentation of the injector involved, its characterization based on the combination of mass flow rate and momentum flux measurements is completed in order to quantify the injector hydraulic efficiency with each fuel under the future test conditions of stages 2 and 3.

3.4.1. Injector geometry

A Bosch injector with solenoid-actuation of the needle was connected to a standard common-rail from which a pressure transducer was measuring the fuel pressure and permitted its control through a proportional-integral-derivative (PID) system. The injector was equipped with a single-hole nozzle drilled axially as shown in Figure 3.5. This cutaway view displays the interface between the needle and the nozzle body. The nominal diameter of the orifice exit was 80 μm. Its conicity of 1.5 implied a diameter of 95 μm at the entrance of the orifice and such geometry was selected in order to avoid cavitation as suggested the review made in *Chapter 2*. For confirmation, the orifice exit was visualized with an optical microscope as shown in Figure 3.6. After image segmentation to detect the hole, the diameter of a disk with equivalent area was calculated as indicated on the figure. Depending on the threshold level, the resulting diameter varies between 80 μm for a restrictive threshold and 84 μm for a more permissive one. As a compromise, a diameter of 82 μm will be considered for further analysis.

A single-hole nozzle was installed despite some potential issues such as a faster pressure build-up in the nozzle sac-hole, a faster needle lift, and a higher injection pressure even at full needle lift [10] compared to a multi-hole one, typical of a production engine. This choice was mostly motivated by the simpler mechanical arrangement for housing the whole injector, in particular in a test rig specifically designed to maximize the development and help the visualization of a unique spray. However, the use of a single-hole nozzle also presents significant additionnal benefits by impeding spray-to-spray interactions, and by limiting the mass injected with the subsequent effect on heat release and ambient conditions alteration.

3.4.2. Mass rate and momentum flux

During the whole test campaign, the energizing duration of the injector has been set and maintained to 8 ms. As already commented in *Chapter 2*, such long signal may not be representative of standard engine injections but it permitted to complete the establishment of the spray and the flame in future combustion tests. Three levels of pressure have been applied, namely 50, 100 and 150 MPa.

Mass flow rate measurements were carried out using the Injection Rate Discharge Curve Indicator (IRDCI) described and operated in the Bosch method [11]. This measurement has been the object of several Ph.D studies at CMT-Motores Térmicos so only a brief summary will be given here. The reader

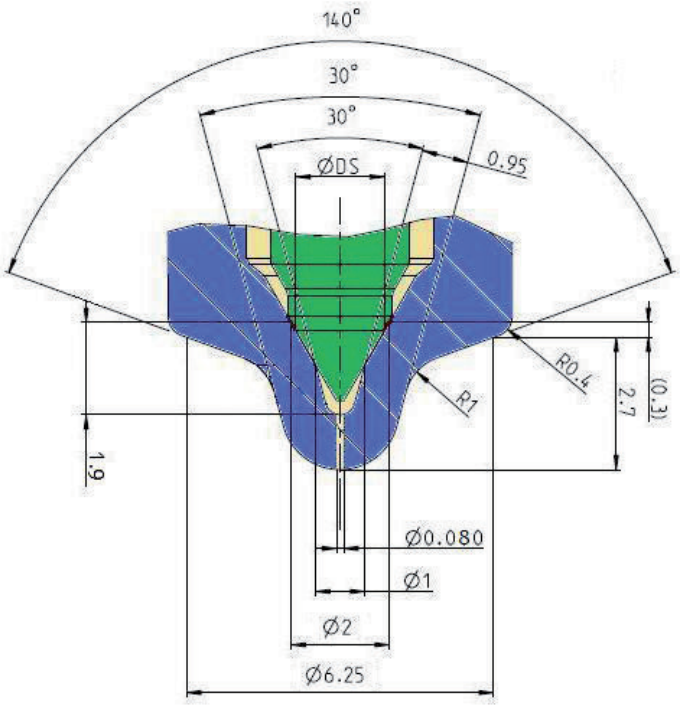

Figure 3.5. *Cutaway view of the injector tip.*

is referred to [12–16] to find further details and deeper analysis on the subject. To sum up, the fuel is injected into a long, pressurized, fuel-filled measuring tube in which the fuel discharge produces a pressure increase proportional to the fuel mass increase. The mass flow rate is related to such pressure increase through an equation derived from the Allievi relationship in stationary fluids:

$$\dot{m} = \frac{(A_t \cdot \Delta P)}{a} \tag{3.1}$$

where A_t is the transversal area of the tube, ΔP is the pressure increase with respect to the stationary pressure and a is the speed of sound within the fuel.

Historically, speed of sound was normally calculated through an empirical correlation as a function of temperature exclusively, obtained from a standard diesel fuel. It aimed at accounting for the slow heating of the rig during tests,

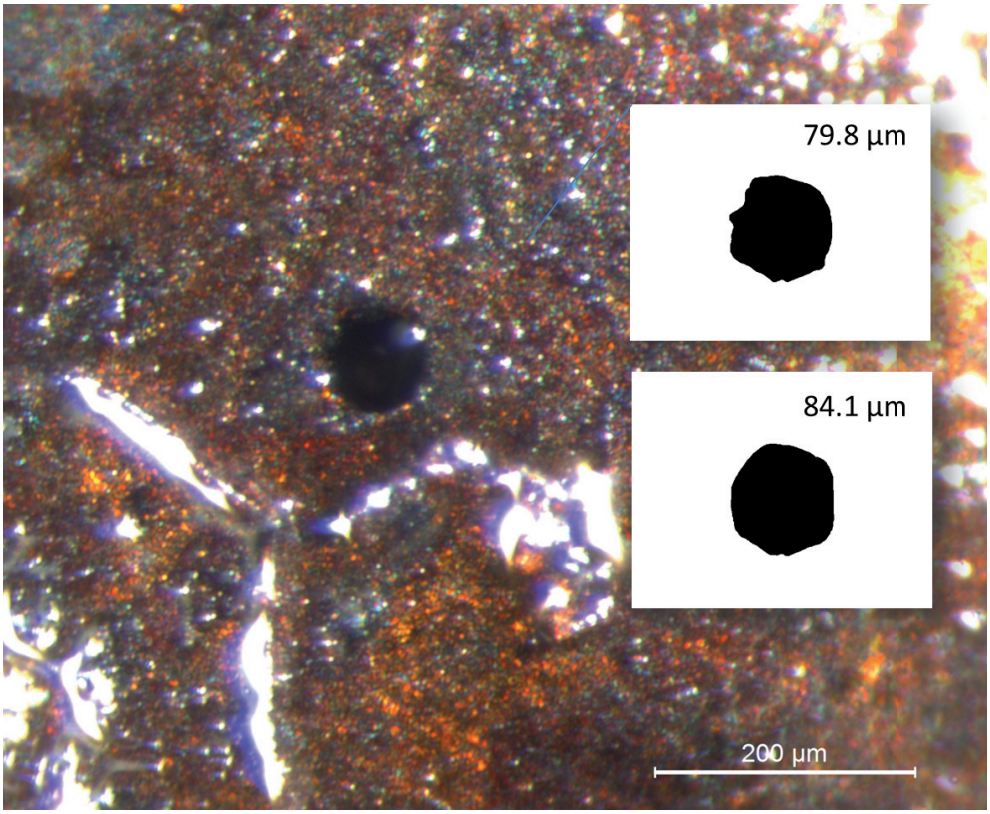

Figure 3.6. *Microscopic picture of the orifice exit. Two images yielding from segmentation with two different thresholds are also displayed. Diameters are those of a disk with the same area.*

typically comprised between 20 and 80°C, and associated to a potential 10 to 20 % error. Nevertheless, in the context of this study, one can expect a significant change of a from one fuel to another while only little information in the literature exists to enable its prediction. Thus, taking advantage of coinciding developments made by Bracho [16, 17], the speed of sound of each fuel (except B30) could be measured with the purpose of completing the calculations of mass flow rate. In addition to fuel temperature effect, Bracho developed a specific experiment and empirical model including the effect of fuel pressure as expressed in Eq. 3.2.

$$a = k_1 + k_2(T_f - T_0) + k_3(P_f - P_0) + k_4(P_f - P_0)^2 + k_5(P_f - P_0)(T_f - T_0) \quad (3.2)$$

where $P_0 = 0.1\ MPa$ and $T_0 = 273\ K$ are references to STP.

The wide ranges of fuel temperature (253-343 K) and pressure (15-180 MPa) operated in her experiment to develop these correlations, as well as the number of test points, allowed for its application to the current study. It has been obtained a good fit between the data and the models whose constants are given in Table 3.5. As suggest the resulting coefficients and the plotting of these models (not represented), speed of sound is almost equivalent for B05, RME, FT1 and expectedly B30, showing differences inferior to 2 % within the whole test matrix. Only the speed of sound of FT2 is slightly lower, typically by 5-6 % rather maintained constant while using any couple of pressure and temperature from the test matrix as inputs. Therefore, although the check had naturally to be made, replacing a single standard correlation by five others, specific of each fuel, may not prove to be essential for the calculation of the mass flow rate, except for FT1. Just as a final remark, the similarity in speed of sound, namely a square root function of the bulk modulus-density ratio, implies that bulk modulus vary in proportion with fuel density for the fuels concerned. In particular, RME higher bulk modulus is consistent with the information mentioned in *Chapter 2*. Because of its lower density but comparable speed of sound, FT1 is expected to have a lower bulk modulus than any of the biodiesel-derived fuels. FT2 with similar density as FT1 but lower speed of sound is likely the fuel with the lowest bulk modulus.

Table 3.5. *Coefficients to be used in Bracho's model (Eq. 3.2) for speed of sound calculation in each fuel. For B30, coefficients have been interpolated.*

	k1	k2	k3	k4	k5	R^2
B05	1440.89	-3.11349	4.1751	-0.00069676	0.0094014	99.59 %
B30	*1446.55*	*-3.10174*	*3.8365*	*-0.0068466*	*0.0099889*	*99.52 %*
RME	1462.42	-3.06884	3.5465	0.00650776	0.0116338	99.33 %
FT1	1434.96	-3.24845	4.3768	-0.00861893	0.0101815	99.58 %
FT2	1373.15	-3.42066	4.4184	-0.00741517	0.0103867	99.64 %

Although with a minor effect expected, two levels of back-pressure have been tested, corresponding to the minimum (5 MPa) and maximum pressures (7 MPa) used in the engine experiments approached thereafter (Stages 2 and 3). Thus, with P_{back} fixed and a issues resolved, Eq. 3.1 was time-resolved by sampling the pressure signal at 100 kHz. The resulting mass rate of injection as a function of time, $\dot{m}(t)$ is plotted in Figure 3.7. A

50 MPa injection pressure case has been selected as it displayed the maximum difference observed among fuels in regard to the needle dynamic of opening and closing. That is, hydraulic delay of FT2, namely the delay between the start of injector energizing and the start of injection, was only ∼60 μs inferior to the rest of fuels. For the two higher injection pressure conditions, injector opening for the five fuels was coincident within the 10 μs sampling period. Therefore, despite biodiesel higher bulk modulus, this hardware configuration did not advance its injection as reported by several authors in *Chapter 2*. On the contrary, FT2 appears instead to be the most propitious to advance injection despite its lower bulk modulus. This result suggests that fuel compressibility may be not such a relevant factor in the needle dynamic. Thus, FT2 lower viscosity, limiting frictions internal to the injector, is likely the cause of its advanced injection. Let us remind the importance of such result since biodiesel advanced injection because of increased bulk modulus was mentioned as one of the potential causes responsible for NO_X increase.

Measurements of the spray momentum flux were operated in a purposely-designed rig [15, 18, 19]. Under a pressurized environment of nitrogen, the force created by the spray impact on a plate is measured by means of a calibrated piezo-electric pressure sensor. The plate, located at a distance of 5 mm of the nozzle exit, is large enough to collect the whole spray. Under the hypothesis of momentum conservation, the force measured by the sensor is equivalent to that at the orifice exit, since the pressure in the chamber is maintained at constant value, and the fuel is deflected radially and perpendicularly to the spray axis. Figure 3.7 shows the corresponding time-resolved momentum flux measurement and confirms the slightly advanced injection of FT2 as well as the conclusions associated over predominance of viscosity over fuel compressibility for the small delays observed at the low injection pressure condition (50 MPa).

Under such long injection conditions, both mass flow rate and momentum flux accommodated a neat "top-hat" rate profile, and thus allowed to extract a reliable average value to establish their quasi-steady condition at full needle lift. As shown for the sample of Figure 3.7, each dataset has been time-averaged between 4 and 8 ms ASOE. Accordingly, results of the whole test matrix, including the three levels of injection pressure and the two levels of back pressure, have been represented in Figure 3.8. Naturally, the five fuels show a similar response to the injection pressure increase by increasing both their mass flow rate and momentum. Although, the small variations of pressure drop produced by lower P_{back} should be in favor of both a higher mass rate and a higher spray momentum, this relationship does not verify systematically. This inconsistency is most likely the result of measurement uncertainty rather than a clear indication that flow-collapsing cavitation occurs in the nozzle.

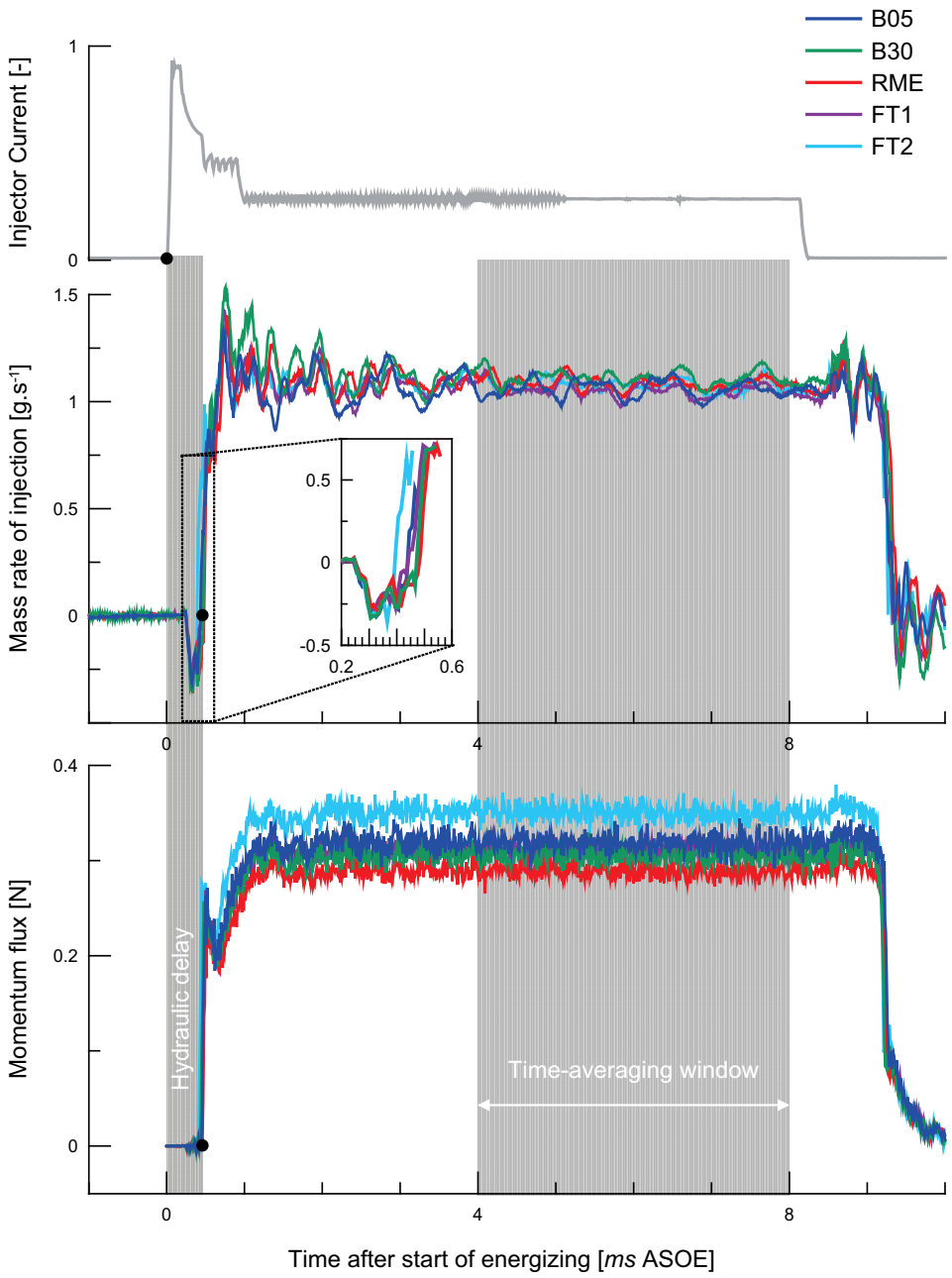

Figure 3.7. *Injector current signal, mass rate of injection and momentum flux as a function of time for* P_{inj}*=50 MPa and* P_{back}*=7 MPa.*

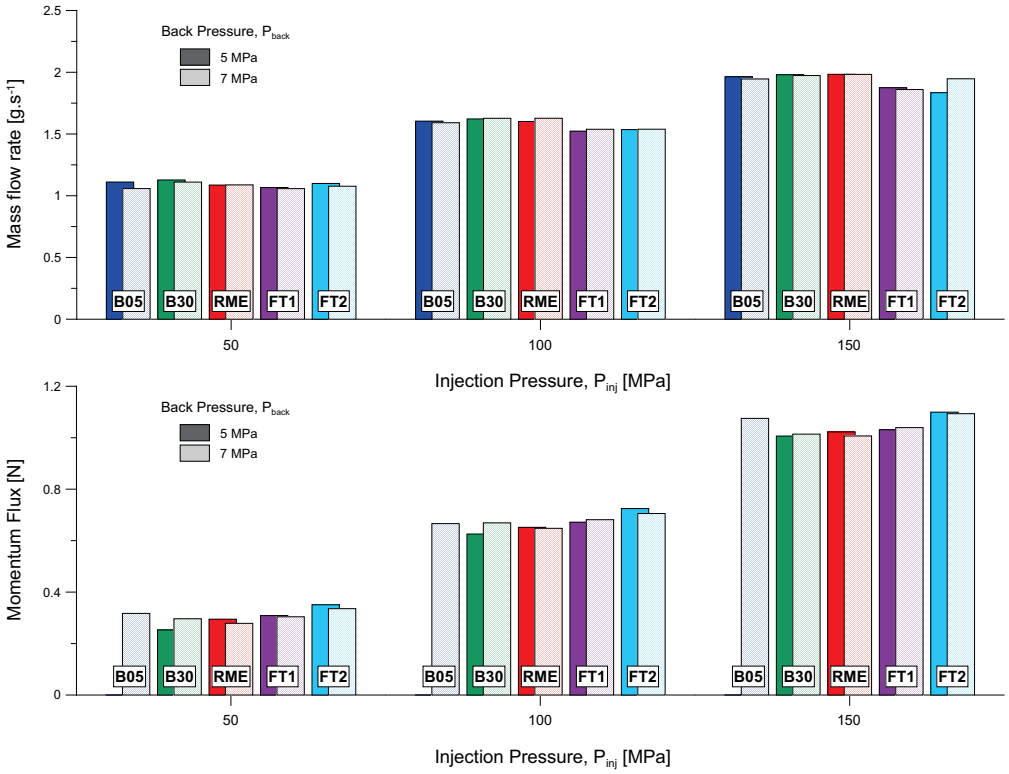

Figure 3.8. *Averaged measurements of mass rate of injection and momentum flux at the three injection pressure levels.*

Considering the fuel effect at each level of injection pressure, mass flow rate is rather equivalent within each of the two groups of fuels, being Fischer-Tropsch fuels almost systematically inferior to biodiesel-derived fuels. This result is consistent with their lower density as stated in Eq. 2.2 and reported in Table 3.1, although under this assumption, more differences may also be expected among biodiesel-derived fuels. By contrast, the fuel effect on the momentum flux isolates FT2 from the rest of fuels. According to Eq. 2.3, none of the fuel properties should actually interfere with that measurement as it only depends on pressure drop and nozzle efficiency. Thus, FT2 higher momentum suggests an increase of the fuel effective velocity. Such increase could be the result of a better discharge, but the previously commented correlation between lower mass flow rate and lower density rather suggests that this is not the case. Thus, Payri *et al.* [19] also observed a similar increase of the velocity when cavitation would arise within the nozzle conduct. As vapor pockets

virtually reduce the conduct area, fuel velocity increases in the rest of the passing section. As the lesser of two evils, this offsetting effect of the nozzle contraction achieves to maintain mass flow rate but therefore impedes the increase expected. This result was actually not expected for conical nozzles [19] but the low viscosity and high volatility of FT2 could be in favor of an easier development of cavitation. In the next section, the purpose will be to determine the nozzle flow efficiency but also to establish clearly if cavitation is really developing with this fuel.

3.4.3. Hydraulic characterization

The hydraulic characterization of a nozzle was derived from the association of mass flow rate (Eq. 3.3) and spray momentum flux (Eq. 3.4) measurements, following the methodology defined in [19].

$$\dot{m}_{eff} = u_{eff} \cdot \rho_f \cdot A_{eff} \tag{3.3}$$

$$\dot{M}_{eff} = u_{eff}^2 \cdot \rho_f \cdot A_{eff} \tag{3.4}$$

with

$$u_{eff} = C_v \cdot u_{th} = C_v \cdot \sqrt{\frac{2 \cdot (P_{inj} - P_{back})}{\rho_f}} \tag{3.5}$$

and

$$A_{eff} = C_a \cdot A_{geo} \tag{3.6}$$

Their combination (system of 2 equations with 2 unknown values) enables an estimation of the effective jet speed at the exit of the orifice and the effective section through which the fuel flows in liquid phase inside the chamber. As given in Eq. 3.5, the coefficient of velocity (C_v) relate the effective velocity with the theoretical one (u_{th}) proceeding from Bernoulli's law (Eq. 2.1), while the coefficient of area (C_a) relate the exit geometric section with the effective one as given in Eq. 3.6. Such area, absolutely virtual, hypothesizes a vector field of velocity with uniform direction and magnitude accounting for two main effects. The first effect rather occurs at low Reynolds number where velocity gradients are radially significant due to the interaction between the fuel and the wall of the conduct. Due to shear stresses, further enhanced with higher fuel viscosity, the liquid vein detaches from the wall forming a boundary layer and inhomogeneity in the velocity profile [16]. As the Reynolds number increases, the more important turbulent viscosity reduces such effect and homogenize

the velocity profile, up to a point where the second effect, namely cavitation, comes into play. As velocity increases, pressure locally decreases down to fuel vapor pressure, forming vapor pockets, typically at the orifice entrance. Such vapor "bubbles" are dragged by the flow until reaching the nozzle exit. Their low density virtually produces a contraction of the exit section, creating an important non-uniformity on the velocity profile. Finally, as mentioned in Section 3.3.2 both coefficients include effects of fuel compressibility and variations of both density and viscosity with temperature since currently, information is missing to isolate and quantify their effect.

The product of these two coefficients gives the discharge coefficient (C_d), historically used to relate the effective mass flow rate with Bernoulli's principle as stated in Eq. 3.7. Some authors use the coefficient of momentum (C_M) to better analyze all the issues associated to that measurement such as spray penetration or mixing. Its relationship with C_a and C_v is expressed in Eq. 3.8.

$$\dot{m}_f = C_v C_a \cdot A_{geo}\sqrt{2\Delta P \rho_f} = C_d \cdot A_{geo}\sqrt{2\Delta P \rho_f} \tag{3.7}$$

$$\dot{M}_f = C_v^2 C_a \cdot A_{geo} 2\Delta P = C_M \cdot A_{geo} \cdot 2\Delta P \tag{3.8}$$

In order to better appreciate the trends, additional measurements of mass flow rate at 30 and 70 MPa have been added to the initial test matrix although, as defined previously, they only permitted to increase the number of data for C_d. Resulting coefficients of the previous analysis have been plotted in Figure 3.9 as a function of the theoretical Reynolds number. B05, B30, RME, and FT1 have a similar behavior, conventional for conical non-cavitating nozzles. It consists in an asymptotical improvement of C_d, caused by an increasing C_v (more homogeneous velocity profiles) while C_a maintains. Regarding FT2, the first remarquable thing is the range of Reynolds number in which it is operating. This effect is produced by its much lower viscosity compared to the rest of fuels. Both coefficients of velocity and momentum are significantly superior in agreement with the higher momentum observed in the previous section. In return, the coefficient of area drops as the Reynolds number increases, dominating the C_v increase, therefore causing a slight reduction of the discharge coefficient. Decreasing C_d is rather unexpected for a conical nozzle as it suggests an apparition of cavitation although these results are not glaring to clearly establish if cavitation is causing the reduction of C_a or if it is due to measurement uncertainty. However, the result and the interest for our study remain actually quite independent from their origin. The point is that FT2 probably suffers inhomogeneities in the velocity profile at the nozzle

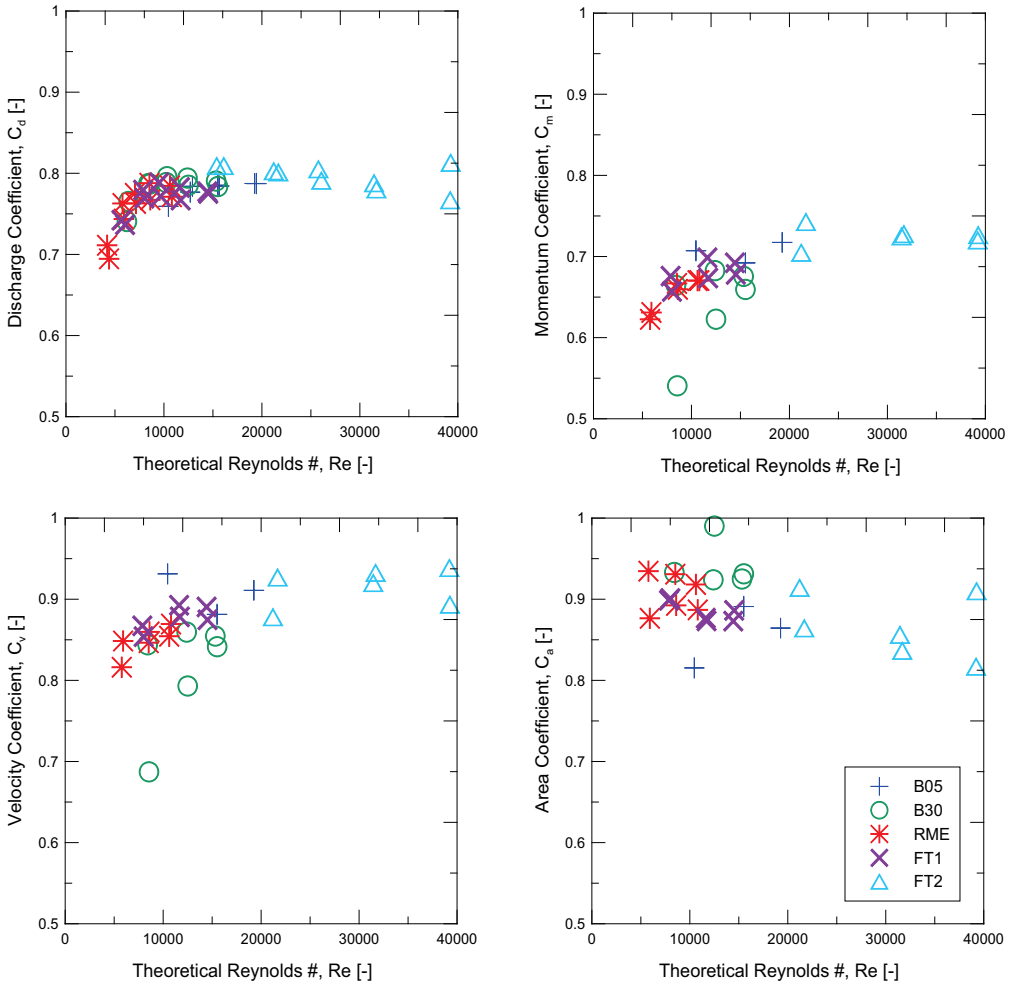

Figure 3.9. *Hydraulic coefficients of the nozzle for the five fuels as a function of the Reynolds number.*

exit, which nonetheless do not engender drastic effects on the mass flow rate. In that sense, mass flow rate remains quite depending from fuel density since C_d maintains, but the higher momentum may produce a faster penetration of the spray, enhance mixing, and should be accounted for further analysis.

3.5. Hot spray test rig

3.5.1. Hardware construction

In order to reproduce Diesel-like conditions, injections have been conducted in a facility based on a modified 2-stroke loop-scavenged single-cylinder Diesel engine. Entrained by a 37 kW electric motor, this engine was converted into a "passive" compression machine as none of the combustion heat release is meant to be leveraged for its functioning. Intake and exhaust being handled by transfers on the cylinder liner, the basic cylinder-head could be easily modified to enable a complete optical access to the high-pressure chamber. With three-

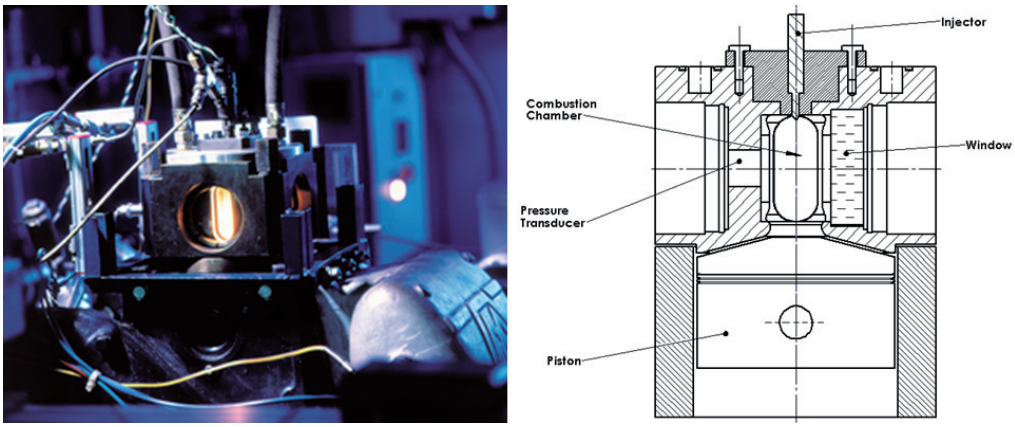

Figure 3.10. *Photograph and cutaway view of the hot spray test rig cylinder-head.*

liter displacement and a compression ratio of 14.8:1, the facility enables conditions of high-temperature and high-density in a cylindrical chamber approximately 10 times larger than that of a conventional diesel engine at TDC. Therefore, the rig permits the development of Diesel sprays in a free field, being its volume large enough to avoid spray impingement against the engine walls. Its relatively low rated rotational speed (500 rpm) allows maintaining such thermodynamic conditions during a relatively long period compared to the typical injection duration of standard HSDI Diesel engines (up to 1.5 ms). In addition, the large volume also limits the effect of endothermic (liquid vaporization) and exothermic (spray combustion) processes on the pressure trace, maintaining ambient conditions and engine speed. As a result, the rig provides chamber thermodynamic conditions at quasi-steady state. Two modes of functioning, namely in open and closed-loop, permit to feed the engine either with pure nitrogen or ambient air. As such, both inert and reacting sprays can

be studied in the same rig with identical boundary conditions. Regulation of engine conditions is made controlling air intake pressure (up to 0.3 MPa) and air temperature (up to 400 K). Data relative to the engine geometry have been collected in Table 3.6.

As regards the cylinder-head in more details, an upper port receives the fuel injector while enabling four lateral orthogonal accesses, as shown in Figure 3.10. One port is used by a pressure transducer whereas the three others are equipped with oval-shaped quartz windows, 88 mm long, 37 mm wide, and 28 mm thick. Accounting for the injector penetration and the sealing peripheral obstruction, the useful area for line-of-sight imaging is 78 mm long and 29 mm wide. Further information about this facility may be found in [20].

Table 3.6. *Hot spray test rig characteristics.*

Hot spray test rig	
Type	Single-cylinder 2-stroke loop-scavenged engine
Displacement	3000 cm^3
Stroke	170 mm
Bore	150 mm
Distance between injector tip and piston head at TDC	87.8 mm
Compression ratio	14.8:1

3.5.2. Operating conditions

As suggested in *Chapter 2*, both air temperature and density play a significant role at all stages of the spray development starting from air entrainment and vaporization of its liquid-phase until the end of its combustion. In this regard, a cross-shaped test matrix has been considered, including five operating conditions as shown in Figure 3.11. This design enable a sweep of three levels of temperature (T_{max}) at constant density (ρ_{max}= 26 $kg.m^{-3}$), and a sweep of three density levels (ρ_{max}) at constant temperature (T_{max}= 800 K). Correspondingly, these operating conditions have been labeled NO, LT, HT, LD, HD, standing respectively for NOminal, Low Temperature, High Temperature, Low Density and High

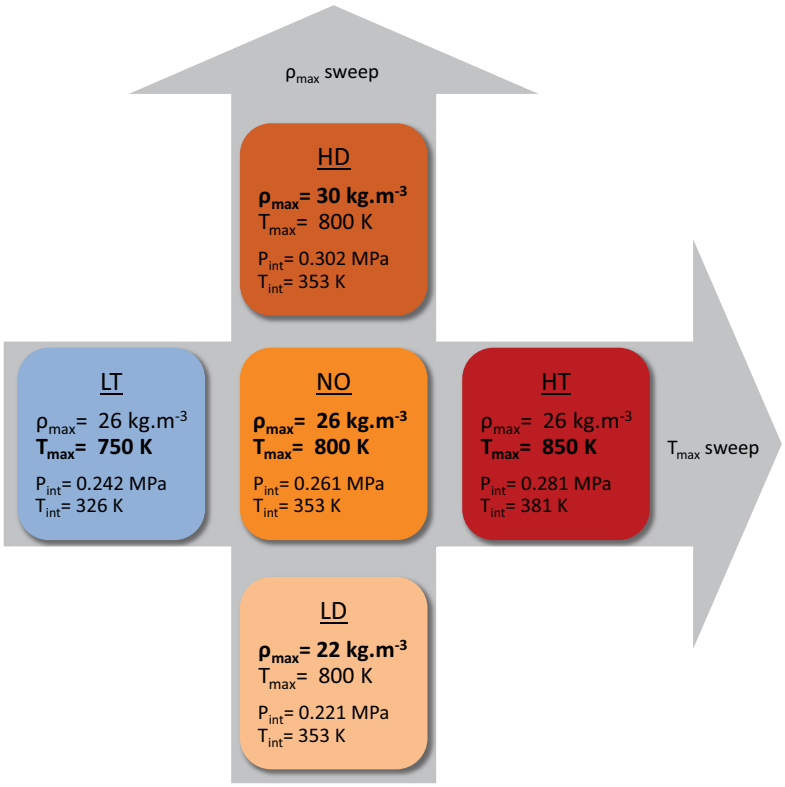

Figure 3.11. *Schematic representation of the engine operating conditions selected for the study.*

Density ambient setup. Note that maximum temperatures and densities were considered in Figure 3.11 although varying ambient conditions must be considered with 8 ms injections. Indeed, the injector was triggered at -16°C ATDC, corresponding approximately to a range of ∼24 CAD, depending on the exact instantaneous angular speed of the engine. By way of background, engine angular velocity was fairly constant during a complete engine revolution, and even more throughout the 24 CAD range of injection. For instance, while the nominal averaged speed was 3 CAD/ms (500 rpm), the 24 CAD average velocity was bounded between 2.835 and 2.885 CAD/ms, corresponding respectively to HD and LD conditions. The rig has always been operated under skip fire mode, i.e. one injection event occurs every 20 engine cycles. This strategy is used to let the system scavenge, recover between injection/combustion cycles and therefore to minimize the cycle-to-cycle interactions.

3.5.3. Engine characterization

To determine the exact intake conditions required by such a test matrix, an accurate characterization of the engine had to be performed previously. A selection of 35 points (couples of intake pressure and temperature) was made, covering the entire range of operating conditions enabled by the engine, as represented in Figure 3.12. Thermodynamic conditions of motored-cycles have been calculated from the cylinder pressure using a first-law thermodynamic analysis accounting for blow-by, heat transfer and mechanical stress (Calmec-derived [21, 22]). The analysis breaks down as follows: first, the trapped mass is estimated using intake temperature, pressure and volume at intake closure (IPC[1]). Once the trapped mass is known, an apparent temperature can be estimated computing the equation of state along the cycle while considering no mass loss. But because of the latter assumption, temperature remains underestimated. For that reason, the apparent temperature at exhaust port opening (EPO) is lower than the measurement of a thermocouple placed right at the entrance of the exhaust duct. This temperature offset actually contains the information of blow-by. Accordingly, the blow-by leakage mass is calculated as the difference between the initial trapped mass and the residual mass, obtained with the cylinder pressure at EPO and the temperature given by the thermocouple. Then, the leakage mass is angularly distributed along the cycle as a linear function of cylinder pressure *via* a simple algorithm based on choked flow equations for gases. The equation of state is applied again, with the new "instantaneous mass", geometric volume and experimental pressure, to estimate temperature and density all along the cycle. The mechanical stress applied to the rod can lead to a mechanical deformation which should be taken into account for the correct calculation of in-cylinder volume evolution. In this particular engine, deformation was estimated to be negligible.

Once the angular-resolved thermodynamic conditions of the 35 points known, the exact intake conditions to carry out the test plan defined in Section 3.5.2 were interpolated as follows. First, both maximum temperature and density were extracted for each condition. The angle of occurrence of both these values varied very little from one test point to another, being typically -3 CAD for temperature and -0.5 CAD for density (-1 CAD for P_{max}). As shown in Figure 3.13, T_{max} had a linear response to intake temperature (T_{int}), independently from intake pressure, and thus independently from ambient density. This result is in agreement with Eq. 3.9 if the polytropic index n is maintained constant for the 35 conditions. Eq. 3.9 is derived from the ideal

[1]Note that in a 2-stroke engine, cyclinder sealing actually occurs at exhaust port closure

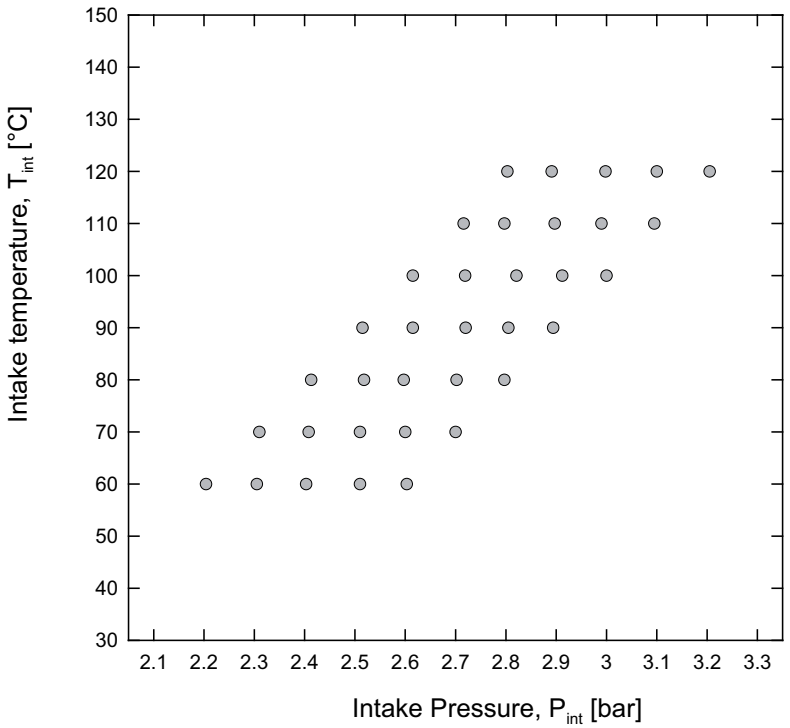

Figure 3.12. *Selected intake thermodynamic conditions for engine characterization.*

gas law in a polytropic process, in which a would be the angle of IPC and b, the angle of maximum temperature (-3 CAD).

$$T_b = T_a \cdot (\frac{V_a}{V_b})^{(n-1)} \tag{3.9}$$

Accordingly, intake temperatures for the five conditions fixed by the test matrix were determined with a linear regression, as reported in Figure 3.13. Next, the estimation of the respective intake pressure (P_{int}) required a succession of two additional interpolations. Maximum density at the two simulated intake temperature conditions (52.7 and 107.4°C) was first derived for the intake pressure sweep as shown in Figure 3.14. Note that this interpolation was not necessary for 80°C as it happened by chance to be the exact intake temperature tested experimentally. Finally, as exposed in Figure 3.15, the linearity between maximum density and intake pressure at each intake temperature condition enables to extract the exact intake pressure by a last interpolation.

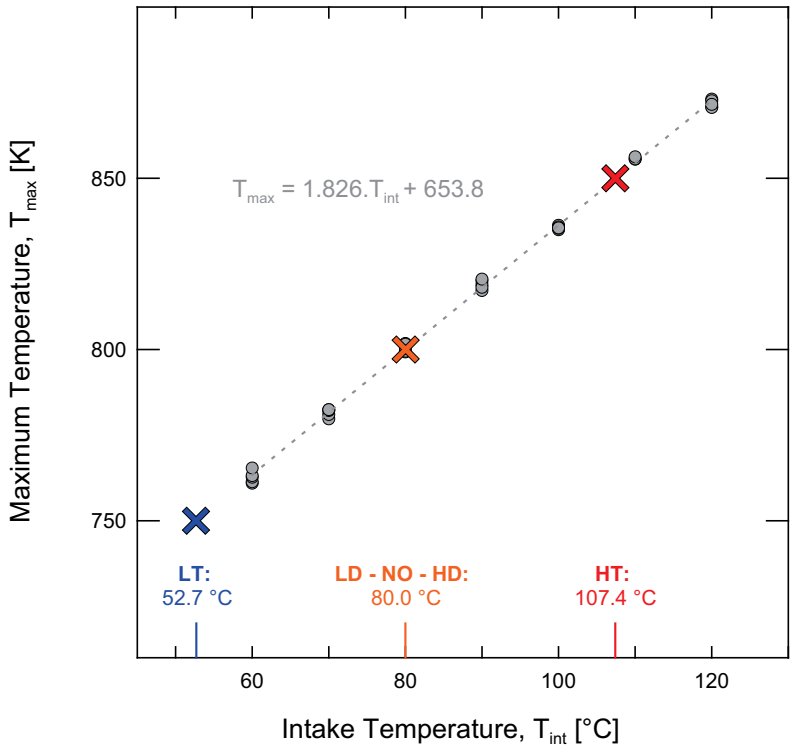

Figure 3.13. *Maximum temperature in the chamber as a function of intake temperature. The circle symbols represent the results from conditions selected for calibration previously showed in Figure 3.12. The cross symbols, issued from the linear regression, represent the conditions to apply to obtain those of the test plan of Figure 3.11.*

A double-check was performed with success by setting the resulting values to the engine and by reiterating the first-law analysis presented in the first paragraph of this section. Intake conditions to carry out the test plan are indicated in Figure 3.11 while the resulting angle-resolved ambient temperature and densities close to TDC are plotted in Figure 3.16 along with injector current and the associated mass flow rate.

3.5.4. Thermodynamic conditions stability with fuel injection

In [23, 24], the use of a multi-hole injector with 130 μm orifices in the present test rig had led to consider carefully the ambient temperature reduction engendered by the fuel vaporization energetic consumption.

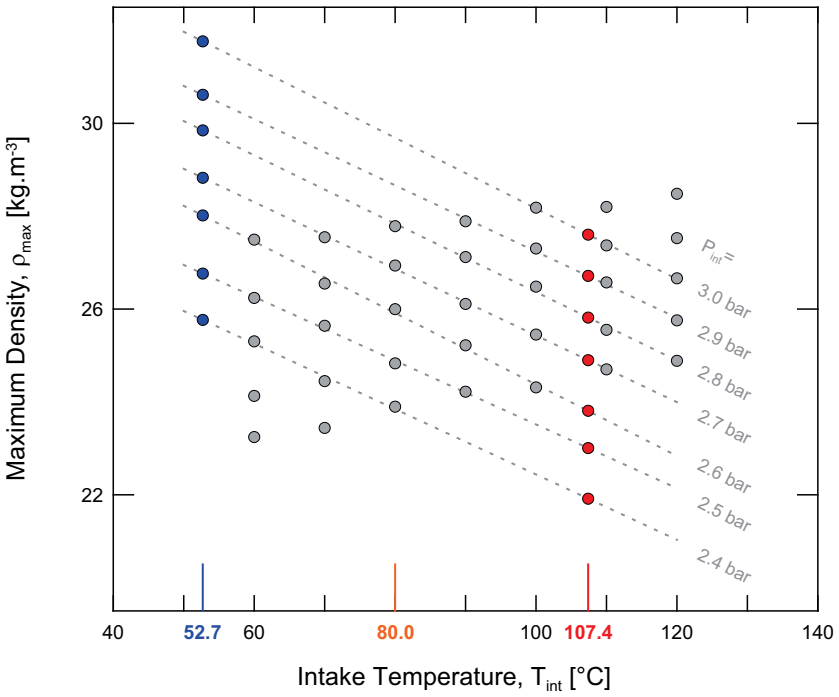

Figure 3.14. *Simulation of the maximum density as a function of intake pressure for the two intake temperatures simulated in Figure 3.13 (LT and HT).*

Therefore, in order to check the conservation of thermodynamic conditions during the injection event in the current study, ambient temperature has been recomputed similarly, considering both inert and reactive environments. For each injected cycle operated in this study, the pressure signal of the following 4 and 9 motored-cycles, respectively for inert and reacting conditions, were systematically acquired and averaged (Cf. Figure 3.17). Note that the two cycles directly following the injection one were not considered in this average since they could contain its footprint due to incomplete scavenging. Thus, the temperature calculation in both inert and reacting conditions was based on the following hypotheses:

- Pressure variations of either the "cycle with injection" or "the motored-cycles average" with that of calibration on the portion prior to injection were assigned to a difference on the trapped mass. Therefore, a correction was first applied to the density in order to match both pressure traces on the section prior to injection. This correction stands on the empirical fact that admission temperature was very well-controlled compared to

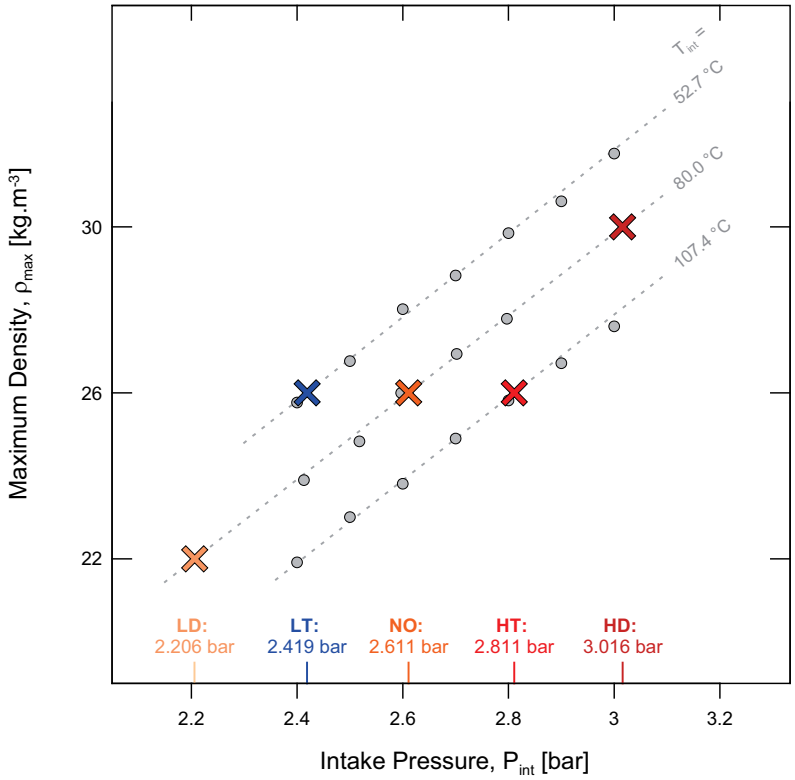

Figure 3.15. *Maximum density as a function of intake pressure for the three intake temperature levels considered in the test matrix.*

the trapped mass and scavenging processes, quite more uncertain in a 2-stroke engine. Though, this correction was always very small, and above all, aimed at making temperatures being strictly equal to that of calibration prior to the injection event.

- Ambient density (previously corrected) was maintained during fuel injection. Such assumption implies that the mass of fuel injected (between 8 and 20 mg) is insignificant respect to the trapped mass (between 4 and 7 g) and that the rate of blow-by leak is not modified by a potential pressure variation (increase in combustion or decrease in inert conditions). Under this assumption, any pressure variation between the injected cycle and the motored-cycles average is entirely assigned to temperature.

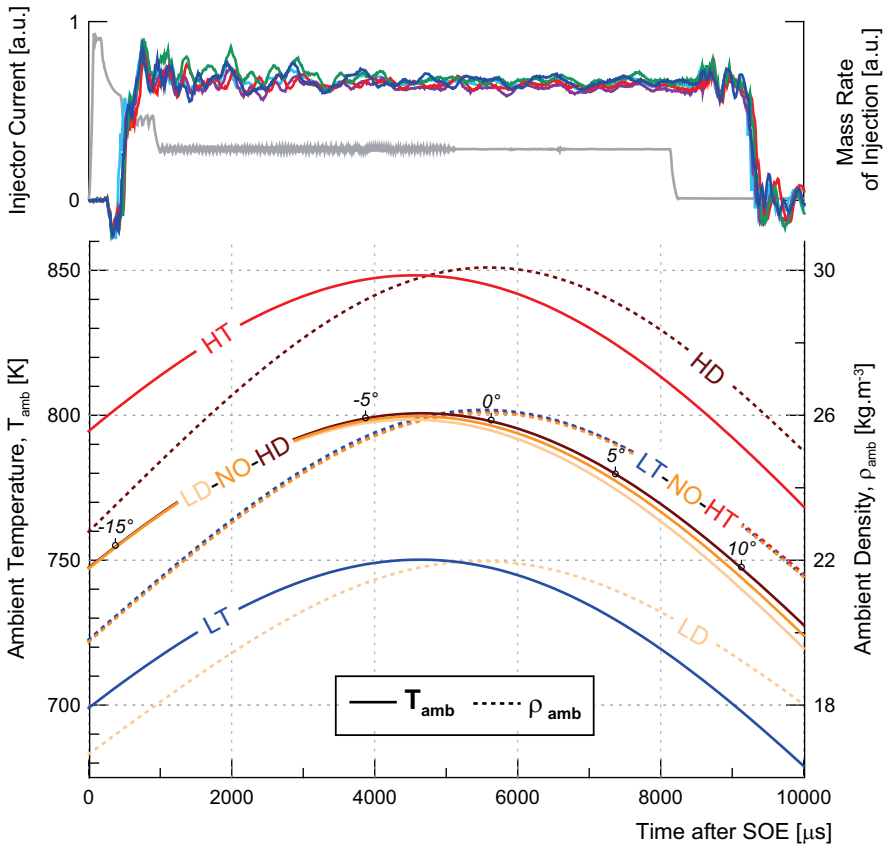

Figure 3.16. *Thermodynamic environment in the TDC vicinity. The 8 ms-energizing time is represented by the injector current along with the resulting mass rate of injection recalled from Figure 3.7.*

As observed in Figure 3.17 (a), pressure of cycles with injection under inert conditions showed very small difference compared to that of motored-cycles, but still could be detected ($\sim$0.05 MPa). Thus, although the temperature assessment could fail in some rare occasions because of cycle-to-cycle dispersion, it permitted to quantify in most of them the small ambient cooling caused by fuel evaporation. Figure 3.18 collects a set of selected inert conditions with the purpose of showing the effects of (a) injection pressure, (b) fuel type, (c) air density (ρ_{max}) and (d) air temperature (T_{max}) on air temperature steadiness. Plot (a) displays the response of B05 at NO condition to the sweep of injection pressure. Expectedly, cooling gets more important as the rate of fuel injection increases, but still remains very low in percentage

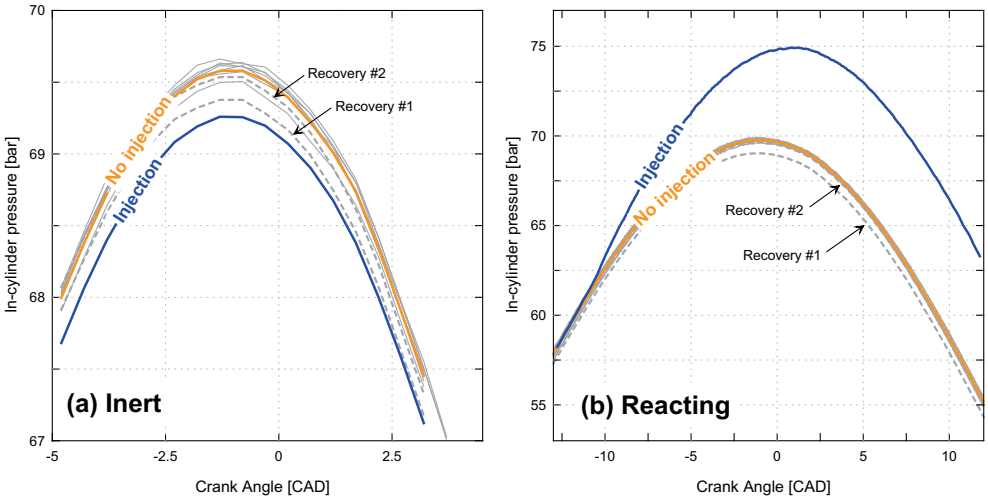

Figure 3.17. *Pressure traces (a) under inert conditions with effect of vaporization heat consumption, and (b) under reacting conditions with effect of combustion heat release. The continuous grey lines shows the 7 motored-cycles used to calculate the "motored-cycles average" (in orange), while dashed lines represent the 2 recovery cycles following the cycle of injection (in blue) that were not considered for the average. The selected example shows RME at HD ambient condition and 150 MPa injection pressure.*

terms (<5 K). In plot (b), injection pressure is fixed at 100 MPa to study the fuel type effect, with the result that it is impossible to make a clear differentiation among the five fuels. Plot (c) shows the density effect at constant temperature. The three "non-injected cycles" had to be plotted as they include a natural temporal offset. In order to limit the curves overlap, the low injection pressure condition was selected. In plot (d), the temperature variation between the motored-cycles average and the cycles with injection has been represented directly to make possible the comparison between the different levels of ambient temperature (LT, NO, and HT conditions).

Both plots (c) and (d) suggest that cooling is more important as either temperature or density levels are increased. However, the result is rather surprising for density since the higher trapped mass should be less sensitive to a constant amount of fuel injected. Therefore, due to the low differences measured, it is rather hazardous to push the interpretation of these results that far. Indeed, the major contribution of these four plots for our study is elsewhere. Firstly, cooling has been detected successfully with an ad-hoc methodology of pressure analysis. Secondly, ambient cooling remains very low,

not to say insignificant at any conditions of the test matrix. In that sense, it validates the choice made of a single-hole injector in order to limit the mass injected despite the long injections performed.

The exact same analysis was reconducted for the reacting environment. As shown in Figure 3.19, the effect of combustion heat release is naturally much more important than fuel vaporization. Correspondingly to Figure 3.18, effects of (a) injection pressure, (b) fuel type, (c) air density (ρ_{max}) and (d) air temperature (T_{max}) on air temperature steadiness are analyzed in Figure 3.19. In (a), (b) and (c), the temperature increase was about 70-80 K compared to the maximum temperature of the motored cycle (800 K). Reasonably, the major differences are observed in (a), namely when the mass rate of injection and the total mass injected are the greatests. In addition to the average, the cycle-to-cycle dispersion of 100 injections has been represented at 100 MPa by means of the interval [T_{air}-σ; T_{air}+σ]. Beyond providing an appreciation of the result reliability, it also raises questions about the causes of such instability. They could be due to the natural measurement uncertainty, but also by heat losses proceeding from soot radiation. An attempt will be made in *Chapter 5* to exploit this cycle-to-cycle dispersion. In plot (b), differences among fuels are also quite limited although more clear than under inert conditions. They appear to be consistent with both the LHV's shown in Table 3.3, and the minor differences observed on mass rate of injection among the fuel selection. Also, a hierarchy of fuel ignition qualities already emerges, consistent in some aspects with the CI calculations loomed in this chapter. While Fischer-Tropsch fuels have the highest reactivity, that of biodiesel-derived fuels is lower, being RME lower compared to B05 and B30. These aspects will be approached in more detail in *Chapter 5* when ignition delay will be considered. Plot (c) shows how ambient temperature increases by decreasing air density, i.e. by decreasing the trapped mass in the cylinder. Again, plot (d) enables the comparison on a temperature increase basis between LT, NO, and HT conditions. Results of ignition delay are consistent but the rate of temperature increase seems quite independent from the temperature starting level. To summarize, despite the large volume, the in-cylinder temperature increase produced by combustion ($\sim$100 K) is significant respect to the temperature sweep proposed in the text matrix, and should be accounted for further analysis.

3.6. Optical diagnostics applied to spray analysis

According to the general methodology introduced in Section 3.2.2, most of the experiments performed in this work correspond to stages 2 and 3 and

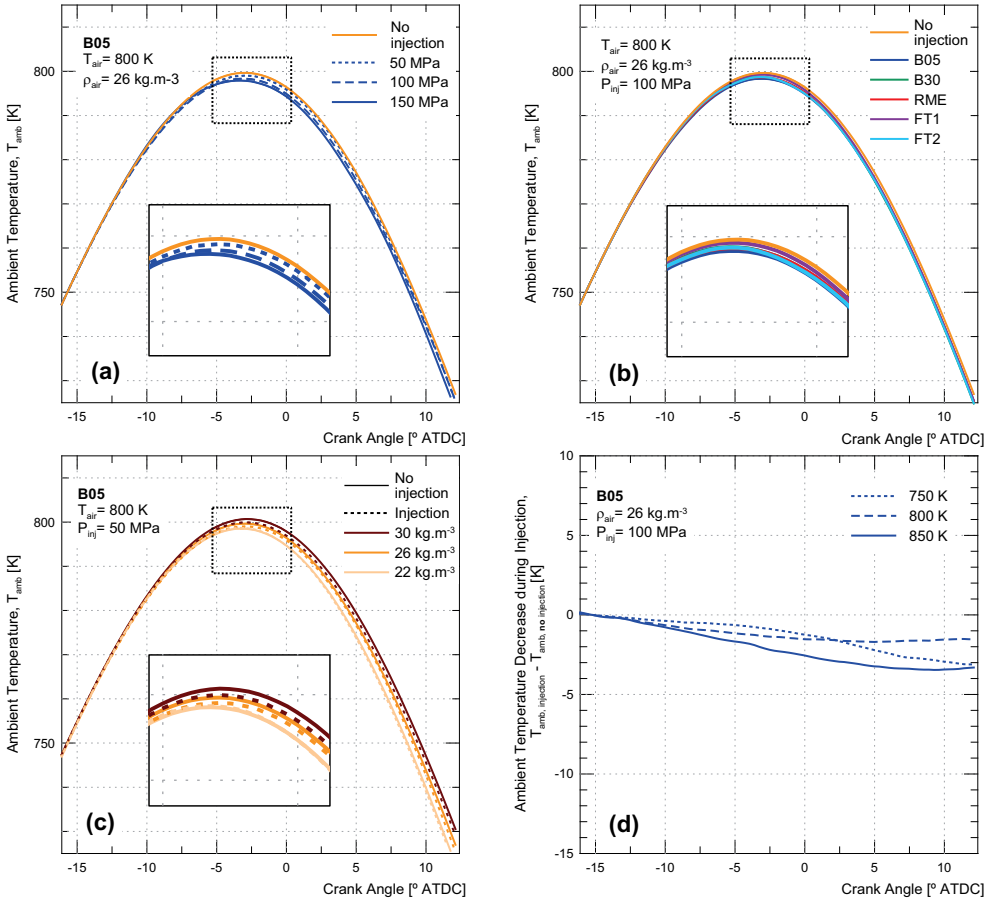

Figure 3.18. *Variation of the in-cylinder temperature with injection under inert conditions. (a) Effect of injection pressure. (b) Effect of fuel type. (c) Effect of maximum ambient density. (d) Effect of maximum ambient temperature.*

have involved the operation of the present test rig, respectively under inert and reacting conditions, with the aim of producing a high-temperature, high-density environment required to produce Diesel-like sprays, and proceed to their diagnostic with optical techniques.

At that point, it may be worth to recall the initial objectives of each stage. Stage 2 aims at covering the purely physical processes, by comparing the relevance of physical variables associated to fuel properties with those typically handled in the range of operation of a Diesel engine. Part of this stage has

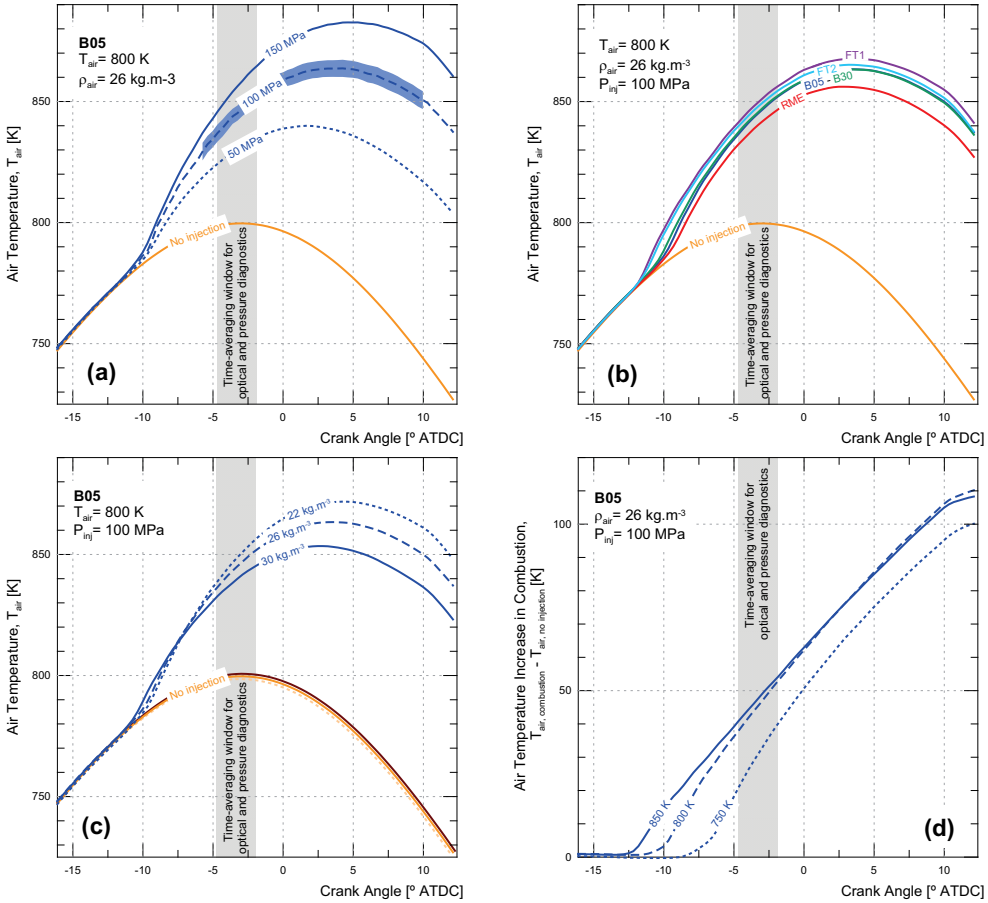

Figure 3.19. *Variation of the in-cylinder temperature with injection under reacting conditions. (a) Effect of injection pressure. (b) Effect of fuel type. (c) Effect of maximum ambient density. (d) Effect of maximum ambient temperature.*

been completed with the assessment of fuel effect on the injector performance, leaving the work on inert sprays yet to be done. Stage 3 adds chemistry to the latter processes by switching nitrogen with air, while repeating the thermodynamic and injection conditions of stage 2. The objective is to extract and assess the component of fuel chemistry with regard to combustion, in order to better understand results of exhaust emissions in production engines.

Accordingly, two optical arrangements have been designed and operated successively. The first setup, labeled "spray mixing and evaporation

setup" is rather simple, involving the unique technique of Mie-scattering imaging collected at high-speed with the purpose of measuring liquid-phase penetration. The initial planning of this stage also included schlieren imaging but difficulties associated to ambient gas flow turbulent structures impeded its use. Thus, the work could be completed during an internship at Sandia National Laboratory, California. Although with a different facility and different fuels, the study permitted to obtain conclusions of interest, extendable to this study. The second optical setup, labeled "combustion and soot formation setup", is more complex involving three techniques operated simultaneously, namely visualization of OH-chemiluminescence, time-resolved laser extinction and 2-color pyrometry imaging. Such techniques permitted relevant insights into processes governing ignition, soot formation and flame temperature. In this case, too, the work has been completed with additional experiments performed during an internship at Meiji University, Japan. Following this introduction, the details relative to these optical techniques are approached with the following outline: First a brief summary of the technique fundamentals is given; then the optical arrangement is presented; and finally details of the post-processing are provided.

Please note that the details relative to the facilities and arrangements of the experiments performed during both internships will not be presented in this chapter, in order to keep the focus into the core of the experimental strategy. Still, the reader will be referred to the publications corresponding to these works where further information can be found. Thus, only the results which present an interest for the present study will be provided in the following chapters.

3.6.1. Spray mixing and evaporation setup

In wave optics, Mie theory, or more precisely the solution of Lorenz-Mie, is a particular solution to Maxwell's equations quantifying light scattering by spherical particles under the hypothesis of kinetic energy conservation (elastic scattering). It applies for particles larger than one tenth of the incident wavelength and stands that most of the incident light is projected forward, i.e. following the same direction as that of the incident wavelength. In opposition, Rayleigh scattering applies for particles much smaller than the wavelength (molecular scale) and diffuses light in a more homogeneous way. Therefore, when a Diesel spray is illuminated, formed by liquid droplets which vaporize as they progress inside the chamber, both regimes coexist, light being Mie-scattered by the liquid phase and Rayleigh-scattered in the vapor region.

However, it is not so much the differences in regard to direction conservation that is leveraged, if not the scattering amplitude. When the spray is either lit from the front as in [23], or backlit with a diffuse background, the small portions of respectively Mie-scattered reflection and refraction are significant enough to identify the liquid-phase as shown in Figure 3.20.

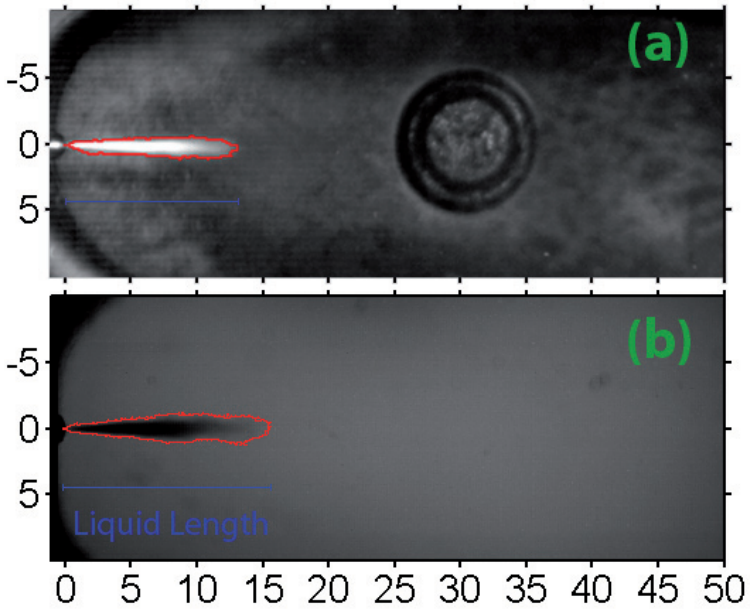

Figure 3.20. *Mie-scattering images of the liquid portion of the spray obtained with direct illumination (a) and back-lightening (b).*

In the present work, the backlit background option was selected. The shadow left by Mie-scattered light from liquid droplets on a diffuse backlit background was collected by a high-speed camera at 8000 fps. As displayed in the optical arrangement of Figure 3.21, illumination was provided by two 150 W quartz-halogen illuminators (Dolan-Jenner PL800) and supplied by 8 mm liquid light guides positioned at 60 mm from the diffuser. Images of the spray were collected by a high-speed CMOS camera (Photron Fastcam-Ultima APX) equipped with a $f/2.8$ lens of 55 mm focal length. Exposure time was limited to 25 μs in order to freeze the spray as much as possible while maintaining a reasonable level of background for contrast. Although such exposure time enabled higher frame rates (up to 40000 fps), the frequency of image acquisition was kept to a relatively lower rate in order to preserve a reasonable spatial resolution (8.9 $pixels/mm$). The camera bit depth was 10

bits, thus providing a discretization of digital intensity with 1024 grey levels. The camera triggering was synchronized with the injector electronic start of injection (SOE). At each injection event, 100 pictures were collected, therefore covering a time range of 12.5 ms from SOE. Each test of the matrix has been repeated 10 times, leading in consequence to a total of 750 injections for the whole study (5 fuels $\times$5 operation conditions $\times$3 P_{inj} $\times$10 injections).

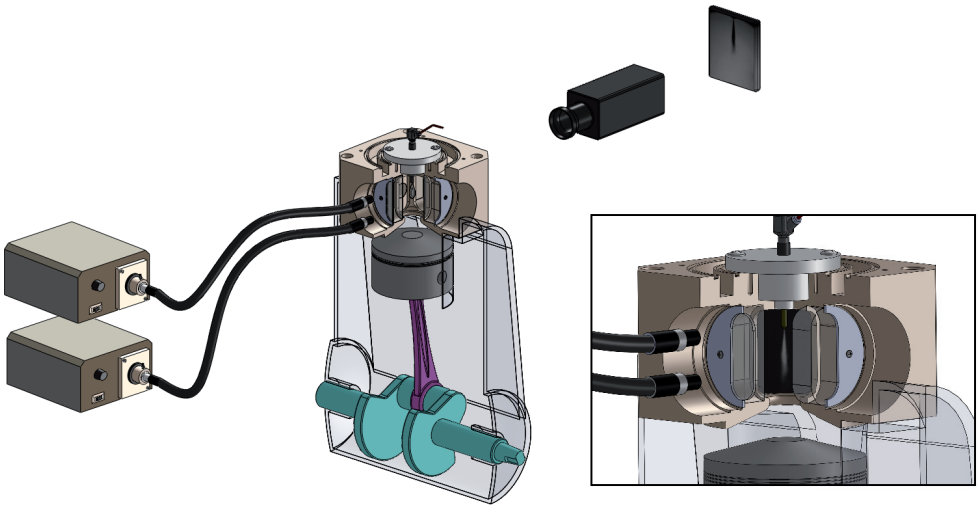

Figure 3.21. *Spray mixing and evaporation optical setup.*

Spray images were later processed by means of a purpose-made algorithm whose output was the measure of the maximum liquid-phase penetration (or liquid length) as shown in Figure 3.20. Such algorithm is extensively described in [25, 26], so only a brief summary will be provided here. Figure 3.22 shows the different steps of the image processing and will serve as the support of the following description.

The routine starts with the background withdrawal, which typically results from the average of several images (a) picked during the first instants prior to the spray emergence. Subtraction of the averaged-background (a) to the original images (b) yields images (c), while removing reflections from the injector and other unwanted interferences (background inhomogeneities, windows reflections, etc.). Note that although (a) and (b) are issued from a direct illumination setup, the resulting image (c) with backlit spray images (a) and (b) is equivalent in absolute values. Once the background removed, a threshold is calculated based on a statistical analysis of each c-type images

and used for their segmentation. The analysis is based upon the principle that images of diesel sprays can be considered as a set of pixel values, each of which belonging to one of two classes according to its digital level: either to the diesel spray itself or to the background. Following this approach, image segmentation can be considered as a classification problem. The discriminant function of the Likelihood Ratio Test (LRT) algorithm for the probability-density functions representing both classes is a quadratic form which minimum gives the optimal decision boundary between the background and the diesel spray distributions. Binary image (d) shows the result after completion of the threshold comparison. Still, some undesirable pixels which do not belong to the spray survive the segmentation. Thus, a connectivity function is applied by checking the connection between neighbour pixels. Only those connected to the centre of mass are finally considered as belonging to the spray as shown in (e). Finally, the distance between the injector tip and the front part of the detected boundary is considered as the maximum liquid-phase penetration and converted into metric-base using the $pixel/mm$ relationship.

3.6.2. Combustion and soot formation setup

Under reactive conditions, a tailored optical setup was designed to measure both soot concentration and temperature while including additional diagnostics aiming at understanding the origins of the potential differences detected when varying either the fuel type or ambient conditions. Thus, the core of the optical arrangement consisted of a laser extinction setup to quantify punctually and precisely soot concentration (KL); and 2-color imaging providing both soot concentration and temperature in the camera line-of-sight. Along with the objectives regarding the fuel effect, the association of these two measurements also offered the opportunity to compare KL measurements of each technique, and possibly employ the more accurate extinction measurement as a reference to calibrate that of the 2-color. To seek further insights into the combustion processes involved, intensified OH-chemiluminescence imaging and further analysis of the pressure signal completed the previous diagnostics operated in this study. They enabled to measure respectively lift-off length and ignition delay. Also, the rate of heat release could be obtained as suggested in the previous section discussing thermodynamic conditions stability. These diagnostics were all applied simultaneously during all the injection events, creating a large dataset first, but above all, it permitted to extract information from the cycle-to-cycle dispertion. For each combination of fuel, operating condition and injection pressure, 100 injections were performed, making a total of 7500 injections.

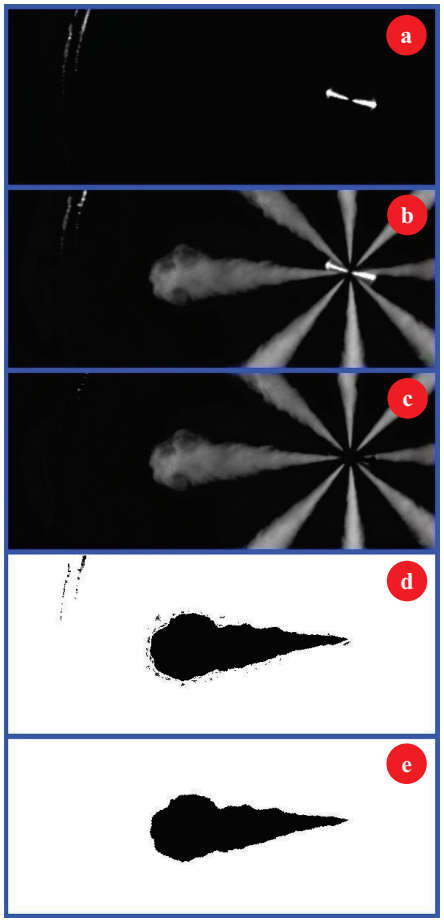

Figure 3.22. *Processing steps of Mie-scattering images. (a) Background image, (b) Spray image, (c) Subtraction of background to spray image (c=b-a), (d) Post-segmentation binary image, (e) Post-connectivity binary image.*

While OH-chemiluminescence, in-cylinder pressure and 2-color sequences were equivalent for the 100 injections, laser extinction moved along 10 flame axial positions and measurement repeated 10 times. The complete optical arrangement is presented in Figure 3.23.

3.6.2.1. Ignition delay and rate of heat release

Acquisition of the in-cylinder pressure was enabled by a pressure transducer (Kistler 6125B) and recorded at a sampling frequency of 100 kHz

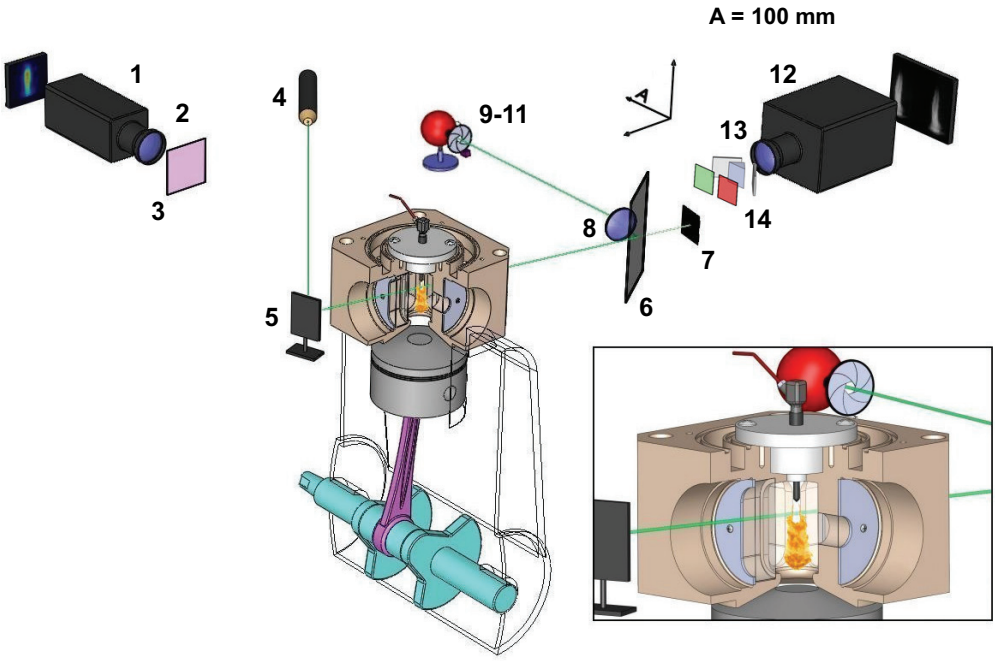

Figure 3.23. *Optical setup of the simultaneous OH-chemiluminescence and laser extinction techniques. 1: ICCD Camera ; 2: UV lens f=100 mm, f/2 ; 3: 310 nm-bandpass filter (FWHM=11 nm) ; 4: Argon-Ion laser ; 5: Mirror ; 6: Beam-splitter; 7: Beam-stop; 8: 50 mm diameter lens (f=250 mm) ; 9: Diaphragm ; 10: 514.5 nm-bandpass filter (FWHM=3 nm) ; 11: Integrating sphere ; 12: High-speed CMOS camera ; 13: lens f=60 mm, f/1.8 ; 14: Stereoscope.*

via a Yokogawa DL716E. Such 10 μs resolution was required to make an accurate measurement of ignition delay. To this end, ignition delay was obtained for each of the 100 cycles by subtracting to the combustion cycle an average of the following and corresponding motored-cycles. Then, the pressure difference (ΔP) was first geometrically-filtered using the Savitzky-Golay method [27], and differentiated as plotted in Figure 3.24. Ignition delay was defined as the first instant exceeding three times the standard deviation of the time-average performed on the first 500 μs (for information, hydraulic delay was about 350 μs). The results for B05 at NO condition and 100 MPa injection pressure are represented with gray lines under their corresponding $\mathrm{d}\Delta P/\mathrm{d}t(t)$. The intention with the corresponding threshold was to detect the ignition delay as it has been defined by Ikegami and Kamimoto [28], namely the time of heat release recovery from the fuel vaporization heat consumption.

Regarding the average ignition delay τ, it was not the result of an average itself, but that of the same sigma-criteria applied to the derivative of the pressure difference between injected and non-injected averaged cycles. The average combustion cycle was the average result of 100 combustion cycles, while that of motored-cycles resulted from 200 cycles proceeding from the third and fourth cycles after combustion. As previously mentioned, the first two cycles following the injection were systematically removed because of scavenging issues. The average of both combustion and motored cycles were calculated through a robust average algorithm using iteratively reweighted least-squares (*Matlab robustfit* function) [29–32] to remove the influence of outliers such as potential failure in the recording.

With the information of instantaneous mass in the cylinder, the pressure increase was converted to heat release applying the first law of thermodynamics (Cf. Eq. 3.10). As for the ignition delay, the heat release was calculated for all cycles, but the average-RoHR was the result of calculations from the robust average of both combustion and motored-cycles. The result shows a small decrease at the beginning because of fuel evaporation, followed by premixed burn which slowly decreases and tends asymptotically to a purely diffusive mode in the last instants, namely a point at which burning rate equals the injection rate. As stated in the previous chapter, the significance of the premixed burn varied strongly depending on fuel reactivity and ambient conditions, i.e. on the fuel amount mixed prior to ignition. These aspects will be approached in more details in *Chapter 5*.

$$RoHR = m \cdot c_{v,air} \cdot \frac{\mathrm{d}\Delta T}{\mathrm{d}t} + \Delta P \cdot \frac{\mathrm{d}V}{\mathrm{d}t} \tag{3.10}$$

with

$$\begin{aligned} c_{v,air} = &-10.4199 \cdot \sqrt{T} \;+\; 2522.88 \;-\; 67227.1 \cdot \frac{1}{\sqrt{T}} \\ &+\; 917124.4 \cdot \frac{1}{T} \;-\; 4174853.6 \cdot \frac{1}{T^{1.5}} \quad [\frac{J}{kg.K}] \end{aligned} \tag{3.11}$$

3.6.2.2. OH-Chemiluminescence

As a reminder of *Chapter 2*, some of the free radicals released during hydrocarbon oxidation can be raised to an excited electronic state by exothermic reactions. The decay from this short-lived state down to groundstate equilibrium produces their chemiluminescence. In particular, OH-chemiluminescence (306 nm) showed to establish as a thin layer surrounding

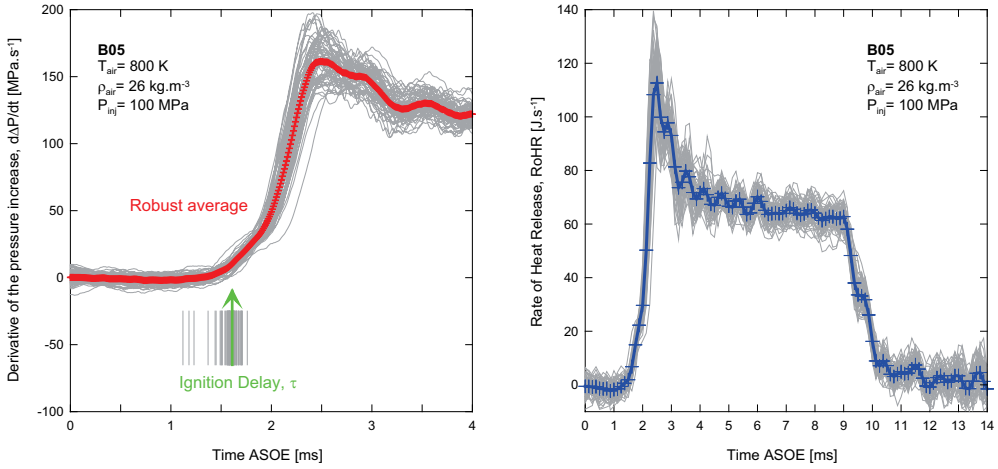

Figure 3.24. *Example of pressure analysis for B05 at 800 K, 26 $kg.m^{-3}$ and 100 MPa injection pressure. On the left, the derivative of the average pressure increase (at high frequency) is represented with the resulting ignition delay. On the right, the corresponding rate of heat release is represented during the whole injection event.*

closely the stoichiometric surface. In the literature, visualization of this exited radical has been widely used to determine the lift-off length, namely the distance between the injector and the first region of high-temperature combustion, in order to characterize the level of air/fuel premixing upstream the flame. Thus, line of sight images of the flame filtered at 310 *nm* were collected to visualize the stoichiometric surface and measure the flame lift-off position relative to the injector for the 7500 injections of this study. A gated 16-bit ICCD camera (Lavision Dynamight) equipped with a 100 *mm*, $f/2$, UV lens was triggered 4 *ms* after the start of injector energizing (ASOE) and acquired one frame per injection cycle. This 4 *ms* delay was selected after preliminary tests using high speed images had shown that the flame required a maximum of 3 *ms* to reach its natural flame length. With this setup, the diffusion flame was then fully established at the time the image was taken. The intensifier gatewidth was set to 1 *ms* and the gain adjusted ($\sim$70 %) to maximize the use of the dynamic range while avoiding image saturation and potential damage to the intensifier. This 1 *ms* range, as enclosed in Figure 3.19, intended to be a good compromise, accounting for thermodynamic variations of cylinder conditions while being representative of the combustion event. Therefore, because it was the unique diagnostic that was not time-resolved, but also because of the major role of lift-off expected over the combustion

process, this 4 to 5 ms ASOE window will be the reference from now on for the rest of diagnostics when time-averaged values will be considered.

Regarding image processing to yield the lift-off length, it was similar to the methodology employed by Higgins *et al.* [33]. Due to its "double-lip" shape, the flame was divided axially and each half-flame was processed independently. Thus, the closest pixel to the injector which exceeded the threshold value (12 % of the camera dynamic range) was considered. Flame lift-off length was the average of the distances between the injector and each point, converted to millimeters with the image resolution of 8.4 $pixels/mm$. Representative samples issued from the dataset of processed images are shown in Figure 3.25.

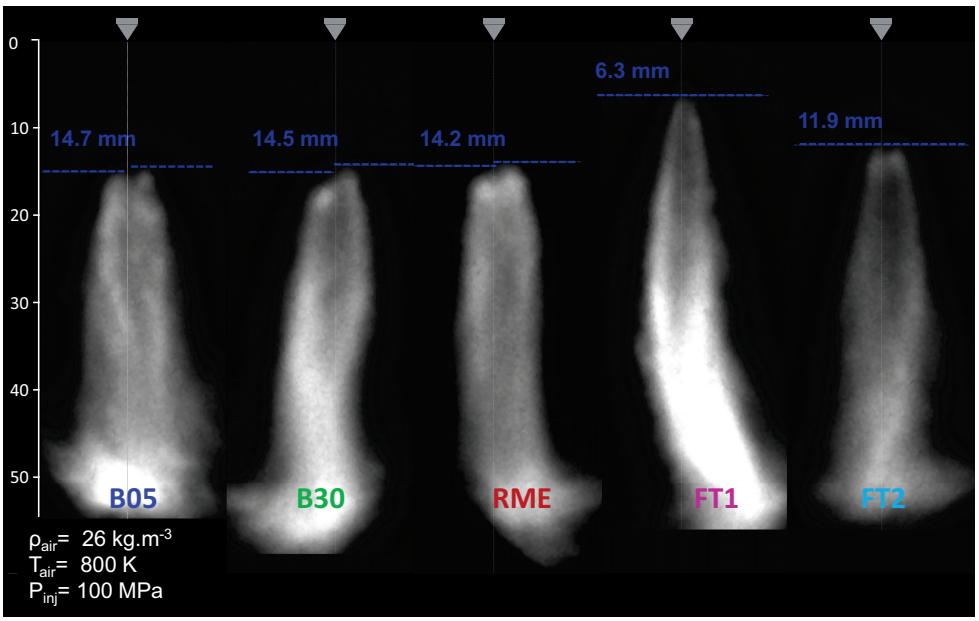

Figure 3.25. *Fuel comparative samples of OH-chemiluminescence images with the corresponding result of lift-off image processing.*

3.6.2.3. Laser extinction

The laser extinction measurement is the quantification of a laser beam attenuation as it goes across an absorbing and scattering medium such as a soot cloud. Since a Diesel flame can be likened to a locally-incandescent soot cloud itself, this technique appears as a key tool to quantify its inner soot volume fraction (f_v). The Beer-Lambert's law relates the transmittance τ,

namely the ratio between the transmitted intensity (I) and the baseline intensity of the incident beam (I_0), with the absorbance $K_{ext}L$ (also called optical density) of the soot aerosol by means of the following relationship [34]:

$$K_{ext}L = -ln\ \tau = -ln(\frac{I}{I_0}) \tag{3.12}$$

In Eq. 3.12, L is the path length through the cloud and K_{ext} is the extinction coefficient averaged along the latter. In other words, this dimensionless number is the difference of magnitude orders between both the up- and downstream signal intensities but remains a priori quite an empirical approach. By way of comparison, the optical density in base 10 (OD) is typically used to characterize optical filters or laser safety goggles (OD=3 glasses divide by a 1000 the incident light at the wavelength specified). Both values of $K_{ext}L$ and OD are therefore related by ln(10) such as $K_{ext}L$ ~2.303·OD. Provided that the optical and physical properties of the soot material are known, the KL-extinction can be converted into soot volume fraction through the Bouguer's law [2], that is, a function of soot volume fraction (f_v), light wavelength (λ) and a dimensionless extinction constant (k_e) integrated along the flame diameter ($L = 2R$):

$$K_{ext}L = \int_{-R}^{R} \mathrm{f_v} \cdot \frac{k_e}{\lambda} \cdot dr = \int_{-R}^{R} \mathrm{f_v} \cdot \frac{k_a \cdot (1 + \alpha_{sa})}{\lambda} \cdot dr \tag{3.13}$$

If at first sight, only the wavelength is known beforehand, a priori the flame diameter can be reasonably captured with imaging. However, the complexity of that conversion relies in the estimation of k_e which includes both absorption and scattering properties of soot. Accordingly, the dimensionless extinction constant (k_e) can be rewritten in Eq. 3.13 as a function of the dimensionless absorption coefficient (k_a) and the scattering albedo (α_{sa}), also referred to in the literature as the scattering-to-extinction ratio. Under the Rayleigh regime for small particles, both these components can be estimated from the particle diameter and the refractive index, being the latter a complex number whose real and imaginary parts account respectively for scattering and absorption. Though, as remark Musculus *et al.* [35] and Williams *et al.* [36], it has been common practice to set k_a=4.9 and α_{sa}=0 given that absorption clearly dominates scattering in the Rayleigh regime. This assumption seemed

[2] This law is actually the result of August Beer's work who published in 1852 an extension of Eq. 3.12 by including the concentration and material properties. Bouguer was actually the first author of Eq. 3.12, but his name had disappeared, although properly quoted and referenced by Lambert. Still, this reverse reference is conscientiously conserved to be consistent with the current literature on the subject.

justified as primary particles of soot are typically small (d∼30-50 nm) in comparison with the light source wavelength. Such assumption of all-absorption extinction held until the works of Choi *et al.* [37] showed that k_e could not be accurately predicted from the Rayleigh limit expression with any of the standard literature values for soot refractive index. Indeed, as primary particles start to form aggregates, scattering becomes significant as suggested in [36–39]. Therefore, as the laser sees a mixture of particles governed by both regimes of Rayleigh and Mie, k_a and α_{sa} vary significantly in consequence. Following Choi's result (k_e=8.6 universally), several works involving diverse configurations of atmospheric laminar flames and laser wavelength proposed other evaluations of k_e (as a whole) with results typically in the range of 8 to 10 [36]. Williams *et al.* [36] showed recently that value of k_e could be as low as 2 in some situations of important soot precursors condensation and absorption (experimental issues). As reviewed in *Chapter 2*, this component is also very present in Diesel flames and could potentially have an effect. Nonetheless, the most recent works involving Diesel-type flames use a value of 8.7 at 632.8 nm (HeNe laser) [40–42].

In this regard, a collaboration between Sandia National Lab., Meiji University and CMT-Motores Térmicos permitted to provide further insights into these issues in the specific context of Diesel flames. *Via* an innovative experimental protocol [40], it was achieved to study the morphology of soot particles sampled from the inner part of diesel and biodiesel flames. Particles were collected intrusively with a grid placed at different axial locations, then observed with TEM imaging (Cf. Figure 3.26) and measured by means of image post-processing. More details and discussions about this technique may be found in [40, 43, 44] while further results will be provided in *Chapter 5*. Figure 3.27 shows the resulting histograms for the primary particle size, aggregate radius of gyration (as an image of the particle size) and mass for both a conventional US diesel (♯2) and a soy-methyl ester biodiesel at 50 mm from the injector. This position (∼middle-flame) corresponded to the core of soot where the number of particles, and in particular agglomerates, was maximum. The size of primary particles appeared to be in the range suggested above and was similar between diesel and biodiesel, independently from the fact that they were isolated or issued from agglomerates. Although the amount of soot collected was lower for biodiesel, the distribution of particles size appeared to be similar as well, while being dominated by primary particles (∼20 nm) and small aggregates. Though, it is to note that in terms of mass and volume, larger aggregates rebalanced the histograms and revealed the relevance of larger aggregates, particularly for biodiesel. At the laser wavelength used in this study, the α_{sa}=0 condition would be valid for particles inferior to 57 nm

($2\pi R_g/\lambda < 0.7$). As a conclusion, while a quantitative relationship between $K_{ext}L$ and soot volume fraction remains affected by small uncertainties in the soot optical properties due to the presence of agglomerates, a relative comparison between these two fuels, and by extension between the five fuels of the present study, should be valid since the soot optical properties are not expected to change significantly. Regarding the path length (i.e. the flame width), it varies during the combustion event but could not be easily measured in the current study. Besides, although flame width may vary when modifying either fuel stoichiometry or air density, differences among fuels and operating conditions should be small. Therefore, experimental results for the extinction diagnostic may be evaluated directly from the $K_{ext}L$ data. Accordingly, the quantity $K_{ext}L$ will be used as the metric to quantify soot measurements in the current study.

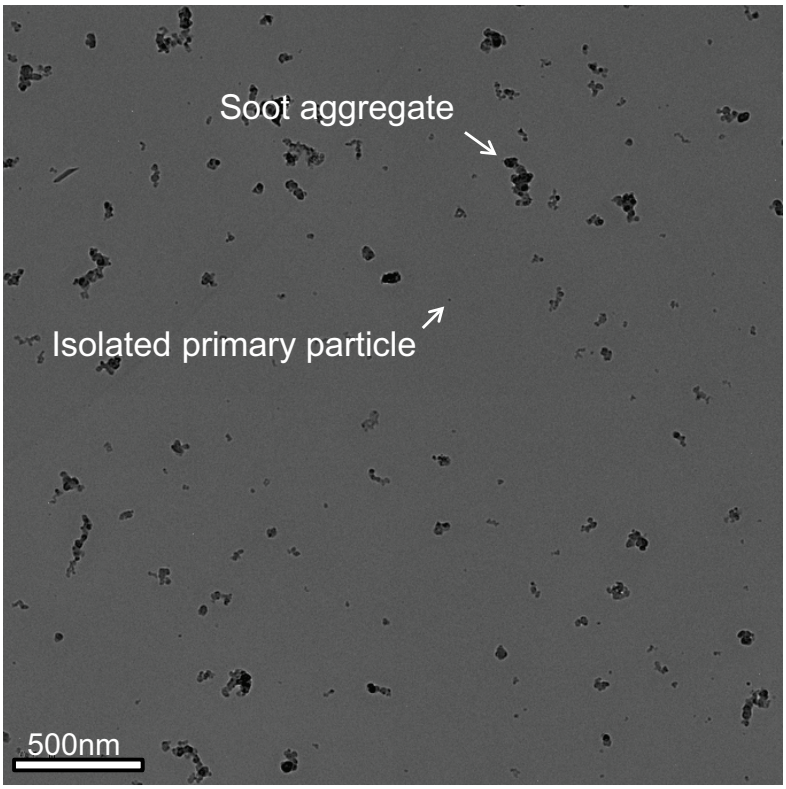

Figure 3.26. *TEM image of soot particles sampled in a biodiesel flame (×6000).*

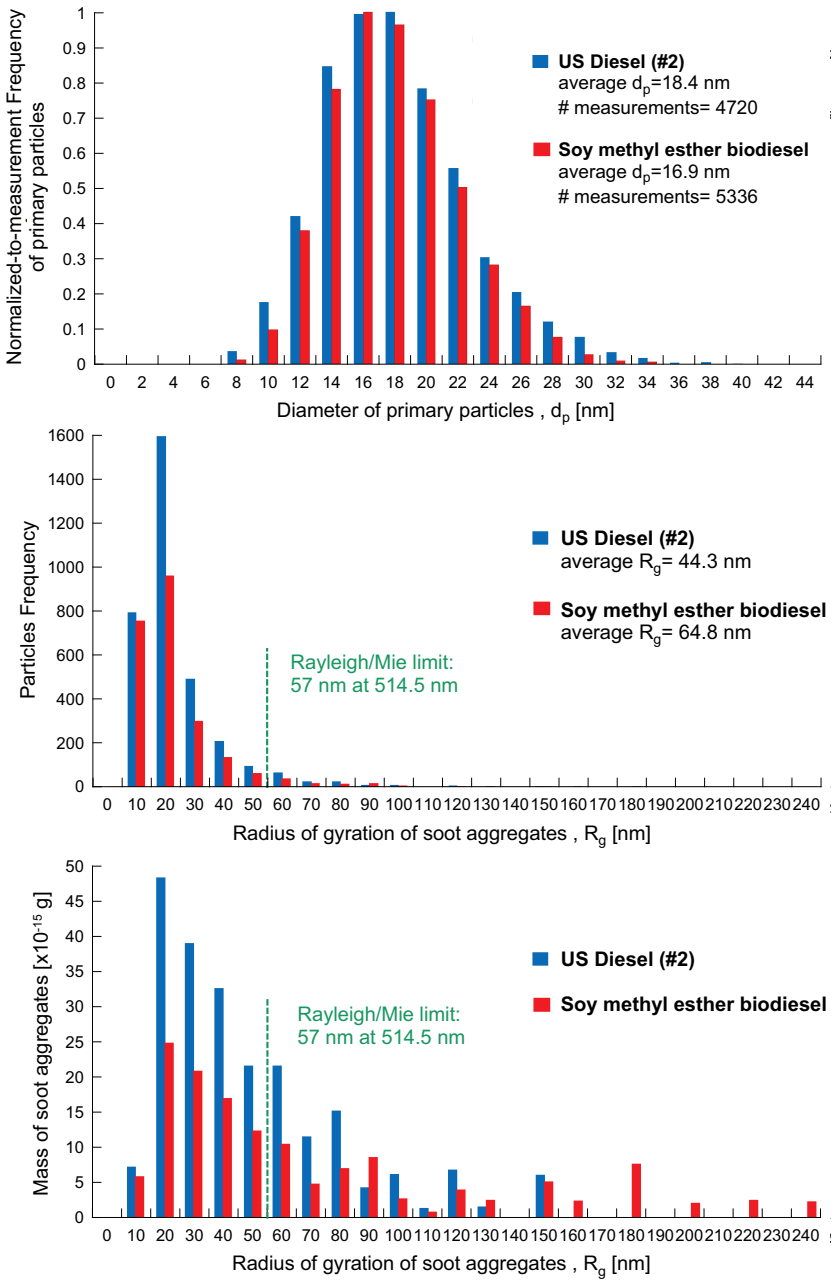

Figure 3.27. *Histograms of primary particles size, particles radius of gyration (size) and mass sampled inside the flame at the most soot-favorable axial position (50 mm).*

Thus, in the experimental framework defined in Section 3.2, measurements of flame opacity have been realized by focusing and passing a $2W$-Argon-Ion (514.5 nm) continuous-wave laser through the fuel jet centerline at different axial positions. At the engine exit, it was deflected by a beam-splitter, collimated by a lens, filtered at 514.5 nm (FWHM=3 nm) and collected by a 100-mm-diameter integrating sphere as shown in Figure 3.23. A diaphragm was placed upstream the filter at approximately 20 mm from the integrating sphere in order to control the collection angle. Note that a beam-splitter was installed instead of a conventional mirror in order to open an optical path to the high-speed 2-color imaging system. Finally, a photodiode mounted on one of the sphere ports and connected to a high-speed amplifier, measured the ambient intensity within the sphere at 100 kHz frequency.

Beyond the soot properties issues approached above, the application of laser extinction in a Diesel environment implies numerous issues and considerations to account prior to any experimental work. Those have been exhaustively and outstandingly reviewed in the work of Musculus *et al.* [35] which served as the reference for the diagnostic implementation and setup of the current study. Accordingly, two major issues have been identified: (1) the so-called "beam steering" induced by the refractive index gradients met along the laser path; (2) the contamination of the transmitted laser signal (I) with the collection of flame luminosity.

Starting with beam steering, the authors explain that *"gradients in temperature, density, or mixture composition [...] can cause gradients in the index of refraction across the width of the extinction beam. Such refractive index gradients deflect the beam as it passes through the combustion chamber. If this "beam steering" causes a portion of the transmitted beam either to be translated to a region of different sensitivity in the detection system or to miss the detector entirely, the resulting change in signal can be interpreted incorrectly as the result of extinction by soot"*. This effect is yet the justification for using an integrating sphere in the arrangement as it enables a reliable measurement of the laser intensity independently from the laser incident angle. However, not all the transmitted light must be collected. As suggested in the first part of this section, soot primary particles may coagulate to form aggregates for which scattering component can be significant. Since the extinction diagnostic accounts for both absorption and scattering, the collection of scattered light may produce an apparent $K_{ext}L$ that is less than the true $K_{ext}L$. Therefore, spatial filtering *via* a diaphragm must be implemented to control the collection angle of the transmitted laser beam. The latter must be properly addressed as it represents a cornerstone for the success of the measurement. It must be set to a value large enough so the

diaphragm do not clip the natural laser deflection (non-caused by soot), while being restrictive enough not to be contaminated by scattered light from soot aggregates. By using a similar methodology as followed in [35], beam steering was measured by high-speed imaging the transmitted beam projection onto a screen. The laser was placed at 50 mm from the nozzle exit and injections of B05 were performed under the 15 combinations of operating conditions and injection pressure defined by the initial test matrix. These appeared to include both non-sooting and highly sooting conditions. Under injected conditions, the core of the laser projection oscillated around the central (and fixed) position defined by motored conditions as shown in Figure 3.28. This effect, caused by the random incident angle between the laser and the spray turbulent surfaces, was also observed in [35] and appeals to consider a "full-angle", i.e. two times the measured angle to account for the direction uncertainty. In the processing of high-speed imaging sequences, only the instant of maximum deflection was considered and quantified. Figure 3.29 shows the result of those beam steering maximum values for the different operating conditions. First, it is to remark that they were slightly higher for the high injection pressure condition, and more generally that no correlation emerged with the sooting level (as a reminder, soot formation is enhanced by high temperature, high density and low injection pressure). Although scattered light from large particle is mostly scattered forward (the 120 $mrad$ forward angle, i.e. 0.1 % of the steradians of a sphere, contains 17 % of the scattered light [35]), such opposite trend rather confirms that beam steering is not dominated by soot. The maximum beam steering was 62.7 $mrad$ for the HD condition at 150 MPa, in agreement with the temporal maximum ($\sim$70 $mrad$ at 10 CAD) obtained in [35]. Accounting that the latter value was ensemble-averaged, beam steering in the present study can be considered as slightly smaller, which could be the result, amongst other things, of the smaller orifice diameter used (smaller flame scale and smaller path length), the lower laser wavelength, and possibly the lower density and temperature conditions.

Although 62.7 $mrad$ was the maximum beam-steering measured, the collection angle has been in practice set to 80 $mrad$. The motivation for that choice is also documented in the study of Musculus *et al.* [35] where the scattering component and subsequent error introduced by extremely large aggregates (40 nm primary diameter and 1000 primaries per aggregate) are calculated using the Rayleigh-Debye-Gans (RDG) theory. While varying the collection angle from 40 and 120 $mrad$, the error on the $K_{ext}L$ measurement because of scattering collection increases linearly from 0 to 4 %, that is, significantly less than the error committed if the beam is clipped by a too restrictive collection angle. Thus, although the authors evaluate beam steering

between 70 and 100 *mrad* through different measurement techniques, they actually recommend increasing the collection angle up to 120 *mrad* in order to fully accommodate beam steering and thus erase the risk of beam clipping for smaller collection angles.

As a final check, the 80 *mrad* angle was examined, similarly to [35], by measuring the laser extinction right at the flame tip of a sooting flame, and in the core of a flame with the lowest possible sooting propensity enabled by the rig. The lowest intake temperature, namely $40°C$ (equivalent to 727 K following the regression of Figure 3.13), lowest intake pressure (1.5 *bar*) and high P_{inj} (150 MPa) were set. Although the latter was probably soot-free, no LII measurements could actually confirm the statement. Still, under both circumstances, no differences were detected between fired and motored cycles, thus validating the previous assessment.

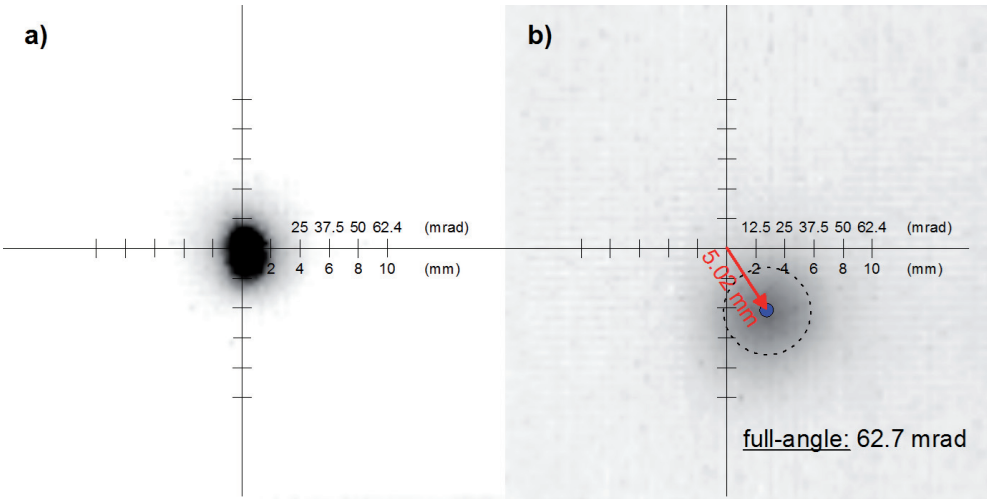

Figure 3.28. *Images of the laser projection onto a screen under (a) motored- and (b) injected-conditions (B05 at HD condition and P_{inj}=150 MPa).*

Once with diaphragm and collection angle adjusted, the second major issue identified above could be considered, namely the signal contamination due to the collection of light proceeding from soot radiation. Indeed, beyond the settlement of beam steering issues, the diaphragm also plays a key role in rejecting broadband combustion luminosity. If the collection angle was apparently increased generously to fully accommodate beam steering, the operation was actually made sparingly in order not to underestimate the real $K_{ext}L$ with collection of improper light from soot radiation. In addition to the

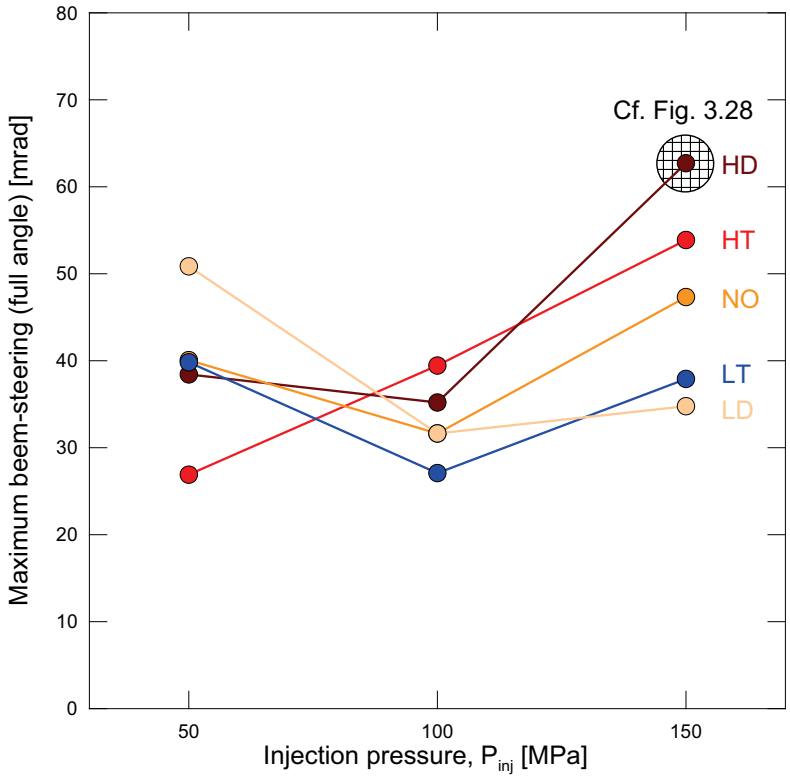

Figure 3.29. *Maximum beam steering at each operating conditions for B05 (measured from laser projection onto a screen).*

diaphragm, a 514.5 nm filter (FWHM=3 nm) was situated at the entrance of the sphere, downstream the iris, with the same purpose. Despite such care taken in filtering spatially and interferentially the collected light, Musculus *et al.* [35] and Pickett *et al.* [45, 46] observed a residual component of soot radiation. At that level, the issue becomes technically challenging to resolve. As such, the flame luminosity component is quantified along the combustion event by making the laser blink at very-high frequency with either a cog-wheel or an acousto-optic modulator (also called Bragg cell). The flame intensity is then measured with the laser off, interpolated, and finally subtracted from the raw intensity (with the laser on) to correct for background flame luminosity. In the arrangement of Figure 3.23, the Argon-Ion laser employed was quite more powerful (2 W) compared to the 10-mW HeNe laser employed in [35, 45, 46]. Once the amplification system was adjusted with the laser power set at its maximum value, soot-rich injections (B05 at AT condition and 50 MPa

injection pressure) were performed with the laser off to quantify the signal fouling. The system showed not to be sensitive to any of the flame radiation. Therefore, by using a slightly smaller collection angle and a more powerful laser requiring less amplification, there was no need to quantify the component of flame luminosity from the collected intensity, which simplified both the optical setup and the post signal processing.

Several other issues that were approached in the study of Musculus and Pickett [35] have been either accounted *per se* or disregarded because they would not apply in this configuration. For instance, engine windows were not subject to soot deposition by thermophoresis. The design of the cylinder-head and the respective orientation of the single-hole injector avoided the flame impingement on the windows. Finally, the authors also discuss the optical properties variations of the window materials due to photo-elastic responses to thermal and mechanical strains which include Fabry-Pérot interferometry, index of refraction variations and birefringence. As recommended, these issues were accounted by making the laser beam enter with a small incident angle respect to the windows faces ($\sim 1^{\circ}$). Optics insensitive to the light polarization state were used while the laser initially with a 3 mm diameter approximately at the optics fiber exit was focused at 3 meters and reached 1 mm diameter in the spray axis region ($\sim 0.076^{\circ}$ full angle).

Tests have been performed for each fuel under the entire test matrix presented above. The laser was moved along the flame centerline from 15 mm to 60 mm to the injector every five millimeters as shown in Figure 3.30. At each axial position, ten injections were completed, resulting in a total number of injections equal to 7500 for the whole combustion study. The I_0 component of Eq. 3.12 was averaged from the three motored cycles following each injection event as shown in Figure 3.31. Accounting for the analog-to-digital conversion and the signal-to-noise ratio of the system, the maximum reliable $K_{ext}L$ that could be measured was 4.8. Accordingly, any calculated $K_{ext}L$ above this electronic limit was equalized to this value instead of being simply disregarded. This initiative permitted to avoid both an overestimation of the $K_{ext}L$ average based on uncertain low-intensity values but also to avoid an underestimation of the $K_{ext}L$ average because data of high sooting propensity were disregarded. Following the recommendation in [35], $K_{ext}L$ from transmittance was calculated prior to time- and ensemble-averaging the results. The apparently "common practice" consisting in averaging raw transmittance data before the calculation of $K_{ext}L$ clearly underestimates the true $K_{ext}L$ and does not respect the linearity between $K_{ext}L$ and the variable of interest, f_v, that quantifies the flame sooting propensity (Cf. Eq. 3.13). As it was suggested earlier, the window for time-averaging was that of OH-

chemiluminescence imaging, i.e. during the quasi-steady period from 4 to 5 *ms* ASOE, with the purpose to place lift-off length and soot formation measurements in the best conditions to study their cross-correlation. In a scattered environment such as the one proposed by the 10 repetitions of Figure 3.31, this proximity between diagnostics will enable to seek further information in the cycle-to-cycle analysis.

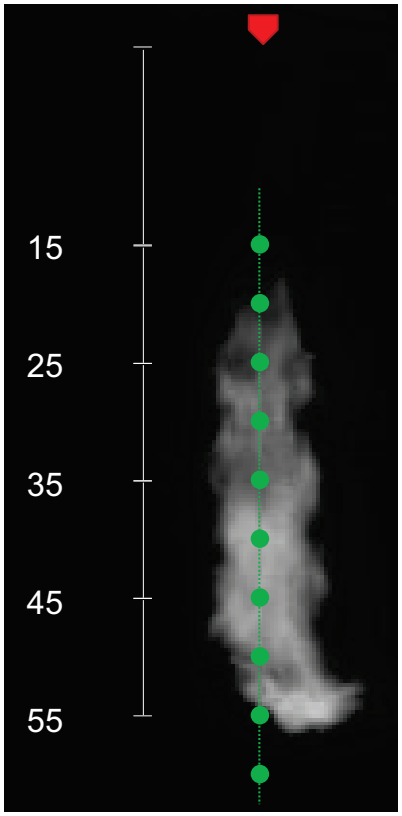

Figure 3.30. *Axial positioning of laser extinction measurements.*

3.6.2.4. 2-color pyrometry

Fundamentals: In numerous investigations, the effects of engine parameters and fuel properties [47–54] on the flame sooting propensity have been considered by using the spatial integrated natural luminosity (SINL) as a criterion to qualify their effect. Though SINL measurements can provide a qualitative measure of in-cylinder soot formation, this technique is not

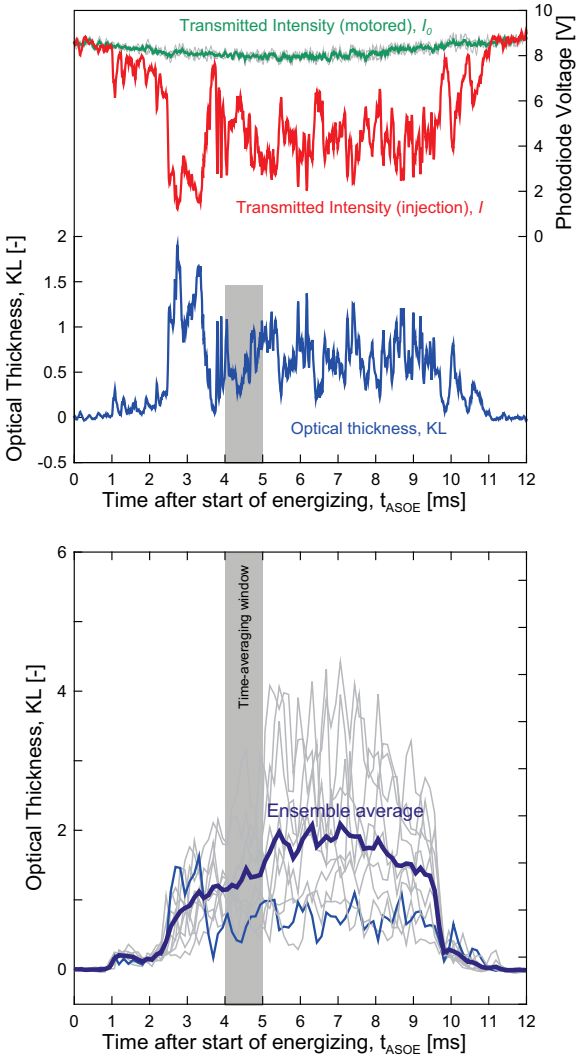

Figure 3.31. *On the top plot: Signal of laser intensity measured in Volts under motored (I_0) and injected conditions (I) for B05 at the NO condition and P_{inj}=50 MPa. Laser intensities for the three motored-cycles are plotted along with the corresponding average (I_0) and the transmitted intensity (I) of a single cycle of injection (Rep. ♯9). The result of Eq. 3.12 applied to these two signals (KL) is plotted under. On the bottom plot: $K_{ext}L$ results for the 10 repetitions are plotted with the resulting ensemble-average. Rep. ♯9 from the top plot has been highlighted. Note that for a better lecture of the figure, a running-average divided the sampling frequency by 12.5, matching by the way the image rate of the 2-color method (8000 Hz).*

quantitative for soot concentration. A decrease of the SINL is typically interpreted as a decrease of soot formation but this lecture may be uncertain considering the high dependence of this diagnostic to the soot temperature (exponent 5 to 11) while it is merely linear with the soot volume fraction [55]. Therefore, offsetting effects of soot temperature and soot volume fraction may be confounding to state on soot occurrence based on SINL. In that sense, the 2-color method appears as a way to resolve such trade-off. Based on the observation of the flame at two different wavelengths, the equations of Planck for soot emissions enable the resolution of a system of two equations accounting for both flame temperature and transparency, i.e. soot concentration. The work of García-Oliver's Ph.D. [56, 57] constituted the starting point and basement know-how with this method.

The two-color (2C) method is a technique of optical thermometry that leverages the presence of incandescent soot within a flame to provide an estimation of flame temperature. Its application is particularly relevant in a Diesel environment given that, as stated in *Chapter 2*, soot radiation dominates by far light emissions during most of the heat release period. In addition, the work of Matsui *et al.* [58] established that the temperature difference between soot particles and surrounding gases is expected to be less than 1 K. Accordingly, the measurement of soot temperature provides a valuable estimation of the true flame (gas phase) temperature.

The starting point of the 2C method is the assumption that radiation from a sooting flame depends on both the temperature and the amount of soot within the flame. This statement can be written as:

$$I_{soot}(T, K_{2C}L) = I_{soot}(T, \lambda, f_v, L) = I_b(T, \lambda) \cdot \epsilon(\lambda, f_v, L) \tag{3.14}$$

In Eq. 3.14, soot radiance I_{soot} (radiation power per unit area, solid angle and wavelength) is a function of both temperature T and soot concentration $K_{2C}L$, while $K_{2C}L$ itself is a function of λ, f_v and L as defined in Eq. 3.13. Now considering Plank's blackbody, the soot radiance I_{soot} can be expressed as the product of the radiance I_b of a blackbody brought to the same temperature (i.e. $I_b > I_{soot}$), and its emissivity ϵ. Thus, emissivity acts like an efficiency term accounting for the flame "transparency", therefore on the amount of soot it contains.

From Planck's radiation law, the blackbody radiance I_b expresses as:

$$I_b(\lambda, T) = \frac{1}{\lambda^5} \cdot \frac{c_1}{(exp(\frac{c_2}{\lambda T}) - 1)} \tag{3.15}$$

where c_1 and c_2 are constants, c_1= 1.1910439·10^{-16} $W.m^2.sr^{-1}$ and c_2= 1.4388·10^{-2} $m.K$.

For the derivation of ϵ, the classical approach for the 2-color method is used; though empirical, it expresses the relationship between $K_{2C}L$ and emissivity as follows:

$$\epsilon(f_v, \lambda, L) = 1 - exp(-\frac{(K_{2C} \cdot L}{\lambda^\alpha}) = 1 - exp(-f_v \cdot \frac{6.3 \cdot L}{\lambda^\alpha}) \tag{3.16}$$

where K_{2C} is a variable proportional to the soot volume fraction, λ is usually expressed in microns and α is a constant whose value vary according to different authors.

In his well-known review, Zhao [34] reports the value obtained by Hottel and Broughton (α=1.39) [59] which has been the reference up-to-day. Very recently, Kamimoto and Murayama [60] reexamined these issues and proposed a value of 1.38. In [61], Musculus employs a function of the wavelength α= 1.22 - 0.245·ln(λ [μm]) providing similar values in the visible range. With regard to the conversion of KL to soot volume fraction, Singh *et al.* [62] use a constant (g=6.3) issued from [63] as written in Eq. 3.16. This historical approach is the one that has been followed for the processing of 2-color images in this study.

Optical setup and calibration: In Figure 3.23, the elements 12 to 14 correspond to the 2-color part of the combustion optical setup. Flame images (256×512 pixels) were collected at 8000 fps with maximum exposure (125 μs) by using the same high-speed CMOS (Photron Fastcam-Ultima APX) as in the inert optical setup. The camera was equipped with a $f/2.8$ lens of 55 mm focal length. A Lavision stereoscope with symmetrical paths of equivalent length permitted to duplicate the image on the sensor without the necessity to rescale the flame size. Each channel of the stereoscope was filtered by means of a narrow interference filter (10 nm FWHM) centered at λ_1= 550 nm (green) and λ_2= 650 nm (red), respectively. As the red component of the flame was typically three times more intense than that of the green one, a 32 % (OD=0.5) neutral filter (not represented) was placed in front of the red channel in order to balance their intensity, and thus leverage the whole dynamic range of the camera while imaging both flames. These wavelengths have been selected in the visible range, according to the advantages commented by Payri *et al.* [57]. As shown in Figure 3.23, the camera was placed behind a beam-splitter, relatively far from the combustion chamber (∼1.2 m). This choice was in part made

because of the complex setup, but above all in order to limit the difference of point of view from each channel. As a result, very similar images were obtained offering same sizes, points of view and collection angles. The spatial resolution was 3.32 $pixel.mm^{-1}$ and the 10 bits dynamic range recorded image intensity over 1024 grey levels. From the trigger, simultaneously sent to the injector, 100 images were collected thus considering a 12.5 ms range from SOE. A raw sample image is shown in Figure 3.32. As a consequence, the number of images to be treated for the 7500 injections was considerable. For reference, 750000 images watched at 24 fps (eyes speed limit) would require 8h42 of visualization. Thus, because not all the images could be checked one by one, a special care had to be taken in the design of the processing algorithm.

In order to use the equations of Planck, the flame luminosity in grey digital levels (DL) had to be converted into spectral radiance (I). Therefore, prior to such conversion applied later in post-processing, a calibration of the CMOS sensor had to be operated. The calibration curve was obtained by energizing a tungsten-ribbon lamp (Osram Wi17G-RIP) at five electrical power conditions previously calibrated themselves. These conditions corresponded to a range of color temperatures comprised between 2000 K and 2700 K, throughout a radiance spectra comprised between 370 nm and 770 nm. The calibration process consisted in placing the calibrated area of the lamp on the same plane as the flame and then imaging the filament while conserving equivalent filtering (window, beam-splitter, neutral and interferential filters, objective aperture, etc.) and conditions of image acquisition (exposure time, resolution, etc.) as for the flame imaging. Accordingly, the radiance for each channel was:

$$\begin{aligned} I_{550} &= (DL_{550} - 3.0645) \cdot 55.192 \cdot 10^{-9} \quad [W.sr^{-1}.m^{-3}] \\ I_{650} &= (DL_{650} - 6.2553) \cdot 21.312 \cdot 10^{-9} \quad [W.sr^{-1}.m^{-3}] \end{aligned} \tag{3.17}$$

As such, it could be obtained a conversion of digital intensity into radiance I_λ for each wavelength. By combining Eq. 3.14 to 3.16, each image pixel resulted in a function of $K_{2C}L$ and T as expressed in Figure 3.32. But prior to the conversion, further operations of image processing were performed as detailed in the next section.

Image processing and calculations: This section details the main steps throughout the processing of 2-color images, permitting the obtention of flame temperature and opacity. The latter are conducted as follows:

- Image segmentation: Prior to the processing of the whole dataset, a criterion of image segmentation had to be established in order to

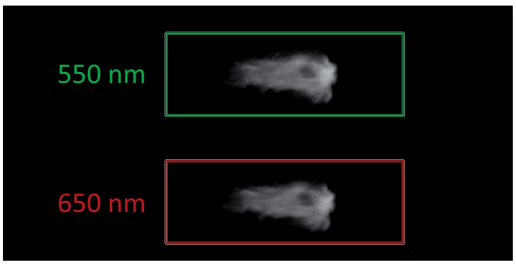

$$I_{550} = \frac{C_1}{550^5 \left[\frac{e^{(C_2/550 \times \boldsymbol{T})} - 1}{1 - e^{(-\boldsymbol{KL}/(550^{\alpha} \times 10^{-3\alpha}))}}\right]}$$

$$I_{650} = \frac{C_1}{650^5 \left[\frac{e^{(C_2/650 \times \boldsymbol{T})} - 1}{1 - e^{(-\boldsymbol{KL}/(650^{\alpha} \times 10^{-3\alpha}))}}\right]}$$

Figure 3.32. *Sample images of the 2-color method with their corresponding radiance calculated from emissivity and Plank equations.*

distinguish pixels belonging to the flame from those belonging to the background and to remove the latter from image processing. As shown in Figure 3.33, calculations of the flame temperature (detailed below) would include the background and the emitting region, therefore impeding any type of averaging to characterize the flame. For that purpose, several thresholds type and values have been tested. Because the background intensity would vary as a function of the proper flame luminosity, a threshold was defined as a percentage of the maximum intensity found in the image. After comparisons between the apparent flame boundary from raw images and that of the segmented image among flames with very different intensities, the best compromising threshold has been chosen equal to 15 %. The set of pixels meeting the condition of thresholds will be referred as $I_{550,th}$ and $I_{650,th}$, respectively for each image.

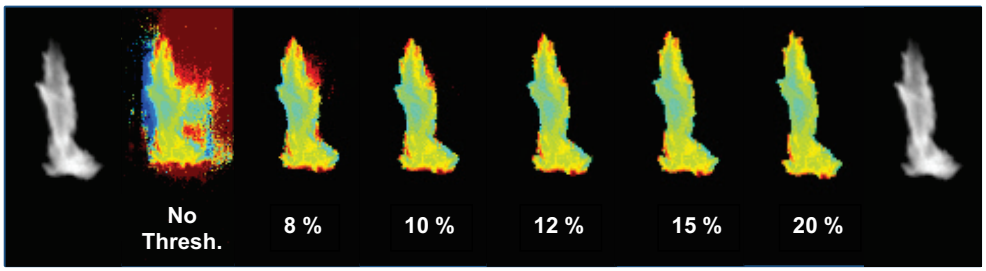

Figure 3.33. *Threshold effect on the segmentation of 2-color images.*

- Spatial calibration: As the calculation of the 2-color method was done pixel by pixel, both flame images required to be perfectly overlaid. Figure 3.34 shows raw and segmented images artificially colored at

different stages of the calibration process. As displayed in the figure, direct superposition of the two half-images without calibration was not satisfactory. The nature of the discrepancy between both images was twofold including a translation and a rotation. The translation component was defined by using a predefined function of *Matlab* (*xcorr2*). By scanning one image onto the other, this function looks for the cross-correlation in terms of geometry and intensity to return the 2-dimensional offset enabling the best match. The result is shown in Figure 3.34. As revealed on the segmented image, a small factor rotation was remaining. This factor could not be accounted by the function and had to be addressed manually. The best match was found typically for a 2 degrees rotation. Due to the computing cost of this function, the code was not executed for every image, and a sophisticated algorithm permitted to average and to check the quality of spatial calibration in several strategic points among the entire dataset. More details may be found in [64].

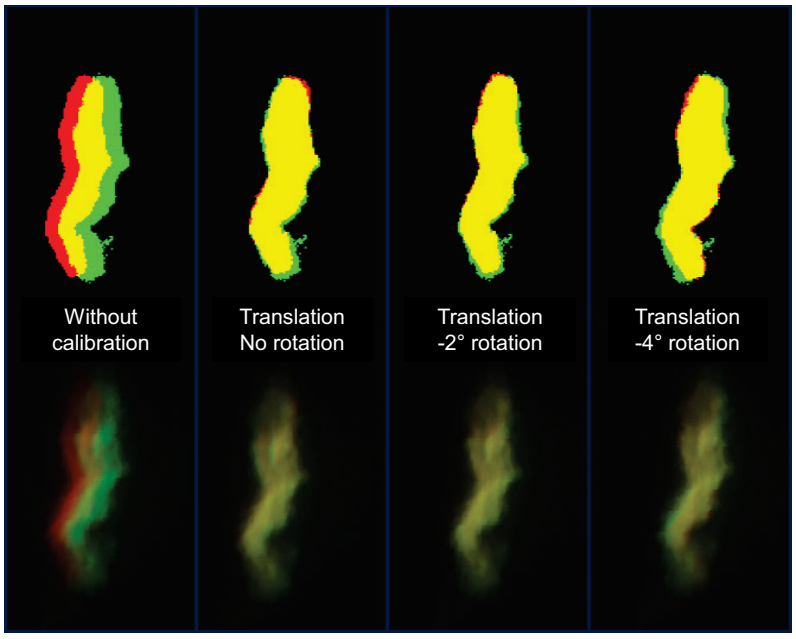

Figure 3.34. *Overlay of the red and green channels before and after spatial calibration. Images have been synthetically colored to better appreciate the match.*

- 2-color resolution: Once images have been segmented, pixels identified as belonging to the flame in at least one of the two flames are considered

(i.e. $I_{550,th} \cup I_{650,th}$) and converted to radiance following Eq. 3.17. The resolution of the 2-color system of equation shown in Figure 3.32 has been widely treated in [56]. Thus, the reader is reported to [56, 57] for more details, particularly about the analysis of uncertainty. From these radiance levels, a corresponding temperature T and soot opacity $K_{2C}L$ are calculated for each pixel by equalizing the $K_{2C}L$ of both channels as follows:

$$[1 - \frac{e^{(C_2/\lambda_1 T)} - 1}{e^{(C_2/\lambda_1 T_{app1})} - 1}]^{\lambda_1 \cdot \alpha_1} = [1 - \frac{e^{(C_2/\lambda_2 T)} - 1}{e^{(C_2/\lambda_2 T_{app2})} - 1}]^{\lambda_2 \cdot \alpha_2} \qquad (3.18)$$

with T_a, the apparent temperature, i.e. the temperature that would have the black body (ϵ=1) at the corresponding radiance; λ_1 and λ_2, the respective wavelengths; c_1 and c_2, the Planck's constant of Eq. 3.15; α_1 and α_2 as expressed by [61] ($\sim$1.38).

Since T cannot be explicited, an iterative method solves the equation. Once T is obtained, KL is calculated. Figure 3.35 shows the solution regions as a function of I_{550} and I_{650}. Error zone EZ ♯1 corresponds to the region with a physically correct solution. If the case is given that pixels belong to error zones EZ ♯3 and ♯4, the solution remains valid but their value is saturated respectively to T >3000 K and KL <0.001. If pixels belong to EZ ♯2, the method does not have a solution as they suppose that emissivity, thus their opacity, is higher than that of the black body ($T_{app} < T_{bb}$). The frontier in terms of KL is arbitrary and has been set to 4.69, being this value the maximum value that could be measured in the region of physical solution. Similarly to the considerations for the extinction method, pixels belonging to EZ ♯2 with emissivity only slightly superior to 1 have been saturated to 4.69, with the same objective not to underestimate the average performed thereafter by clipping regions of high KL.

- Control: Finally, because of the concern presented above regarding the large amount of data, time-resolved videos presenting a compilation of results and averages of interest have been produced in order to perform a check on the solution validity, the method of averaging and the cycle-to-cycle dispersion. Figure 3.36 shows a print screen of one of these. They enabled the visualization of 10 to 100 images of the same instant. This test appeared to be particularly useful as it permitted to find out that a set of tests had been performed with failing conditions of collection angle and eliminate them from averaging in this respect.

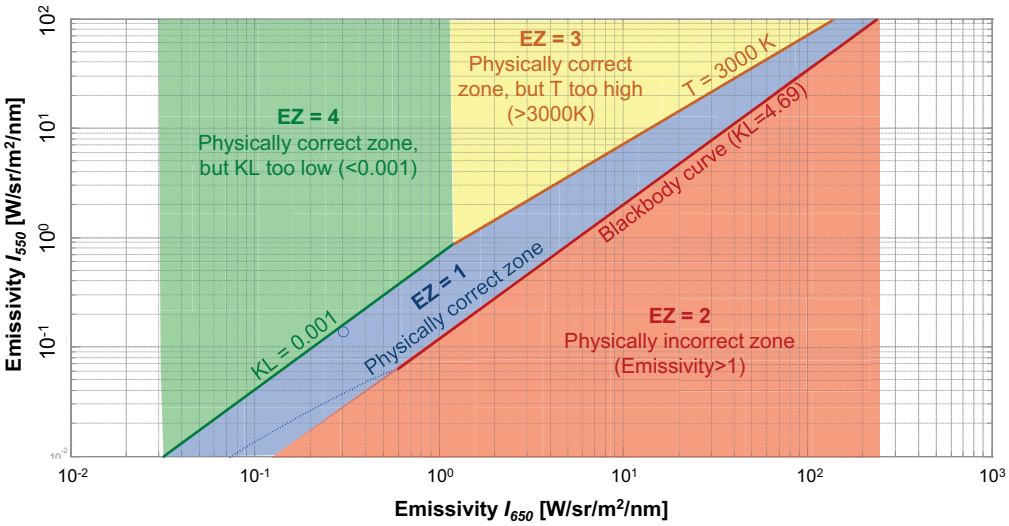

Figure 3.35. *Schematic of the solutions found by the 2-color processing code.*

- Averaging: As for the rest of time-resolved techniques, the instants between 4 to 5 ms, corresponding to OH-chemiluminescence have been considered. At 8000 fps, this represented 8 images for each image sequence, thus in total 800 images for each of the 75 points of the test matrix. Two types of averaging have been operated after the 2-color calculations (i.e. on T and KL), once again with the intention to preserve the linearity between KL and f_v. The first one has been labeled "zero-dimensional" (0D), and consisted in averaging these 800 images in order to compare the 75 tests conditions and study the effect of fuel properties, thermodynamic conditions and injection pressure. The second type of average had for objective to compare the KL measurements from both laser extinction and 2-color method. Therefore, a range of pixels has been selected on the line followed by the laser corresponding to the flame core. Five radial pixels ($\sim$1.5 mm) were averaged at each axial position to draw the axial profile of both temperature and KL. Further details will be given in *Chapter 5* while approaching the results.

3.7. Conclusion

A methodology has been defined with the objective to measure the impact of fuel properties in comparison to the variation of typical engine

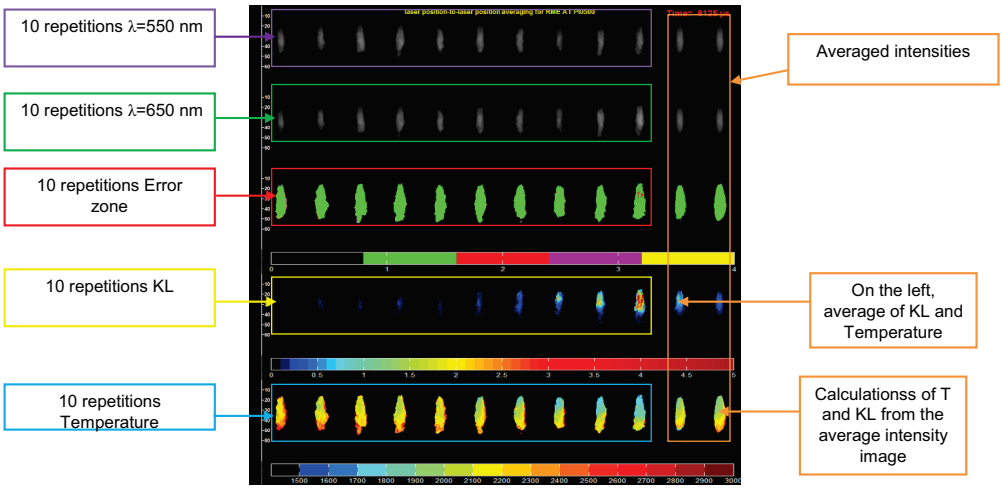

Figure 3.36. *Print screen of the resuming videos of control.*

parameters, including thermodynamic conditions and injection pressure. The design of experiments has taken an incremental approach to determine the fuel effect at the key stages of the injection/combustion process identified in the previous chapter. For this purpose, fuel physical and chemical properties were first addressed, as well as their effect on the fuel injection system. As a second step, the optical facility permitting their injection into a Diesel environment was presented along with the corresponding test matrix of thermodynamic conditions. Beyond their own contribution, these specifications moreover defined the boundary conditions of two experiments applying optical measurements to inert and reacting sprays respectivelly. Considerations and analysis of these optical techniques were complex, such that their fundamentals, apparatus and processing assets have been introduced and detailed in this chapter as well, in particular for the laser extinction technique newly applied in the department. The following two chapters will therefore now focus on the analysis of results from these two experiments in order to fullfill the objectives defined in *Chapter 2*.

References

[1] Allocca L., Mancaruso E., Montanaro A., Sequino L., Vaglieco B.M., *Effects of mineral and biodiesel fuel compositions on spray evolution and mixture distribution.* Thermofluidynamic processes in Diesel engines, Valencia, Sept. 14-17, 2010.

[2] Jääskeläinen H., *Biodiesel Standards & Properties*. DieselNet Technology Guide. "http://www.dieselnet.com/tech".

[3] Kinast J.A., *Production of Biodiesels from Multiple Feedstocks and Properties of Biodiesels and Biodiesel/Diesel Blends*, Prepared for U.S. Department of Energy, NREL Report, NREL/SR-510-31460, 2003.

[4] Lapuerta M., Canoira L., Ráez J., "Improved Method for Determining the Atmospheric Distillation Curve of Biodiesel Fuels from Reduced Pressure". *Ind. Eng. Chem. Res.*, Vol. 50, pp. 7041-48, 2011.

[5] Sadeghbeigi R., *Fluid Catalytic Cracking Handbook: An Expert Guide to the Practical Operation, Design, and Optimization of FCC Units*, 3rd Ed., Gulf Publishing Company, 2012.

[6] Siebers D., "Scaling Liquid-Phase Fuel Penetration in Diesel Sprays Based on Mixing-Limited Vaporization". *SAE Paper 1999-01-0528*, 1999.

[7] Rodríguez Fernández J., *Estudio bibliográfico y experimental de las emisiones y prestaciones de un motor trabajando con biodiesel*. Tesis Doctoral, Universidad de Castilla-La Mancha, Departamento de Mecánica Aplicada e Ingeniería de Proyectos, 2007.

[8] Thomas A., "Fats and Fatty Oils", in *Ullmann's Encyclopedia of Industrial Chemistry*, John Wiley & Sons, 2007.

[9] Coates J., "Interpretation of Infrared Spectra, A Practical Approach", in *Encyclopedia of Analytical Chemistry*, pp. 10815-37, John Wiley & Sons, 2000.

[10] Baert R.S.G., Frijters P.J.M., Somers B., Luijten C.C.M., de Boer W., "Design and operation of a high pressure, high temperature cell for HD diesel spray diagnostics: guidelines and results". *SAE Paper 2009-01-0649*, 2009.

[11] Bosch W., "The fuel rate indicator: a new measuring instrument for display of the characteristics of individual injection". *SAE Paper 660749*, 1966.

[12] Arrègle J., *Análisis De La Estructura Y Dinámica Interna De Chorros Diesel*. Tesis Doctoral, Universidad Politécnica de Valencia, Departamento de Máquinas y Motores Térmicos, 1997.

[13] Payri R., Salvador F.J., Gimeno J., Bracho G., "A new methodology for correcting the signal cumulative phenomenon on injection rate measurements". *Experimental Techniques*, Vol. 32, pp. 46-49, 2008.

[14] Hermens S., *Influence Of Diesel Injector Nozzle Geometry On The Injection And Combustion Process*. Tesis Doctoral, Universidad Politécnica de Valencia, Departamento de Máquinas y Motores Térmicos, 2008.

[15] Gimeno J., *Desarrollo y Aplicación De La Medida Del Flujo De Cantidad De Movimiento De Un Chorro Diesel*. Tesis Doctoral, Universidad Politécnica de Valencia, Departamento de Máquinas y Motores Térmicos, 2008.

[16] Bracho G., *Experimental And Theoretical Study Of The Direct Diesel Injection Process At Low Temperatures*. Tesis Doctoral, Universidad Politécnica de Valencia, Departamento de Máquinas y Motores Térmicos, 2011.

[17] Payri R., Salvador F.J., Gimeno J., Bracho G., "The effect of temperature and pressure on thermodynamic properties of diesel and biodiesel fuels". *Fuel*, Vol. 90, pp. 1172-80, 2011.

[18] Desantes J.M., Payri R., Salvador F.J., Gimeno J., "Measurements of Spray Momentum for the Study of Cavitation in Diesel Injection Nozzles". *SAE Paper 2003-01-0703*, 2003.

[19] Payri R., García J.M., Salvador F.J., Gimeno J., "Using spray momentum flux measurements to understand the influence of diesel nozzle geometry on spray characteristics". *Fuel*, Vol. 84 pp. 551-61, 2005.

[20] Bermúdez V., García J.M., Juliá E., Martínez S., "Engine with Optically Accessible Cylinder Head: a Research Tool for Injection and Combustion Processes". *SAE Paper 2003-01-1110*, 2003.

[21] Armas O., Rodríguez J., Payri F., Martín J., Agudelo J.R., "Effect of the trapped mass and its composition on the heat transfer in the compression cycle of a reciprocating engine". *Appl. Therm. Eng.*, Vol. 26, pp. 2842-53, 2005.

[22] Payri F., Molina S., Martín J., Armas O., "Influence of measurement errors and estimated parameters on combustion diagnosis". *Appl. Therm. Eng.*, Vol. 26, pp. 226-36, 2006.

[23] Pastor J.V., Pastor J.M., Gimeno J., Nerva J.-G., "The effect of Biodiesel fuel blend rate on the Liquid-phase fuel penetration in Diesel engine conditions". *SAE Paper 2009-24-0051*, 2009.

[24] Pastor J.V., Payri R., Gimeno J., Nerva J.-G., "Experimental Study on RME Blends: Liquid-Phase Fuel Penetration, Chemiluminescence, and Soot Luminosity in Diesel-Like Conditions". *Energy Fuels*, Vol. 23, pp. 5899-915, 2009.

[25] Pastor J.V., Arrègle J., Palomares A., "Diesel spray image segmentation with a likelihood ratio test". *Appl. Opt.*, Vol. 40, pp. 1-10, 2001.

[26] Pastor J.V., Arrègle J., García J.M., Zapata L.D., "Segmentation of diesel spray images with loglikelihood ratio test algorithm for non-Gaussian distributions". *Appl. Opt.*, Vol. 46, pp. 888-99, 2007.

[27] Orfanidis S.J., *Introduction to Signal Processing*, Prentice-Hall, 1996.

[28] Ikegami M., Kamimoto T., "Conventional Diesel Combustion", in *Flow and Combustion in Reciprocating Engines*, Chapter 6, Springer-Verlag, 2009.

[29] DuMouchel W.H., O'Brien F.L., *Integrating a Robust Option into a Multiple Regression Computing Environment*. Computer Science and Statistics: Proceedings of the 21^{st} Symposium on the Interface, Alexandria, VA, 1989.

[30] Holland P.W., Welsch R.E., "Robust Regression Using Iteratively Reweighted Least-Squares". *Commun. Statis.-Theor. Method.*, Vol. A6, pp. 813-27, 1977.

[31] Huber P.J., *Robust Statistics*. John Wiley & Sons, 1981.

[32] Street J.O., Carroll R.J., Ruppert D., "A Note on Computing Robust Regression Estimates *via* Iteratively Reweighted Least Squares". *The American Statistician*, Vol. 42, pp. 152-54, 1988.

[33] Higgins B., Siebers D.L., "Measurement of the Flame Lift-Off Location on DI Diesel Sprays Using OH Chemiluminescence". *SAE Paper 2001-01-0918*, 2001.

[34] Zhao H., Ladommatos N., "Optical diagnostics for soot and temperature measurement in diesel engines". *Prog. Energy Combust. Sci.*, Vol. 24, pp. 221-55, 1998.

[35] Musculus M.P.B., Pickett L.M., "Diagnostic considerations for optical laser-extinction measurements of soot in high-pressure transient combustion environments". *Combust. Flame*, Vol. 141, pp. 371-91, 2005.

[36] Williams T.C., Shaddix C.R., Jensen K.A., Suo-Anttila J.M., "Measurement of the Dimensionless Extinction Coefficient of Soot within Laminar Diffusion Flames". *Int. J. Heat Mass Trans.*, Vol. 50, pp. 1616-30, 2007.

[37] Choi M.Y., Mulholland G.W., Hamins A., Kashiwagi T., "Comparisons of the soot volume fraction using gravimetric and light extinction techniques". *Combust. Flame*, Vol. 102, Vol. 161-9, 1995.

[38] Zhu J., Choi M.Y., Mulholland G.W., Gritzo L.A., "Soot Scattering Measurements in the Visible and Near-Infrared Spectrum". *Proc. Combust. Inst.*, Vol. 28, 439-46, 2000.

[39] Smyth K.C., Shaddix C.R., "Elusive History of m=1.57-0.56i for the Refractive Index of Soot. Brief Communication". *Combust. Flame*, Vol. 107, pp. 314-20, 1996.

[40] Kook S., Pickett L.M., "Soot volume fraction and morphology of conventional and surrogate jet fuel sprays at 1000-K and 6.7-MPa ambient conditions. *Proc. Comb. Inst.*, Vol. 33, pp. 2911-18, 2011.

[41] Kook S., Pickett L.M., "Soot Volume Fraction and Morphology of Conventional, Fischer-Tropsch, Coal-Derived, and Surrogate Fuel at Diesel Conditions". *SAE Paper 2012-01-0678*, 2012.

[42] Nerva J.-G., Genzale C.L., Kook S., Garcia-Olivier J.M., Pickett L.M., "Fundamental Spray and Combustion Measurements of Soy Methyl-Ester Biodiesel". *Int. J. Engine Res.*, published online 30 August 2012, pp. 1-18, 2012.

[43] Nerva J.-G., Yamaguchi T., Iguma H., Nishigai H., Kondo K., Takano S., Aizawa T., Genzale C., Pickett L.M., "Transmission Electron Microscopy of Soot Particles sampled directly from a Biodiesel Spray Flame". *SAE Paper 2011-01-2046*, 2011.

[44] Aizawa T., Nishigai H., Kondo K., Yamaguchi T., Nerva J.-G., Genzale C., Kook S., Pickett L.M., "Transmission Electron Microscopy of Soot Particles Directly Sampled in Diesel Spray Flame - A Comparison between US♯2 and Biodiesel Soot". *SAE Paper 2012-01-0695*, 2012.

[45] Pickett L.M., Siebers D.L., "Soot formation in diesel fuel jets near the lift-off length". *Int. J. Engine Res.*, Vol. 7, pp. 103-30, 2006.

[46] Pickett L.M., Siebers D.L., "Fuel Effects on Soot Processes of Fuel Jets at DI Diesel Conditions". *SAE Paper 2003-01-3080*, 2003.

[47] Fang T., Lin Y.-C., Foong T.M., Lee C.-F., "Biodiesel combustion in an optical HSDI diesel engine under low load premixed combustion conditions". *Fuel*, Vol. 88, pp. 2154-62, 2009.

[48] Mueller C.J., Boehman A.L., Martin G.C., "An experimental investigation of the origin of increased NOx emissions when fueling a heavy-duty compression-ignition engine with soy biodiesel". *SAE Paper 2009-01-1792*, 2009.

[49] Beatrice C., Bertoli C., Del Giacomo N., Guido C., Migliaccio M., "In-cylinder Soot Evolution Analysis in a Transparent Research DI Diesel Engine Fed by Oxygenated Fuels". *SAE Paper 2002-01-2851*, 2002.

[50] Cheng A.S., Upatnieks A., Mueller C.J., "Investigation of the impact of biodiesel fuelling on NOx emissions using an optical direct injection diesel engine". *Int. J. Engine Res.*, Vol. 7, pp. 297-318, 2006.

[51] Cheng A.S., Upatnieks A., Mueller C.J., "Investigation of Fuel Effects on Dilute, Mixing-Controlled Combustion in an Optical Direct-Injection Diesel Engine". *Energy Fuels*, Vol. 21, pp. 1989-2002, 2007.

[52] Beatrice C., Capaldi P., Del Giacomo N., Guido C., Mancaruso E., Vaglieco B.M., "Analysis of Impact of Diesel Fuel/Biodiesel Blends on a Modern Diesel Combustion System Performance by Means of Injection Test Rig, Optical and Real SC Engine Experiments". *SAE Paper 2009-01-0484*, 2009.

[53] Klein-Douwel R.J.H., Donkerbroek A.J., Van Vliet A.P., Boot M.D., Somers L.M.T., Baert R.S.G., Dam N.J., Ter Meulen J.J., "Soot and chemiluminescence in diesel combustion of bio-derived, oxygenated and reference fuels". *Proc. Combust. Inst.*, Vol. 32, pp. 2817-25, 2009.

[54] Fang T., Lee C.F., "Bio-Diesel Effects on Combustion Processes in an HSDI Diesel using Advanced Injection Strategies". *Proc. Combust. Inst.*, Vol. 32, pp. 2785-92, 2009.

[55] Mueller C.J., Martin G.C., "Effects of oxygenated compounds on combustion and soot evolution in a DI diesel engine: Broadband natural luminosity imaging". *SAE Paper 2002-01-1631*, 2002.

[56] García-Oliver J.M., *Aportaciones Al Estudio Del Proceso De Combustión Turbulenta De Chorros En Motores Diesel De Inyección Directa*. Tesis Doctoral, Universidad Politécnica de Valencia, Departamento de Máquinas y Motores Térmicos, 2004.

[57] Payri F., Pastor J.V., García-Oliver J.M., Pastor J.M., "Contribution to the application of two-colour imaging to diesel combustion". *Meas. Sci. Technol.*, Vol. 18, pp. 2579-98, 2007.

[58] Matsui Y., Kamimoto T., Matsuoka S., "A study on the time and space resolved measurement of flame temperature and soot concentration in a DI diesel engine by the two-color method". *SAE Paper 790491*, 1979.

[59] Hottel D.C., Broughton F.P., "Determination of true temperature and total radiation from luminous gas flames". *Ind. Eng. Chem.*, Vol. 4, pp. 166-75, 1932.

[60] Kamimoto T., Murayama Y., "Re-examination of the emissivity of diesel flames". *Int. J. Engine Res.*, Vol. 12, pp. 580-600, 2011.

[61] Musculus M.P.B., "Measurements of the Influence of Soot Radiation on In-Cylinder Temperatures and Exhaust NO_2 in a Heavy-Duty Diesel Engine". *SAE Paper 2005-01-0925*, 2005.

[62] Singh S., Reitz R.D., Musculus M.P.B., "2-Color Thermometry Experiments and High-Speed Imaging of Multi-Mode Diesel Engine Combustion". *SAE Paper 2005-01-3842*, 2005.

[63] Gray W.A., Muller R., *Engineering Calculations in Radiative Heat Transfer*, Permagon Press, 1974.

[64] David G., *Mesure de la température et de la concentration en suies de flammes Diesel"*. Projet de Fin d'Étude, Institut Supérieur de l'Automobile et des Transports, 2011.

Chapter 4

Fuel effects on spray mixing and vaporization under inert conditions

Contents

4.1. Introduction

Following the objectives presented in the previous chapters and according to the experimental methodology defined, the purpose of the following chapter

is to address the effect of fuel properties on the spray development under inert conditions. By isolating the physical aspects related to fuel injection and spray formation, this step has been shown to be essential prior to the assessment of the potential fuel effects during the combustion process.

In the previous chapter, the boundary conditions of this experiment have been defined, including the determination of ambient conditions and their stability along the injection processes, the mass flow rate and momentum flux through the injector nozzle, and the fuel intrinsic properties. Also, the optical technique employed, namely Mie-scattering high-speed imaging, has been detailed along with its corresponding processing. Thus, the analysis below focuses on the results exclusively and divides in two parts. In the first section, results of the maximum liquid-phase penetration for the five studied fuels are shown. These results enable a discussion of the fuel effect over the processes of atomization and evaporation. A statistical analysis is conducted to identify which are the fuel properties with a significant impact, and assess both their sensitivity and their implication respect to the physical parameters controlled by the engine. Accordingly, an empirical model able to predict the liquid length from both engine and fuel variables is proposed. In the second study, results on vapor phase penetration obtained at Sandia National Lab. are presented, although in other conditions and with different fuels, but whose analysis should extend to the selection of fuels used in the present work. The analysis focuses on mixing and the differences observed between the transient penetration of diesel and biodiesel sprays. Finally, the relevant conclusions are retrieved and presented in the conclusion section.

4.2. Maximum liquid-phase penetration

4.2.1. Analysis methodology

The maximum liquid-phase penetration (or liquid length) of the five fuels has been measured under three injection pressure levels and five engine operating conditions, sweeping both ambient temperature (T_{amb}) and density (ρ_{amb}). For each of the 75 points defined by this test matrix, ten replications of the test were conducted for statistical purpose. Images of these 750 injections were collected at 8000 fps during 12.5 ms. Accordingly, Figure 4.1 shows a sample of the ensemble-average time-resolved liquid-phase penetration with the standard deviation associated to each instant. In addition, the figure displays the ambient thermodynamic conditions and the spray images sequence

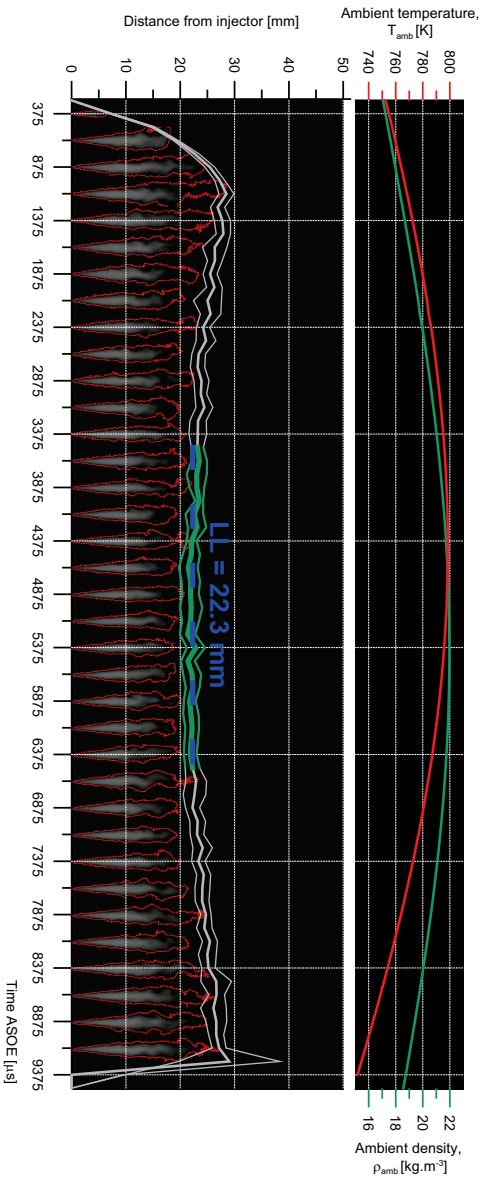

Figure 4.1. *Representation of the ensemble-average and standard deviation of FT1 at Low Density (22 $kg.m^{-3}$; 800 K) and 50 MPa injection pressure. Images (1 out of 2) from one cycle have been added for illustration. The time-averaging window (3500-6500 μs ASOE) is represented in green and the time-averaged value dashed blue line. $\rho_{amb}(t)$ and $T_{amb}(t)$ are represented in the upper part of the figure.*

from one of the ten cycles used to yield the average after that background was subtracted. For clarity, only one out of two images is depicted.

4.2.1.1. Considerations of steady and unsteady-state thermodynamic conditions

As is usual for the processing of liquid length, results have been first analyzed considering a steady-state environment such as the test rig aims at reproducing. Under this assumption, the liquid length remains constant with time because of the steady-state thermodynamic conditions surrounding the spray. Thus, results were first ensemble-averaged as represented in Figure 4.1 with a thick continuous line; the cycle-to-cycle standard deviation is shown in thinner lines. Thereafter, a window for time-averaging was selected near the engine TDC, consistent with a reasonably stabilized liquid-length region. In order to respect as much as possible the conditions fixed by the test matrix, the time-averaging window has been centered respect to the maximum temperature T_{max} and the maximum density ρ_{max}. Depending on the engine operating conditions, the maximum temperature T_{max} was reached between -3.1 and -2.8 ATDC (4500 and 4625 μs ASOE) and the maximum density ρ_{max} between -0.5 and -0.1 ATDC (5500 and 5625 μs ASOE). Consequently, the time-averaging window was slightly extended between 3500 and 6500 μs ASOE for all test cases, considering a total of 25 images per injection. The corresponding range has been highlighted in Figure 4.1 and the resulting average plotted in dashed blue line. This *steady-state approach* enabled to compare the 75 results of liquid length all at once.

Nonetheless, in view of the relatively long injections performed in this study (8 ms) compared to the engine speed (500 rpm), the spray was exposed to significant pressure variations along the injection event ($\sim$24 CAD). In Figure 4.1, it can be observed that T_{amb} oscillates by more than 50 K while ρ_{amb} does by up to 7 $kg.m^{-3}$. For each operating conditions, the resulting time-derivatives of temperature and density are plotted in Figure 4.2, showing variations between -20000 and 20000 $K.s^{-1}$ in terms of ambient temperature and between -2000 to 2000 $kg.m^{-3}s^{-1}$ in terms of ambient density. As a result to these variations, the cylinder pressure leaves its mark on the ensemble-averaged liquid length, offering the opportunity to consider the liquid length with an *unsteady-state approach* similarly to the works of Fisher *et al.* [1, 2]. In order to evaluate whether such variation of pressure and density within the cycle of our tests could be useful to reproduce any realistic situation or not, it is worthy to compare with results presented by Benajes *et al.* [3, 4]. In that work, the author considers motored cycles from a single-cylinder heavy-duty

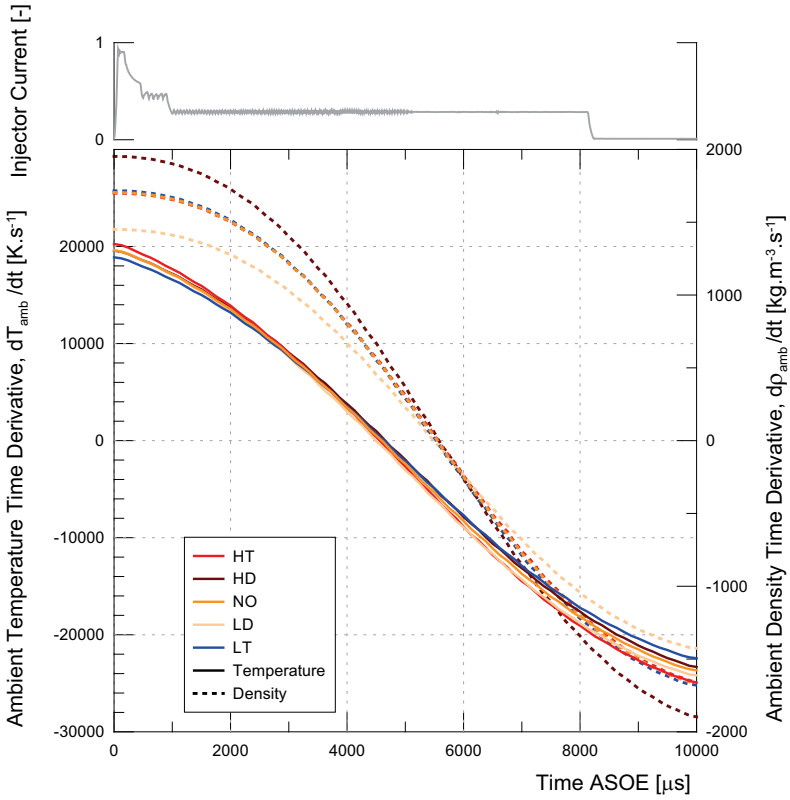

Figure 4.2. *Temperature and density time-derivatives during the injection event.*

engine operating under PCCI mode. Table 4.1 collects the angle ranges where this engine reaches similar time-derivative values to those of our test rig. Due to the higher engine speed, these regions correspond to the early range in the compression stroke (Cf. "prior to"), the late range in the power stroke (Cf. "after"), and the range close to TDC ("Cf. "in the range"). Although quite narrower than in the test rig, these three regions have interest nonetheless as they belong to the typical injection range for HCCI combustion (∼-90 CAD), and the close-to-TDC region for more conventional combustion modes.

Under this assumption, almost the entire sequence could be leveraged by associating each image of the spray with its corresponding couple of T_{amb} and ρ_{amb}. Only few images were removed in order to avoid the influence of start- and end-of-injection momentum transients. For instance, in the test case shown in Figure 4.1, the range has been restricted between 1375 and 8875 μs ASOE. From a statistical point of view, such kind of approach is

Table 4.1. *Corresponding angular range of temperature and density time-derivatives in the single-cylinder heavy-duty Diesel engine operated in [3, 4] at different operating conditions.*

	Engine speed	*1200*	*1200*	*1800*	*1800*	*[rpm]*
	IMEP	*1.35*	*2.4*	*2.4*	*3.2*	*[bar]*
	CR	*14.4*	*14.1*	*14.1*	*14.1*	*[-]*
-20000 to 20000 $K.s^{-1}$	prior to	-71	-76	-97.5	-98	[CAD]
	in the range	-1.8 to 5.8	-5.8 to 1.8	-1 to 3.8	-1.1 to 3.9	[CAD]
	after	71	73	93	92	[CAD]
-2000 to 2000 $kg.m^{-3}.s^{-1}$	prior to	-35	-48	-57.5	-67	[CAD]
	in the range	-6 to 5	-2.8 to 3.2	-2.5 to 1.5	-1.7 to 0.9	[CAD]
	after	35	48	57.5	68	[CAD]

fairly advantageous as it multiplies the number of combinations. Accordingly, the statistical analysis considers about 300 combinations of temperature and density per fuel instead of the five ones originally handled by the test matrix. The initial test matrix is then extended and discretized as shown in Figure 4.3. Moreover, the relative proximity among the five original operating conditions enables a smooth transition between the points of this new "continuous test matrix". Finally, blow-by, heat transfer and mechanical stresses induce a phase-shift between temperature and density traces, reducing the collinearity between both variables and the possible bias it may produce in the statistical analysis.

4.2.1.2. Determination of the empirical model

In order to assess the effect of fuel physical properties compared to engine parameters in regard to spray atomization and vaporization processes, the statistical analysis has been conducted with the objective to produce an empirical model able to predict the liquid length based on the simple off-engine measurements presented in the previous chapter. In this respect, an analysis was performed upstream with the purpose to first estimate the variables potentially involved in the establishment and the control of the liquid length. As a starting point, one-dimensional spray models aiming at predicting the mixture fraction field represented a valuable approach for the research of relevant variables.

In regard to Diesel applications, one of the first models of this kind was impulsed by Siebers [5] who developed a scaling-law based on the mixing-

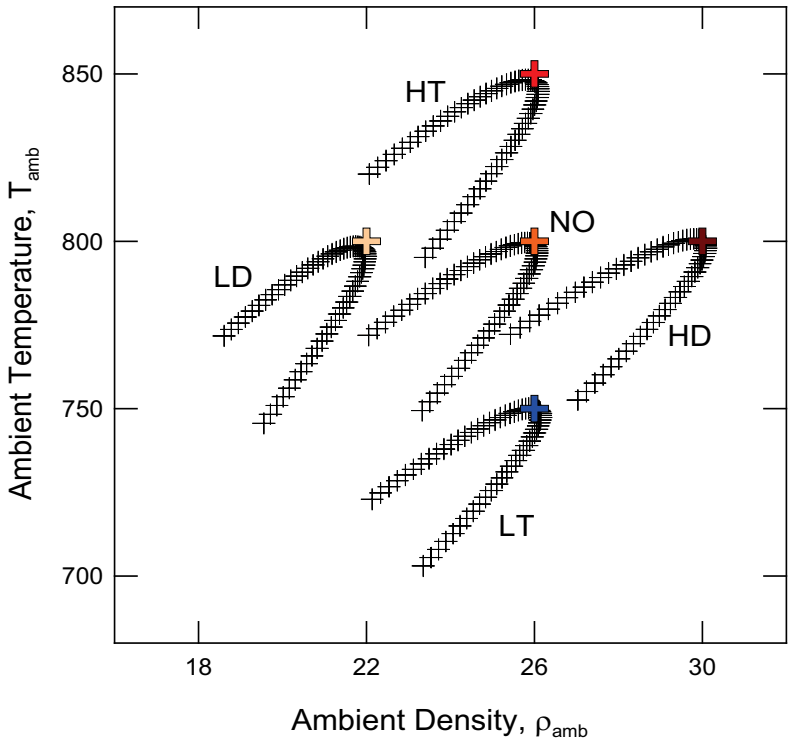

Figure 4.3. *Continuous test matrix enabled by the consideration of instantaneous in-cylinder conditions in the unsteady-state approach.*

limited and momentum conservation hypotheses. These models have been further developed by García-Oliver *et al.* [6, 7], and Kattke and Musculus [8, 9], while including a better approach of the spray radial distribution. By assimilating the Diesel spray to a gas jet, these models convert an a priori complex two-phase flow problem into a single-phase one, in which a portion of fuel vaporizes instantaneously when surrounded by enough enthalpy to heat up and vaporize, independently from droplets size and diffusion timescales at their surface. The appropriate mixture fraction where this energy equilibrium is achieved is referred to as $Y_{f,evap}$ and the liquid length is then defined as the spray axial position where this specific mixture fraction level is reached.

Following this hypothesis, a scaling-law for liquid length can be derived as in [10] based on turbulent spray mixing considerations. The axial mass fraction within the quasi-steady part of a diesel spray could be obtained from:

$$Y_f = K \cdot d_0 \sqrt{\frac{\rho_f}{\rho_{amb}}} \cdot \frac{1}{X} \tag{4.1}$$

where K is a spray constant, d_0 is the nozzle diameter, ρ_f and ρ_{amb} are the fuel and ambient densities respectively, and X is the spray axial coordinate. Thus, the liquid length (LL) is defined by:

$$LL = K \cdot [d_0 \sqrt{\frac{\rho_f}{\rho_{amb}}}] \cdot \frac{1}{Y_{f,evap}} \tag{4.2}$$

In Eq. 4.2, the term in brackets is widely known in the literature as the *"equivalent diameter"* and characterizes the spray mixing scales (i.e. momentum). Such *"mixing factor"* considers both in-cylinder and fuel physics (as described in *Chapter 3*), by including the ratio of fuel and ambient densities. The last term of Eq. 4.2 is usually referred to as the *"energy factor"* as it accounts for the spray vaporization processes. It can be rewritten in term of enthalpies such as in Eq. 4.3 and 4.4, where T_{amb} is the ambient gas temperature, $T_{f,0}$ is the initial fuel temperature and T_{evap} is the temperature of saturation when the fuel is entirely vaporized. Therefore, this parameter depends on both fuel properties and ambient thermodynamic conditions [10, 11], by involving the specific heat capacity of the liquid fuel ($c_{pl,f}$) and its latent heat of vaporization ($L_{v,f}$) on one hand, and the ambient temperature (T_{amb}) on the other hand. In our parametrical study, the specific heat capacity of the ambient ($c_{p,amb}$) was that of nitrogen and the fuel initial temperature (T_0) was not varied.

$$\Delta h_{amb}(T_{amb}, T_{evap}) \cdot (1 - Y_{f,evap}) = Y_{f,evap} \cdot \Delta h_f(T_{f,0}, T_{evap}) \tag{4.3}$$

$$\frac{1}{Y_{f,evap}} = 1 + \frac{\int_{T_{f,0}}^{T_{evap}} c_{pl,f} \cdot \mathrm{d}T + L_{v,f}(T_{evap})}{\int_{T_{evap}}^{T_{amb,\infty}} c_{p,amb} \cdot \mathrm{d}T} \tag{4.4}$$

The evaluation of these fuel thermal properties is not straightforward, as they are specific to each fuel and particularly sensitive to variations of ambient temperature and pressure. This assessment would require an additional calorimeter-type experiment, particularly complex in view of the pressure and temperature ranges operated in a Diesel engine. Available in the literature, an estimation may be obtained by selecting a surrogate with similar properties than the realistic fuel involved. In this particular context, the

literature [12] suggests the choice of an alkane with similar volatility although lower density (no aromatics). In the previously mentioned 1D-models, the phase change is typically resolved by considering equilibrium between liquid and vapor phases. These operations are resolved combining the empirical correlations of Lee-Kesler for liquid/vapor equilibrium, and Pitzer and/or Watson to estimate the latent heat of vaporization. These correlations require a large number of inputs such as the surrogate saturation conditions, acentric factor, and both its specific heat of liquid and gas phases, the latter being derived from other empirical correlations, typically polynomial functions of ambient temperature. Thus, these inputs may be available for alkanes or short hydrocarbons, but become difficult to derive for blends, and definitely do not exist (and do not even make sense) for realistic fuels. In addition, the correlations this intermediate data is derived from are likely obtained in conditions far from that of a Diesel engine.

Therefore, a lag still exists between the fundamental understanding brought by 1D-models and their application with practical fuels. From that perspective, it makes sense to seek for the relevance of easily obtainable variables, maybe with a less fundamental approach but with the ability to mimic the previously mentioned variables, in order to produce empirical correlations more directly applicable with available and daily handled variables in the Diesel engine community such as those obtained with ASTM standards. These theoretical considerations have been leveraged and guided the selection of relevant variables among both fuel properties and engine parameters presented in the previous chapter. As a result, the following model for the dependence of liquid length has been considered for the statistical analysis:

$$LL = K \cdot d_{noz}^{a} \cdot T_{amb}^{b} \cdot P_{inj}^{c} \cdot \rho_{amb}^{d} \cdot \rho_{fuel}^{e} \cdot \nu_{fuel}^{f} \cdot T_{10\,\%}^{g} \cdot T_{50\,\%}^{h} \cdot T_{95\,\%}^{i} \qquad (4.5)$$

In Eq. 4.5, variables accounting for engine physics are the ambient temperature (T_{amb}), ambient density (ρ_{amb}), and injection pressure (P_{inj}). Since the nozzle diameter was not varied in this study, d_{noz}^{a} was consequently part of the constant factor (k). An injection pressure exponent has been retained, despite the fact that injection velocity (and thus injection pressure) has theoretically no influence on liquid length under the mixing-limited assumption. The relevance of this exponent will then serve to discuss the validity of the latter hypothesis when varying fuel properties and ambient conditions.
Regarding the fuel physical properties, they were represented in the model by its density (ρ_f), viscosity (ν_f) and three selected points from the distillation

curves ($T_{X\,\%}$) accounting for T_{evap}. A unique temperature could not be considered as for a pure single-component fuel, due to the high level of molecular heterogeneity revealed by the distillation curves for at least three of the fuels involved. Part of the objective was also to find the most relevant point of the distillation curve for modeling. Fuel density is that of the ASTM standard, thus measured at close to STP conditions. The effect of temperature on fuel density previously measured (Cf. Figure 3.3), has not been considered for two reasons. Firstly, because the temperature of the fuel injected remains up-to-day a great unknown, and secondly because, for consistency, fuel compressibility effects should be accounted as well, given that they can possibly offset entirely the temperature effect under high pressure conditions. Fuel viscosity has also been considered although Siebers' type models apparently do not hint at any direct effect. But, fuel viscosity could indirectly affect the spray spreading angle which is a constant input for these models fixing the mixing quality of the spray, and for which a prior experimental calibration is typically required. Furthermore, the review in *Chapter 2* showed that fuel viscosity may also have an effect on the droplets size distribution, and hence could potentially be a parameter of interest in case the mixing-controlled hypothesis does not verify. For these two reasons, the relevance of fuel viscosity deserved to be tested in the model.

The statistical analysis consisted in the coefficient estimations for a multiple linear regression. In this respect, Eq. 4.5 had to be first converted into a sum of logarithmic terms as follows:

$$\begin{aligned} ln(LL) = K &+ a \cdot ln(d_{noz}) + b \cdot ln(T_{amb}) + c \cdot ln(P_{inj}) + \\ &+ d \cdot ln(\rho_{amb}) + e \cdot ln(\rho_{fuel}) + f \cdot ln(\nu_{fuel}) + \\ &+ g \cdot ln(T_{10\,\%}) + h \cdot ln(T_{50\,\%}) + i \cdot ln(T_{95\,\%}) \end{aligned} \tag{4.6}$$

The operation was realized with the *robustfit* function of *Matlab*. The statistical significance of each term was evaluated with the *p-value* returned by the proper function. The significance level was fixed to 0.05, i.e. when *p-value* was less than 0.05, the null hypothesis was rejected and the variable was considered as statistically significant. The coefficient of determination (R^2) and the root mean square error (RMSE) permitted to assess the quality of the prediction. In order to compare correlations with a different number of parameters, reliability has been calculated using specific R-squared (R^2_{spe}).

Results of this analysis are presented in the following section. As a first step, coefficients b, c, d from Eq. 4.5 corresponding to engine physical properties, have been evaluated for each fuel independently under both steady

and unsteady conditions. This analysis permitted to study the response of each fuel to a variation of engine-derived variables and compare their respective sensitivity. Then, the consideration of both steady and unsteady-states permitted to address the temporal adjustment of the liquid spray into the varying thermodynamic conditions surrounding it. The second step consisted in determining the fuel relevant properties in regard to the length of the liquid phase, and in assessing their effect compared to engine-derived variables. Thus, results from the whole dataset have been concatenated and fuel physical variables included in the model testing, in order to produce a model able to predict liquid length for a large range of fuels based on an appropriate selection of both fuel and engine physical variables.

4.2.2. Results and discussion

Prior to enter the discussion on the previously detailed statistical analysis, this section includes some of the results of liquid length under the *steady-state approach* in the plots of Figure 4.4 to 4.6. In view of the large amount of results, only the most relevant ones are shown but the whole set of numerical results is available in Appendix to this chapter.

4.2.2.1. Quasi-steady-state conditions

The liquid length at different injection pressure levels is plotted in Figure 4.4 for the five studied fuels. Significant differences can be observed from one fuel to another given the reduction by more than a factor of two between RME and FT2. Both these fuels construct respectively the upper and lower boundaries of the tested fuels. In that sense, Figure 4.4 shows similar trends as in distillation curves of Figure 3.2 regarding two fuels encasing the others by upper and lower boundaries, which illustrates the high influence of fuel volatility. Such result was expected since the association between liquid length and distillation curves is widely diffused in the literature [10, 13–15]. Nonetheless, the comparison among the three RME-derived fuels turns out to be in opposition with Siebers conclusions' [15] stating that the lower volatility components in a multi-component fuel control liquid length. The results obtained are more likely in agreement with Higgins *et al.* [10] and Canaan *et al.* [14], suggesting that the liquid length is more depending on the average volatility ($\sim T_{50\,\%}$ for linear distillation curves). With the same fuels but different injector and conditions, it was even obtained in [16] that liquid length scaled with the RME blending ratio, but this relationship does not confirm with this dataset. Regarding the fuel origin, this result is consistent

with recent works involving similar alternative fuels and showing both a shorter liquid length for Fischer-Tropsch Diesel (FTD) [17] and a higher one for biodiesel [1, 18, 19] compared to conventional diesel. However, fuel volatility does not clarify the differences observed among B05, B30 and FT1, suggesting that other fuel properties may be involved.

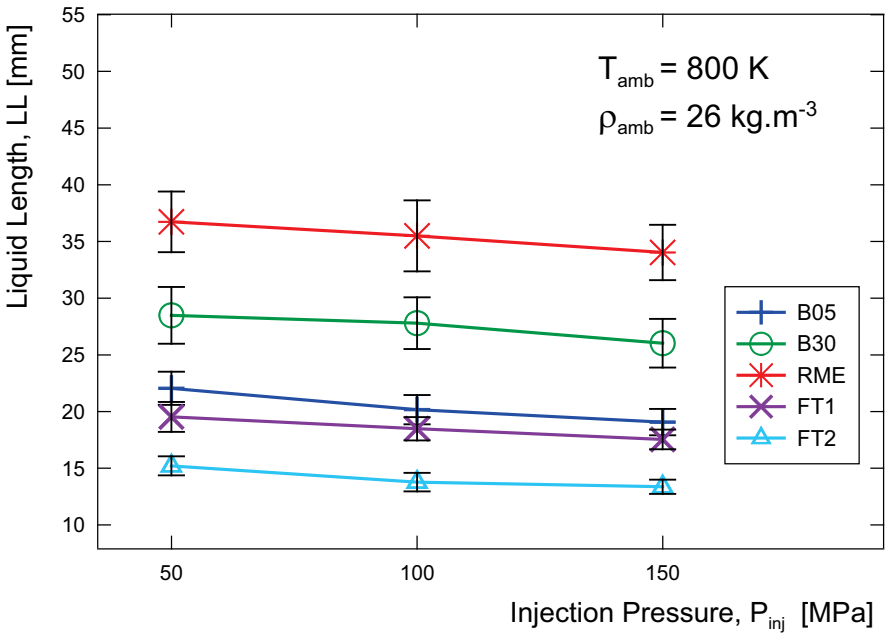

Figure 4.4. *Injection pressure effect on liquid length for the five studied fuels at the NO ambient condition.*

A minor decrease of the liquid length can be observed among all the fuels when injection pressure is increased. Though only the NO-condition is represented, the same trend has been observed for the four other operating conditions. This effect is opposite to that observed by Pastor *et al.* in [16, 20] while the same fuels were injected using a multi-hole nozzle. Although care had been taken in the processing, it was suspected that ambient cooling increased significantly with injection pressure (i.e. mass rate) to cause the liquid length growth. Because it is unlikely that the different nozzle geometry is responsible of such an effect, this result confirms the authors' concern about the conservation of ambient temperature. Thus, the small decrease of liquid length with increasing injection pressure observed in this single-hole nozzle could be the result of either a slightly increased angle (i.e. mixing) as observed in [21] or a decrease of droplets size as suggested in the review of *Chapter 2*. It

must be noted that this second option would challenge the mixing-controlled hypothesis stated by Siebers [5] by suggesting that diffusion and convection time scales at the droplet surface are producing this effect. However, all proportions guarded, the effect observed remains too low to reconsider the validity of the latter hypothesis and still represents a valuable and practical contribution for Diesel spray modeling.

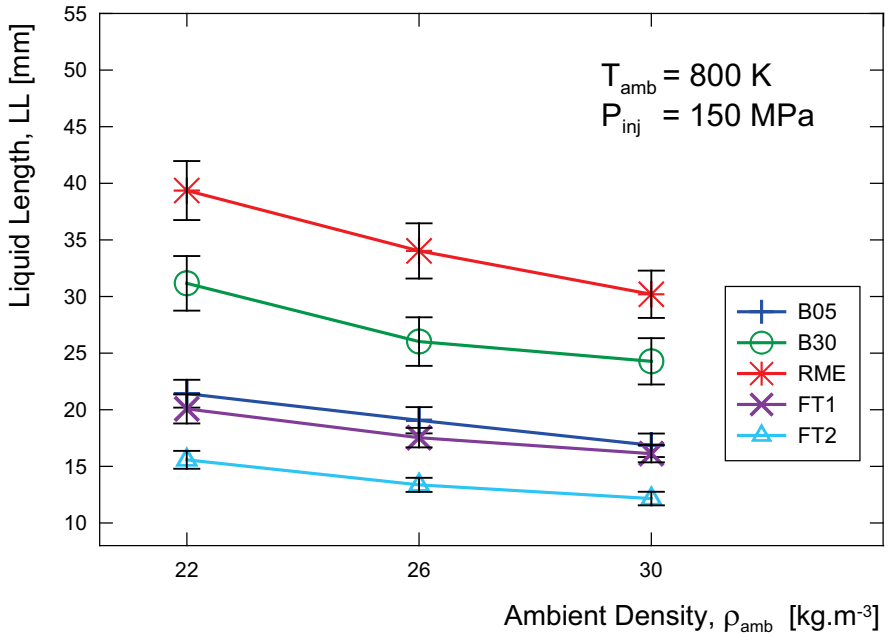

Figure 4.5. *Ambient density effect on liquid length for the five studied fuels at 150 MPa injection pressure.*

The effects of ambient temperature and ambient density have been represented in Figures 4.5 and 4.6 respectively. Since injection pressure showed a small impact on the liquid-phase penetration, only the 150 MPa injection pressure condition has been represented. Similarly to Figure 4.4, the fuel hierarchy is conserved and remains partially consistent with the ambient pressure distillation curves. For all the fuels concerned, an increase on both ambient parameters leads to a reduction of the liquid length with a particularly significant effect to highlight for temperature. Indeed, a 13 % increase of ambient temperature decreases the liquid length by up to 43 %, while a 36 % increase of ambient density only decreases the liquid length by up to a 25 %. Accordingly, the purpose of the following section is to assess more precisely

the weight of these parameters by means of the previously described statistical analysis.

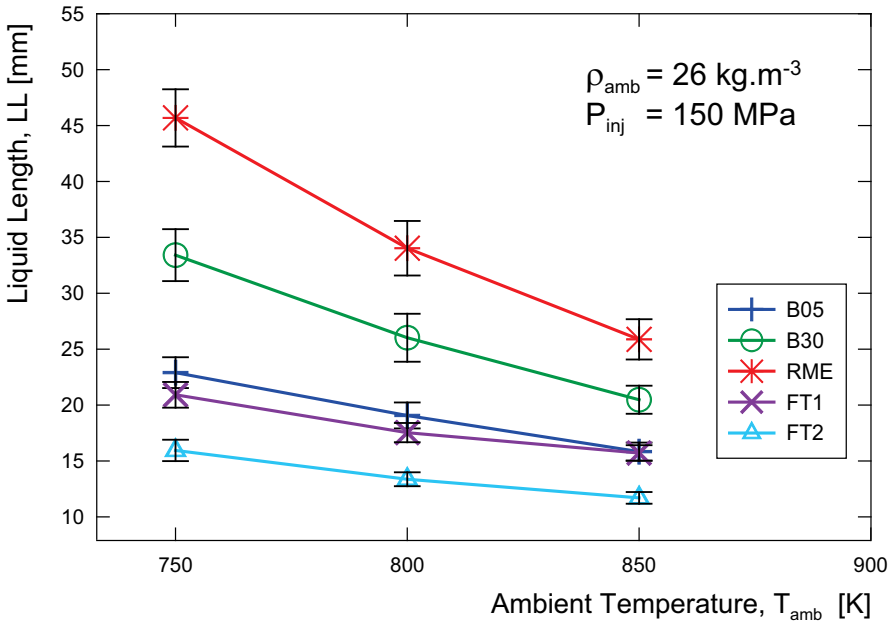

Figure 4.6. *Ambient temperature effect on liquid length for the five studied fuels at 150 MPa injection pressure.*

4.2.2.2. Statistical regression for engine-depending physical processes assessment

In a first instance, the statistical analysis has been applied to each fuel independently while introducing to the model the variables depending on engine settings exclusively. In this way it is proposed to evaluate if each of the five fuels responds with the same sensitivity to parameters conventionally varied in a production engine.

Thus, T_{amb}, ρ_{amb} and P_{inj} effect have been assessed and the resulting exponents collected in Table 4.2. Theoretical exponents derived from García-Oliver's model [6] using heptadecane as a surrogate have been added to the table header for comparison. Considering either steady or unsteady approaches, both the impact of ambient conditions and the irrelevance of injection pressure are confirmed for all the fuels, in agreement with the previous observations. Nonetheless, the exponents accounting for the effects of

Table 4.2. *Results from the statistical analysis for assessment of engine physical conditions under both steady and unsteady conditions. Statistically insignificant exponents (p-value> 0.05) appear in italic.*

Parameter		Cte	d_0	T_{amb}	P_{inj}	ρ_{amb}	-	-
Exponents		-	a	b	c	d	R^2	RMSE
Theoretical		-	1	-1.58	0	-0.5	-	-
B05	*Steady-State*	3.0324E+11	-	-3.11	-0.10	-0.68	99.0	0.28
B30		3.7266E+10	-	-2.80	*-0.02*	-0.70	92.6	0.91
RME		3.2664E+15	-	-4.39	*-0.04*	-0.82	99.0	0.59
FT1		5.3889E+09	-	-2.55	-0.09	-0.63	99.3	0.19
FT2		1.1733E+10	-	-2.68	-0.10	-0.67	97.9	0.26
All fuels		1.2095E+11	-	-2.98	*-0.06*	*-0.69*	15.3	6.95
B05	*Unsteady-State*	3.0139E+11	-	-3.12	-0.10	-0.66	96.5	0.60
B30		3.9238E+10	-	-2.81	-0.02	-0.69	89.4	1.23
RME		7.9248E+12	-	-3.55	-0.01	-0.75	88.9	2.02
FT1		4.4816E+09	-	-2.54	-0.09	-0.60	97.4	0.43
FT2		3.1336E+09	-	-2.53	-0.09	-0.58	95.5	0.44
All fuels		9.9393E+08	-	-2.42	-0.05	-0.39	11.3	6.82

ambient conditions, namely density and more particularly temperature, turn out to be higher than those proposed by the scaling law. The comparison among the fuels of their respective effect reveals a relative homogeneity except for RME. RME is indeed more likely affected by variations of in-cylinder conditions compared to the rest of fuels.

If now considered the comparison between results from steady and unsteady-state, it can be observed that, except for RME, the resulting exponents are remarkably close. This indicates that the parametrical study enabled by these unphased and temporally varying conditions provides the same results as the 15 "fixed" conditions from the initial test matrix. Therefore, this observation suggests that a spray under unsteady conditions behaves as a succession of steady states of the spray. In other words, it means that there is no delay in the adjustment of the spray to its environment under the range of pressure derivatives studied. This result is in entire agreement with the recent study from Fisher *et al.* [2] showing a good match between liquid length measurements and successive predictions from Siebers steady-state scaling-

law [5]. These results validate the use of Siebers' scaling law [5] under unsteady conditions as a succession of steady-states. Note that in García-Oliver's [7] and Kattke and Musculus's model, the in-cylinder history is already accounted [8, 9], although this result suggest it is not essential. Similarly, it extends the use of other empirical liquid length models derived from measurements obtained in steady-state environments [10], to such unsteady environment. These conclusions are supported by the high correlations reliability that has been evaluated through both the R-squared parameter and the RMSE which are, except for RME, consistent between steady and unsteady-state conditions.

The differences observed on the exponents for RME as well as the decay observed on R^2 and RMSE suggest that this fuel may not follow the same conclusions as depicted above and that the characteristic time of vaporization for a droplet of such a dense, viscous and low volatility fuel may be significant compared to the spray flow field development. In [1], Fisher *et al.* performed a similar analysis as in [2] while using two biodiesel fuels derived from different feedstock. Similarly, the authors observe that biodiesel liquid length is not directly related to instantaneous in-cylinder temperature and density, and suggest that biodiesel may be more subject to thermodynamic history. An attempt has been made to quantify the biodiesel time-response, namely the delay between the minimum liquid length of the empirical model (between T_{max} and ρ_{max}, closer to T_{max}), and the experimental minimum. Such delay was positive and thus consistent, however the quality of the result showed to be highly affected by our relatively low camera frequency. Yet, no clear trends were found when this delay was correlated with engine parameters or with the liquid length itself. Thus, both data and correlations were not robust enough to be presented in this manuscript and more investigation on the subject would be needed to understand this phenomenon of inertia.

Finally, just in in order to put in evidence the meaning of looking for relevant variables among fuel properties, all fuels liquid length results have been introduced into the statistical analysis tool and correlated exclusively with engine-derived variables ("All fuels" line of Table 4.2). As obviously expected, although no significant change is to report on the exponents' value, the very low R^2 shows that physical parameters issued from the engine setup are not sufficient to predict liquid length so that it is now necessary to introduce fuel physical properties to achieve a fuel-type free prediction.

4.2.2.3. Statistical regression for fuel physics assessment

An analogous statistical analysis has been conducted while introducing variables from fuel physical properties selected in the upper corresponding

section. Firstly, these variables may be themselves separated in two groups by considering on one hand fluid-mechanical properties (i.e. fuel density and viscosity), and on the other hand evaporative properties (i.e. $T_{10\,\%}$, $T_{50\,\%}$ and $T_{95\,\%}$ from distillation curves). Similarly to the previous section, no significant differences have been observed between steady and unsteady-state considerations. Thus, in order to leverage the higher number of input data, the *unsteady-state approach* was considered and its corresponding results are reported in Table 4.3.

Table 4.3. *Results from the statistical analysis for assessment of engine physical conditions and fuel physical properties under unsteady-state conditions. Statistically insignificant exponents (p-value>0.05) appear in italic.*

Parameter			Cte	d_0	T_{amb}	P_{inj}	ρ_{amb}	ρ_f	ν_f	$T_{10\,\%}$	$T_{50\,\%}$	$T_{95\,\%}$	-	-
Exponents		♯	-	a	b	c	d	e	f	g	h	i	R^2_{spe}	RMSE
Theoretical			-	1	-1.58	0	-0.5	0.5	-	-	-	-	-	-
All fuels	*Unsteady-State*	(1)	9.9393E+08	-	-2.42	-0.05	-0.39	-	-	-	-	-	11.3	6.82
		(2)	1.0000E+00	-	-	-	-	0.71	0.22	-1.14	5.41	-4.53	78.2	3.45
		(3)	8.2699E-08	-	-2.78	-0.06	-0.61	5.99	-	-	-	-	88.7	2.57
		(4)	6.8209E+09	-	-2.72	-0.06	-0.55	-	0.62	-	-	-	79.5	3.15
		(5)	9.4517E+06	-	-2.68	-0.06	-0.54	-	-	1.27	-	-	75.1	3.80
		(6)	3.2668E+06	-	-2.66	-0.06	-0.54	-	-	-	1.39	-	69.0	4.10
		(7)	1.5327E+06	-	-2.51	-0.06	-0.47	-	-	-	-	1.27	45.4	5.01
		(8)	2.2874E-03	-	-2.74	-0.06	-0.61	4.39	0.26	-	-	-	94.6	1.62
		(9)	1.8131E+10	-	-2.85	-0.07	-0.63	-	-	-1.23	6.94	-5.45	97.9	0.97
		(10)	**6.1213E-05**	**-**	**-2.63**	**-0.06**	**-0.60**	**4.39**	**-**	**-**	**0.54**	**-**	**94.4**	**1.57**
		(11)	1.0000E+00	-	-2.85	-0.07	-0.63	6.61	1.70	-0.90	-2.89	-0.06	98.1	0.93

As a first approximation, physical properties issued from the engine operation and fuel physical properties have been compared in correlations (1) and (2). This first simplistic comparison suggests that fuel properties have more contribution in the prediction of liquid length than engine-derived physical variables in the range operated. However, it should be acknowledged that negative coefficients for $T_{10\,\%}$ and $T_{95\,\%}$ remain physical non-senses. Thus, care must be taken to keep physical rationality while identifying the variables controlling the liquid length instead of chasing systematically the highest R^2 scores. Accordingly, fuel parameters have been associated one by one to engine-derived physical variables in correlations (3) to (7). Fuel density stands out as the most significant parameter for liquid length prediction, and all by itself already enables a reasonable level of prediction in correlation (3). In correlations (8) and (9), the fuel fluid-mechanics properties and fuel evaporative properties are respectively associated to engine physical

properties. The result shows that each sub-group of fuel physical variables is a good contributor for empirical modeling, although once again, the negative exponents for $T_{10\,\%}$ and $T_{95\,\%}$ are physical non-senses. Thus, correlation (10) shows an association of both fluid-mechanics and evaporative properties using subjectively the most essential and reliable parameters, namely fuel density and the distillation curve midpoint. The choice of conserving fuel density while removing viscosity was motivated by the previous variable analysis from 1D-models, and the finally only very weak influence of viscosity in the correlations. This analysis suggested that fuel density, beyond its potential effect in terms of energy balance, was already intrinsically involved in the mixing factor (exponent 0.5), while viscosity may only have affected spray angle, and both atomization and vaporization if the mixing-limited had not been previously verified. $T_{10\,\%}$ and $T_{95\,\%}$ have also been removed in favor of $T_{50\,\%}$ because the former show more instability in the correlations. In view of the distillation profiles, $T_{50\,\%}$ is also believed to be more representative of the LL trends, while $T_{10\,\%}$ and $T_{90\,\%}$ are more "collapsed". As commented above, the best illustration of this effect is given by RME-derived fuels having similar $T_{90\,\%}$ (because of their respective RME content) but having significantly different liquid lengths. This result is in agreement with Higgins *et al.* [10] and Canaan *et al.* [14] suggesting that the average volatility (represented by $T_{50\,\%}$) is a better predictor of liquid length than the lowest volatility fractions (represented by $T_{90\,\%}$) as stated by Siebers in [15]. This result motivated the test of a new variable, issued from the distillation curves, and resulting from the temperature integral throughout the whole recovery percentage. However, because of the quasi-linear profiles of distillation curves, this variable did not have a significant contribution compared to $T_{50\,\%}$. Though, this approach may find more substance with stair-shaped distillation curves such as when varying the blend rate of two pure compounds for example. Finally, correlation (11) has been added just in order to show the maximum reliability these parameters were capable of, for comparison with upper correlations.

On balance, correlation (10) may be considered as the most significant among the 11 other correlations shown in the table, although some others may also be employed depending on data availability. The reason for this is that most of the fuel physical variables selected are in one way or another inter-correlated and indirectly functions or "images" of the true controlling variables for liquid length, namely the latent heat of vaporization (L_v) and the liquid-phase heating component (enthalpy increase), i.e. a function of the liquid specific heat capacity (c_{PL}) and the temperature increase between T_0 and T_{evap}. If $T_{50\,\%}$ may intuitively be associated to T_{evap}, the significant role played by fuel density in this respect is more opaque. In addition, assuming

constant T_0 (reasonable) and constant $c_{PL}(T)$ among the fuels, $T_{50\,\%}$ would have a linear effect in the liquid enthalpy component which is not the case in correlation (10).

Therefore, in order to understand better the relevance of fuel density and $T_{50\,\%}$, the latent heat of vaporization (L_v) and the specific heat capacity of the liquid-phase ($c_{p,l}$) have been calculated at different temperature levels for a selection of alkanes following the methodology described above. Results for five linear alkanes along with isooctane are shown in Figure 4.7. Typically, both density increases and volatility decreases for linear alkanes when increasing their molar mass. Caution: this reciprocity does not systematically extend when compared with branched alkanes, unsaturated and oxygenated hydrocarbons. Both higher density and lower volatility of linear alkanes are due to stronger Van der Waals interactions reinforcing the cohesion and the rapprochement between molecules as the chain gets longer. For similar reasons, as an alkane gets more ramified, the length of the core chain gets smaller than the corresponding linear isomer, causing lower density and higher volatility. Thus, as suggested by the arrows on the figure, isooctane (ρ_f= 692 $kg.m^{-3}$ and T_{evap}=98.5°C at STP) is for instance closer in terms of density and volatility to n-heptane (ρ_f= 684 $kg.m^{-3}$ and T_{evap}=98°C at STP) than to n-octane (ρ_f= 704 $kg.m^{-3}$ and T_{evap}=126°C at STP).

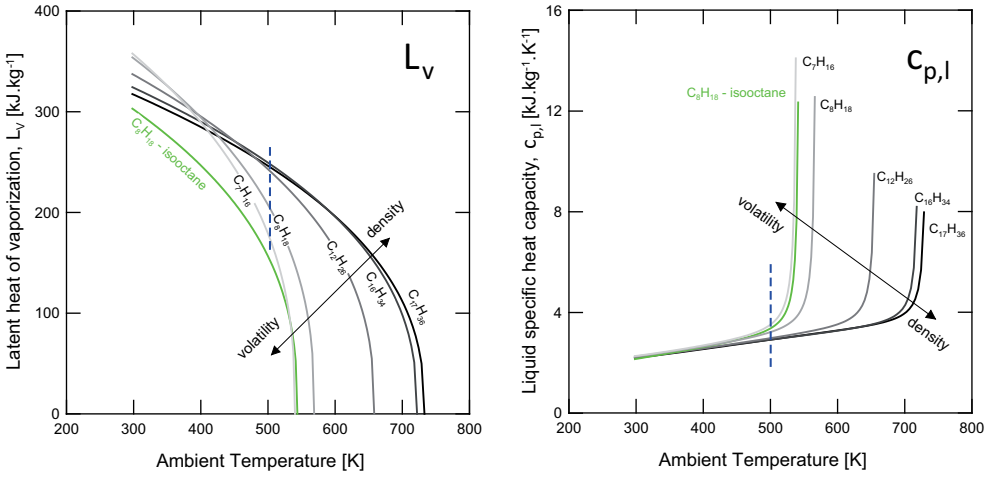

Figure 4.7. *Calculated latent heat vaporization L_v (Pitzer), and specific heat capacity $c_{p,l}$ (Rowlinson-Bondi) of isooctane and five linear alkanes.*

Now considering these alkanes at constant temperature (Cf. dashed lines in Figure 4.7) which could be the vaporization temperature T_{evap} defined in Eq. 4.3 and 4.4, it can be observed that the latent heat of vaporization increases with increasing density (or decreasing volatility), whereas the specific heat capacity $c_{p,l}$ decreases. Note that some authors relate this higher latent heat of vaporization with the higher cost for large molecule to break the liquid surface and get released as a gas. However, if considered the total liquid enthalpy increase (e.g. between 350 and 500 K), the heat consumption is only slightly smaller for larger molecules. Still, these offsetting effects are interesting as they suggest that the important exponent found for fuel density in the previous correlations makes sense and mostly accounts for the increase of latent heat when increasing density. The lower than expected exponent of $T_{50\,\%}$ in correlation (10) is also consistent with the lower $c_{p,l}$ and the lower heat dedicated to liquid fuel heating.

With linear alkanes density and volatility are reciprocal, which suggests that either ρ_f or $T_{50\,\%}$ would be enough to capture the effect of different $c_{p,l}$ and L_v. However, with the introduction of branched, unsaturated and oxygenated hydrocarbons, it is likely that each variable responds differently, such as two hydrocarbons may have the same density and different volatility (or vice-versa). Therefore, as suggested by their respective statistical significance (p-$value<0.05$), it becomes a requirement to consider both these variables in order to balance undesirable effects and get a better prediction. In conclusion, this small analysis confirms the relevance of both fuel density and distillation curve midpoint selected in correlation (10) for the creation of an empirical model predicting the liquid length for realistic fuels.

4.3. Vapor-phase penetration

In this second study, results obtained at Sandia National Lab. are presented, although injecting two other fuels in different conditions. Nonetheless, the result of the analysis is relevant as it can very likely extend to the selection of fuels used in the present work. Thus, only the analysis focusing on mixing and the differences observed between the transient penetration of diesel and biodiesel inert sprays is presented but the complete study, including reacting conditions and a detailed description of both the installation and the techniques employed may be found in [19].

Schlieren imaging permitted to visualize the vapor-phase penetration of both a conventional US diesel ♯2 (D2) and soy-biodiesel (BD) sprays under inert conditions. Each fuel was injected into an ambient environment of

900 K with equivalent density and injection pressure and the high frequency of image acquisition enabled a detailed description of the injection event (∼170 images/inj.). In Figure 4.8, the ensemble-averaged penetration at 900 K is shown as solid lines. The liquid-phase penetration also measured in the study is shown in dashed line for reference. During the initial penetration of the injection, the liquid and vapor phases overlap until the liquid-phase reaches its maximum penetration or liquid length. After the spray reaches this penetration distance, only the vapor-phase continues its progression through the chamber up to the vessel wall. The jet slows down as it continues to penetrate and entrain ambient gases, following a typical square-root dependency with time [22]. Although not represented on the figure, the vapor penetration of biodiesel at 900 and 1000 K overlapped perfectly, confirming the expected irrelevance of ambient temperature in the process of mixing.

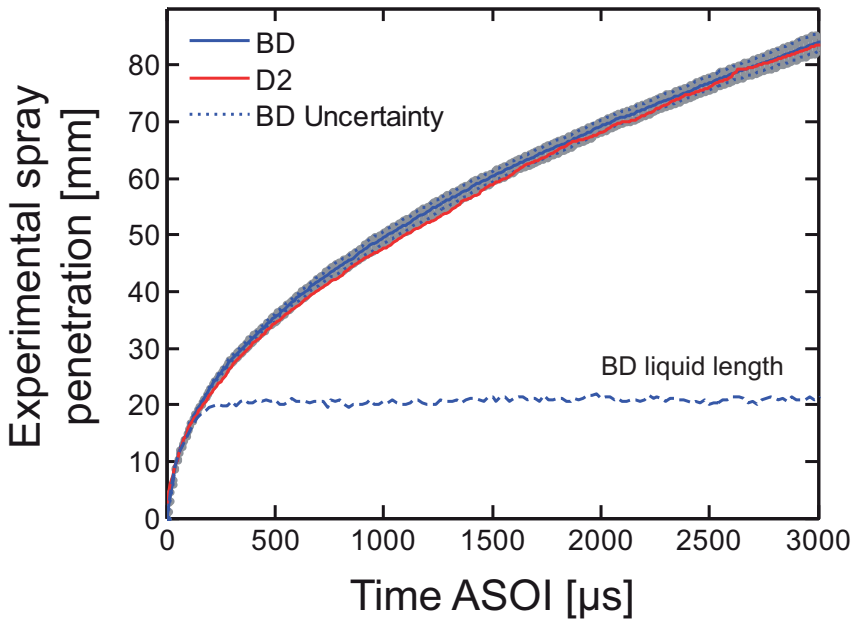

Figure 4.8. *Experimental results of the jet vapor penetration for both diesel and biodiesel under non-reactive conditions at 900 K.*

Comparing the two fuels jets, biodiesel appears to have a slightly faster penetration rate than diesel (D2), demonstrated more easily by the difference in penetration in Figure 4.9, which shows as much as 2 mm higher penetration for biodiesel. However, the differences are slight, especially when considering the experimental uncertainty. The shaded line surrounding the mean biodiesel

penetration at the bottom is the 95 % confidence interval for the ensemble average of the data. The overlap between mean value and the shaded region shows that the statistical difference between the two fuels is only marginal.

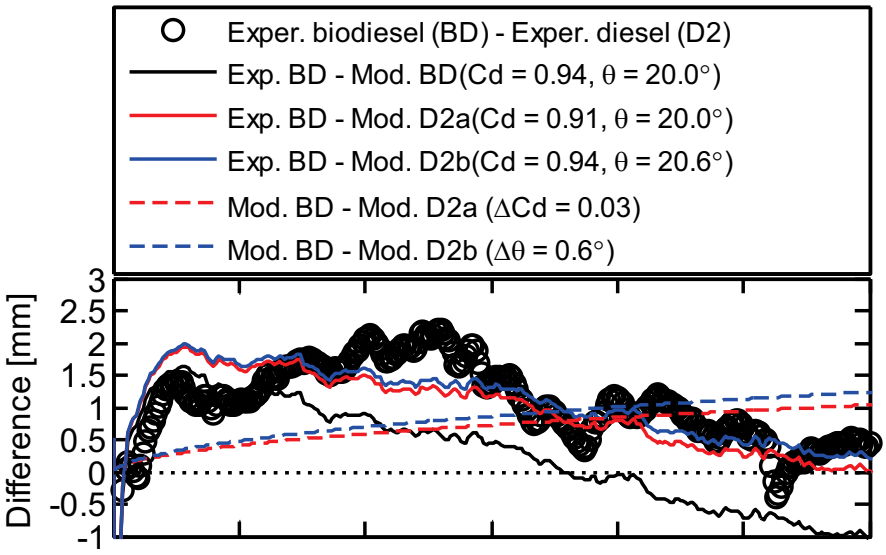

Figure 4.9. *Difference of biodiesel experimental penetration with respect to diesel, or penetration modeling predictions with different discharge coefficient (C_d) or different full spreading angle (θ).*

If real, the faster penetration of biodiesel could be the result of two factors: (1) a narrower spreading angle and/or (2) a higher spray momentum. Investigations of the measured spreading angle were not conclusive to establish a spreading angle effect in this study. The difficulties with assigning a spreading angle *via* schlieren imaging in this high-temperature/high-pressure environment are well-known since subtle differences in both optical setup and image processing yield different results for spreading angle but not penetration. Indeed, the radial borders of the schlieren images typically have too much uncertainty to conclude that biodiesel has a smaller spreading angle compared to diesel. Regarding (2), there is also an indication that biodiesel may have a slightly higher spray momentum. It may be reminded that the higher fuel density of biodiesel does not affect spray momentum when injection pressure is held constant and momentum changes only if the nozzle flow coefficients change. In the study, the discharge coefficient was also measured and appeared to increase from 0.91 with diesel to 0.94 with biodiesel, indicating that biodiesel would have higher momentum. Uncertainties in these coefficients deserve

attention, however, particularly because the fuel and injector temperature were slightly (10 K) different, which increases the uncertainty. In a previous study from Genzale *et al.* [18], flow coefficient measurements performed for the same fuels using the same injector temperature controller, but with a different, 0.108-mm nozzle, showed only an 0.01 units higher nozzle flow coefficients for biodiesel compared to diesel. This difference is also within the experimental uncertainty.

Given the uncertainties associated with spreading angle and spray momentum, and also with the measured penetration itself, it is helpful to address the effect that these parameter variations have on predicted jet penetration. The Musculus and Kattke jet model described in [8, 9] was used to model spray penetration with different assumptions for nozzle coefficients and spreading angle. Modeling results are given in Figure 4.9, displayed as difference in the modeling result compared to the biodiesel experimental or modeling data. Three model predictions are represented in the figure. One is for biodiesel with the discharge coefficient set to the experimental value of 0.94 and a full spray angle of 20°. The model predictions for biodiesel toggle about the experimental data, starting out too low but ending too high, although never varying from the experimental data by more than 2 mm. Two other model predictions are shown for diesel fuel. D2a uses the same spreading angle as BD and the measured discharge coefficient, while D2b assumes the same nozzle coefficients and a higher spreading angle. The lower penetration of diesel (positive values in Figure 4.9) is well predicted with either a 0.6° spreading angle increase or a 0.03 decrease in discharge coefficient (according to our measurements) compared to that of biodiesel, amounting to about 1 mm lower penetration by 3000 μs in each case. This modeling exercise is useful because it shows the extent that changes in spreading angle or flow coefficients affect penetration. It also shows that these subtle variations produce predictions that fall within the experimental uncertainty. Ultimately, it can be concluded that the differences in penetration for biodiesel and diesel jets are not significant enough to ascertain a causal effect of either spreading angle or flow coefficients on the penetration and represent an indication that the biodiesel spreading angle may be similar to that of fossil diesel.

This result is also in agreement with recent studies from Payri *et al.* [23], comparing conventionnal diesel and gasoline, and from Kook *et al.* [24], involving six fuels among which the same conventional D2 and similar Fisher-Tropsch fuels to those employed previously in this work. Figure 4.10 shows the results of vapor-phase penetration and similarly, both measurements and analysis were conclusive that the same vapor penetration is expected independently from the fuel type. As a consequence, this is an indication

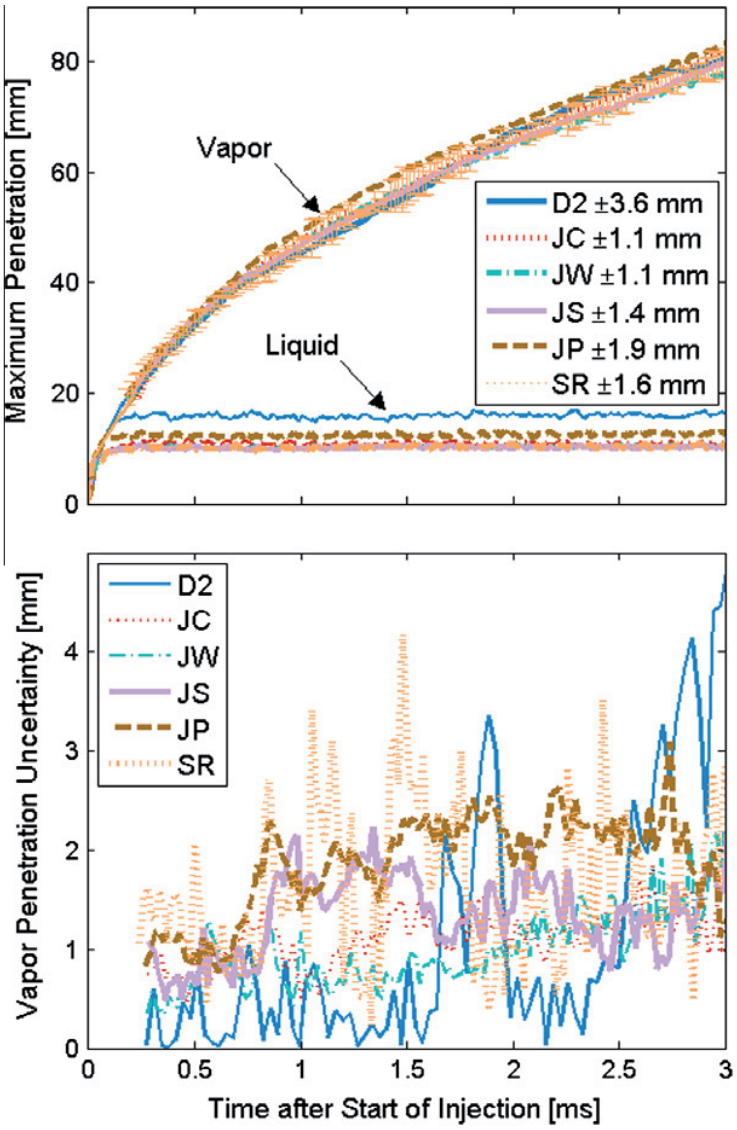

Figure 4.10. *Vapor penetration distance (top) and its uncertainty (bottom) from schlieren images. The penetration is a cycle average of five injections. The uncertainty bands for SR fuel are shown at the top of the figure. Also shown are liquid penetrations for the same operating conditions. D2: No. 2 diesel; JC: Conventional JP-8; JW: World average Jet A blend; JS: Fischer-Tropsch fuel; JP: Coal-derived fuel; SR: Surrogate fuel (23 % m-xylene, 77 % n-dodecane). Source: [24].*

that the total ambient entrainment and fuel-air mixing are virtually the same among all these fuels. By extension, this conclusion should apply to the five fuels tested in the initial test matrix. This result is fundamental in regard to spray modeling, as it suggests that potential variations of the local mixture equivalence ratio when varying the fuel origin proceed exclusively from the differences in the A/F stoichiometric ratio. In terms of mixture fraction field, this translates in similar values among fuels, only modified by the square-root relationship of fuel density from the equivalent diameter.

4.4. Conclusion

In order to assess the effect of fuel properties in respect to the physical processes associated to spray development, mixing and vaporization, measurements of both the liquid- and vapor-phase penetrations have been conducted in two different experimental facilities.

Measurements of the maximum liquid penetration (i.e. liquid length) were performed involving the five fuels and the facility presented in the previous chapter. According to the methodology defined, liquid length has been related to fuel properties and varying ambient conditions in a statistical analysis permitting the assessment of each group of variables. The consideration of the temporal evolution of thermodynamic conditions for the processing of liquid length high speed images permitted to multiply the number of samples for a more robust statistical analysis by extending and discretizing the initial test matrix. This study revealed the following conclusions:

(I) Under all tested conditions, Fischer-Tropsch fuels showed to have a shorter liquid length than RME-derived fuels, for which the liquid length increased when the RME percentage was increased. The fuel hierarchy for liquid length was the following: FT2<FT1<B05<B30<RME. This trend was maintained for all engine settings and suggested that fuel volatility was not sufficient to understand differences among fuels.

(II) The qualitative effect of engine-derived variables, namely T_{amb}, ρ_{amb} and P_{inj}, already available in the literature for conventional diesel fuel has been confirmed and could be extended to both biodiesel and Fischer-Tropsch fuels. In particular, the irrelevance of P_{inj} confirmed the mixing-limited hypothesis for alternative fuels, i.e. the irrelevance of droplet size and diffusion timescales at their surface. This result enables their use in 1D-models based on this assumption.

(III) For all the fuels except RME, the comparison between the two statistical approaches (steady/unsteady) revealed that the spray liquid-phase adjusts instantaneously to in-cylinder conditions. This result suggests that under time-derivatives up to 20000 $K.s^{-1}$ and 2000 $kg.m^{-3}.s^{-1}$, the spray liquid length behaves as a succession of steady-states, enabling both the use of Siebers' scaling law [5] and the use of empirical liquid length models derived from steady-state measurements, to unsteady conditions.

(IV) Fuel physical properties have been assessed against the physical properties resulting from engine operating conditions and translated into correlations for empirical modeling. Several of these correlations, associating either fluid-mechanics properties or evaporation properties, appeared to be valuable, while showing the significance of fuel density beyond its natural implication in mixing (equivalent diameter). An analysis including data of latent heat of vaporization and specific heat capacity of alkanes suggested that fuel density was a reliable mirror, mostly accounting for the latent heat of vaporization. $T_{50\,\%}$ appeared to be more representative of the overall fuel volatility compared to $T_{90\,\%}$ sometimes employed in the literature.

(V) According to the previous conclusion, an empirical correlation was proposed accounting for engine parameters, fuel fluid-mechanics properties and evaporation properties: $LL \propto T_{amb}^{-2.63} \cdot P_{inj}^{-0.06} \cdot \rho_{amb}^{-0.60} \cdot \rho_{fuel}^{4.39} \cdot T_{50\,\%}^{0.54}$

Measurements of the vapor-phase penetration rate have been carried on injection the conventional diesel ♯2 diesel and soy-biodiesel in similar conditions of thermodynamic ambient and injection pressure. Relevant conclusions of this study are the following:

(I) Under inert conditions, the vapor penetration of biodiesel at 900 and 1000 K overlap perfectly, confirming that ambient temperature is not relevant in the mixing process of the spray.

(II) Comparing the two fuels, penetration appeared to be very similar between ♯2 diesel and biodiesel, with the biodiesel jet penetrating only slightly more. Higher penetration for biodiesel could be caused by a better discharge coefficient of injection or a lower spreading angle, but these factors, as well as the penetration difference itself are within the experimental uncertainty.

(III) The similarity in penetration suggests that an equivalent field of equivalence ratio and therefore a similar fuel mixture fraction distribution

exist for diesel and biodiesel. Thus, because biodiesel is oxygenated, and has a similar mixture fraction distribution as diesel, it necessarily has a lower stoichiometry distribution compared to diesel fuel. In agreement with recent works involving alternative fuels, this result is believed to be extendable to the five fuels initially involved in this work, so that any potential variations of the local mixture equivalence ratio when varying the fuel origin proceed exclusively from the differences in the A/F stoichiometric ratio.

Appendix

Fuel	T_{amb}	ρ_{amb}	P_{inj}	ΔP	ρ_f	ν_f	$T_{10\,\%}$	$T_{50\,\%}$	$T_{95\,\%}$	LL
	$[K]$	$[kg.m^{-3}]$	$[MPa]$	$[MPa]$	$[kg.m^{-3}]$	$[mm^2.s^{-1}]$	$[K]$	$[K]$	$[K]$	$[mm]$
B05	798.0	29.7	50	43.2	833	2.50	205	293	356	19.34
	798.0	29.7	100	93.2	833	2.50	205	293	356	18.42
	798.0	29.7	150	143.2	833	2.50	205	293	356	16.87
	845.2	25.8	50	43.7	833	2.50	205	293	356	17.83
	845.2	25.8	100	93.7	833	2.50	205	293	356	16.55
	845.2	25.8	150	143.7	833	2.50	205	293	356	15.84
	795.4	21.7	50	45.1	833	2.50	205	293	356	24.01
	795.4	21.7	100	95.1	833	2.50	205	293	356	22.68
	795.4	21.7	150	145.1	833	2.50	205	293	356	21.42
	747.5	25.9	50	44.5	833	2.50	205	293	356	25.64
	747.5	25.9	100	94.5	833	2.50	205	293	356	24.87
	747.5	25.9	150	144.5	833	2.50	205	293	356	22.90
	796.8	25.8	50	44.1	833	2.50	205	293	356	22.05
	796.8	25.8	100	94.1	833	2.50	205	293	356	20.17
B05	796.8	25.8	150	144.1	833	2.50	205	293	356	19.07
B30	798.0	29.7	50	43.2	849	3.10	223	304	347	24.53
	798.0	29.7	100	93.2	849	3.10	223	304	347	26.15
	798.0	29.7	150	143.2	849	3.10	223	304	347	24.28
	845.2	25.8	50	43.7	849	3.10	223	304	347	24.16
	845.2	25.8	100	93.7	849	3.10	223	304	347	23.07
	845.2	25.8	150	143.7	849	3.10	223	304	347	20.48
	795.4	21.7	50	45.1	849	3.10	223	304	347	30.58
	795.4	21.7	100	95.1	849	3.10	223	304	347	31.86
	795.4	21.7	150	145.1	849	3.10	223	304	347	31.17
	747.5	25.9	50	44.5	849	3.10	223	304	347	30.93
	747.5	25.9	100	94.5	849	3.10	223	304	347	32.08
	747.5	25.9	150	144.5	849	3.10	223	304	347	33.41
	796.8	25.8	50	44.1	849	3.10	223	304	347	28.49
	796.8	25.8	100	94.1	849	3.10	223	304	347	27.80
B30	796.8	25.8	150	144.1	849	3.10	223	304	347	26.03
RME	798.0	29.7	50	43.2	878	4.41	321	334	345	31.67
	798.0	29.7	100	93.2	878	4.41	321	334	345	29.57
	798.0	29.7	150	143.2	878	4.41	321	334	345	30.20
	845.2	25.8	50	43.7	878	4.41	321	334	345	27.80
	845.2	25.8	100	93.7	878	4.41	321	334	345	27.57
	845.2	25.8	150	143.7	878	4.41	321	334	345	25.88
	795.4	21.7	50	45.1	878	4.41	321	334	345	39.14
	795.4	21.7	100	95.1	878	4.41	321	334	345	40.63
	795.4	21.7	150	145.1	878	4.41	321	334	345	39.36

Continued on next page

Appendix – continued from previous page

Fuel	T_{amb} [K]	ρ_{amb} [$kg.m^{-3}$]	P_{inj} [MPa]	ΔP [MPa]	ρ_f [$kg.m^{-3}$]	ν_f [$mm^2.s^{-1}$]	$T_{10\,\%}$ [K]	$T_{50\,\%}$ [K]	$T_{95\,\%}$ [K]	LL [mm]
	747.5	25.9	50	44.5	878	4.41	321	334	345	38.71
	747.5	25.9	100	94.5	878	4.41	321	334	345	45.85
	747.5	25.9	150	144.5	878	4.41	321	334	345	45.69
	796.8	25.8	50	44.1	878	4.41	321	334	345	36.73
	796.8	25.8	100	94.1	878	4.41	321	334	345	35.50
RME	796.8	25.8	150	144.1	878	4.41	321	334	345	34.03
FT1	798.0	29.7	50	43.2	784	3.44	250	297	352	18.26
	798.0	29.7	100	93.2	784	3.44	250	297	352	17.33
	798.0	29.7	150	143.2	784	3.44	250	297	352	16.12
	845.2	25.8	50	43.7	784	3.44	250	297	352	17.07
	845.2	25.8	100	93.7	784	3.44	250	297	352	15.90
	845.2	25.8	150	143.7	784	3.44	250	297	352	15.72
	795.4	21.7	50	45.1	784	3.44	250	297	352	22.31
	795.4	21.7	100	95.1	784	3.44	250	297	352	20.79
	795.4	21.7	150	145.1	784	3.44	250	297	352	20.08
	747.5	25.9	50	44.5	784	3.44	250	297	352	23.28
	747.5	25.9	100	94.5	784	3.44	250	297	352	22.22
	747.5	25.9	150	144.5	784	3.44	250	297	352	20.92
	796.8	25.8	50	44.1	784	3.44	250	297	352	19.53
	796.8	25.8	100	94.1	784	3.44	250	297	352	18.48
FT1	796.8	25.8	150	144.1	784	3.44	250	297	352	17.54
FT2	798.0	29.7	50	43.2	773	1.29	177	200	242	13.53
	798.0	29.7	100	93.2	773	1.29	177	200	242	13.09
	798.0	29.7	150	143.2	773	1.29	177	200	242	12.15
	845.2	25.8	50	43.7	773	1.29	177	200	242	13.08
	845.2	25.8	100	93.7	773	1.29	177	200	242	12.36
	845.2	25.8	150	143.7	773	1.29	177	200	242	11.70
	795.4	21.7	50	45.1	773	1.29	177	200	242	16.69
	795.4	21.7	100	95.1	773	1.29	177	200	242	15.92
	795.4	21.7	150	145.1	773	1.29	177	200	242	15.58
	747.5	25.9	50	44.5	773	1.29	177	200	242	18.75
	747.5	25.9	100	94.5	773	1.29	177	200	242	16.92
	747.5	25.9	150	144.5	773	1.29	177	200	242	15.94
	796.8	25.8	50	44.1	773	1.29	177	200	242	15.21
	796.8	25.8	100	94.1	773	1.29	177	200	242	13.77
FT2	796.8	25.8	150	144.1	773	1.29	177	200	242	13.37

References

[1] Fisher B.T., Knothe G., Mueller C.J., "Liquid-phase penetration under unsteady incylinder conditions: soy- and cuphea-derived biodiesel fuels versus conventional diesel". *Energy Fuels*, Vol. 24, pp. 5163-80, 2010.

[2] Fisher B.T., Mueller C.J., "Liquid penetration length of heptamethylnonane and trimethylpentane under unsteady in-cylinder conditions". *Fuel*, Vol. 89, pp. 2673-96, 2010.

[3] Benajes J., Novella R., García A., Arthozoul S., "Partially premixed combustion in a Diesel engine induced by a pilot injection at the low-pressure top dead center". *Energy Fuels*, Vol. 23, pp. 2891-902, 2009.

[4] Benajes J., Novella R., García A., Arthozoul S., "The role of in-cylinder gas density and oxygen concentration on late spray mixing and soot oxidation processes". *Energy*, Vol. 36, pp. 1599-611, 2011.

[5] Siebers D., "Scaling Liquid-Phase Fuel Penetration in Diesel Sprays Based on Mixing-Limited Vaporization". *SAE Paper 1999-01-0528*, 1999.

[6] García-Oliver J.M., *Aportaciones Al Estudio Del Proceso De Combustión Turbulenta De Chorros En Motores Diesel De Inyección Directa*. Tesis Doctoral, Universidad Politécnica de Valencia, Departamento de Máquinas y Motores Térmicos, 2004.

[7] Pastor J.V., López J.J., García J.M., Pastor J.M., "A 1D model for the description of mixing-controlled inert diesel sprays". *Fuel*, Vol. 87, pp. 2871-85, 2008.

[8] Musculus M.P.B., Kattke K., "Entrainment Waves in Diesel Jets". *SAE Paper 2009-01-1355*, 2009.

[9] Musculus M.P.B., "Entrainment waves in decelerating transient turbulent jets". *J. Fluid Mech.*, Vol. 638, pp. 117-40, 2009.

[10] Higgins B.S., Mueller C.J., Siebers D., "Measurements of fuel effects on liquid-phase penetration in DI sprays". *SAE Paper 1999-01-0519*, 1999.

[11] Desantes J.M., Pastor J.V., Payri R., Pastor J.M., "Experimental characterization of internal nozzle flow and diesel spray behavior. Part II. Evaporative conditions". *Atomization Sprays*, Vol. 15, pp. 517-43, 2005.

[12] Pitz W.J., Mueller C.J., "Recent progress in the development of diesel surrogate fuels". *Prog. Energ. Combust.*, Vol. 37, pp 330-350, 2011.

[13] Browne K., Partridge I., Greeves G., "Fuel Property Effects on Fuel/Air Mixing in an Experimental Diesel Engine". *SAE Paper 860223*, 1986.

[14] Canaan R.E., Dec J.E., Green R.M., Daly D.T., "The influence of fuel volatility on the liquid-phase fuel penetration in a heavy-duty D.I. diesel engine". *SAE Paper 980510*, 1998.

[15] Siebers D., "Liquid-phase fuel penetration in diesel sprays". *SAE Paper 980809*, 1998.

[16] Pastor J.V., Pastor J.M., Gimeno J., Nerva J.-G., "The effect of biodiesel fuel blend rate on the liquid-phase fuel penetration in diesel engine conditions". *SAE Paper 2009-24-0051*, 2009.

[17] Azimov U., Kim K.S., "Visualization of gas-to-liquid (GTL) fuel liquid length and soot formation in the constant volume combustion chamber". *J. Therm. Sci. Technol.*, Vol. 3, pp. 461-73, 2008.

[18] Genzale C.L., Pickett L.M., Kook S., "Liquid penetration of diesel and biodiesel sprays at late-cycle post-injection conditions". *SAE Paper 2010-01-0610*, 2010.

[19] Nerva J.-G., Genzale C.L., Kook S., García-Oliver J.M., Pickett L.M., "Fundamental spray and combustion measurements of soy methyl-ester biodiesel". *Int J. Engine Res.*, published online 30 August 2012, pp. 1-18, 2012.

[20] Pastor J.V., Payri R., Gimeno J., Nerva J.-G., "Experimental Study on RME Blends: Liquid-Phase Fuel Penetration, Chemiluminescence, and Soot Luminosity in Diesel-Like Conditions". *Energy Fuels*, Vol. 23, pp. 5899-915, 2009.

[21] Allocca L., Montanaro A., Cipolla G., Vassalo A., "Spatial-temporal characterization of alternative fuel sprays from a second-generation common-rail fuel injection system for Euro4 passenger car application". *SAE Paper 2009-01-1856*, 2009.

[22] Naber J.D., Siebers D.L., "Effects of Gas Density and Vaporization on Penetration and Dispersion of Diesel Sprays". *SAE Paper 960034*, 1996.

[23] Payri R., García A., Domenech V., Durrett R., Plazas A.H., "An experimental study of gasoline effects on injection rate, momentum flux and spray characteristics using a common rail diesel injection system". *Fuel*, Vol. 97, pp. 390-9, 2012.

[24] Kook S., Pickett L.M., "Liquid length and vapor penetration of conventional, Fischer-Tropsch, coal-derived, and surrogate fuel sprays at high-temperature and high-pressure ambient conditions". *Fuel*, Vol. 93, pp. 539-48, 2012.

Chapter 5

Fuel effects on spray combustion

Contents

5.1. Introduction

In the previous chapter, the influence of fuel physical properties in the process of mixture fraction field establishment has been isolated from the other physical variables proceeding from the engine operating conditions. The object of this second analysis is now to explore the effect of fuel properties under reacting conditions. Naturally, the outcomes from the previous chapter will be accounted, in particular the mixture fraction values in the upstream region of the flame, in order to observe their impact during combustion. In this second set of experiments, the rig and its corresponding test matrix were conserved, while oxygen concentration was switched from 0 to 21 % (in volume). OH-chemiluminescence, laser extinction and 2-color imaging presented in *Chapter 3* as the "combustion and soot formation setup" have been operated simultaneously and associated to the pressure trace analysis to understand the fuel effect on both combustion phenomenology and emissions formation. Such combination of techniques allowed studying spray autoignition, flame lift-off length, and both temperature and density of the soot cloud, while accounting for their potential interactions. A search for relationships between these measurements is performed, first to identify the role played by the fuel at each of these key stages/regions, but also to confirm and improve the understanding of the combustion phenomenology. Results and analysis will be contrasted with those obtained in the exhaust of production or single-cylinder engines.

The influence of thermodynamic and injection processes will be first addressed for each fuel separately, with the purpose to check and compare their own sensitivity with respect to these parameters intrinsic to engine functioning. Subsequently, an attempt is made to extract the fuel properties responsible for the differences observed. As described in *Chapter 3*, the methodology of data processing will remain incremental, typically starting with conventional averaged values and then, if possible and relevant, extending to a cycle-to-cycle analysis in order to extract additional information of the whole experimental dataset and its associated dispersion.

5.2. Relationship between fuel ignability and lift-off length

Although flame lift-off length is a long-time measured parameter, details of the mechanisms responsible for its establishment remain uncertain and are still subject to investigation today. Historically, mechanisms leading to stabilization of the flame lift-off were explained through the gas jet theory by which Peters [1] suggested that the latter establishes at the location where the propagation velocity of a premixed flame front and local convective velocity of the flow offset. Recently, another perspective was explored by Pickett *et al.* in [2], based on the observation that fuels with shorter ignition delays also had shorter lift-off lengths. In [3], the authors also observed the emergence of small ignition kernels developing near the flame base, suggesting that lift-off establishment and stabilization may be connected with local ignition processes. In [4], these statements were pushed further by forcing ignition *via* a laser pulse in the upstream region of the natural lift-off length. The spray showed to ignite quite readily, then facing lift-off stabilization close to the laser ignition spot during a relatively long period ($\sim$10 ms) before returning to its natural position. Thus, the latter work suggests that more than just related, the establishment of the lift-off in Diesel conditions may be driven by the very processes of autoignition.

In the following analysis, fuel properties relevant in both processes of autoignition and flame lift-off establishment are first identified, and their relevance assessed in respect to the physical variables proceeding from the engine operating conditions. Then, because fuel properties are expected to have an impact on phenomena described above, the opportunity is given to explore the validity of both Peters and Pickett statements in the context of this study.

5.2.1. Ignition delay, a parametric study

As reviewed in *Chapter 2*, fuel ignitability is fundamentally a characteristic of the fuel molecular structure. The propensity of a hydrocarbon molecule to ignite stands in its ability to first break one of its bonds whose strength varies respect to parameters such as position or branching degree. In *Chapter 3*, the chemical composition and molecular morphology of the fuels involved was approached although with the limitations associated with the characterization of real multi-component fuels.

Ignition delay has been measured through the analysis of the pressure trace following the methodology described in *Chapter 3* and illustrated in Figure 3.23. In view of both the absence of CN measurements for all fuels, and the uncertainty of CI calculations, ignition delay is then the first experimental approach connecting the fuel chemical content loomed in *Chapter 3* and the practical ignition qualities of the fuel under Diesel-like conditions. As reviewed in *Chapter 2*, the experimental protocol is actually very similar to that of CN measurements through the ASTM D-6890 standard. In that sense, ignition delay measurements at the baseline condition (NO, 100 MPa) may be seen as an alternative option to address fuel ignitability, while presenting the advantage to be obtained in the specific conditions of our experiment, more relevant of the conditions of a modern engine in terms of injection technology and ambient conditions [5]. In addition, by varying injection and ambient conditions the opportunity is given to assess the fuel effect in comparison.

5.2.1.1. Dispersion of ignition delay measurements

Before entering into a deeper analysis of the specific parameters governing the ignition delay, it is proposed to quantify the dispersion of the measurement. As presented in *Chapter 3*, a 3σ-threshold (99.7 % reliability) was used as a criterion to detect the ignition pressure rise aiming at detecting the time of recovery from fuel vaporization. Figure 5.1 shows the measurements histograms for two points of the test matrix which are representative of the overall dispersion and will be later used for the analysis of lift-off length dispersion. Typically, the coefficient of variation (CoV), defined as $\sigma_\tau/\overline{\tau}$ was 5 %. For 67 tests out of 75, CoV was inferior to 6 % and the maximum was 8.5 %. At both these conditions, the histogram shows a typical Gaussian shape with a relatively low standard deviation, which attests for the stability of ignition processes in our facility.

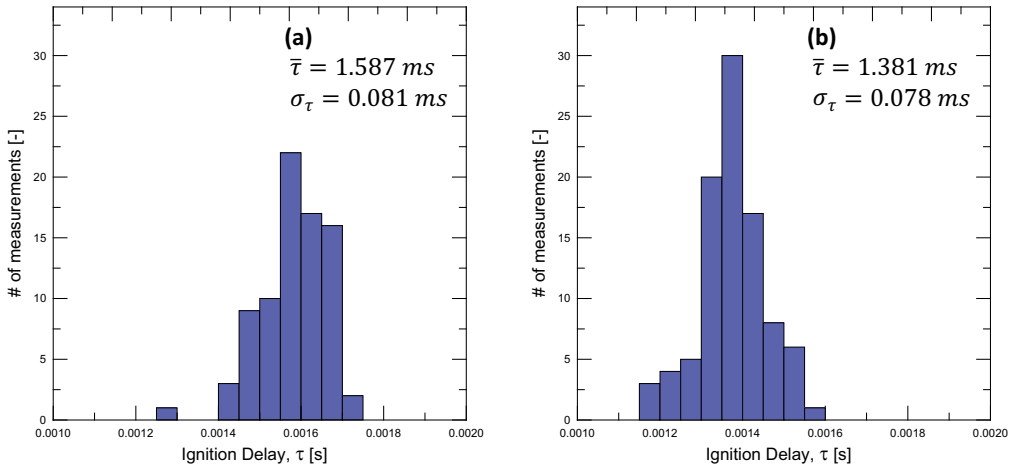

Figure 5.1. *Histograms of ignition delay measurements. In (a), B05 at 800 K, 30 kg.m^{-3} and 50 MPa injection pressure; and in (b): FT2 at 800 K, 26 kg.m^{-3} and 50 MPa injection pressure.*

5.2.1.2. Analysis of ignition delay results

In a first approach, ignition delay measurements have been analyzed for each fuel separately following a standard method for the analysis of ignition delay (τ) results, namely by fitting an Arrhenius-type equation[1] to the experimental data. In Eq. 5.1, ignition delay is a function of the fuel activation energy (E_a) and the ambient temperature (T_a), while A and R are respectively a pre-exponential factor and the universal gas constant.

$$\tau = A \cdot exp(\frac{E_a}{R \cdot T_a}) \tag{5.1}$$

Figure 5.2 shows different representations of ignition delay as a function of ambient temperature. In the six plots, the dashed lines represent the Arrhenius regression of each fuel obtained while using the whole test matrix dataset (15 points/fuel). Symbols of the NO condition at 100 MPa injection pressure have just been added for reference. In the five remaining plots, fuels are considered individually and the effect of injection pressure added. The Arrhenius-fits of each fuel are recalled and their corresponding equations formulated.

[1]Note that Eq. 5.1 is an adaptation of the classical Arrhenius equation, typically expressing a reaction rate k (in s^{-1}) instead of a delay.

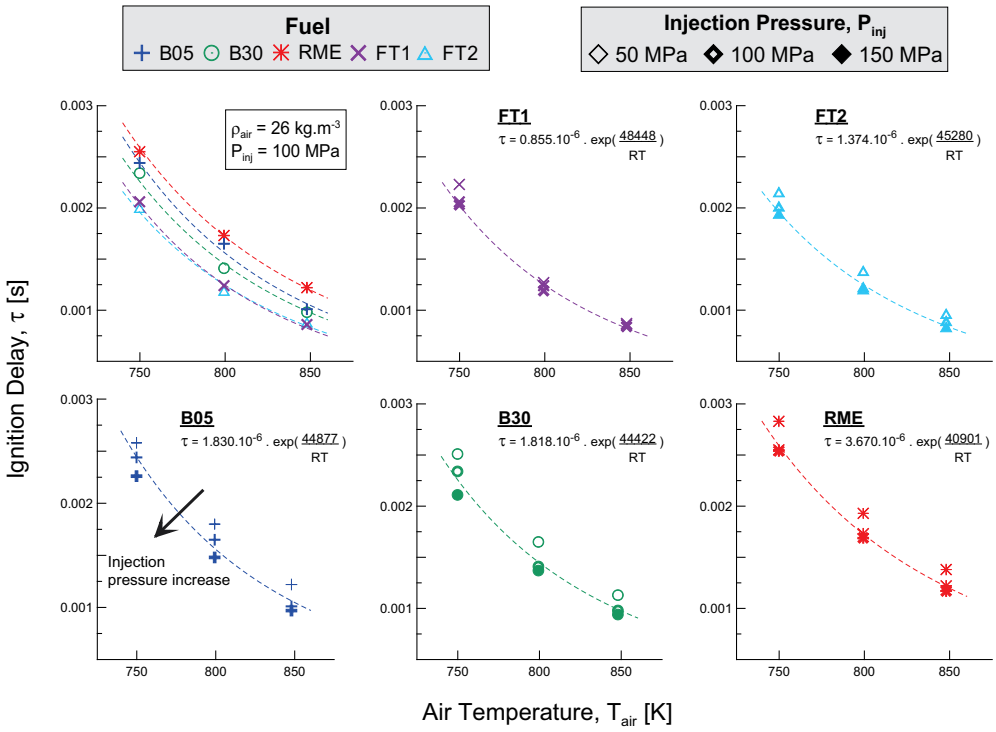

Figure 5.2. *Arrhenius plot of the ignition delay for the five selected fuels. The top left hand plot displays the fuel stratification at P_{inj}= 100 MPa, while the five other plots show the injection pressure effect for each fuel. Different symbols are used for each fuel and their thickness varies with the injection pressure level. LD and HD thermodynamic conditions are not represented.*

Starting with the upper left-hand corner of the figure, the plot aims at comparing the five fuels. A stratification emerges of fuel ignitability according to the following hierarchy: FT1∼FT2<B30<B05<RME. As expected, this stratification does not rigorously follow the one issued from CI calculations showed in Table 3.4. For the record, these correlations suggested that fuels with lower density and lower volatility were more prone to ignite. Among all of them, correlation (1) now appears to be the most predictive as it both minimizes the differences between FT1 and FT2, and predicts RME lower ignitability. Therefore, although CI correlations appeared to be consistent in terms of trends, this observation confirms that the weight attributed to fuel density and volatility is different out of the range limiting their use.

Higher ignitability of Fischer-Tropsch fuels is in agreement with their absence of aromatics, their high level of saturation, and thus their lower density respect to RME-derived fuels. However, both fuels show very similar results despite their significant differences in terms of volatility (chain length), suggesting that their comparable density is more representative of their ignition qualities. In opposition, although with similar volatility but different density, B05 and FT1 show significant differences in ignition results. Regarding the comparison between RME-derived fuels, the longer ignition delay of RME and its relative position compared to B05 and B30 is rather surprising at a first glance. However, this result is in agreement with the conclusions of Section 3.3.3, where it was found that RME degree of saturation was inferior to that of B05 and B30 despite its lack of aromatics. Thus, it seems that RME higher density compared to the other fuels overcomes the effect of its lower volatility. B30's lower ignition delays compared to B05 are difficult to explain based on measurements of the level of unsaturation, but results remain consistent with their respective CN measurements (Cf. Table 3.4), excluding by the way an error due to experimental uncertainty. Such effect could possibly be due to the use of a cetane improver escaping our detection of the saturation level by Fourier Transform Infrared Spectroscopy. In view of these results, fuel density, as a marker of the fuel level of saturation, appears to be more relevant regarding ignition processes than fuel volatility, namely a parameter representative of its chain length.

Now looking at the E_a terms of each model, the result is somewhat remarkable as it seems that the higher the activation energy is, the faster ignition occurs, which is quite in opposition with the trend expected. If it is likely that the pre-exponential factor A accounts for a "constant chemical delay" intrinsic to each fuel, a chance also exists that it accounts for particular and local conditions of the mixture, thereby calling into questions the previous conclusions. Indeed, although the Arrhenius equations represent a good starting point, it must not be lost sight of the fact that this kind of analysis generally applies to homogeneous reactors. Therefore, mixing parameters such as ρ_a and P_{inj}, inherent to a spray matter may have an impact and should be accounted properly in consequence.

In the five remaining plots of Figure 5.2, fuels are considered individually, and results of the three injection pressure levels have been added. In order to both simplify the reading of the plot and isolate the injection pressure effect from that of ambient density, LD and HD symbols (at 800 K) have been removed leaving only the temperature sweep part of the test matrix (at 26 $kg.m^{-3}$). At the three temperature conditions and for the five fuels, increasing injection pressure decreases ignition delay. Whereas globally the

effect is rather moderate, it may be observed that such reduction seems more pronounced between 50 and 100 MPa than between 100 and 150 MPa. In Figure 5.3, the objective is then to compare this effect with both ambient condition variables, namely ρ_a and T_a. Once again, the top left-hand plot displays the fuel stratification and shows that it also maintains at the three levels of injection pressure. In the five continuing plots, the entire test matrix is now represented, and both air temperature and injection pressure effects already available in the previous figure can be observed. Though, emphasis is made on the sweep of ambient density within the dashed circles. Under all conditions, increasing air density from 22 to 30 $kg.m^{-3}$ at constant ambient temperature also produces a moderate decrease of ignition delay.

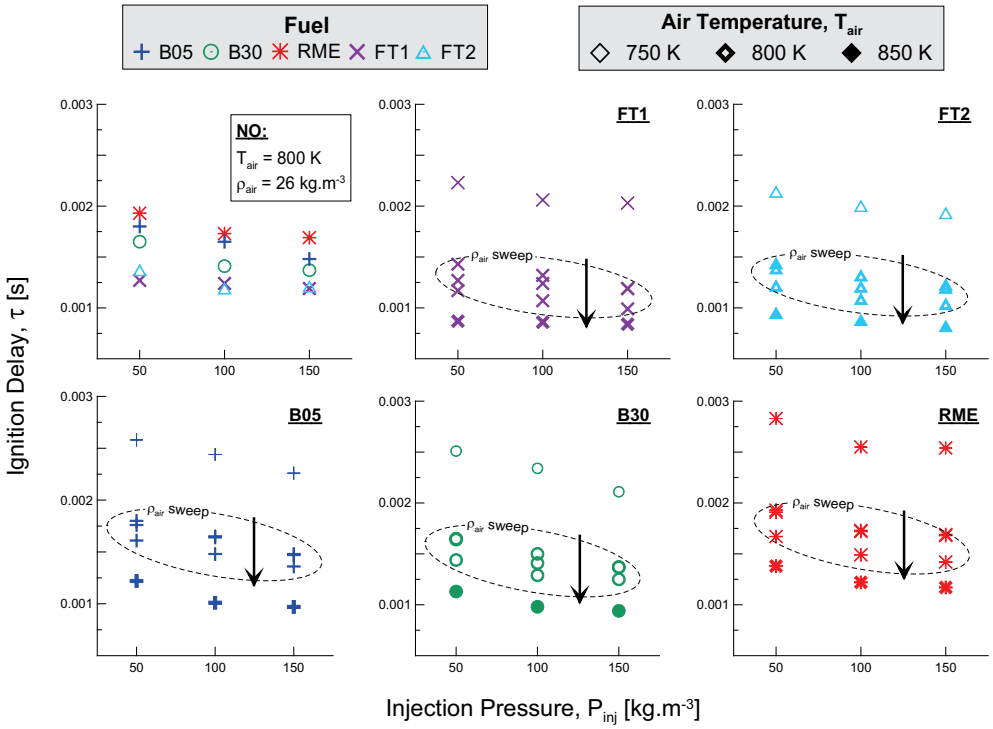

Figure 5.3. *Ignition delay as a function of injection pressure for the five selected fuels. In top left hand plot, it can be observed the fuel stratification at the NO-condition, while the five other plots detail the effects of P_{inj}, T_a and ρ_a for each fuel. Different symbols are used for each fuel and their thickness varies with the air temperature level.*

The analysis of both injection pressure and ambient density effects is comparable in a way that faster and better mixing makes the release of vapor

and the reach to ignition conditions faster and consequently leads to shorter ignition delays.

5.2.1.3. Empiricial modeling

Hence, these results highlight the role played by such mixing parameters on ignition delay as a consequence of the modifications they produce on the spray mixing characteristics. However, their interpretation remains qualitative and questionable in terms of relevance. For instance, by modifying either ambient density or injection pressure, ignition delay varies in a range of about 500 μs (10 to 50 %), but these variations are obtained multiplying injection pressure by three, whereas air density is only increased by about 50 %. Therefore, these effects need to be quantified more accurately and assessed in comparison with the variations of fuel characteristics involved.

As a result, such assessment may help to further understand the combustion phenomenology by addressing the significance of both mixing and chemical timescales in the process of Diesel ignition. Indeed, two limiting hypotheses may be considered as the boundary conditions of this analysis:

(I) the *Mixing-controlled ignition* for which the first chemical reactions would be triggered once a specific mixture fraction is reached to overcome the activation energy. This statement would be an analogy to the mixture level required for vaporization ($Y_{f,evap}$, introduced previously in *Chapter 4*), while substituting instantaneous vaporization by spray ignition.

(II) the *Chemical kinetics-controlled ignition* for which ignition processes would only be controlled by the chemical reaction rate fixed by averaged ambient conditions, independently from the local mixture state and any of the spray mixing processes, since mixing is assumed to be fast enough not to be dominant.

To address this topic, the two variables have been added to the Arrhenius-type equation, as written in Eq. 5.2, in order of extract their effect from the results of ignition delay. Fuel exit velocity (u_f) was calculated out of Eq. (2.1) following Bernoulli's equation.

$$\tau = A \cdot exp(\frac{E_a}{R \cdot T_{amb}}) \cdot \rho_{amb}^{a} \cdot u_f^{b} \tag{5.2}$$

The exponents of ρ_{amb} and u_f were quantified through a statistical analysis whose results and error associated are collected in Table 5.1. To help the comparison, results corresponding to the conventional Arrhenius equation (Eq. 5.1) are also indicated. For each fuel, the exponents found for ρ_{amb} and u_f are negative and thus consistent with the observations made above. Quantitatively, the weight of ρ_{amb} and u_f is enclosed between -0.20 and -0.45 quite homogeneously among the fuels. Reminding Section 2.3, the effect of injection pressure is found to be slightly superior to that of the study by Molina [6] where in a similar analysis the exponent of injection pressure was 0.2 (equivalent to 0.1 for u_f). At any rate, the impact of both mixing variables remains minor in comparison to the effect of ambient temperature. Indeed, if the term $exp(\frac{E_a}{R \cdot T_{amb}})$ were replaced by T_{amb}^c , c would get to values around -6. Thus, their contribution only slightly improves the model reliability with both the decrease of the RMSE and the increase of the specific R-squared, typically from 93 to 98 %. To summarize, although they are good refining parameters permitting the model to reach higher reliability, mixing parameters are very likely not any major issue in the empirical prediction of the ignition delay of a Diesel spray.

Table 5.1. *Results of the statistical analysis for the assessment of engine physical parameters in the prediction of ignition delay.*

Factor	A	E_a	ρ_{amb}	u_f	-	-
	-	$[J.mol^{-1}]$	$[kg.m^{-3}]$	$[m.s^{-1}]$	-	-
Exponents	**-**	**-**	**a**	**b**	R^2_{spe}	**RMSE**
(a) B05	1.83E-06	44877	-	-	92.1	0.000116
	2.36E-05	44689	-0.21	-0.3	98.7	0.000051
(b) B30	1.82E-06	44422	-	-	91.4	0.00012
	3.08E-05	44247	-0.32	-0.29	98.5	0.000059
(c) RME	3.67E-06	40901	-	-	95.7	0.000082
	5.95E-05	41040	-0.41	-0.24	97.3	0.000078
(d) FT1	8.55E-07	48448	-	-	95.4	0.000087
	1.98E-05	45920	-0.45	-0.22	97.1	0.000073
(e) FT2	1.37E-06	45280	-	-	93.3	0.000092
	2.59E-05	45049	-0.44	-0.24	97.4	0.000064
(f) All fuels	1.64E-06	45000	-	-	78.3	0.0002
	3.51E-05	44474	-0.34	-0.31	83.6	0.000186

Thus, reconsidering the two previous hypotheses, the statistical analysis suggests that chemical kinetics timescales are more likely to control ignition delay compared to mixing timescales, being ignition heavily dominated by ambient temperature. Under the specific terminology relating chemical reaction timescales to physical ones, this statement translates into a low Damköhler number ($Da << 1$) or a high Karlovitz number ($Ka >> 1$). In order to better illustrate this effect and the consequences on the combustion process, schlieren images have been retrieved from preliminary tests and are shown in Figure 5.4. This technique is sensitive to the first and second derivative gradients of the refractive index within the media observed [7, 8]. Because the low effect of injection pressure on ignition delay is a particularly pertinent situation, three injections of conventional diesel varying injection pressure at the same three levels are shown under thermodynamic conditions close to LD. This configuration of the schlieren setup, called "darkfield schlieren", enables three levels of intensity, being the liquid in black, the background in grey and the vapor in white on the resulting image [8]. As observable in the sequence, spray penetration is expectedly significantly faster as the pressure increases on the first instants prior to ignition. However, all the sprays ignite almost simultaneously in the head-vortex region, thus shifting ignition location further downstream. The first chemical activities are detectable at around 1280 μs and continue until nearly 1680 μs ASOE when the diffusion flame starts to establish. Now reconsidering results from the previous chapter and recording *Chapter 2* (Section 2.3), it is quite expected that injection pressure does not modify the mixture fraction field quantitatively, if not the velocity at which it establishes. Therefore, each of the three sprays consists of very different fields of both temperature and mixture fraction at the time and position of ignition. As suggested by the statistical analysis, chemical timescales thus seem to stifle local processes occurring among the wide range of "temperature/stoichiometric air-fuel ratio couples" enabled by each spray. Accordingly, ignition of the mixture remains sensitive to ambient temperature and oxygen concentration, but rather in space-averaged terms and thus quite in a "zero-dimensional way". This observation, proceeding from a process presented as fundamentally local in *Chapter 2*, was rather unexpected. In that sense, this figure further corroborates the results from the statistical analysis, while probably being more illustrative of the low relevance of mixing parameters on the ignition process. Besides, it also suggests a relationship between injection pressure, ignition delay and ignition location which will be approached in Section 5.2.3.

At this point, an empirical model based on physical parameters from the engine has been established for each fuel independently. Clearly, given

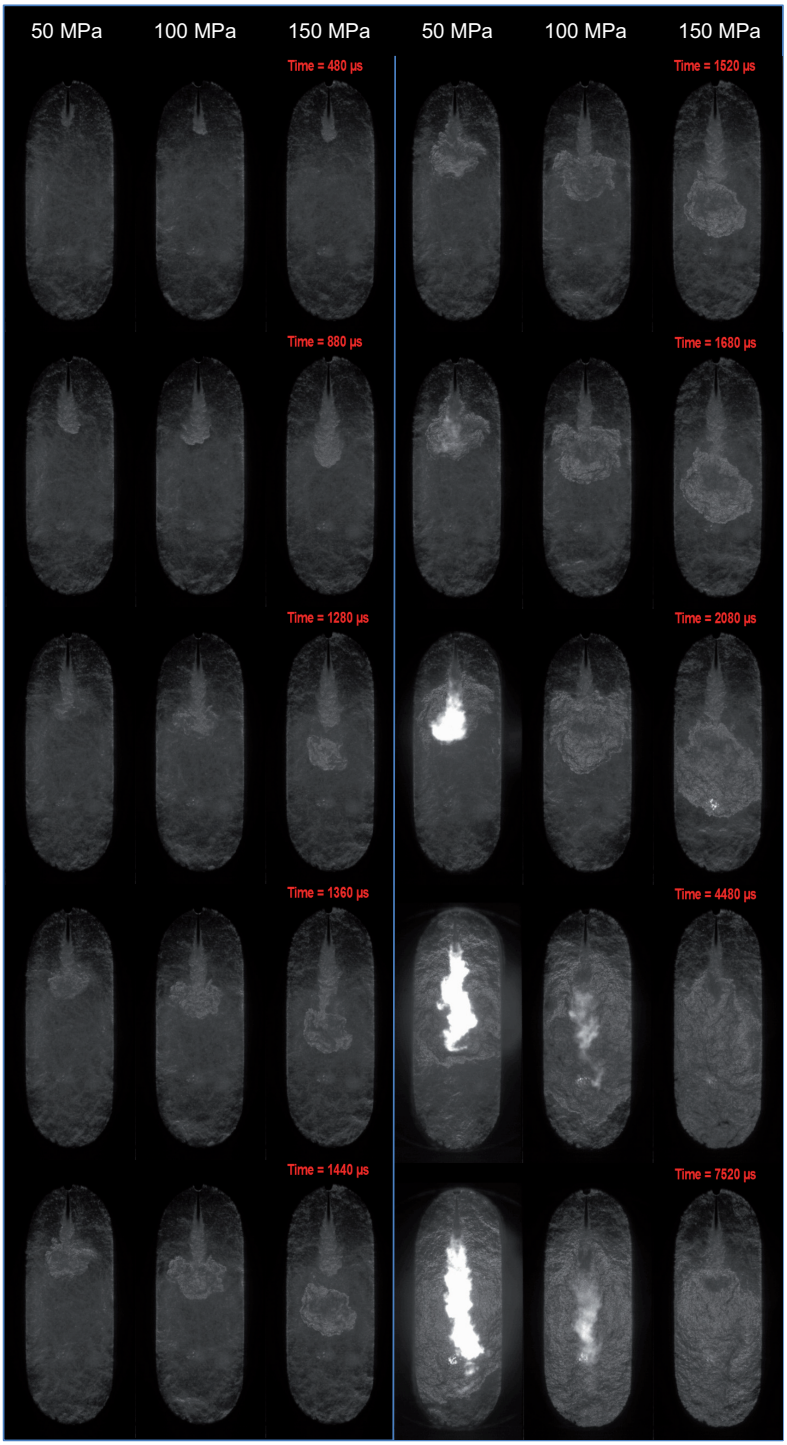

Figure 5.4. *Darkfield schlieren imaging of three injections of conventional diesel at 50, 100 and 150 MPa. Thermodynamic conditions are identical for the three tests: 22 kg.m^{-3}, 815 K, 21 % oxygen in volume.*

the differences of results among the five fuels, a model exclusively based on engine physical parameters without accounting for their own properties fails in predicting ignition delay (Cf. correlation f of Table 5.1). The next step is then to explore and identify the relevant fuel properties involved in the processes of ignition delay. First, the fuel stoichiometry appears to be a natural parameter to test as proposed in [3, 9]. Then, as both suggested by ASTM correlations and commented in the first qualitative description of the results, fuel volatility and particularly fuel density appeared to be good correlating parameters of ignition delay and their effect should now be quantified. Therefore, the fuel specific correlation of Eq. 5.2 has been extended with the latter fuel properties as expressed in Eq. 5.3.

$$\tau = A \cdot exp(\frac{E_a}{R \cdot T_{amb}}) \cdot \rho_{amb}^{a} \cdot u_f^{b} \cdot f_{st}^{c} \cdot \rho_f^{d} \cdot T_{10\,\%}^{e} \cdot T_{50\,\%}^{f} \cdot T_{90\,\%}^{g} \tag{5.3}$$

Table 5.2 shows the result of the statistical assessment of Eq. 5.3 exponents. In (1) and (2), physical parameters from the engine and physical properties of the fuel are tested each separately. The significantly higher reliability of (1) suggests that engine physics (P_E) prevails over fuel physical variables (P_F) in the prediction of τ within the range of this study. In (3), fuel stoichiometry is added and contributes to improve the model reliability by 10 %. The positive sign of the exponent indicates that fuels with a higher A/F stoichiometric ratio are easier to ignite. This result is remarkable as it goes against the mainstream idea stating that the oxygen content of RME-derived fuel helps ignition. Also, in view of the low effect of mixing parameters evidenced above, the effect of fuel stoichiometry is rather believed to be an indirect effect of fuel ignitability properties, since A/F ratio typically increases with long non-oxygenated molecules. Correlation (4) is based on the ASTM-D976 standard where fuel density and the mid-boiling point were used in the correlation. The model confirms the trend expected that lowering fuel density while heightening the distillation curves (decreasing volatility) is favorable to faster ignition. It also confirms the observations made earlier about density being clearly dominant over volatility. Finally, two extra points of the distillation curve are added in correlation (5) with no major contribution. Although the trend of (5) is confirmed and R-squared increases slightly respect to (4), the signs of $T_{10\,\%}$ and $T_{90\,\%}$ are inconsistent with the previous statements and only seems to be an artifact offsetting the increase of both ρ_f and $T_{50\,\%}$ exponents. As a consequence, correlation number (4) appears as a more reliable and reasonable choice as it accounts with physical sense to both fuel properties and variables proceeding from the engine functioning.

Table 5.2. *Results of the statistical analysis for the assessment of fuel physical properties towards ignition delay prediction.*

Factor		A	E_a	ρ_a	u_f	f_{st}	ρ_f	$T_{10\,\%}$	$T_{50\,\%}$	$T_{90\,\%}$	-	-
		-	$[J.mol^{-1}]$	$[kg.m^{-3}]$	$[m.s^{-1}]$	[-]	$[kg.m^{-3}]$	$[°C]$	$[°C]$	$[°C]$	-	-
Exponents		-	-	**a**	**b**	**c**	**d**	**e**	**f**	**g**	R^2_{spe}	**RMSE**
	(1)	3.51E-05	44474	-0.34	-0.31	-	-	-	-	-	83.6	0.000186
	(2)	4.70E-27	-	-	-	-	7.74	1.78	-9.14	7.64	23.5	0.000294
All fuels	(3)	2.02E-03	44244	-0.36	-0.26	1.56	-	-	-	-	93.5	0.000115
	(4)	**5.43E-13**	**44336**	**-0.37**	**-0.25**	**-**	**2.76**	**-**	**-0.13**	**-**	**96.5**	**0.000067**
	(5)	3.54E-26	44238	-0.39	-0.26	-	6.89	1.63	-8.22	6.85	97.9	0.000088

As a result of this section, ignition delay has been examined qualitatively before further analysis through a statistic method providing a more quantitative dimension to the first observations. At first, empirical models specific to each fuels permitted to highlight the strong influence of chemical kinetics compared to mixing processes. Seeking further clarifications into kinetics, the fuel effect appeared to have less impact than ambient temperature for the fuel selection considered. Yet, while the effect of fuel density and volatility was consistent with the models used for the calculation of CI, it was also in agreement with the expectations issued from the chemical structure analysis completed in the previous chapter. A fuel-independent empirical model accounting for both engine functioning variables and fuel physical properties was then produced, able to predict ignition delay with more than 95 % accuracy. Given the complexity and the number of chemical reactions involved in the process of ignition, these empirical correlations offer a certain interest for "fast modeling". Such a result does not aim at replacing all the recent effort made on kinetics models in CFD but it contributes to the understanding at an engineering level and may benefit for 0-D or 1-D modeling in on-board ECU systems. For this purpose, additional fuels should be considered and further experiments should be performed to account for the ambient oxygen concentration (EGR rate) as it plays a key role in ignition processes.

5.2.2. Lift-off length, a parametric study

Lift-off length, namely the distance between the nozzle tip and the flame base, is an important parameter for Diesel combustion understanding as it hints at the amount of fuel-air premixing occurring prior to the first region of high temperature heat release. This parameter has already been widely used in the literature and revealed to be a particularly precious tool for the

understanding of soot formation processes. The reader may refer to *Chapter 2* where several studies of interest are discussed, to find further information on the subject. Thus, line of sight images of OH-chemiluminescence were collected to visualize the stoichiometric surface [10] and measure the flame lift-off position relative to the injector *via* image post-processing. Regarding details of the optical setup, test procedure and image processing, the reader may refer to *Chapter 3*. In this section, a similar analysis to that for ignition delay is applied to evaluate the results of lift-off length measurement. The test repeatability is firstly approached; then, averaged results are analyzed intending to address the significance of fuel properties respect to both thermodynamic and injection setups; finally, a quantification of these effects is proposed through a statistical analysis.

5.2.2.1. Dispersion of lift-off length measurements

Unlike ignition delay measurements, dispersion of the lift-off length was quite significant from one cycle to another. Figure 5.5 shows histograms of measurements matching the same batch of experiments as in Figure 5.1 in addition to a sample of 10 images for each test. Each dataset represents the minimum and the maximum of the coefficient of variation (CoV) among the 75 test combinations, although the maximum standard deviation (σ_{LOL}=6.59 mm) was reached for the RME at 750 K, 26 $kg.m^{-3}$ and 100 MPa injection pressure. In (a), this ratio reaches 30 % for $\overline{LOL}$=10.70 with results contained between 4 and 18 mm. In (b), CoV is minimum but still reaches 13 % for $\overline{LOL}$=12.61. Lift-off length measurements appear then to be always strongly scattered. However, the number of injections for each point of the test matrix was 100. Occasionally, in particular conditions of long lift-off lengths and specific position of the optical mounting the flame could eventually miss the camera field of view. Still, the number of lift-off measurements was always superior to 70. Thus, the length of the 95 % confidence interval ($CI_{95\,\%}$), defined in Eq. 5.4, was found to reach a maximum value of 2.6 mm ($\sigma/\sqrt{n}$=0.66).

$$CI_{95\,\%} = \left]\overline{LOL} - 1.96 \cdot \frac{\sigma}{\sqrt{n}} \;;\; \overline{LOL} + 1.96 \cdot \frac{\sigma}{\sqrt{n}}\right[\tag{5.4}$$

In statistical terms, this means that for any additional repetition of the test, the average has a 95 % probability to stay within this interval. Therefore, the average measurement of lift-off length were considered as reliable and significant enough to be treated *per se* and used thereafter in a statistical analysis of variable assessment.

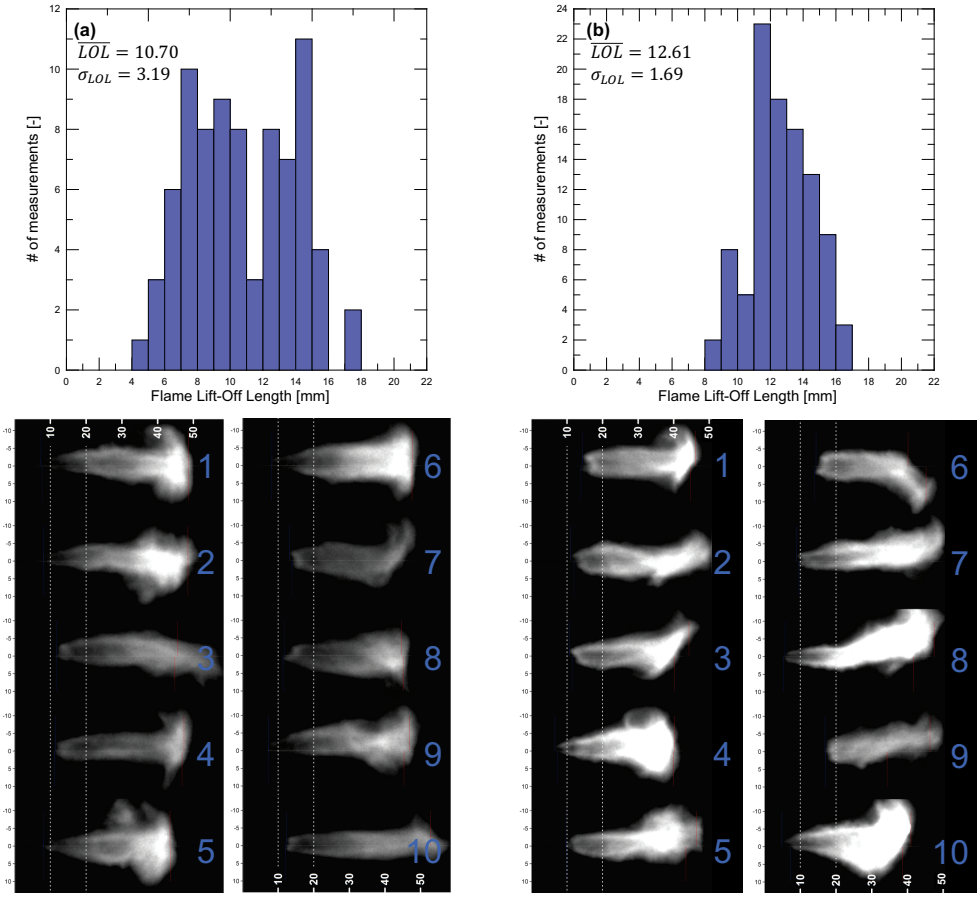

Figure 5.5. *Histograms of lift-off length measurements. In (a) the maximum $\sigma_{LOL}/\overline{LOL}$ ratio: B05 at 800 K, 30 kg.m^{-3} and 50 MPa injection pressure; and in (b) the minimum: FT2 at 800 K, 26 kg.m^{-3} and 50 MPa injection pressure.*

5.2.2.2. Analysis of lift-off length results

Figure 5.6 shows the average lift-off length as a function of thermodynamic and injection conditions for the five fuels separately. In plot (a), results of the temperature sweep at constant air density (26 $kg.m^{-3}$) and constant injection pressure (100 MPa) are represented. For all the fuels, the plot shows how the lift-off length decreases in a significant way as ambient temperature increases. The trend appears to be asymptotic: thus, extrapolating the lift-off length to air temperature levels above 850 K suggests that the lift-off length could collapse into a common value where neither the fuel nor the

ambient temperature would have effect anymore. Regarding the comparison among fuels, RME-derived fuels show similar results and therefore a similar sensitivity to ambient temperature. Meanwhile, the two Fischer-Tropsch fuels have significantly shorter lift-off lengths and their sensitivity to a temperature increase seems lower within this range of study. Similar trends were observed for the 50 and 150 MPa injection pressure levels.

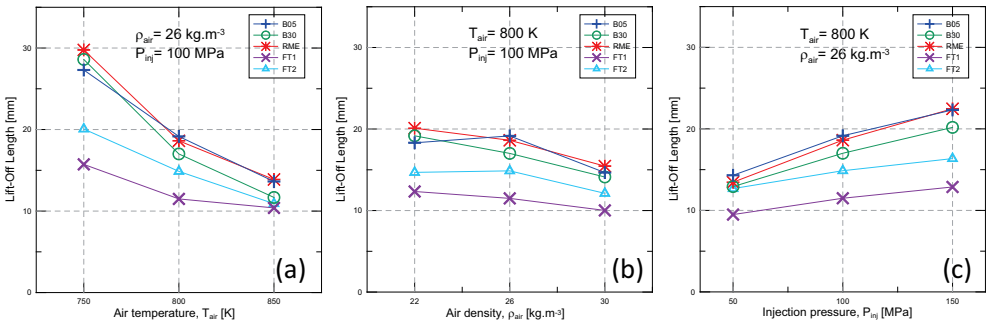

Figure 5.6. *Effect of (a) ambient temperature T_{amb}, (b) ambient density ρ_{amb}, and (c) injection pressure P_{inj}, on the lift-off length for the five studied fuels.*

The effect of ambient density is shown in plot (b). For the air density sweep part of the test matrix is now used, varying density between 22 and 30 $kg.m^{-3}$ at 800 K and 100 MPa. In the same way as observed for the temperature effect, an increase of ambient density shortens the lift-off length for all the fuels studied. However, the effect is significantly less important than the temperature effect with a decrease of the lift-off length inferior to 5 mm for a 36 % increase of air density. There is no clear trend showing that one fuel is more sensitive than another to such a density increase. According to that, the fuel hierarchy observed in the temperature sweep is conserved with shorter lift-off length values for the Fischer-Tropsch fuels and longer ones for RME-derived fuels.

Finally, the effect of injection pressure is represented in (c), for the NO operating condition. When the injection pressure is increased, lift-off length increases as well. Although the trend is always the same among different fuels, sensitivity is quite different, with both Fischer-Tropsch fuels being less responsive to the injection pressure than biodiesel-derived fuels. In order to give a quantitative dimension to these observations, the effect of injection velocity (u_f), ambient density (ρ_{amb}) and ambient temperature (T_{amb}) were assessed statistically to solve Eq. 5.5. Similarly to ignition delay, fuels have been first tested separately to check their sensitivity to these engine physical

parameters. As detailed in *Chapter 3*, air density and temperature have been time-averaged during the exposure window of the OH-chemiluminescence imaging under reacting conditions as shown in Figure 3.19. The resulting exponents for empirical modeling through Eq. 5.5 are summarized in Table 5.3.

$$LOL = k \cdot u_f^a \cdot \rho_{amb}^b \cdot T_{amb}^c \tag{5.5}$$

where u_f is calculated following Eq. 2.1.

In a consistent way for all the fuels, the increasing effect of spray velocity as well as the decreasing effects of both air density and air temperature are confirmed for all the fuels. As for ignition delay, air temperature is clearly the dominant factor. Fuel-to-fuel modeling reaches a very high reliability above 90 %. Logically, the model precision drops when all fuels are mixed. Following a quick comparison of the lift-off results with those of the liquid length, the analysis will focus on the fuel properties able to refine the experimental model in order to better predict the lift-off length without having to go to empirical models specific to each fuel.

Table 5.3. *Results from the fuel-specific statistical analysis.*

Term	K	u_f	ρ_{amb}	T_{amb}	-	-
Exponents	-	**a**	**b**	**c**	R^2	**RMSE**
Theoretical	-	**1**	**-0.77**	**-3.32**	-	-
B05	1.50E+15	1.02	-0.84	-5.28	93.9	1.48
B30	3.91E+17	1.02	-0.81	-6.13	98.4	0.73
RME	9.59E+14	1.02	-0.96	-5.15	96.5	1.13
FT1	3.17E+08	0.63	-0.62	-2.82	94.8	0.55
FT2	2.20E+13	0.79	-0.87	-4.47	94.7	0.83
All Fuels	1.88E+15	0.88	-0.75	-5.26	73.9	2.81

5.2.2.3. Comparison with liquid length results

In *Chapter 4*, the maximum liquid-phase penetration was measured under inert conditions. However, as suggested in *Chapter 2*, only few works have approached this measurement under reactive conditions [11]. Although this was not the case either in this study, Figure 5.7 proposes a comparison between inert liquid length and lift-off length values. The figure first highlights how the range of liquid length values is wider than that of lift-off lengths'. Most of

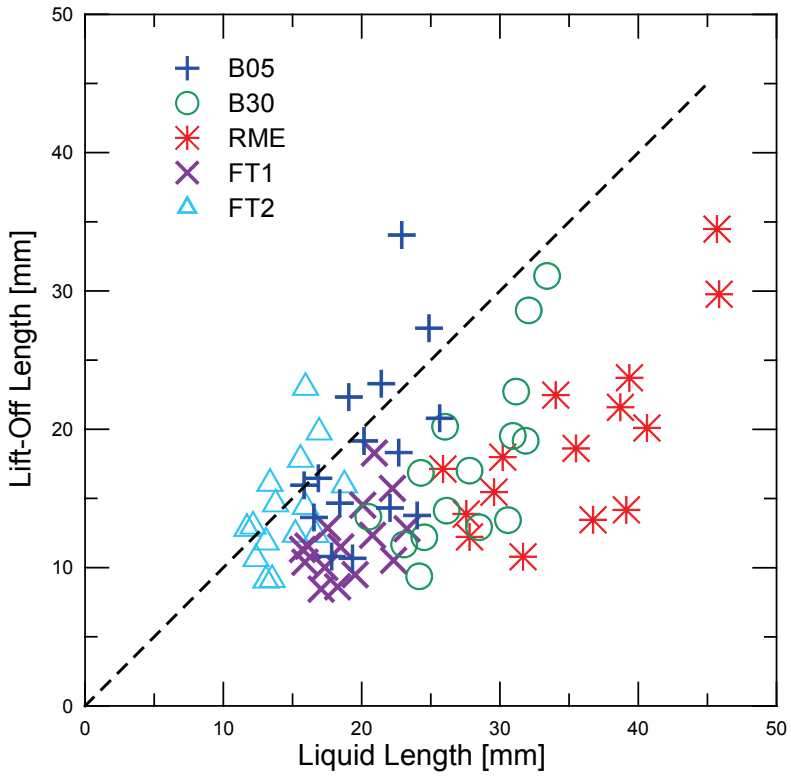

Figure 5.7. *Averaged lift-off length as a function of averaged liquid length for the five fuels under all test matrix conditions.*

liquid length values fall between 10 and 40 *mm*, while lift-off length remains between 10 and 25 *mm* with a couple of scattered points above 30 *mm* (highest injection pressure). But the most noteworthy point is certainly that lift-off length is shorter than non-reacting liquid length in 63 out of 75 test conditions, whereas only few conditions involving FT2 and B05 at the highest injection pressure conditions permit full vaporization prior to lift-off length. As a consequence, it is most likely that heat release from the lift-off region is interacting with liquid vaporization, probably shortening liquid length while cooling down the premixed burn occurring at the flame base. In [11], diesel ♯2 and biodiesel liquid lengths were maintained between inert and reactive conditions, but lift-off length was also significantly longer not to have any effect. The uncertainty on the effect that may have such local cool down or even the fact of having liquid achieving to penetrate inside the flame is high, and should be considered for future work as it may affect all the

processes occurring downstream including soot formation processes. Under these conditions, natural complete vaporization could not be a requirement for the establishment of lift-off if local heat release assumes an extra cost of fuel vaporization, or lift-off could establish to its natural position being driven by the conditions on the spray sides while being insensitive to the fuel phase in the centerline. Lift-off length stabilization is then a complex association of physical and chemical processes, either inherent to the engine operation or to the fuel properties. In the next section, two major theories for its establishment are tested in the statistical method to seek further insights in such governing processes.

5.2.3. Evaluation of Peters and Pickett theories on the mechanisms of lift-off stabilization

5.2.3.1. In average terms

As commented several times already, lift-off length is a long-time measured parameter with demonstrated influence on soot formation, but the detailed mechanisms responsible for its establishment remain uncertain and are still subject to investigation [12]. Historically, diesel spray lift-off length stabilization was explained through the gas jet theories in which Peters [1] mentioned that flame lift-off stabilizes at the location where the velocity of propagation of a premixed flame front and the local convective velocity of the flow offset. This statement is expressed by means of Eq. 5.6 where u_f is the velocity of Bernoulli, f_{st} is the stoichiometric mixture fraction, D_t is the thermal diffusion, s_L is the propagation velocity of the laminar flame front and k is a constant value.

$$LOL = k \cdot \frac{u_f \cdot f_{st} \cdot D_t}{s_L^2(f_{st})} \tag{5.6}$$

Siebers [13] extended this theory to the diesel jet application by bringing an additional term accounting for the spray cone angle (Eq. 5.7).

$$LOL = k \cdot \frac{u_f \cdot f_{st} \cdot D_t}{s_L^2(f_{st})} \cdot \frac{1}{tan(\frac{\theta}{2})} \tag{5.7}$$

Considering that diffusivity and laminar flame velocity depend on ambient temperature, ambient pressure (i.e. density) and fuel properties, the empirical model of Eq. 5.5 has been improved by adding the fuel stoichiometry as follows:

$$LOL = k \cdot u_f^a \cdot \rho_{amb}^b \cdot T_{amb}^c \cdot f_{st}^d \tag{5.8}$$

As concluded in *Chapter 4*, spray angle is not expected to change drastically from one fuel to another and was not included in consequence. Following the analysis made by Peters [1], the theoretical exponents a, b, and c are respectively 1, -0.77 and -3.32. Before including the fuel stoichiometry factor, it can first be looked back at the result obtained in Table 5.3 to check the experimental response of each fuel to engine parameters respect to the theoretical model. The linear trend with the spray velocity is respected for biodiesel-based fuels but not for Fisher-Tropsch fuels. The effect of air density is also well estimated but air temperature has, except for FT1, much more effect experimentally than expected with the gas jet theory.

Table 5.4 shows the results of the experimental modeling including all the lift-off length results from the five fuels. In (1), the low-efficiency correlation of Table 5.3 with no contribution of fuel properties has been recalled to help the comparison with improved correlations. Correlation (2) includes fuel stoichiometry but the model quality barely improves respect to (1). As suggested above with the low effect of mixing, this result hints at the fact that the fuel effect on ignition is somewhat more complicated than just a stoichiometry issue, and confirms that fuel chemical structure and the kinetics associated have to be accounted. Besides, one can find some inconsistencies when using the final correlation, e.g. the fact that velocity exponent is clearly lower than unity, which is intrinsically in disagreement with the combustion velocity stabilization hypothesis.

Table 5.4. *Comparison between Peters and Pickett theories on the lift-off stabilization.*

Term		k	u_0	ρ_{air}	T_{air}	f_{st}	τ	-	-
Exponents		**-**	**a**	**b**	**c**	**d**	**e**	R^2_{spe}	**RMSE**
Theoretical		**-**	**1**	**0.77**	**3.32**	**-**	**-**	**-**	**-**
All Fuels	(1)	1.88E+15	0.88	-0.75	-5.26	-	-	73.9	2.81
All Fuels	(2)	3.83E+17	0.64	-0.56	-5.2	1.9	-	79.3	2.33
All Fuels	(3)	24.134	0.92	-	-	-	0.92	91.3	1.55

Another path of research was explored by Pickett *et al.* in [2, 3]. The authors first observed that fuels with shorter ignition delays also had shorter lift-off lengths, later suggesting that lift-off stabilization may be resulting from

the agglomeration of ignition events (kernels) occurring at the flame base. Additionally, in [4], the same authors achieved to modify the flame morphology by forcing ignition upstream the natural region of lift-off establishment. The flame appeared to be easily ignited by the laser and lift-off stabilized close to the laser ignition spot for a relatively long time ($\sim$10 ms) before returning to its natural position. Therefore, these works state that ignition position is fundamental for the understanding of lift-off stabilization. An illustration of such connection between ignition position and lift-off length may be observed by reconsidering Figure 5.4 where shifted ignition location had already been observed among the three injection levels because of constant ignition delay, faster spray penetration, and of course the maintenance of this reaction in a position ahead of the flame, throughout the jet head-vortex region. Thus, although the flame lift-off length may be difficult to distinguish on schlieren images, one can still perceive how the heat release region gets closer to the nozzle as injection pressure decreases, supporting that lift-off length scales with ignition position in a consistent way with the previous considerations.

In the absence of systematic acquisition of chemiluminescence or schlieren images to detect ignition position with accuracy, Figure 5.8 displays a comparison between lift-off length and ignition delay. In (a), all the 75 points of the test matrix have been represented using different symbols to embody the three levels of injection pressure. In (b), the same results are plotted but highlighting fuel origin and ambient temperature conditions. Note that data from LD and HD at 800 K have been removed from (b) for ease of reading. Although plot (b) mostly aims at identifying the test conditions of plot (a), it also permits to reconsider with a different perspective the previous observations made about fuel stratification and the significance of ambient temperature over both processes of ignition and lift-off length. Yet the key information arises from plot (a) by revealing the existence of a simple relationship in which lift-off length appears to be depending only on ignition delay and injection velocity. Indeed, the entire test matrix turns out to be reducible to three groups in a linear fashion, such that each of them corresponds to a level of injection pressure, independently from thermodynamic conditions and fuel origin. Therefore, a simple time-speed relation confirms the key role played by ignition location on lift-off stabilization processes, in agreement with Pickett's approach.

Further quantification of this connection between ignition and lift-off processes is provided by correlation (3) from Table 5.4. According to the analysis of Figure 5.8, the model only involves spray velocity (u_f) and ignition delay (τ), but enables a significant improvement in terms of predictability compared to the previous ones. A nearly linear trend is obtained for

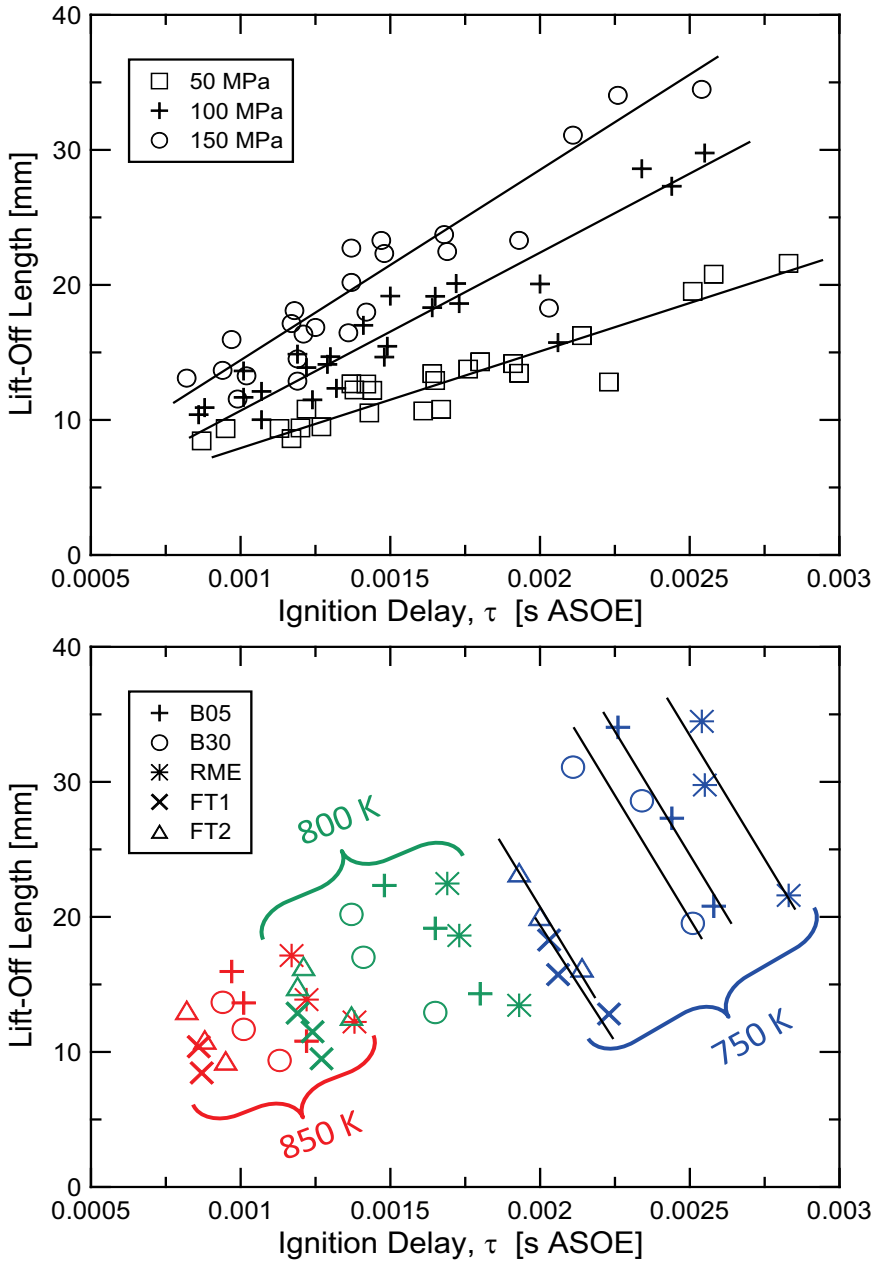

Figure 5.8. *Relationship between ignition delay and lift-off length. Results from the five fuels under the entire test matrix are plotted in (a) while only the temperature sweep data has been shown in (b).*

each parameter, further confirming the previous discussions. As for the quasi-linearity of τ, it also indicates that ignition exponents obtained in Table 5.2 for both fuel properties (primarily density) and thermodynamic conditions (primarily temperature) are almost directly extendable to lift-off length predictions. To conclude, the contribution issued from these results is important as it supports one of the two major conceptual approaches regarding lift-off length establishment, by approving under a large set of thermodynamic conditions and different fuel origins that a strong relationship exists between the latter and ignition location. In addition, an empirical model based on easily accessible inputs for any type of engines (ignition delay and injection pressure) permits to obtain a reasonable estimation of the lift-off length assuming free spray conditions.

5.2.3.2. Cycle-to-cycle approach

The previous correlation between ignition position and lift-off length stemmed from ensemble-averaged results of nearly 100 injections performed during each of the 75 tests of the initial test matrix. However, reconsidering histograms of Figures 5.2 and 5.6, such relationship does not appear to extend on a cycle-to-cycle basis, as scattering for lift-off length measurements is significantly more important than it is for ignition delay. Thus, because injection velocity is also considered to be a cycle-to-cycle robust process, other parameters must be interacting with the lift-off stabilization to which a treatment of average values is not sensitive to.

To identify the origin of such dispersion, recourse has been made once again to schlieren high-speed images retrieved from past experience with the technique. Figure 5.9 shows the juxtaposition of selected instants from two injection sequences in identical test conditions. As in Figure 5.4, the fuel employed is a commercial diesel (Repsol) with properties similar to the B05's used in this work, while thermodynamic conditions are exactly those of LT at 150 MPa injection pressure. The 4 ms injections were shorter however than the injections performed in this study. Under this "focused Schlieren" configuration [7, 8], highly deflected rays are clipped in the Fourier plane by an iris, thus resulting in a dark region on the image, whereas low-deflected rays such as those of the background go through the iris, get collected by the camera lens, and form a bright region on the image. In a Diesel flame context, these highly deflected rays are the markers of liquid, vapor and combustion products.

The purpose of the figure is to illustrate how two injections performed with the same boundary conditions can prompt comparable ignition position while

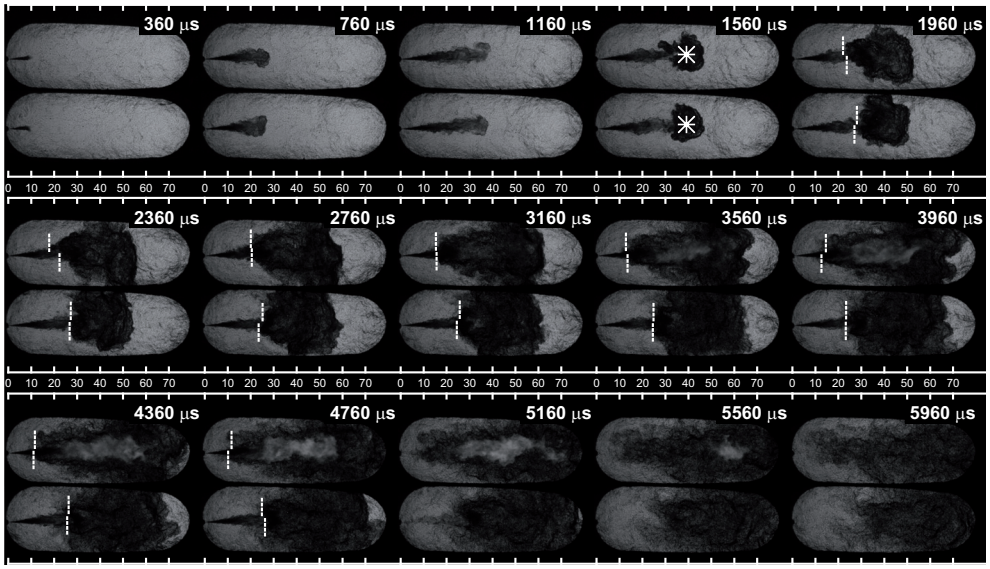

Figure 5.9. *Brightfield schlieren imaging sequence of two injections under the same test condition: conventional diesel, BT and 150 MPa injection pressure.*

ending with different lift-off length during OH-chemiluminescence imaging (exposure from 4 to 5 ms ASOE). On the first three instants prior to ignition, spray penetration is similar between the two injections, confirming that spray velocity and ambient density are alike for each. On the forth shadowgraph, ignition occurs simultaneously at a comparable position as symbolized by the stars. However in the following frames, where intend has been made to detect and materialize lift-off length with dashed lines, it can be observed how the flame development differs from one injection to the other. Whereas the bottom flame establishes and maintains lift-off at around 25 mm until the end of the combustion process, the top sequence starts with a similar lift-off but continuously shortens down to 10 mm. Therefore, in a test configuration such as the one serving as the core of this work, namely with longer injections of 8 ms and OH^* imaging triggered between 4 and 5 ms ASOE, these two injections would certainly result in very different lift-off lengths. It is likely then that the delay initially imposed to reach flame steady state thus explains the high level of dispersion observed for lift-off length compared to ignition delay measurements.

Paradoxically, although this comparison seems to dissociate the effect of ignition position over lift-off length, it fairly confirms the concept held in [4]. In this study, Pickett and co-workers state that a reservoir of high-temperature

combustion products forms after ignition and interacts at the flame base *via* natural heat diffusion by promoting the conditions of autoignition of the mixture. While it is expected that this process stabilizes in a quiescent environment as permitted by a combustion vessel, the contribution of heat convection could potentially be significant in the turbulent environment of the hot spray test rig, where ambient is set in motion during the piston compression stroke and strangled at the entrance of the cylinder-head. The turbulent character of the environment inside the chamber was revealed with extra-sensitive schlieren imaging (using small illumination angle [8]), and the important variability of the flow circulation pattern could possibly be responsible for the dispersion observed with lift-off length measurements. A closer look at the schlieren images shows how hot combustion gases effectively appear to be convected upstream in the upper sequence, while the bottom repetition rather seems able to maintain these hot products downstream. This apparently binary behavior with flames recirculating combustion products, and others that do not, is also suggested by the "double Gaussian" distribution of the lift-off length results in Figure 5.5. Further validation of this effect should be carried out with the objective to treat each distribution separately, and eventually remove recirculated flames from the free spray consideration in order to avoid an underestimation of the lift-off length ensemble-averaged value. Under these conditions, it is believed that averaged ignition delay remains a good correlating variable of the lift-off length because this effect is grinded by averaging or it affects all the tests in the same way. The latter observations already prompted deeper investigation in this direction, including CFD modeling of in-cylinder-head flow pattern, comparisons of the spray penetration with that measured in a quiescent one, and will represent part of the future work published by the group.

Finally, another observation of interest suggested by Figure 5.9 provides a seamless transition to the next section. Indeed, as lift-off length keeps decreasing in the upper sequence, soot starts to form and its radiation becomes significant. This close relationship between lift-off and soot formation has been mentioned already by several authors, but to the author's knowledge, such transition from non-sooting to sooting regime has not been observed during a same injection event. In the following section, aspects of soot formation in relation with lift-off length are analyzed by matching lift-off length and soot opacity measurements in both an average and cycle-to-cycle approach.

5.3. Relationship between lift-off length and soot formation

In the previous section, the relationship between ignition position and lift-off length has been established for a selection of fuels under a large set of operating conditions. The following section now proposes to move a step forward by studying the relationship between lift-off length and soot formation processes. In the past, numerous studies have reported that enhancing air entrainment upstream of the flame, and thus lowering the equivalence ratio at the lift-off length, can reduce flame sooting propensity [2, 14–21]. Often, it has been reported that soot formation may even be avoided if mixtures fall below a critical level of mixture fraction. When the cross-sectional average equivalence ratio at the lift-off length decreases to a value less than approximately 2, soot would no longer be formed within the fuel jet [19, 22]. However, if most of these results were obtained varying engine operating conditions such as injection pressure, thermodynamic conditions and ambient oxygen concentration, only few have considered the involvement of alternative fuels [2, 23] or oxygenated fuels [22]. As stated by Svensson and co-workers [23], stoichiometry at lift-off length may not be exclusive to explain differences in soot formation in the context of a fuel change. Inside the diffusion flame, a partially premixed fuel-rich combustion zone forms soot precursors that are the foundation for soot growth downstream. Aside from fuel oxygenation effects on mixture stoichiometry, the molecular structure of the fuel could also strongly affect the progression of soot formation downstream of the lift-off length, as suggested by Pickett and Siebers [15]. Therefore, these aspects need further investigation to develop a more complete picture of the processes leading to soot formation with alternative fuels.

The objective of this section is first to show and analyze results of KL-flame opacity measurements on the centerline as thermodynamic, injection and fuel properties are varied. Next, such analysis is completed by soot sampling measurements realized in another experimental context including different fuels and conditions, but whose results can extend to our study as well. Finally, the relationship between the lift-off length and KL measurements is discussed to study their interaction. Analysis is led in average terms first and then *via* a cycle-to-cycle approach with the purpose to potentially extract additional information.

5.3.1. Axial flame opacity measurements, a parametric study

In *Chapter 3*, practical details relative to the laser extinction technique have been provided permitting to quantify the flame opacity. To summarize, KL measurements were obtained by passing a punctual laser through the flame soot cloud, and by collecting the transmitted intensity with an integrating sphere, thus providing an integral measurement of the soot volume fraction (f_v) met by the laser along its path within the flame. The KL value was obtained from the conversion of the intensity drop between the transmitted and baseline intensities on a logarithmic scale (Eq. 3.14). Measurements were performed at 10 positions along the flame centerline, between 15 and 60 mm every five millimeters. At each axial position, the calculated optical thickness, KL was time-averaged between 4 and 5 ms ASOE to be synchronized with OH-chemiluminescence, and ensemble-averaged for 10 injections.

In Figures 5.10 and 5.12, the effects of respectively ambient density and temperature on soot opacity are shown for each fuel separately. Ensemble-average KL measurements as a function of the laser distance from the injector are plotted, while removing the points where the spray liquid-phase interfered and affected the measurement accuracy. Considering the five fuels at once, it can be observed that differences are small between B05, B30, FT1 and FT2. Only RME shows significantly minor levels of soot compared to the rest of fuels. Besides, each fuel demonstrates self-consistent trends in KL with either ambient temperature or density in that both parameters enhance flame sooting propensity. Under such conditions, higher soot levels are believed to be the result of both reduced lift-off length and faster reaction rates of soot formation. Regarding the KL-evolution along the flame axis, all fuels show similar profiles. As an overall trend, soot rapidly reaches a peak fairly upstream within the sooting region as a whole, before decreasing gradually down to the flame tip, beyond which no more laser extinction is detected ($\sim$55-60 mm). Independently from the fuel origin, such peak appears between 30 and 35 mm for both the highest density and temperature conditions. When either ambient temperature or density is decreased, the peak shifts further downstream by up to 10 mm in agreement with the observations made by Pickett and Siebers [15]. The systematic repetition of such bell-shaped profiles, extensively observed by other authors as well [2, 11, 19, 21, 24–26], enables to consider the peak-KL value by itself as a characteristic result. Thus, while a constant injection pressure was maintained (50 MPa) in both Figures 5.10 and 5.12, Figures 5.11 and 5.13 compare the corresponding peak-KL values including the two extra levels of injection pressure. As observable on the bar charts, increasing injection pressure reduces in-flame soot occurrence. It is to note however, that the step

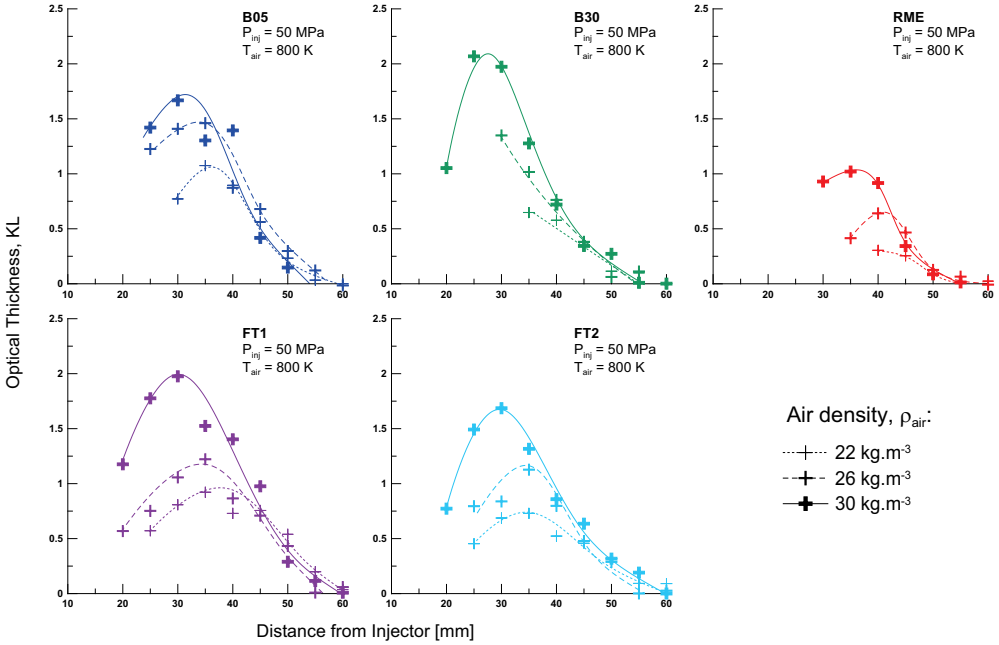

Figure 5.10. *Effect of ambient density on flame optical thickness (KL) along its centerline for the five tested fuels at 50 MPa.*

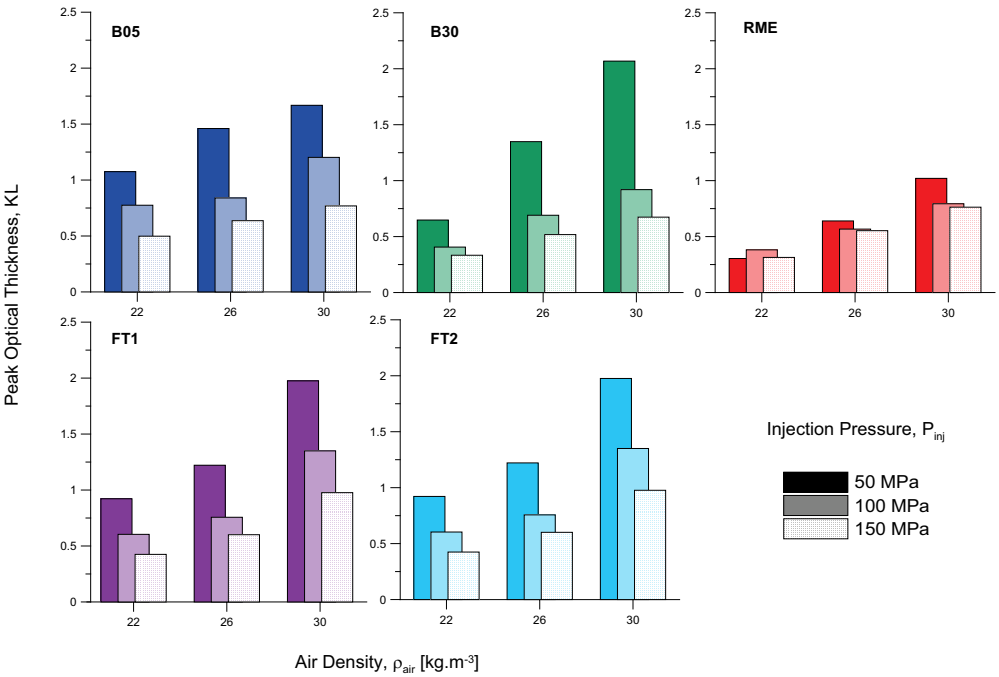

Figure 5.11. *Peak-KL values for the five tested fuels at 800 K under different injection pressure and ambient density conditions (constant temperature part of the test matrix).*

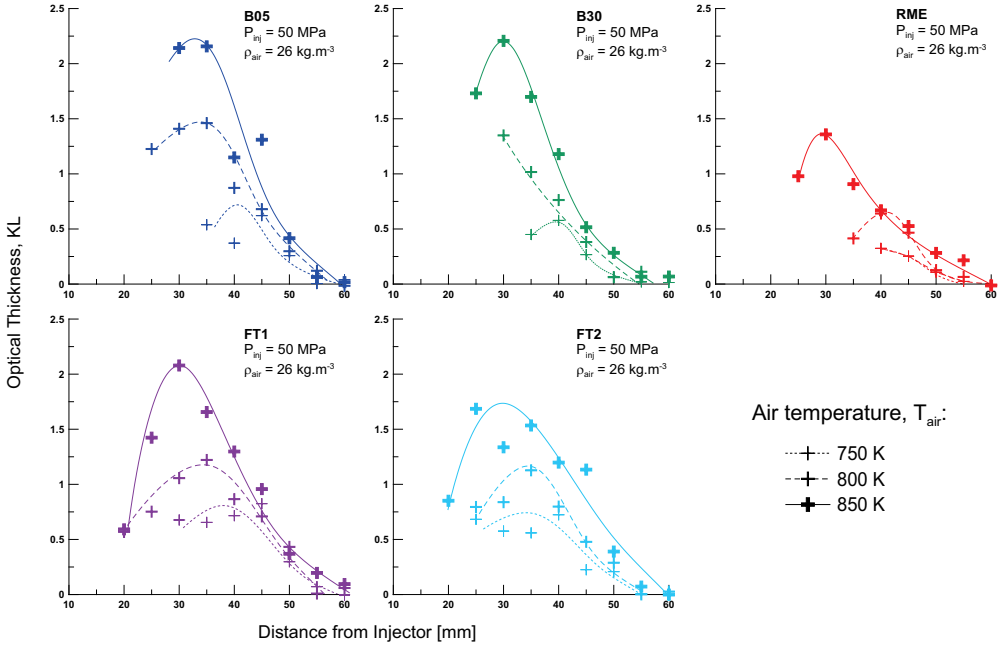

Figure 5.12. *Effect of ambient temperature on flame optical thickness (KL) along its centerline for the five tested fuels at 50 MPa.*

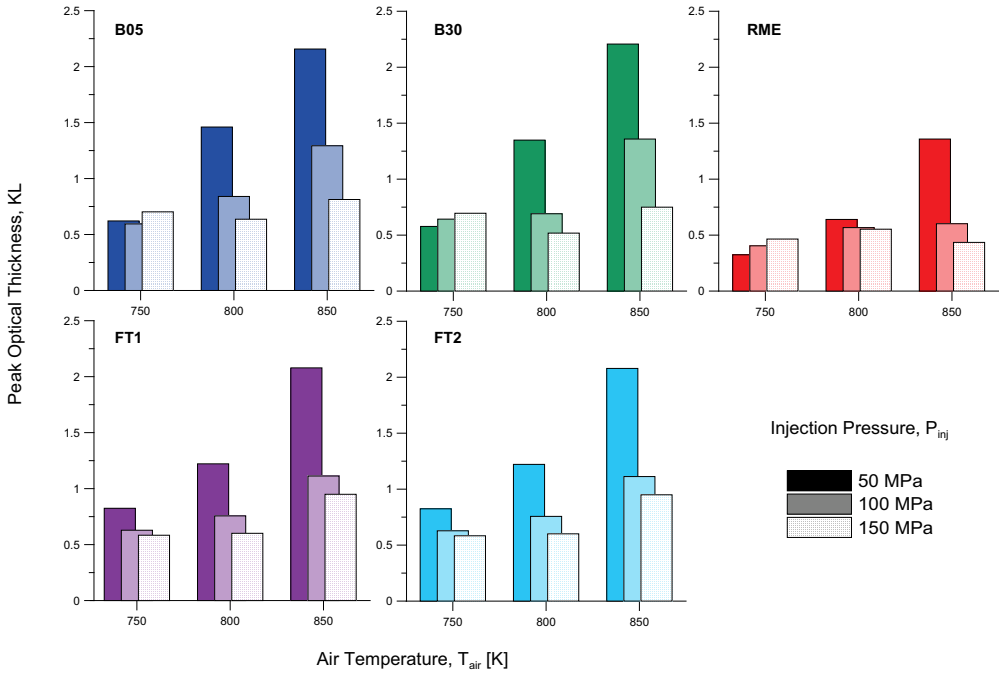

Figure 5.13. *Peak-KL values for the five tested fuels at 26 $kg.m^{-3}$ under different injection pressure and ambient temperature conditions (constant density part of the test matrix).*

from 50 to 100 MPa is more significant than that from 100 to 150 MPa. The overall effect of injection pressure is primarily the result of twofold sources: (1) the increase of lift-off length and, (2) the decrease of soot residence time throughout the flame. Accordingly, the minor impact of the 100 to 150 MPa step could be the result of (1) the typical asymptotical decrease of mixture fraction as a function of axial distance from the injector (similar to an inverse exponential function [27]) making stoichiometric variations in the lift-off region less significant for larger distances than the nearly linear dependence of lift-off length with injection pressure (Cf. Figure 5.6(c)); or (2) a minor decrease of residence time compared to the 50-100 MPa step, caused itself by a minor increase of spray velocity, the latter scaling with the square root of injection pressure drop.

Reconsidering the asymmetric bell-shaped profiles previously mentioned, it should be reminded that they correspond to the typical structure of a flame that fully established and achieved steady-state. These plume-shaped flames should not be confounded with Dec's widely diffused conceptual model [28] issued from the observations of a transient state of penetration. As a result, Dec's model depicts a qualitative soot concentration increasing continuously from the rich premixed combustion region (slightly downstream of the lift-off length) until the flame tip, where a head-vortex embraces the highest levels of soot. Causes for soot rarefication on the downstream part of steady-state flames may find different origins. First, the natural spray dynamics (spreading angle) promotes the convection aside of both soot precursors and particles towards the oxidation surface, which reduces the flame width (i.e. path length L), but also and mainly the soot volume fraction (i.e. extinction coefficient K) as distance increases from the nozzle. Also, as reviewed in *Chapter 2*, recent works from Kosaka *et al.* [29] and Bruneaux *et al.* [30] revealed the existence of a thick and lean surface of OH radicals located at the inner periphery of the stoichiometric surface, and from which OH radicals may be convected and/or diffused inside the flame to proceed to internal oxidation of soot particles. In order to further investigate these processes, the next section exposes a morphological study of soot particles sampled directly from the soot core region.

5.3.2. Morphology of in-flame soot particles

As concluded above, the bell-shaped KL profiles display a peak of soot concentration located between the lift-off length and the flame length, marking the limit between a region dominated by soot formation upstream, and a region dominated by soot oxidation downstream. Among these profiles, RME-

biodiesel is the unique fuel showing a significant reduction. Hence, questions are raised about the link between biodiesel lower profile, soot formation rates and soot morphology at a microscopic level. Paths of soot particles growth, including the nucleation of PAHs soot precursors, coalescence, and primary particles agglomeration, have already been introduced in *Chapter 2*, but have never been physically experimented with diesel flames and, a fortiori, let alone with alternative fuels flames. Whereas these growing paths are expected to prevail in the soot forming region, detailed mechanisms associated to soot processes are more uncertain once within the oxidation-dominated region. As suggested above, soot vanishing from this region is primarily the result of particles trajectory in the typical flow pattern of a conical spray which naturally pushes products aside towards the oxidation layer. Accordingly, surviving particles should pursue their growth until the flame tip, but inner OH oxidation may also occur and interact as suggested in [29, 30]. Therefore, in addition to the fuel effect, one might wonder how these soot particles transform along this path and how the microscopic stages of soot formation processes established for conventional flames actually fit into such context.

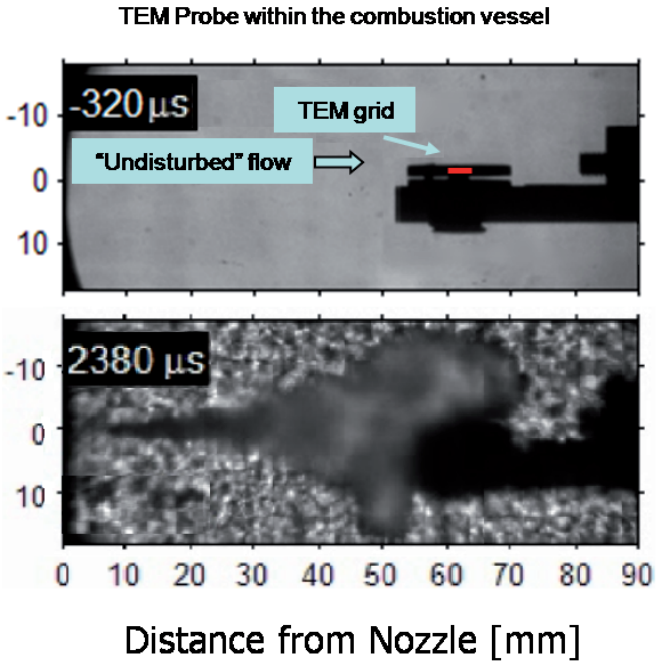

Figure 5.14. *Implementation of the soot sampler in the combustion chamber.*

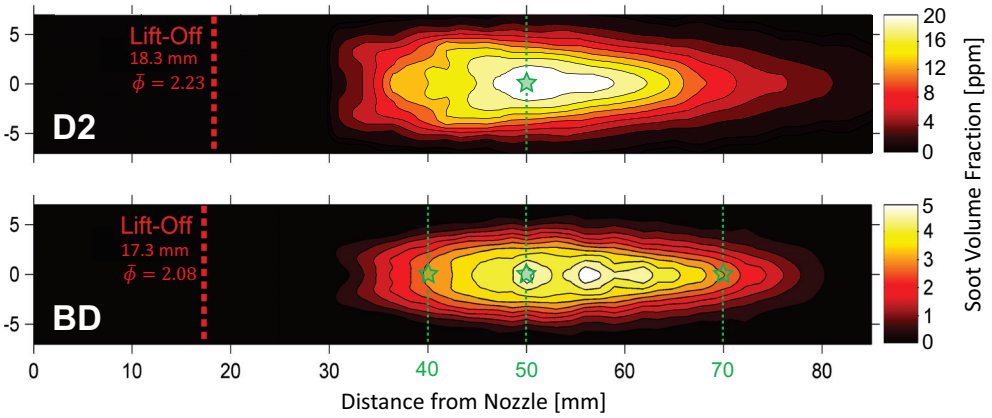

Figure 5.15. *Location of axial soot sampling respect to the flame structure. The figure background displays results of two-dimensional soot volume fraction for SME-biodiesel (BD) and conventional diesel ♯2 (D2) flames at 1000 K, 22.8 kg.m*$^{-3}$ *and 150 MPa injection pressure [11, 31].*

In the following section, soot particles have been sampled from both conventional diesel and soy methyl ester biodiesel flames by placing intrusively a TEM grid at 50 *mm* from the injector, inside the soot core region, as illustrated in Figure 5.14. In order to track soot particles development along the flame, additional samples at 40 and 70 *mm* have been realized for the biodiesel flame. In Figure 5.15, these three locations are spotted onto the respective soot volume fraction fields measured in another experiment under matching operating conditions [11]. Each of these three positions correspond to a strategic location within the flame, respectively the formation-dominated region (40 *mm*), the near-peak region (50 *mm*) and the oxidation-dominated region (70 *mm*). Grids were then observed with a Transmission Electron Microscope (TEM), and images later processed in order to characterize and measure the soot particles collected. Specifically for the comparison between diesel and biodiesel, new images of the biodiesel 50 *mm*-grid were taken in addition to the first catch for diesel, improving both the microscope setup and the image post-processing. Results issued from the latter will be referred as "reprocessed". In this document, it has been chosen only to present the main results and analysis from a series of works carried out in collaboration between Sandia National Lab., Meiji University and CMT-Motores Térmicos. To obtain deeper details on the experimental facility, operating conditions, sampling technique and image processing, it may be referred to the following

publications [31, 32]. Next subsections present some quantitative results on soot particles size, morphlogogy and development.

Figure 5.16 shows examples of TEM original images of soot particles sampled respectively at 40, 50 and 70 mm from the injector. At a first glance, observation of the images reveals the presence of both primary particles and soot agglomerates at the three locations. The fact that both states of particles development coexist for each fuel and all along the flame for biodiesel is already a significant result in itself.

5.3.2.1. Soot projected area ratio (A)

As a first step of image processing, the projected area ratio of soot (A) was calculated dividing the number of pixels considered as soot by the total number of pixels of the image (2048 $\times$2048). Pixels belonging to soot particles were selected by segmenting TEM images with a threshold manually adjusted so that eventual spot-like damages were excluded as much as possible. The resulting soot projected area ratio (A) estimated the density of soot particles sampled on the grid as shown in Figure 5.17. Regarding the comparison between diesel and biodiesel (BD rep.), the result is consistent with the higher sooting propensity of the diesel flame observed in Figure 5.15. As for biodiesel axial samples, the figure reveals a peak of soot density at the 50 mm position consistent with both Figure 5.15 and the bell-shaped KL profiles obtained in the previous section. However, although the 40 and the 70 mm positions appear to have very similar soot volume fractions levels in Figure 5.15, fewer particles were collected at 70 mm, suggesting the importance of the local jet velocity in the convection of soot particles up to the grid.

5.3.2.2. Primary particle diameter (d_p)

In the second stage of image processing, each element identified as a primary particle while considering all particles type (i.e. both isolated primary particles and agglomerates) was measured at least two times (orthogonal directions), mostly because of their non-circularity. This operation was rather manual, but enabled by a Graphical User Interface (GUI) permitting to consider each particle individually. The resulting histograms of primary particles diameter measurements are shown in Figure 5.18. All appear to be close to normal distributions permitting to consider average values as a significant result.

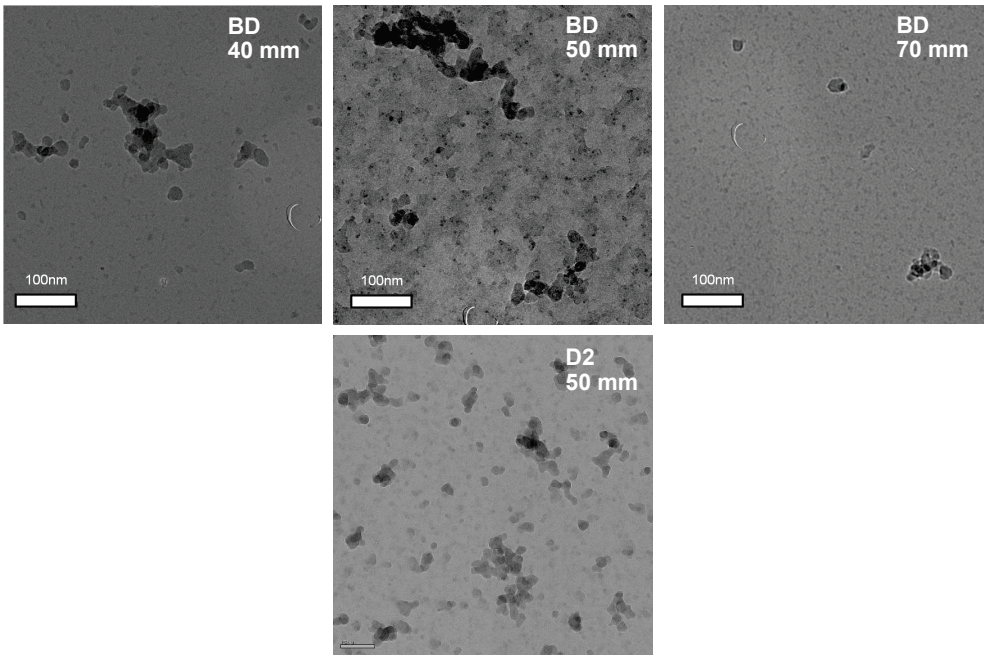

Figure 5.16. *TEM images of soot particles directly sampled in a biodiesel spray flame at 40 mm, 50 mm and 70 mm from the injector nozzle.*

First considering the fuel effect, 5336 and 4720 measurements were performed for biodiesel and diesel at 50 *mm* respectively, leading to average sizes of 16.9 and 18.4 *nm*. Despite biodiesel's slightly smaller value, the whole distributions of primary particles size remain fairly similar. Above all, the discrepancy between biodiesel at 50 *mm* and its reprocessing suggests that the difference between diesel and biodiesel may be contained within the experimental uncertainty, and therefore that primary particles' size of diesel and biodiesel should be considered as close or even equivalent. In this regard, this result provides another perspective and possibly completes the actual picture of biodiesel particles morphology already studied with samples from exhaust gases. The most recent work on the subject was conducted by Lapuerta and coworkers [33] and concluded that soot primary particles obtained with biodiesel fuel were significantly smaller than with conventional diesel, while employing a similar TEM analysis of soot agglomerates. Although only partially in agreement with results from the present study, the authors also confirmed a result widely diffused in the literature stating that biodiesel soot is considerably more reactive to oxidation as a result of its nanostructure which

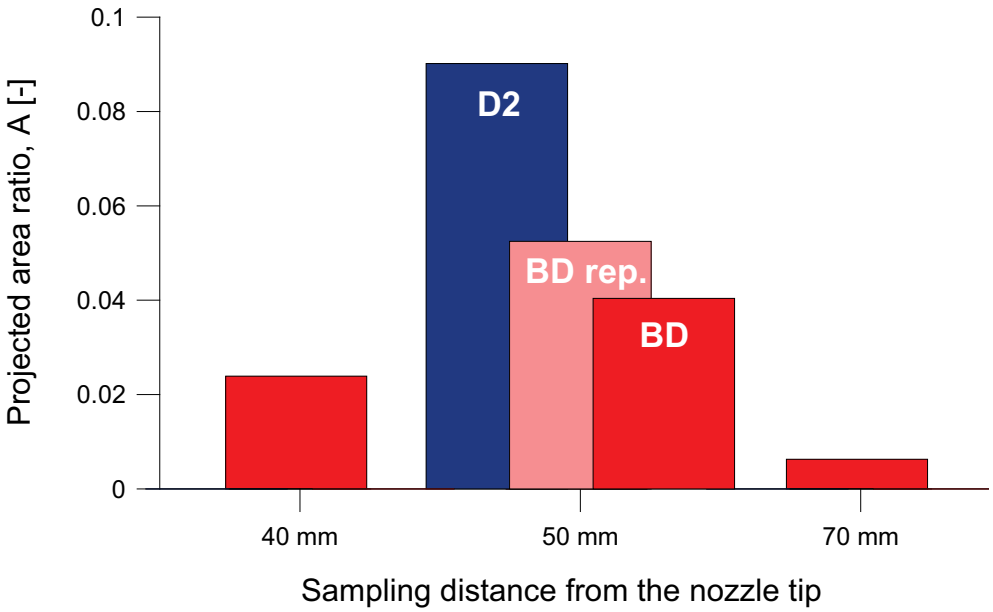

Figure 5.17. *Projected area ratio of soot particles on TEM images. Label "BD" is to be compared with measurements at 40 and 70 mm, while BD reprocessing (BD rep.) is to be compared with D2.*

enables faster oxidation rates [34–38]. For information purposes only, it must be noted that the causes of such faster oxidation still vary depending on the authors. On one hand, Song *et al.* [36] report more disordered and amorphous structures for biodiesel, in agreement with Vander Wal and Mueller [39] who relate that increasing the degree of fuel oxygenation leads to an increasing degree of amorphous nanostructure characterized by narrow fringe-length distributions with smaller means and broader and larger tortuosity histograms. On the other hand, Lapuerta *et al.* [33] obtained opposite trends with biodiesel reaching more ordered graphite-like structures (i.e. higher degree of graphitization) and lower amorphous carbon concentration, but maintaining faster oxidation due to the higher curvature of its carbon fringes. Thus, despite the lack of consensus about the details leading biodiesel structure to faster oxidation, the correlation between the higher reactivity of biodiesel soot and its morphology [35] remains widely accepted in the literature. Accordingly, a possible explanation of the difference between our results and those of Lapuerta *et al.* [33] regarding primary particles diameter could be that formation of soot primary particles is similar in quantitative terms (same size), but the growth is qualitatively different at a nanostructural level so that

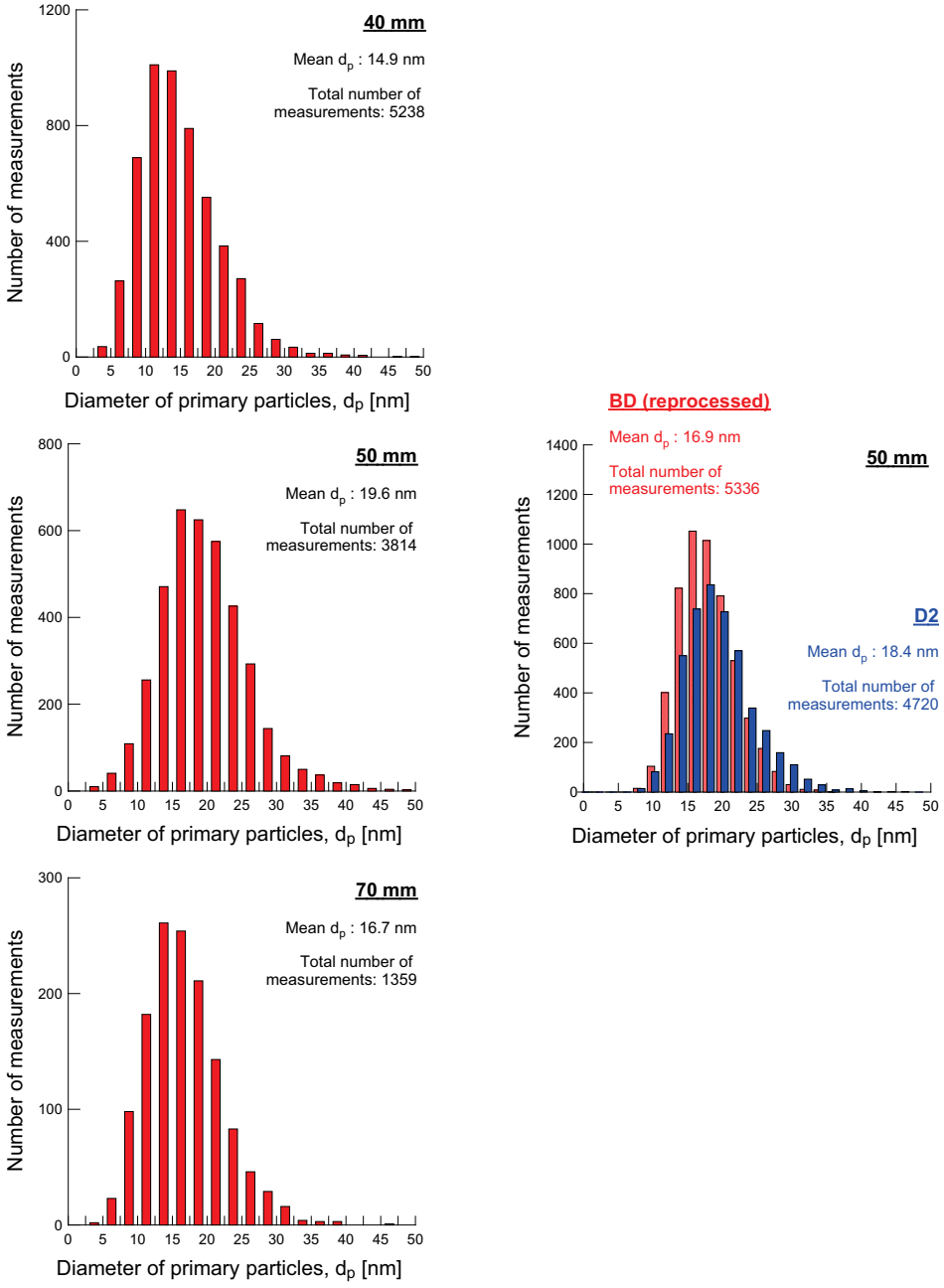

Figure 5.18. *Size histograms of primary particles sampled from diesel and biodiesel flames at 40 mm, 50 mm and 70 mm from the injector nozzle.*

particles oxidation is enhanced when going through the reactive layer, leading to smaller primary particles in the exhaust.

Regarding the position effect, respectively 5238, 3814 and 1359 measurements were taken out of each set of 25 images at 40, 50 and 70 mm from the injector. Although soot density on the grid was higher for the 50 mm position than for the 40 mm position, a higher number of measurements were taken at 40 mm because primary particles were less agglomerated and easier to recognize. The averaged primary particle diameter grows from 14.9 to 19.6 mm between 40 and 50 mm, expectedly as a result of the formation process known as "surface growth" or crystallization [40, 41]. Similarly to both the projected area ratio and soot volume fraction trends, maximum d_p is obtained at 50 mm from the injector. Thus, d_p shrinks to 16.7 nm between 50 and 70 mm, while going through the soot oxidation-dominated region. Analogous observations by Yamaguchi *et al.* [42] and Kondo *et al.* [43] have later confirmed this trend while using different fuel, facility, conditions, sampler, and six sampling positions every 10 mm in a longer flame (lower ambient density). If all the uncertainties associated to this novel experimental technique are clarified, the impact of this result could be important as it suggests that soot oxidation actually occurs inside the flame, and therefore partially questions the concept of diffusion flame for Diesel flames [28] in its strictest approach, namely the fact that soot oxidation occurs when going through the stoichiometric surface exclusively.

5.3.2.3. Radius of gyration (R_g)

The next step to characterize in-flame soot morphology was to calculate the radius of gyration for each soot particle in order to obtain an indicator of the overall-averaged particle size (primary particles + soot aggregates). The radius of gyration of soot aggregates R_g was calculated using the projected shape of each soot particle on binarized TEM images following the pixel-based Eq. 5.9:

$$R_g^2 = \frac{1}{n_{pxl}} \cdot \sum_{i=1}^{n_{pxl}-1} r_i^2 \tag{5.9}$$

where m is the number of pixels per aggregate and r_i is the distance between each pixel belonging to the aggregate and the centroid (digital) of the particle.

This parameter has been first used to complete the previous section by checking the consistency between d_p measurements taken from an isolated

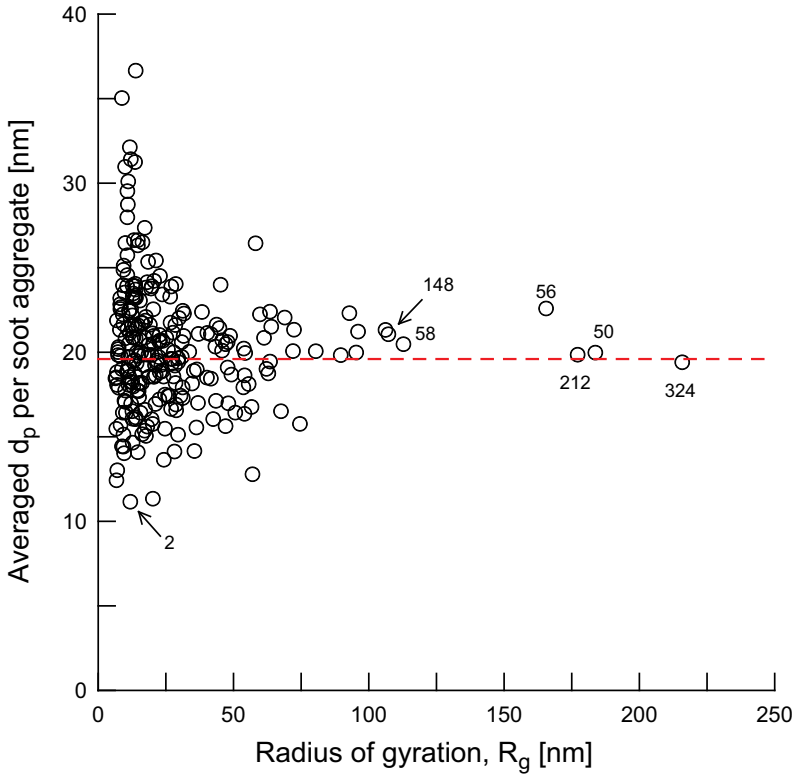

Figure 5.19. *Specific primary particles average diameter (obtained considering each particle individually) as a function of the particle radius of gyration (isolated primary particles and agglomerated confounded). The case represented is biodiesel at 50 mm (first processing). The dashed line corresponds to the overall average (19.6 nm). The numbered labels represent the number of measurements taken for the corresponding particles.*

primary particle and a more complex soot agglomerate. In Figure 5.19, the average d_p specific to each particle element has been plotted against its proper radius of gyration (R_g) for the first processing case of biodiesel at 50 mm. The radius of gyration was calculated following Eq. 5.9. While further analysis about it is provided in the next section, the important point at present is to understand that it represents the particle size. As indicate the numerical labels on the figure, two measurements were typically taken for an isolated primary particle (low R_g), while up to 300 could be performed for the largest agglomerates (high R_g). As expected, the plot shows more scattered measurements for smaller particles, and the dispersion decreases as R_g and the number of measurements increase. However, the average of d_p (19.6 nm

represented in dashed line) does not seem to be significantly affected by the particle size and complexity. Therefore, the size of primary particles seems to be independent from the fact that they are issued from an isolated primary particle or from a larger aggregate.

Similarly to the analysis of Figure 5.18, Figure 5.20 shows the distribution of R_g at the three sampling positions on a logarithmic scale in order to highlight the lower levels. In view of the difference between the two processing of biodiesel grids at 50 mm, it must be accounted that quantitative values are significantly affected by the experimental methodology so that only comparisons between analogous processing should be considered. Accordingly, the comparison between diesel and biodiesel suggests that soot aggregates have a very similar size, R_g being nearly equal to 18 nm for both fuels. Once again, this result is quite contrary to measurements reported in the literature of samples taken from exhaust gases, and for which it is typically concluded that biodiesel combustion produces smaller particles [44]. Even more startling is that larger soot aggregates over 150 nm of gyration radius can be observed only for the biodiesel fuel case. However, comparably to primary particles, biodiesel faster oxidation rates could explain the differences observed between soot sampled from the flame core and soot sampled from exhaust gases.

In respect to the comparison between axial positions, histograms display the respective average values of 9.3, 28.2 and 14.9 nm. Similarly to the trends observed for soot density and primary particle diameter, a peak of particle size appears at 50 mm from the injector tip. At the 40 mm position, the data is relatively homogeneous and most of the particles have a radius of gyration centered on 20 nm, demonstrating that the processed objects are mainly primary particles. Moving to 50 mm, the number of objects drastically drops, data becomes more scattered and larger aggregates up to 220 nm appear. The majority range is 30 nm but this barely represents 40 % of all measured aggregates. At 70 mm, close to the tip region of the flame, no more large aggregates were collected and the few aggregates left are centered on the 30 nm radius of gyration range. A possible scenario to explain such observations could be that: (1) From 40 to 50 mm, in parallel to the increase of the primary particle diameter itself, the high number of homogeneous primary particles present at 40 mm aggregates to form larger structures at 50 mm; (2) From 50 to 70 mm, the biggest particles dissociate while the smallest ones complete rapidly their oxidation; (3) At 70 mm, the collected particles result from the incomplete oxidation of the largest particles observed at 50 mm. The fact is that a parallelism seems to exist between the growth/shrink of primary particles and the coagulation/dissociation of larger agglomerates all along the flame corroborating that both processes may coexist as mentioned above.

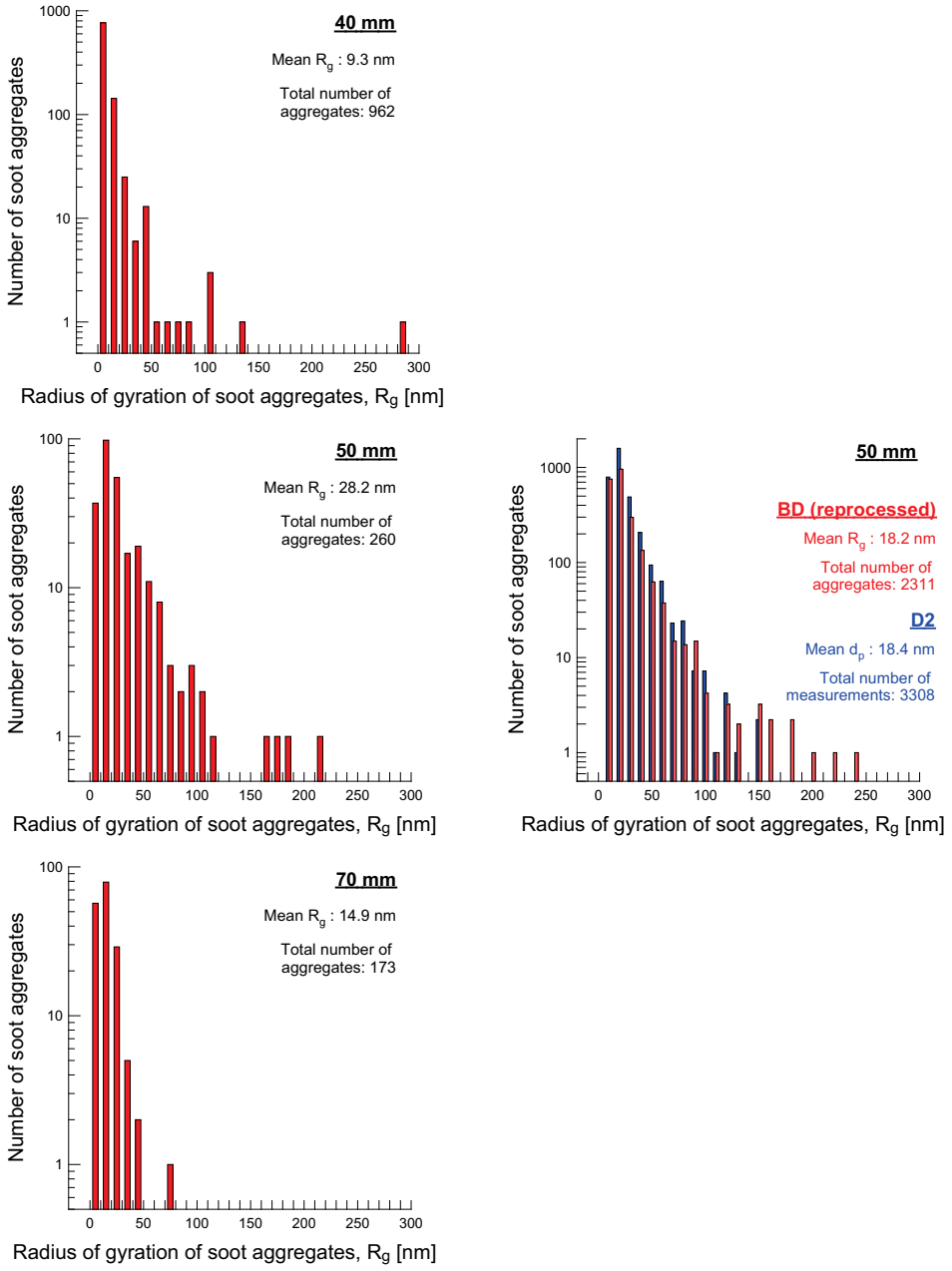

Figure 5.20. *Histogram of radius of gyration of soot aggregates sampled from diesel and biodiesel flames at 40 mm (a), 50 mm (b) and 70 mm (c) from the injector nozzle.*

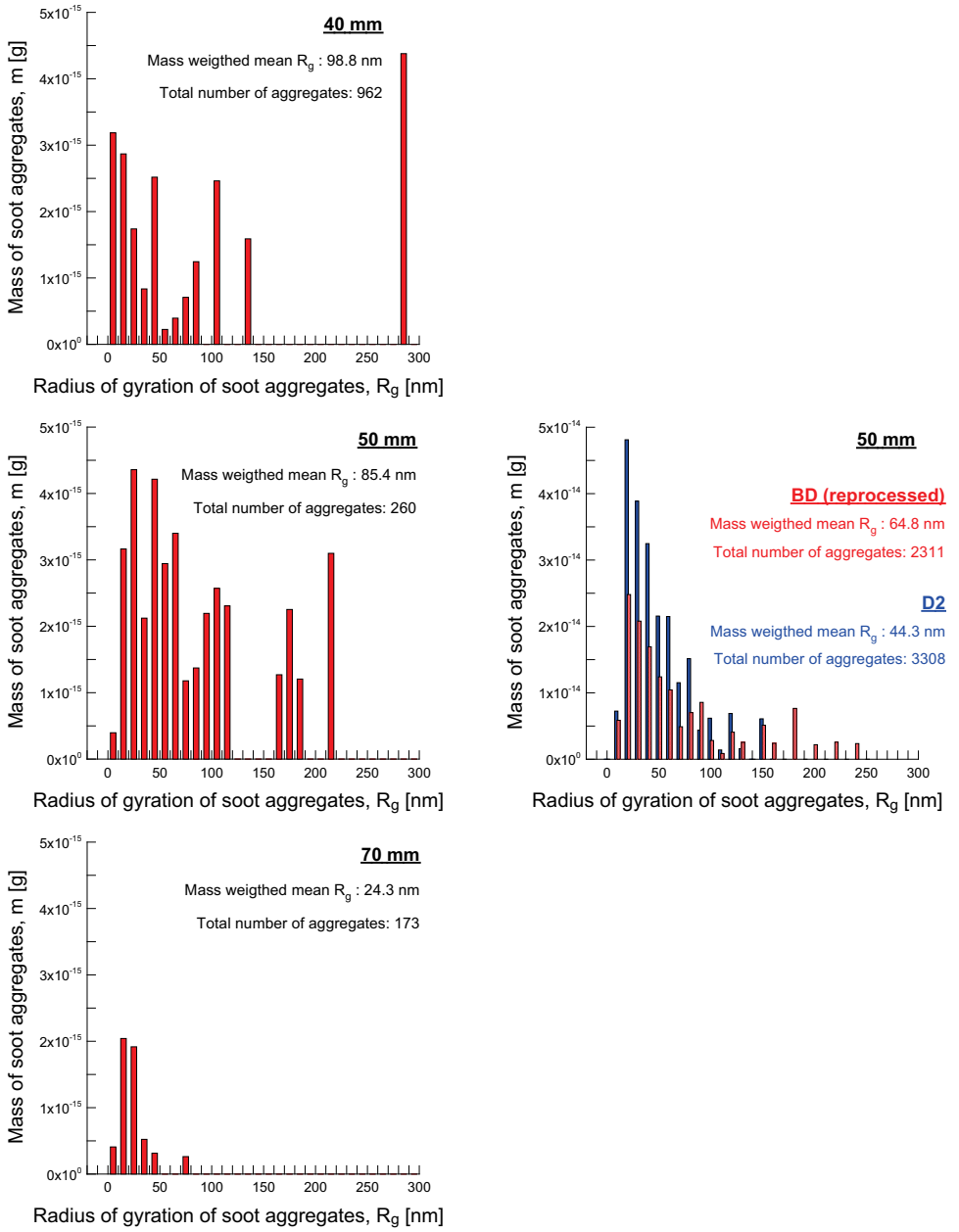

Figure 5.21. *R_g mass distribution of soot aggregates sampled from diesel and biodiesel flames at 40 mm (a), 50 mm (b) and 70 mm (c) from the injector nozzle.*

In Figure 5.21, number-based data from in Figure 5.20 have been converted into mass representation using the average primary particle diameter d_p, the approximate number of primary particles within the aggregate n_p, and a representative value for soot density: ρ_{soot}= 2000 $kg.m^{-3}$ [45, 46]. The number n_p was obtained following Eq. 5.10:

$$n_p = (\frac{A_a}{A_p})^{\alpha} \tag{5.10}$$

where α is an empirical coefficient accounting for the overlapping effect and whose value has been set to 1.09 according to [47]. A_a is the projected area soot aggregate considered, and A_p is the projected area of the averaged primary particle (A_p=$\pi d_p^2/4$). This data does not pretend to be quantitatively accurate but does show what would be the trend of mass distribution for the data showed in Figure 5.20. These histograms highlight the importance of the few large aggregates in the mass balance. Biodiesel mass-weighted average (64.8 nm) is significantly higher than diesel's (44.3 nm) due to the lower number of small-size aggregates and the presence, as commented above, of very large aggregates over 150 nm. At 40, 50 and 70 mm, the mass-weighted averages R_g of soot aggregates were found to be respectively 98.8, 85.4 and 24.3 nm. Although the average R_g at 40 mm is higher than at 50 mm, the overall distribution shows the same trend as observed for number-based histograms, probably highly affected by a unique large aggregate.

5.3.2.4. Fractal dimension (D_f)

As a final diagnostic of TEM images, the fractal dimension of soot aggregates D_f was considered to characterize soot particles morphology. Expressed by the power-law relationship of Eq. 5.11, this parameter estimates the self-similarity properties of soot aggregates, while being the ratio of the logarithm of the number of primary particles in single agglomerate to the logarithm of the "primary particle/soot aggregates" size ratio [47, 48]. As a result, D_f qualifies the shape of soot agglomerates between two limits as illustrated in Figure 5.22, namely a truly linear agglomerate (D_f=1) and a truly circular agglomerate (D_f=2[2]). In [49], Lapuerta *et al.* provide a finer definition by warning that *"agglomerates with similar size and fractal*

[2]Note that maximum D_f is equal to 2 (equivalent to a disk) because of the two-dimensional treatment given to the images. In [48], Lapuerta *et al.* established a more sophisticated methodology permitting to account for the tri-dimensionality of soot aggregates and for which maximum D_f is equal to 3 (equivalent to a sphere). This algorithm is currently under implementation in the processing codes.

dimension may have different shapes, this difference being characterized by the pre-factor k_f. Whilst the fractal dimension accounts for the irregularity and the clusterization of the agglomerate structure, [...] the pre-factor expresses how the space is being filled up by the agglomerate mass, independently of its size [...] and how the primary particles are packed. It has been associated with the lacunarity and with the porosity of the agglomerate".

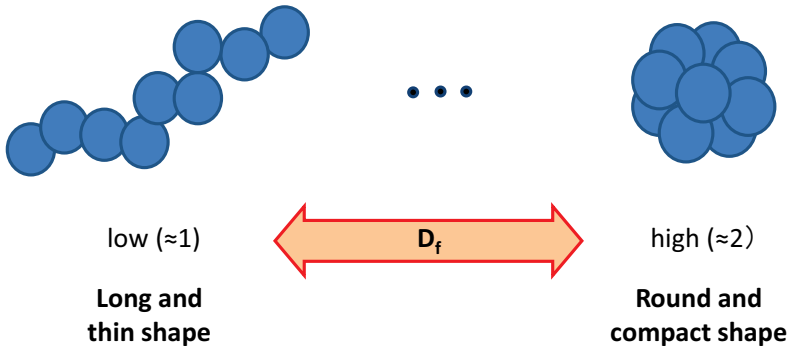

Figure 5.22. *Schematic representation of the fractal dimension (D_f) significance for soot agglomerates.*

Thus, in a representation analogous to the previous figures, Figure 5.23 shows the plots of the number of primary particles n_p as a function of R_g/d_p in logarithmic coordinates for both the fuel and the sampling location comparisons. The slope of the linear regression which fits each population of soot aggregates, provides the mean fractal dimension D_f, while the pre-factor value k_f is equal to the y-intercept (R_g/d_p=1). In order be consistent with the meaning of Eq. 5.11, isolated primary particles (n <2) have been removed directly from the calculation of D_f. Before entering deeper consideration, it must be highlighted that all values of D_f and k_f are reasonably similar. While Lapuerta *et al.* [49] report a wide dispersion of pre-factor values from the literature, D_f is consistent with the 1.6-1.8 narrow range obtained by several authors. This result implies that soot aggregates sampled from the soot core region are not drastically different in term of morphology respect to aggregates sampled from exhaust gases.

As a result of the comparison between diesel and biodiesel soot particles, diesel aggregates appear to be sensitively more circular (higher D_f) and more dense (higher k_f), thus suggesting a more compact structure than biodiesel. This result is in line with the previous argumentation suggesting that biodiesel oxidation rate is faster. By being more open to oxygen molecules attacks,

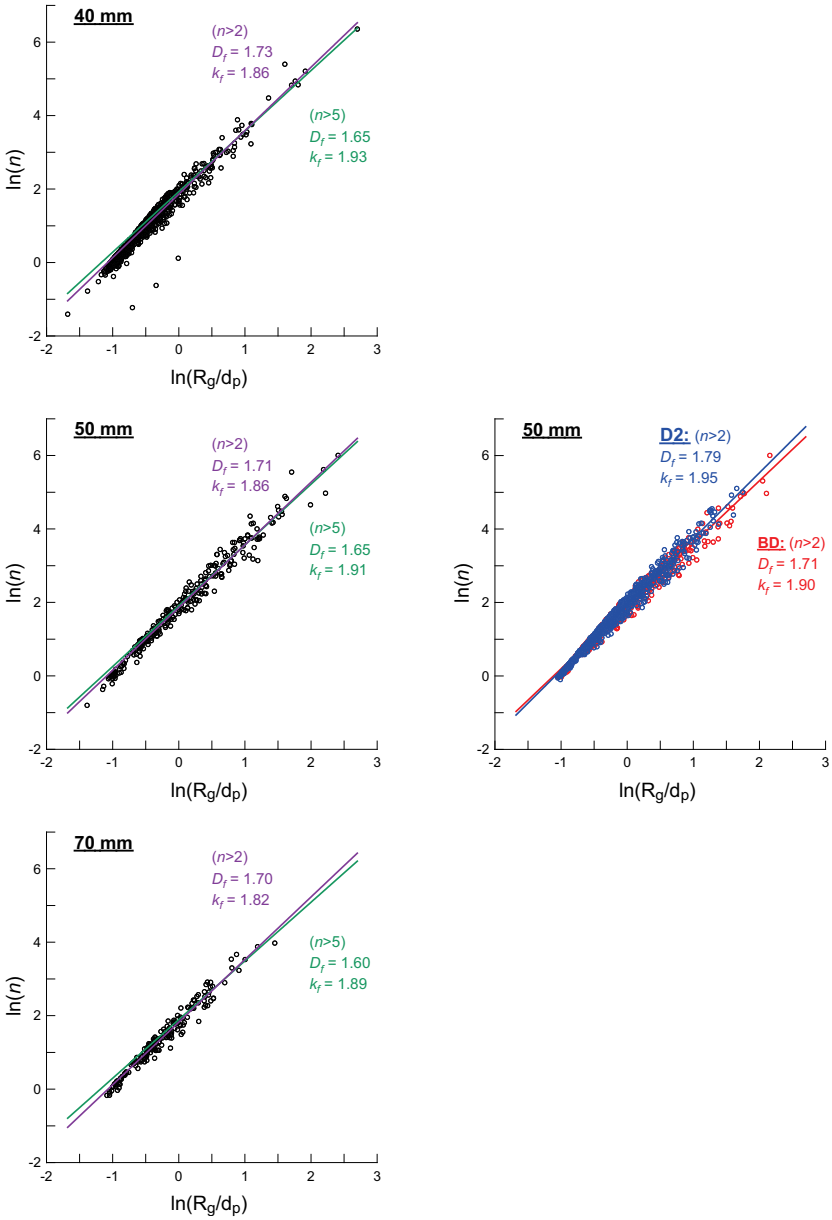

Figure 5.23. *Logarithmic plots of R_g/d_p for soot in biodiesel spray flame at 40 mm (a), 50 mm (b) and 70 mm (c). Each open circle represents a measured soot aggregate. The slope of the linear regression line represents the fractal dimension D_f. The y-intercept (R_g/d_p=1) corresponds to the pre-factor k_f.*

biodiesel aggregates oxidation could be enhanced, therefore reducing their size in the exhaust.

$$n_p = k_f \cdot (\frac{R_g}{d_p})^{D_f} \tag{5.11}$$

Regarding the comparison between biodiesel axial positions, it must be noted first that a second threshold for n_p has been tested (n_p=5) to detect a possible influence of the aggregate size on the fractal dimension. Although D_f decreases and k_f increases slightly with such higher threshold, the values D_f∼1.70 and k_f∼1.90 turn out to remain quite constant from one sampling position to the other. Similarly to the morphological consistency between agglomerates sampled from the soot core and from the exhaust, this result suggests that the latter also maintain a self-similar morphology through both growing and oxidations processes when going across the flame.

As a final word concluding this research with in-flame soot sampling, some hypothesis have been proposed, discussed and compared with the actual knowledge on soot sampled from exhaust gases, but it should be noted that the influence of soot sampling method and the process of TEM image analysis still needs careful examination before their validation and the start of further discussions on the evolution and oxidation of soot inside the flame. A lot of uncertainties are inherent to the experimental setup such that obtained results should be considered with the highest precaution. The specific issues to be carefully examined in the future include the influence of different temperature and flow conditions at different locations in the flame on the process of soot sampling onto the grid surface, oxidization of soot particles after they are sampled onto the grid surface by continuing exposure to burning/burnt gases, and the reliability of TEM image analysis processes in which complicated three dimensional shape, and structure of the soot aggregate needs to be recognized and measured only from its low-resolution projected images and by different operators.

5.3.3. Effect of A/F ratio at lift-off length

After this parenthesis dealing with soot morphology, let us reconsider the parametric study representing the guideline of this document. In Section 5.3.1, different trends in sooting propensity were observed while varying fuel origin and operating conditions. As reviewed in *Chapter 2*, a region develops downstream to the lift-off length, called premixed burn, where all the oxygen entrained is consumed. Products from this rich combustion, mostly PAHs, are

believed to be the precursors of soot formation in the diffusion part of the flame. Accordingly, the amount of soot formed within the flame is expected to be highly depending on the equivalence ratio at the lift-off length, but only few studies approached these considerations when varying fuel composition and origin [2]. Thus, with a similar approach to the one that permitted to establish a relationship between ignition location and lift-off length, this section aims at studying the connection between sooting propensity and results of lift-off length obtained in Section 5.2.2. A cycle-to-cycle analysis is first carried on before approaching this effect through the different parameters of the experimental study in average terms.

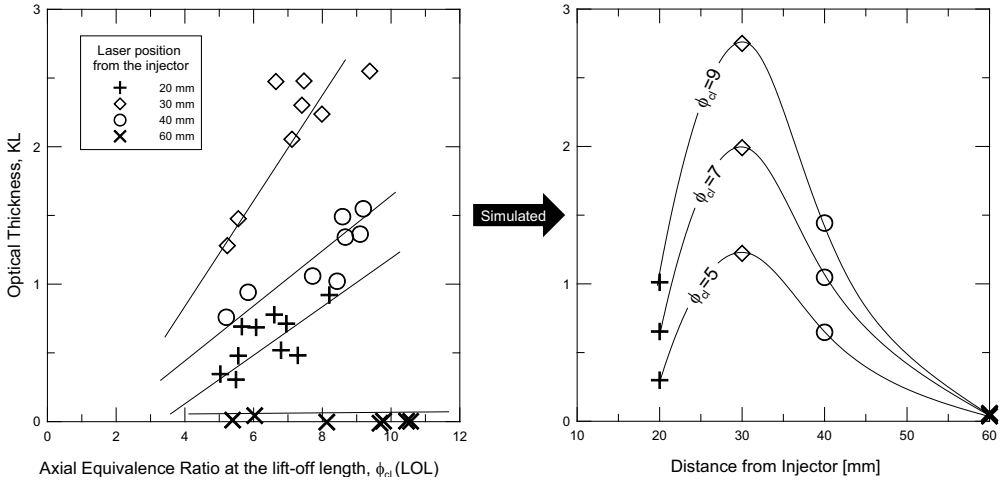

Figure 5.24. *The relationship between the cycle to cycle dispersion of lift-off length and KL measurements. The case represented is FT1 at the HT operating condition and 50 MPa injection pressure.*

In Section 5.2.2.1, a high dispersion on the lift-off length measurements was reported, possibly generated by the turbulent character of the flow inside the cylinder-head. The source of such dispersion remains to be confirmed but, without entering these considerations, it is proposed to investigate how the cycle-to-cycle dispersion of the flame lift-off length affects KL measurements, and thus to check if the connection between lift-off length and soot formation reported by other authors also extends to a cycle-to-cycle approach. Figure 5.24 shows single-shot measurements of KL at different axial position for FT1 in the HT operating condition at 50 MPa injection pressure. As described in *Chapter 3*, such measurements have been time-averaged between 4 and 5 ms ASOE in synchronization with the exposure

of OH-chemiluminescence imaging. KL measurements are plotted against the centerline equivalence ratio (ϕ_{cl}) at their corresponding lift-off length. The estimation of ϕ_{cl} was made *via* a 1-D spray model based on the gas/diesel jet similitude, mixing limited assumption and Gaussian radial profiles. Inputs to the model included the equivalent diameter (Cf. *Chapter 3*), fuel stoichiometry, and a constant spreading angle equal to 20° according to the conclusions from *Chapter 4*. Further details relative to the model hypotheses and methodology can be found in [27]. The plot shows that at any position of the flame, soot propensity increases in a quasi-linear trend with ϕ_{cl} (i.e when lift-off length decreases). The effect is fairly significant at 30 mm, near the soot-peak region, more moderate 10 mm upstream and downstream, and null at 60 mm near

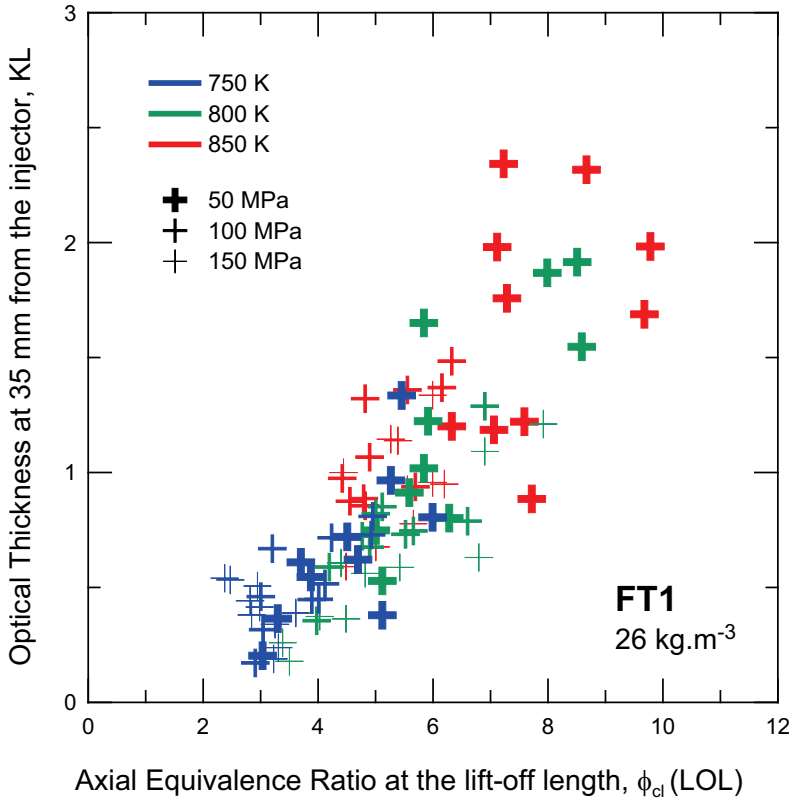

Figure 5.25. *Cycle-to-cycle measurements of the KL factor at 35 mm from the injector correlated with their corresponding equivalence ratio (ϕ_{cl}) in the lift-off region. The case represented is FT1 at constant air density (26 $kg.m^{-3}$), under the temperature sweep and all injection pressures.*

the flame tip. In this respect, the result at 60 mm is essential as it indicates that the flame length is maintained, and therefore that variations of lift-off length are not the result from a simple shift of the entire flame along its own axis. This issue could indeed produce similar results, for instance at 30 mm, by having variations of KL created by measurements taken from the peak and from both formation- and oxidation-dominated portions of the flame. If flames at iso-ϕ_{cl} (iso-lift-off in that case) are now considered, one can observe that the axial dependence of KL, typically the bell-shaped profile introduced above, is conserved. This, as a result, suggests that cycle-to-cycle dispersion modifies KL axial profiles similarly to what is known as "homotopic paths" in algebraic topology, including a first connection upstream at $2< \phi_{cl} <3$ and another at the flame tip. In that sense, the plot demonstrates that the high dispersion of lift-off length measurements is reflected directly on those of KL as a result of different sooting propensity, and not due to flame shifting. Therefore, by showing that it extends to a cycle-to-cycle approach, the hypothesis made by other authors stating that the equivalence ratio the lift-off length significantly influences soot propensity of Diesel flames is reinforced. Moreover, while most of the studies treating this topic create variations of lift-off length by modifying conditions of temperature, density or injection pressure, this cycle-to-cycle effect further suggests the exclusivity of lift-off air entrainment in the control of soot formation.

A consequence of the "homotopic character" of KL profiles is that a fixed laser position now can be considered in order to compare different cycles from different tests; as long as the "flame scale", i.e. both air and fuel densities (equivalent diameter), are maintained. In Figure 5.25, KL measured at 35 mm for all test repetitions of FT1 have been plotted, while including both the air temperature and injection pressure sweeps. Despite the significant scattering, a linear trend can be extracted, showing an increase of the KL factor in response to the mixture enrichment in the lift-off region. By extrapolation, the trend further suggests that flames with an equivalence ratio such that $2< \phi_{cl} <3$ would not produce soot anymore. As observable in Figure 5.26, similar trends and threshold for non-sooting regime were observed for all fuels, therefore confirming that modification of air entrainment upstream to the lift-off length, either created by engine-derived variables (excluding ρ_{amb} and resulting rescaling) or by the cycle-to-cycle dispersion, determines strongly soot formation within the flame.

The value of ϕ=2 as the ultimate threshold permitting to reach non-sooting conditions was also obtained by Pickett *et al.* [19] and Mueller *et al.* [22]. However, this value applied to the cross-sectional average equivalence ratio, meaning that 50 % of the total amount of air required to burn the fuel

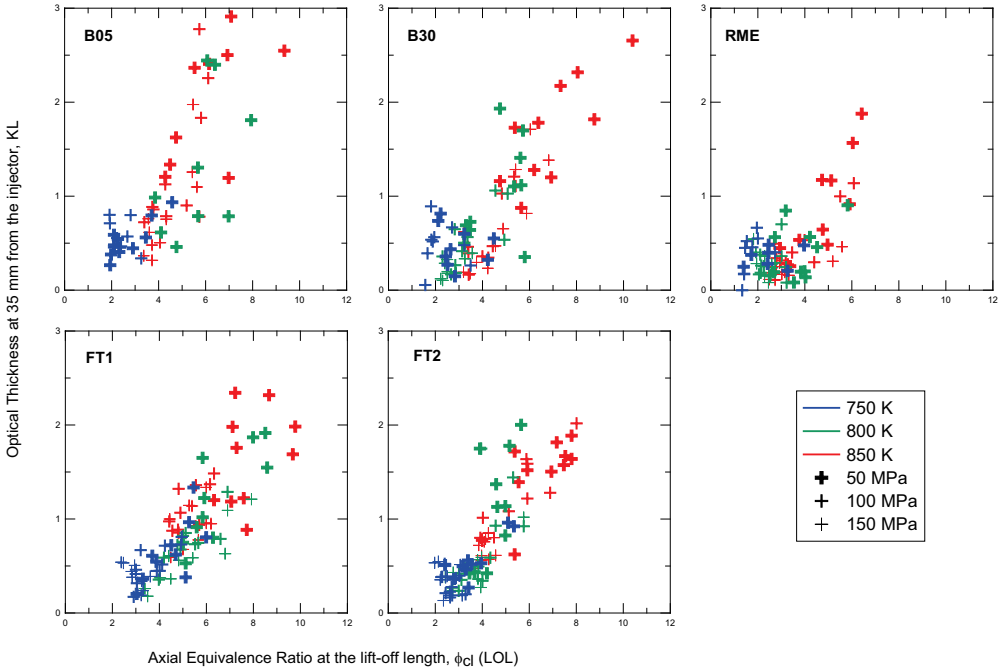

Figure 5.26. *Cycle-to-cycle measurements of the KL factor at 35 mm from the injector correlated with their corresponding equivalence ratio (ϕ_{cl}) in the lift-off region. All fuels are represented at constant air density (26 kg.m^{-3}), under the temperature sweep and all injection pressures.*

injected needs to be entrained prior to the lift-off length in order to avoid soot formation. Given that centerline and cross-averaged equivalence ratio are related by nearly a factor 2 with the Gaussian-type of radial profile selected for modeling [50], the result of this study actually suggests that leaner mixtures (87.5 % entrainment for ϕ_{cl}=2.5) are even required to reach the non-sooting regime. Results from Figure 5.15 are also consistent with this conclusion since it is very unlikely that both flames would turn out to be completely soot-free with $\overline{\phi}$=2.

In order to better compare the five fuels and assess the effect of their chemical composition on flame sooting propensity, ensemble-average values of peak-KL have been represented in Figure 5.27 as a function of the centerline equivalence ratio at the lift-off length, while including results from the entire test matrix (75 combinations). With the purpose to properly consider the density sweep in this analysis (i.e. accounting for the flame-scale issue), the KL-factor for both LD and HD operating conditions has been normalized to

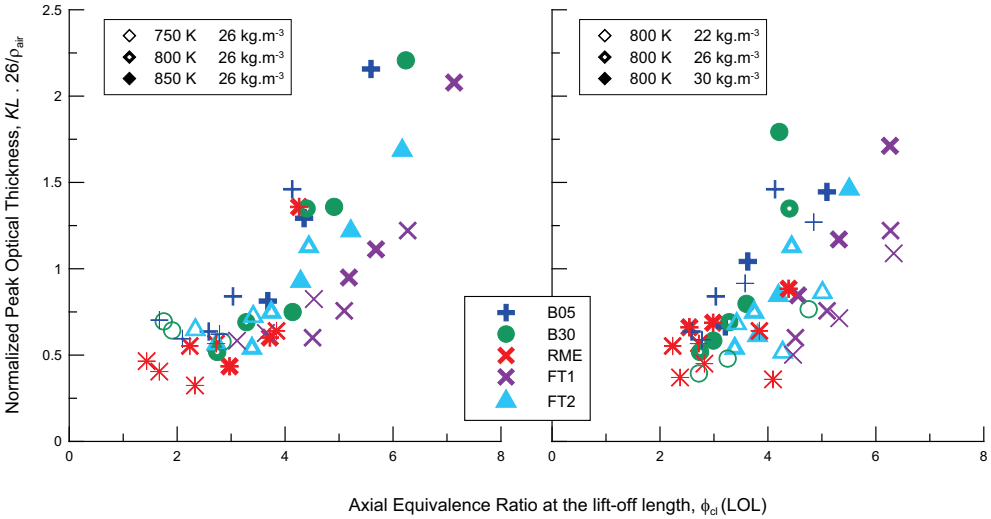

Figure 5.27. *Ensemble-averaged peak-KL as a function of the calculated equivalence-ratio on the centerline at the lift-off length (ϕ_{cl}). The whole test matrix (5 fuels ×5 operating conditions ×3 injection pressure levels) is represented.*

the nominal density (26 $kg.m^{-3}$). Sweeps of air temperature (no flame re-scale) and air density are shown respectively on the left and right sides of the figure. In general terms, the result is consistent with previous ones, in that all fuels display a trend to lower peak-KL with mixture leaning at the lift-off length. Any variation of engine-derived variables seems to influence soot propensity mainly through air entrainment at the lift-off length, as already suggested by Figures 5.25 and 5.26. Therefore, the trend confirms that, for each fuel considered individually and for all the conditions explored, the main factor controlling soot formation within the flame is air entrainment before lift-off length.

Considering all fuels at once, most of them appear to collapse into a similar trend, except for FT1, which enables richer mixtures at the flame base for peak-KL levels similar to the rest of fuels. Quantitatively, this makes the four fuels concerned by the first linear trend reach non-sooting conditions for $1< \phi_{cl} <2$, whereas this limit is more easily achieved for FT1 with $2< \phi_{cl} <3$. According to *Chapters 2* and *3*, lower sooting propensity of Fischer-Tropsch fuels was expected due to the absence of aromatics in their formulation. Indeed, aromatics intrinsically contained into the fuel may potentially serve as a basis for soot formation in the same manner as soot precursors issued from the rich premixed burn. However, this expected lower propensity clearly does not verify

for FT2. Such inconsistency opens a discussion but unfortunately does not permit to establish a clear and emphatic trend for the effect of fuel properties. Different lectures of the results are possible, leading to two scenarios:

(I) The first one consists in considering FT1 as the marginal fuel by either conceding that its difference belongs to experimental uncertainty, or by recording FT1's extremely short lift-off length, in particular compared to its corresponding liquid length (LOL$\sim$0.5 $\times$LL). Under this assumption, the effect of fuel properties appears to be indirect in regard to soot formation as for the rest of engine-derived variables. Thus, fuel properties may be able to modify the lift-off length, but soot propensity remains controlled by the equivalence ratio at the latter. Accordingly, fuels already containing oxygen in significant proportion, such as RME or even B30, enhance flame leaning at iso-LOL, but do have equivalent levels of soot whenever different ambient conditions enable to consider results at iso-ϕ_{cl} (LOL). Also, fuels with a higher level of unsaturation (containing aromatics, cyclic, polycyclic or double-bonded molecules), and so intrinsically more prone to soot formation, would offset this penalty by permitting more mixing upstream the lift-off length, as a result of their longer lift-off length, itself a result of their longer ignition delay and lower ignitability. On the opposite, paraffinic fuels such as Fisher-Tropsch, balance their natural low-sooting propensity by their higher ignitability and their subsequent shorter lift-off length. Therefore, by extending its application to fuel properties, this lecture suggests the total exclusivity of mixture quality at the lift-off length in the control of soot formation, even beyond its role detected when varying engine-derived parameters.

(II) The second scenario consists in considering FT2 as the marginal fuel. By reconsidering Figure 5.7 where lift-off length and liquid length were compared, FT2 actually appears as the most prone to vaporize entirely before lift-off length, and then to avoid liquid evaporation inside the diffusion part of the flame. More generally, *Chapter 4* suggested that its shorter molecule implied a lower cost of evaporation (lower L_v). Under this assumption, it might be hypothesized that the mixture cooling engendered by FT2 evaporation is lower than the rest of fuels in both the upstream and downstream regions of the lift-off length. Such lack of cooling could accelerate soot formation rates in comparison with the rest of fuels and virtually increase FT2 sooting propensity.

To conclude, soot formation processes were presented in *Chapter 2* as driven by mixture richness, temperature (higher formation rates), residence

time, and of course fuel chemical composition. While soot residence time was highly varied through three levels of injection pressure, the parametric study, including in addition variations of both ambient temperature and density, revealed that soot formation processes in the context of a Diesel-like flame are rather controlled by the quality of spray mixing, and more particularly by the flame capacity to entrain oxygen before entering the oxygen-free, high-temperature region. Thus, a "mechanical" modification of the lift-off length, either created by the cycle-to-cycle dispersion or by engine-derived variables, affects directly flame sooting propensity. Regarding, the effect of fuel chemical composition, this big picture established for lift-off length equivalence ratio also extends in general terms, such that fuel oxygen content seems equivalent to the any other indirect enhancements of lift-off oxygenation. But several uncertainties remain to clarify, in particular regarding the role of aromatics or that of local cooling, and would probably require a more refined experimental environment, liquid length measurements under reactive conditions, and a more specific fuel selection.

5.4. Relationship between soot formation and both local flame temperature and RoHR

Although previously acknowledged by several other authors, connections between ignition position, lift-off length, and soot formation have been confirmed in the previous sections. As a final stage for this study, it is now proposed to examine the correlation between soot formation and flame temperature.

In *Chapter 2*, benefits of Diesel engines with respect to other power-production devices have been reviewed, revealing their lead in terms of fuel consumption and efficiency. Nonetheless, a weak point was also highlighted, namely the well-known trade-off of PM/NO_x emissions, which has been concentrating considerable research efforts in the past twenty years. This issue has already been widely studied while considering the engine as a "black box", but only few studies have approached these aspects by working on the fundamental properties of the flame using optical diagnostics, and obviously even fewer applied the latter to understand the implications of replacing conventional diesel by alternative fuels. Whereas no real consensus exists about the effect of Fischer-Tropsch fuels on exhaust emissions, numerous studies agree on that biodiesel permits to decrease PM emissions while causing an increase of NO_x. In *Chapter 2*, it was suggested that such reduction could be the result of higher flame temperatures, that is, a critical parameter

in the most preponderant mechanism for NO_x formation in Diesel engines (Zeldovich). Because no major difference is actually expected on the adiabatic flame temperature, higher flame temperatures may be produced by a decrease of soot radiation losses, along with several other mechanisms. In a real engine, all these mechanisms occur simultaneously, and continuously interact, which complicates their separation and their own assessment. In probably the most extensive study regarding the breakdown of these mechanisms, Mueller *et al.* [51] refuted experimentally the very widespread idea that faster ignition, either caused by a shorter hydraulic delay and/or a higher CN, was the origin of biodiesel higher NO_x emissions. In agreement with these conclusions, previous results from this study showed that RME has a similar hydraulic delay to other fuels, and even a slightly longer ignition delay. In the same work, Mueller *et al.* therefore concluded that two other factors were most likely responsible for the typical 10 % increase of NO_x emissions, namely (i) a faster combustion, making the whole process happen at higher temperature (closer to TDC), and (ii) soot radiation, cooling down the flame locally. However, as for many studies conducted in facilities of this kind, these two processes remained difficult to isolate.

With the objective to contribute to a better understanding of such processes, while focusing on the consequences involved by the use of alternative fuels, the 2-color method has been employed simultaneously with the OH-chemiluminescence imaging and laser extinction technique. Double-imaging of the flame was collected at high speed, and each channel was filtered at a different visible wavelength. Image post-processing resolved a succession of equations, whose details were given in *Chapter 3*, in order to determine the soot cloud opacity and its corresponding temperature. It is important to remind that flame temperature is assumed to be that of soot according to the discussion provided in [50]. Due to the large amount of data (750000 images) and the difficulty to extract relevant information from 2-D maps of KL and temperature, a methodology of data processing labeled "0-D" and "1-D processing" has been developed whose details are given below. It is important to note that both these averaging methods were operated on the resulting 2-D maps of temperature and KL, i.e. once 2-color calculations were performed on each single image. The intention was to preserve the linearity between KL and f_v since calculations based on average images of intensity do not permit it. To complete the analysis, calculations of the RoHR on the steady portion of the flame have been compared to the steady energy rate injected in order to possibly detect the effect of soot radiation on combustion efficiency. Therefore, beyond the measurement of flame temperature for different fuels under different engine setups, the objective of this section is threefold: (i) to

compare the KL measurement from both laser extinction and 2-color imaging techniques; (ii) to contribute to the understanding of the relationship between soot formation and flame temperature within a conventional Diesel free flame, and (iii) to assess soot radiation losses in regard to combustion efficiency.

5.4.1. 0-D processing of 2-color imaging, a parametric study

As for the other time-resolved techniques, the time-interval between 4 and 5 ms was considered with the intention of matching results with those of OH-chemiluminescence. At the frame rate of 8000 fps, this resulted in considering 8 images per injection sequence (out of 100), thereby reducing the total amount of images to process down to 800 for each of the 75 points of the test matrix. The "0-D processing" aimed at obtaining one single result for every test condition with the purpose to study the effect of fuel properties, thermodynamic conditions and injection pressure. It simply consisted in ensemble-averaging each set of 800 images while including all the pixels belonging to the flame (post-segmentation). Given the spatial inhomogeneity of both flame temperature and KL, but also the cycle-to-cycle dispersion among the 100 injection events, the results are not claimed to be perfectly accurate in quantitative terms through this approach, but they represent an indicator of interest in regard to the comparison among the 75 test conditions. In Figures 5.28 and 5.29, 0-D results of KL and soot temperature have been represented for the sweeps of ambient temperature and ambient density respectively, while accounting for the three injection pressure levels. Experimental results have been completed with estimations of the adiabatic flame temperature (T_{ad}) obtained by means of *Chemkin* calculations at equilibrium and stoichiometric A/F ratio. For this, three surrogates were selected based on a criteria matching approximately chemical formulas, namely heptadecane ($C_{17}H_{36}$) for B05, B30 and FT1; dodecane ($C_{12}H_{26}$) for FT2; and methyl-oleate ($C_{19}H_{36}O_2$)) for RME. The following hierarchy is obtained: $T_{ad}(C_{12}H_{26}) < T_{ad}(C_{17}H_{36}) < T_{ad}(C_{19}H_{36}O_2)$, but only few Kelvins actually separate the three surrogates as previously suggested in this introduction.

First examining KL opacity, both figures display consistent results with laser extinction (Cf. Figure 5.11 and 5.14), in that flame sooting propensity decreases with increasing injection pressure and decreasing both ambient temperature and density. When such three trends are associated, flames even switch to non-sooting regime as can be seen with the three RME-derived fuels at 750 K and 150 MPa injection pressure. In regard to the fuel comparison, results are globally consistent with laser extinction. RME is confirmed to enable a significant reduction of soot formation but results from other fuels

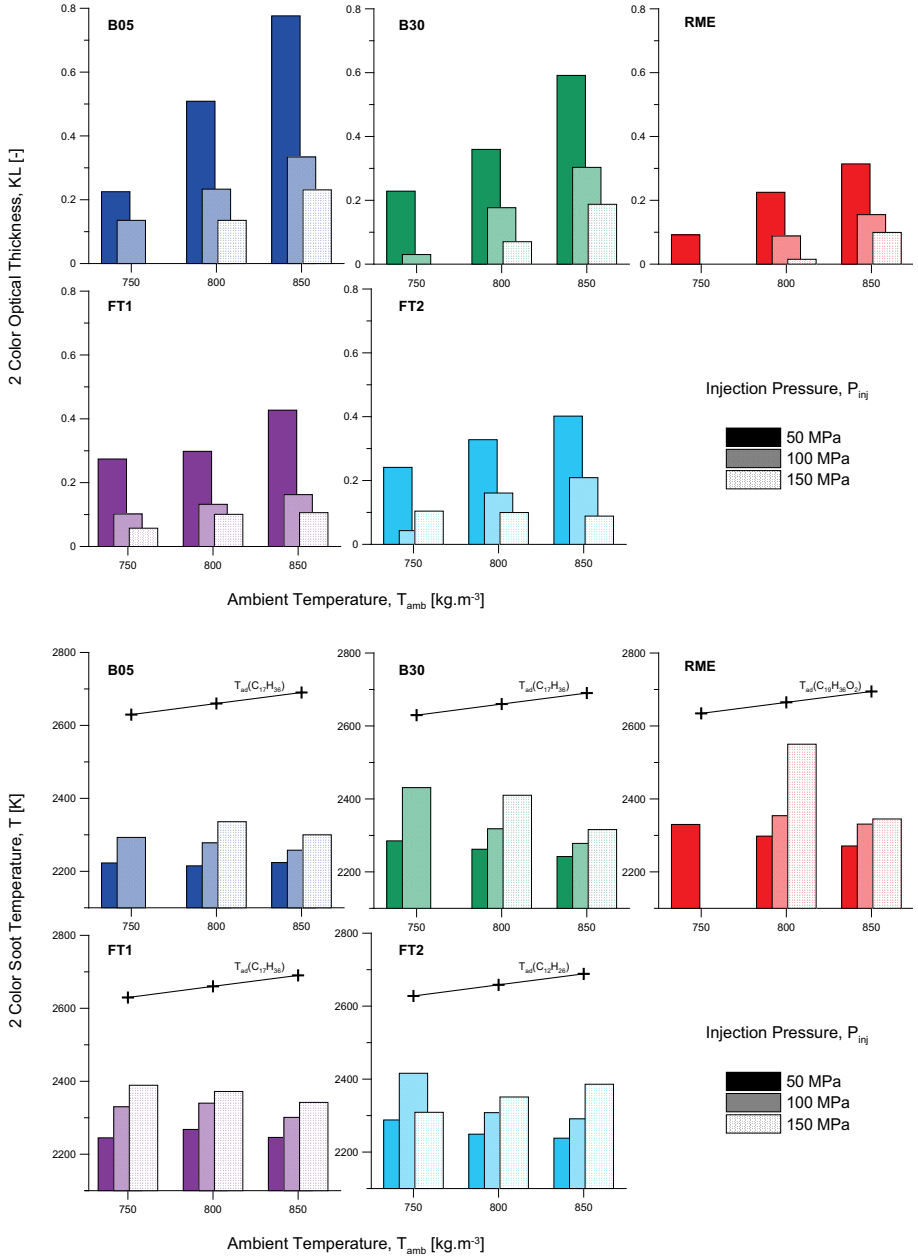

Figure 5.28. *Result of the 0-D processing of 2-color images for the five tested fuels at 26 kg.m^{-3} under different injection pressure and ambient temperature conditions (constant density part of the test matrix).*

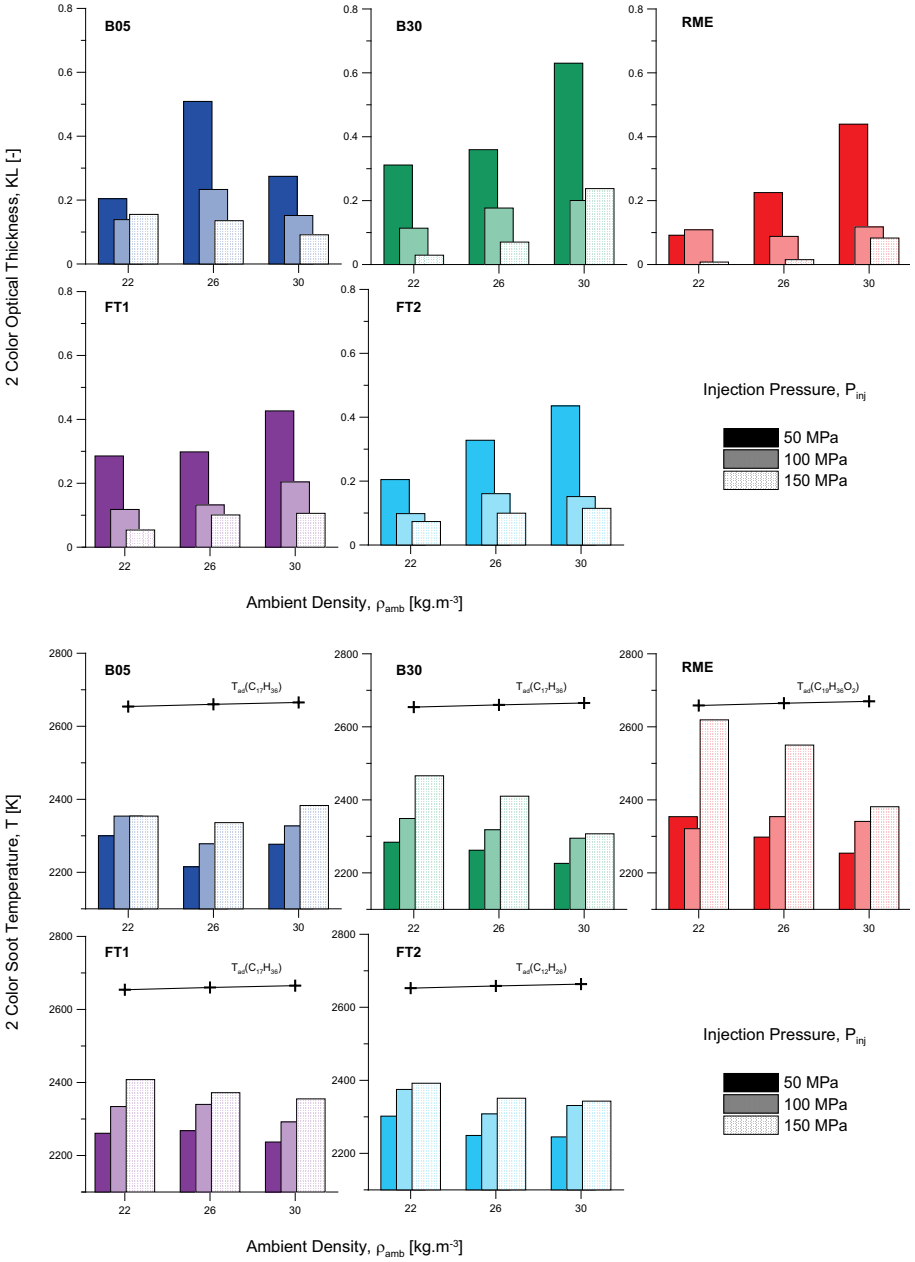

Figure 5.29. *Result of the 0-D processing of 2-color images for the five tested fuels at 800 K under different injection pressure and ambient density conditions (constant temperature part of the test matrix).*

are perhaps less homogeneous than they were with laser extinction. While B05 appears to have the highest sooting propensity, the two Fischer-Tropsch fuels are only slightly more prone to form soot than RME. More in accordance with natural expectations, B30 is also positioned between B05 and RME. In view of this description, values of B05 at 22 and particularly at 30 $kg.m^{-3}$ do not respect such trends and are believed to be underestimated due to an experimental or data processing issue. As a result, the hierarchy of sooting propensity is slightly different than the one extracted from laser extinction with RME<FT1=FT2<B30<B05.

Regarding the flame temperature, it is worth noting first that all the temperatures obtained fall into a reasonable range of $T_{ad}-400\ K$ to T_{ad}. Above all, the response of temperature is particularly interesting as the trends in regard to injection pressure, ambient thermodynamic conditions and fuel type appear to be the exact inversion of those observed for KL. In other words, flame temperature increases with decreasing ambient density and increasing injection pressure. Even more startling is that flame temperature decreases with increasing ambient temperature, thus causing a higher drop respect to the adiabatic flame temperature. As for the fuel hierarchy for flame temperature, it is then the inverse of the one previously obtained for KL: B05<B30<FT1=FT2<RME. Therefore, flame temperature appears to be directly connected to flame sooting propensity, suggesting that energy consumption from soot radiation (and possibly soot inception in a minor extent) plays a significant role in the reduction of flame local temperatures. This further proposes that the trade-off of PM/NO_x emissions, typical of exhaust measurements, actually extends to the scale of the flame, converting the latter into a source (possibly the main one) for this well-known issue. Accordingly, RME shows the highest levels of temperature in response to its lower sooting propensity, which is in entire agreement with results of exhaust emissions obtained by other authors [44].

Besides, further observations also provide a good perception about 2-color results. For instance, FT2 at 150 MPa unexpectedly happens to maintain a similar KL throughout the ambient temperature sweep. Although responding differently from the general trend, the result is positive in that flame temperature increases in return by about 100 K, in accordance with the adiabatic temperature trend. For the record, adiabatic temperature increases almost linearly with ambient temperature, thus one can also expect a similar increase at equivalent sooting levels. Therefore, this effect, although off-trend, reinforces somehow the confidence in the 2-color method. Another example echoing this view is provided by RME at 22 $kg.m^{-3}$ and 150 MPa injection pressure. As observable on KL results, the flame is close to reach

the non-sooting regime but a few remaining kernels of soot, although far from covering the whole flame area, still permit to measure an extremely low KL (KL~0.008) and a corresponding flame temperature almost equal to the adiabatic temperature. By extrapolation, it can be reasonably conceived that flames in the non-sooting regime, for which the absence of soot does not permit to evaluate the flame temperature, should reach temperature values even closer or equal to the adiabatic temperature. As this result is theoretically expected, it also reinforces the confidence in the 2-color method.

5.4.2. 1-D processing of 2-color imaging, a comparison with KL from extinction

The simultaneous use of both laser extinction and 2-color pyrometry provides a great opportunity to compare the KL-opacity resulting from each technique. Before contrasting experimental results between the two techniques, it is proposed to evaluate their relationship on the theoretical level.

5.4.2.1. Theoretical background

Considering the thermal equilibrium of Kirchhoff in which emissivity ϵ equals absorption α, the relationship between absorption (α), transmissivity (τ) and scattering (s) becomes:

$$\epsilon = \alpha = 1 - \tau - s = 1 - exp(-K_{ext}L) - s \tag{5.12}$$

where τ is expressed as a function of $K_{ext}L$ as in Eq. 3.12. In Section 3.6.2.3 where laser extinction was discussed, it was stated that under the Rayleigh regime for small particles, absorption was dominant enough so that scattering could be disregarded. Under this assumption, the scattering component s of Eq. 5.12 would be equal to 0. Therefore, emissivity of both 2-color and laser extinction would be comparable as in Eq. 5.13:

$$1 - exp(-K_{ext}L) - s = 1 - exp(\frac{-K_{2C}L}{\lambda^{\alpha}}) \tag{5.13}$$

Hence, with the wavelength used for laser extinction (514.5 nm), and α=1.38 [52, 53], it can be obtained:

$$K_{ext} = 2.502 \cdot K_{2C} \tag{5.14}$$

The resonance given to the relationship showed in Eq. 5.14 would be stronger if it could be demonstrated that it extends to the cases for which large aggregates are responsible for significant light scattering. When this issue was loomed with laser extinction, it was stated that the historical k_a=4.9 for small particles had to be replaced by an empirical coefficient k_e accounting for scattering, varying in the range of 8 to 10 as a function of the "mixing ratio between Mie and Rayleigh particles". In the most recent studies for Diesel flames, it had been set to 8.7. In the 2-color method, the equivalent empirical coefficient permitting the conversion from KL to f_v would be $\frac{g}{\lambda^{1-\alpha}}$ such as:

$$\frac{g}{\lambda^{1-\alpha}} = \frac{6.3}{0.5145^{0.38}} = 8.12 \sim k_e \tag{5.15}$$

The proximity between both empirical coefficients suggests that they have been obtained under similar conditions, each accounting properly for scattering issues. Therefore, although each technique had its own way to express empirically the uncertainties associated to light scattering, they appear to provide quite a good match.

5.4.2.2. Analysis of 1-D temperature and KL results

After considering results with a 0-D approach, the second type of analysis consisted in a reduction to one dimension of KL and temperature maps. For such analysis, here called "1-D processing", the same time-interval and images have been considered. Since one of the objectives set out in this introduction was to compare KL measurements from both laser extinction and 2-color imaging techniques, a range of pixels was selected along the laser path corresponding to the flame centerline. Five pixels ($\sim$1.5 mm) were averaged radially to draw the axial profiles of both temperature and KL represented in Figures 5.30 and 5.31. In the previous section, it has been shown that KL-factors from each method were intrinsically different and related by approximately a factor 2.5. This correction has then been applied to results of the 2-color method in both figures, and KL-results from the laser extinction technique have been added to help the comparison. Also, *Chemkin* results of adiabatic flame temperature have been recalled on both figures.

First considering results of KL, the comparison between both techniques shows a very good match. If initially, a calibration of the 2-color method had been imagined based on the more accurate measurements of laser extinction, the results rather suggest that the latter is not required. Axial profiles follow the typical bell shape obtained with extinction while reaching similar

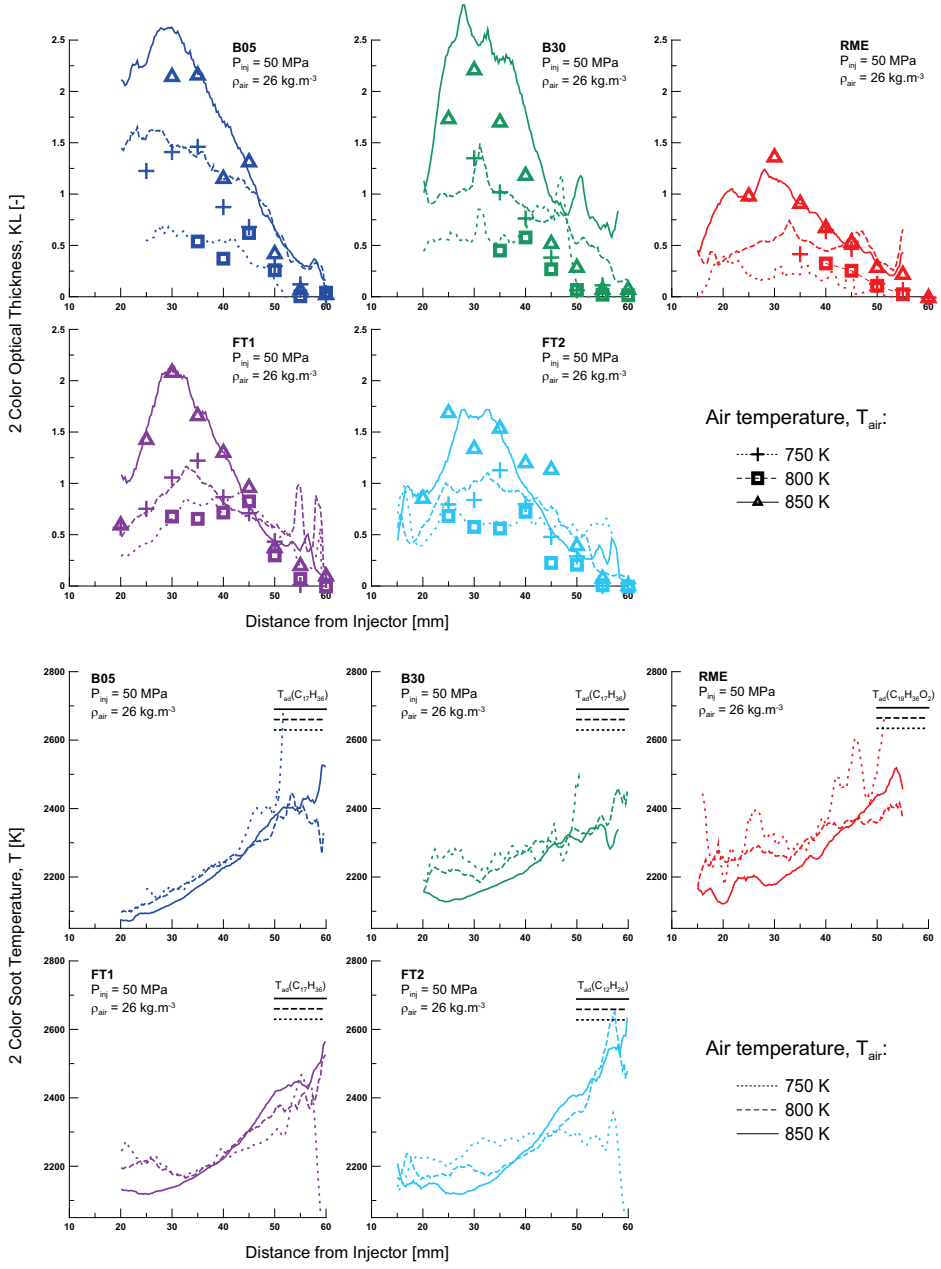

Figure 5.30. *KL and temperature results for the 1-D processing of 2-color images with the five tested fuels at 26 kg.m^{-3} and 50 MPa injection pressure under different ambient temperature conditions.*

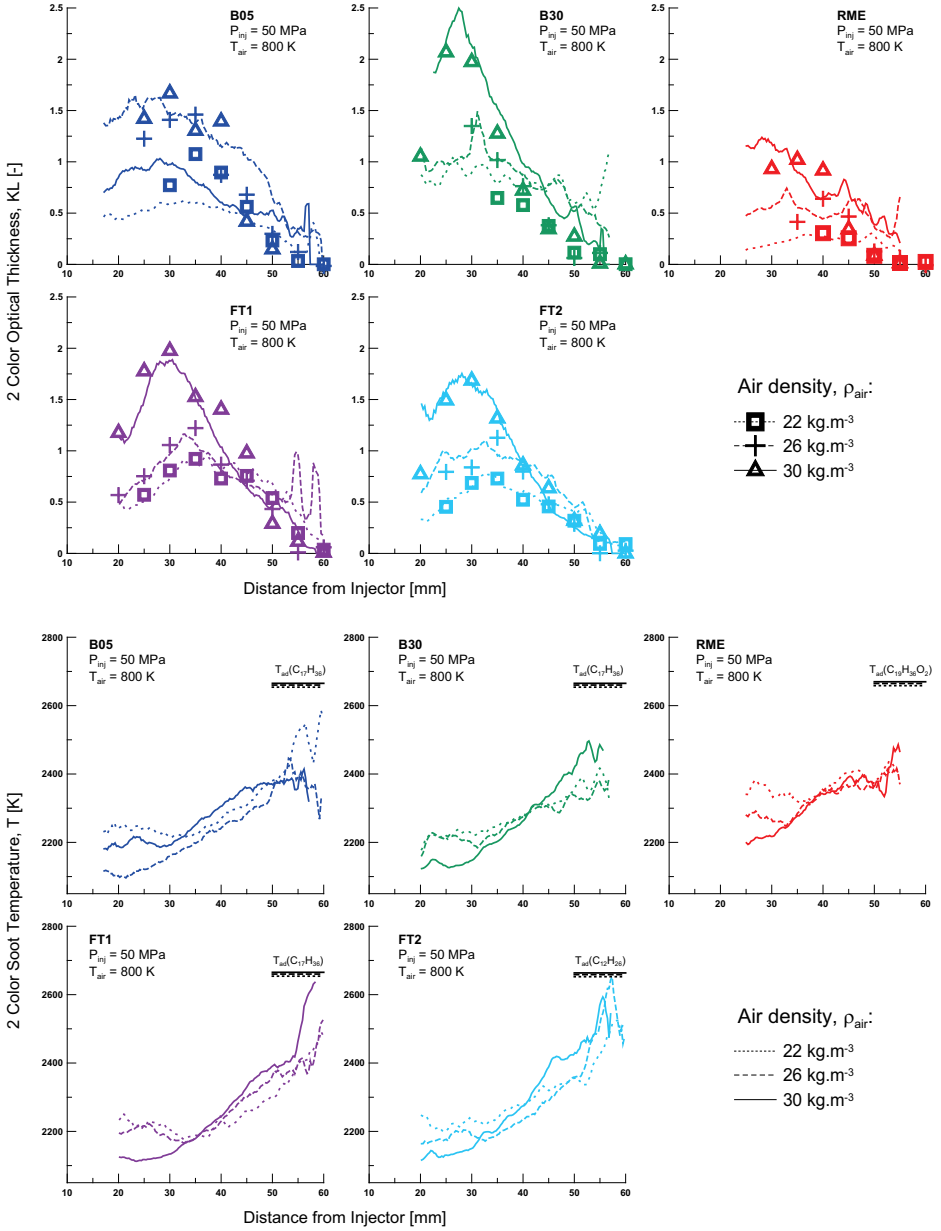

Figure 5.31. *KL and temperature results for the 1-D processing of 2-color images with the five tested fuels at 800 K and 50 MPa injection pressure under different ambient density conditions.*

KL-values in most of the punctual measurements of laser extinction. This result is important on several fields. First, the contribution is important in terms of concepts about the very technique of 2-color imaging. In [54], it was considered that optical thickness of Diesel-like flames was so great that luminosity collected from a line-of-sight technique of imaging such as the 2-color would mostly proceed from the flame surface facing directly the camera, while avoiding completely the contribution from the flame backside. Doubts were consequently raised about what is exactly measured by this technique. In this context, this result therefore suggests that 2-color is able to account for the whole flame depth in the same manner as laser extinction does. Secondly, this result promotes the use of the 2-color imaging in other experiments by furnishing a validation of the technique for KL measurements, namely a measurement fundamentally issued from laser extinction. In practice, this contribution is important as the 2-color imaging technique is much easier to set up, provides a better spatial resolution (2-D *vs.* punctual), and permits in addition the assessment of the flame temperature.

Concerning the axial profiles of temperature, their shape varies from those of KL in that temperature keeps increasing all along the flame axis until the flame tip, similarly to laminar atmospheric flames. Beyond this consistency with the literature, this trend also provides further confidence in the technique. Indeed, the previous section might have suggested that a lower KL was systematically and "foolishly" balanced by a higher level of temperature and *vice-versa*. Results actually show that the method is sensitive and reliable enough to measure a common increase of both KL and temperature before reaching a region where temperature keeps increasing while KL decreases due to soot rarefaction and oxidation. Typically the temperature increases from 2200 to 2600 K, reaching eventually the adiabatic temperature at the flame tip. However, results are not fully homogeneous and may be a bit confusing somehow. Still, an interesting trend emerges considering the parametric study of ambient temperature and density. In the previous section, it has been shown that higher sooting conditions, enabled by either higher ambient temperature or density actually produced a decrease of the flame temperature, in opposition to the trend observed for the adiabatic temperature. On a one-dimensional basis, this statement remains valid on the upstream part of the flame exclusively. Once soot rarefies, typically downstream the 40 mm position (KL <1), flame temperature recovers and tends to reach the adiabatic value, naturally greater for higher ambient temperatures. With flames typically reaching the peak-KL at 30-35 mm, such small and lean downstream portion of the flame (typically between 40 and 55 mm) does not weigh heavy enough in the 0-D average to reverse the trends observed in the previous section.

5.4.3. Effect of soot radiation on the RoHR

As a final stage of this study, an attempt has been made to evaluate the combustion efficiency and its possible deterioration due to soot radiation. When brought to a temperature superior to that of the engine walls, soot radiation produces an imbalance of the Kirchhoff's law of thermal radiation. Thus, heat transfers to the walls, and converts into a loss of thermal efficiency for the engine. In the previous section this effect manifested by a decrease of the flame temperature when sooting propensity was increased, and in consequence should reflect on the pressure trace analysis. Hence, the combustion efficiency η was estimated following Eq. 5.16, where RoHR is the rate of heat release, $\dot{m}_f$ is the mass rate of injection and LHV is the fuel lower heating value. Thus defined, this parameter is similar to the *Calmec parameter* as defined in [55–57] but expressed in time-derivative terms whereas the latter accounts for the integral value throughout the entire combustion event.

$$\eta = \frac{RoHR}{\dot{m}_f \cdot LHV} \tag{5.16}$$

The obtaining of these three parameters has been detailed in depth in *Chapter 3*. To briefly summarize, LHV has been measured with a calorimeter for each of the five fuels, while $\dot{m}_f$ was obtained through measurements in an Injection Rate Discharge Curve Indicator. With 8 ms-long injections, mass flow rate stabilized quickly as displayed by Figure 3.7, which permitted to easily obtain a time-average on the steady portion of the curve. As for calculations of the RoHR, they were obtained through a pressure trace analysis based on the first law of thermodynamics as expressed in Eq. 3.12. This analysis accounted for heat transfer (convection), blow-by and mechanical deformation characterized under motored conditions (non-injected cycles). In combustion, assumption was made that such factors remained unchanged, which seems reasonable a priori when considering that one single spray is injected into a large volume, while only producing a 5 to 10 *bar* pressure increase. Under this assumption, the whole energy injected ideally converts into heat, without further increasing blow-by or convection, therefore leaving soot radiation as the unique possible leak of energy. As a result, non-sooting flames ought to reach efficiency levels close to 100 %, and any drop of combustion efficiency should be created by soot radiation. At that point, it may be important to remark that such assessment is permitted by the particularly long injections performed, so the possibility is given to consider a steady-state portion on the RoHR trace. Thus, fuel burns in the strictest definition of a diffusion flame, namely at the same rate as it is injected without residual heat

release from the premixed burn (Cf. Figure 3.7 and 3.24). In some occasions, time was particularly long to reach this steady-state, such as in conditions of high injection pressure and low temperature, where an important quantity of fuel mixes prior to the complete establishment of the diffusion flame. Thus, the typical 4 to 5 ms interval could not be considered because a remaining component of premixed burn would often lead to an overestimation of both the time-averaged RoHR and the combustion efficiency. For that reason, the time-interval of analysis was further delayed to 5 to 8 ms ASOE. According to this description, results have been reported in Figures 5.32 and 5.33, for respectively the sweeps of ambient temperature and density.

First looking at the overall result, most of the tested conditions fall in a range between 90 and 100 %, except for RME at the lowest temperature condition whose incoherency manifestly attests of an error. In view of the sensitivity of this result, which includes the error associated to each variable, this level of quality in the assessment already represents an achievement and a good starting point. On one hand, both figures show results in accordance with the expectations emitted in this introduction. For instance, efficiency for the three RME-derived fuels drops by about 10 % while increasing ambient temperature, in agreement with the consequent higher sooting propensity. Similarly, their efficiency drops from 26 to 30 $kg.m^{-3}$ in the ambient density sweep. Note that at 22 $kg.m^{-3}$, the efficiency is particularly low for the five fuels possibly due to mixing issues. Finally, RME shows a higher efficiency in comparison to the four others fuels, consistently with its significantly lower sooting propensity. On the other hand, several other points call into questions the quality of the results. First, Fischer-Tropsch fuels do not respect any of the trends suggesting that soot radiation could be affecting combustion efficiency. Above all, one result is particularly striking, that is the efficiency decrease with injection pressure, while this variable is by far the most effective in reducing flame sooting propensity. This issue may find an explanation in the starting assumption, fixing an equivalent thermal flux of convection between non-injected and firing cycles. As pressure and mass injected increase, the higher temperature rise (Cf. Figure 3.19) may increase the thermal flux of convection sufficiently enough to overcome the gain given by radiation, and perceive efficiency degradation. Further assessment should then be performed in this direction to refine the results.

Therefore, in view of the high level of uncertainty associated to this measurement, it is difficult to assert that typical variations of 10 % observed are the unique result of flame radiation created by different levels of soot formation. Nevertheless, the methodology and experimental facility are

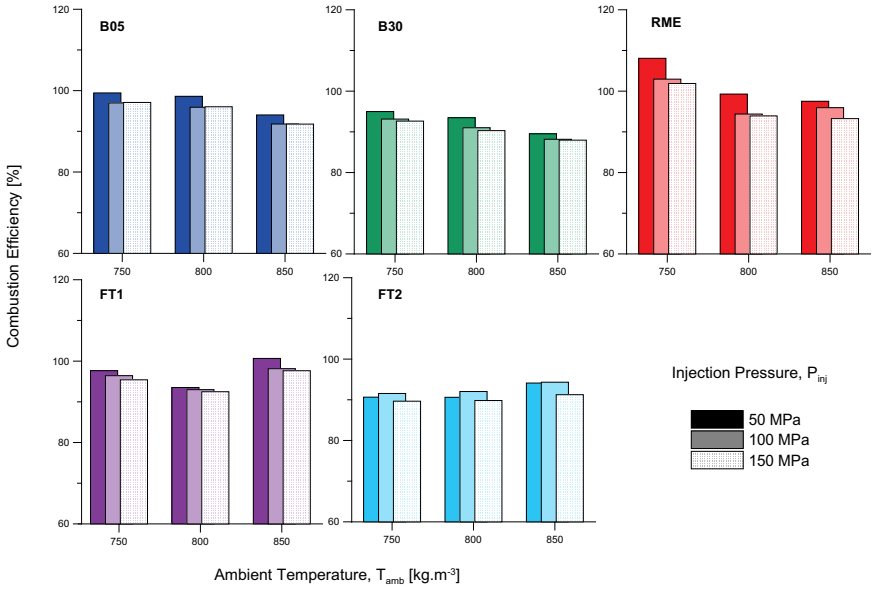

Figure 5.32. *Combustion efficiency for the five tested fuels at 800 K under different injection pressure and ambient density conditions.*

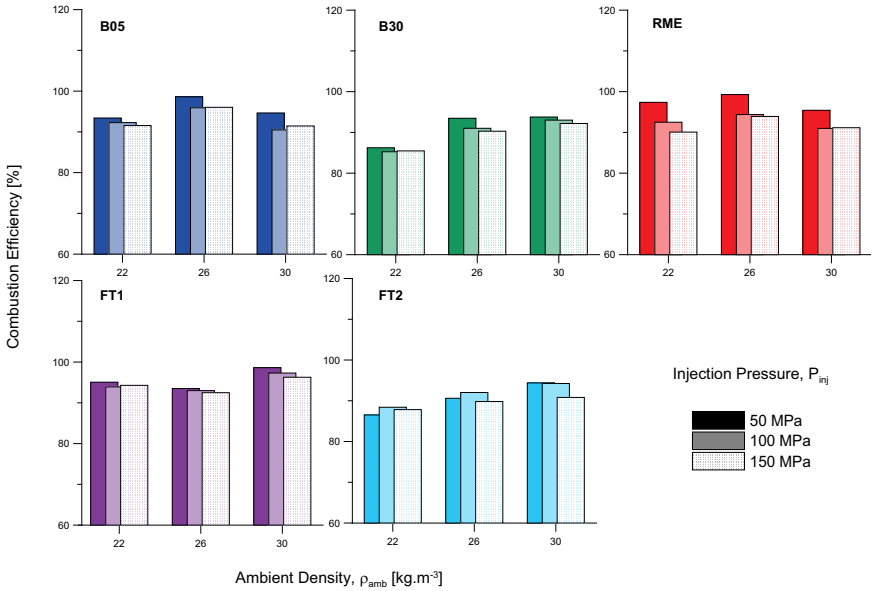

Figure 5.33. *Combustion efficiency for the five tested fuels at 800 K under different injection pressure and ambient density conditions.*

believed to be adequate to account for this factor, which nowadays still represent a great unknown for Diesel combustion.

5.5. Conclusions

After the detailed approach of *Chapter 4* discussing the fuel effect on the spray development under inert conditions, this chapter studied the fuel impact on the spray in a reactive environment, while accounting for the knowledge acquired previously. Several key parameters and stages of the combustion process have been considered, including ignition, lift-off length (and the equivalence ratio associated), soot formation, flame temperature and soot radiation. The focus has also been made on the connection existing between these processes using the different fuels as an additional variable to overall test matrix.

Fuel ignition qualities have been measured revealing the following hierarchy: FT1∼FT2<B30<B05<RME. With the purpose to provide a more quantitative dimension to the latter, particularly in regard to the typical parameters varied in an engine, ignition delay has been examined through different statistic approaches. Empirical models specific to each fuels first suggested that chemical kinetics was more likely to control ignition delay compared to mixing processes. Seeking further clarifications into the fuel effect on chemical kinetics, fuel properties appeared to have less impact than ambient temperature for the fuel selection considered. Still, the fuel density, as a marker of the fuel level of saturation, appeared to be more predictive regarding ignition processes than its volatility, namely a parameter representative of its chain length and volatility. A fuel-independent empirical model accounting for both engine functioning variables and fuel physical properties was then produced, able to predict ignition delay with more than 95 % accuracy.

Results of lift-off length have then been considered and revealed a comparable hierarchy: FT1<FT2<B30∼B05∼RME. In a similar statistical assessment, the key role played by ignition position in the establishment of the lift-off length has been confirmed with engine-derived variables, while extending to alternative fuels. This study therefore supports one of the two major conceptual approaches regarding lift-off length establishment by observing its relevance under a large set of thermodynamic conditions and different fuel origins that a strong relationship exists between the latter and ignition location, Also, an empirical model based on easily accessible inputs for any type of engines (ignition delay, injection pressure, and cylinder pressure)

permitted to obtain a reasonable estimation of the lift-off length assuming free spray conditions.

By measuring the soot thickness with laser extinction, RME appeared to have a much lower sooting propensity than the rest of fuels. All the fuels displayed bell-shaped profiles, varying with cycle-to-cycle dispersion. Using both average results and the cycle-to-cycle dispersion, it was confirmed that, for each fuel considered individually and for all the conditions explored, the main factor controlling soot formation within the flame was air entrainment before lift-off length, while switching to non-sooting regime at a fixed ϕ_{cl}. Although most of the fuels apparently reached this regime with $\phi_{cl}\sim 2$, the analysis was actually more confusing, and opened to different interpretation. Once again, both averaged values and cyclic dispersion were used to demonstrate the validity of these relationships. Engine conditions and the proper oxygen content in fuel proved to be determinant in the leaning of the mixture to the base of the flame to reduce diesel soot formation.

This work on the fuel effect over soot formation processes has been completed under different conditions with the observation and characterization of soot particles sampled directly from the flame core. Soot particles showed similarity in both morphology and evolution throughout the formation/oxidation processes, despite the significantly different amount of soot formed within the flame. Diesel aggregates appeared to be sensitively more circular (higher D_f) and denser (higher k_f) than biodiesel thus suggesting a more compact structure than biodiesel. Regarding the comparison between axial positions, the results suggested the self-similar evolution of particles morphology throughout both growing and oxidations processes when going across the flame.

In the analysis of the 2-color method, flame temperature appeared to be directly connected to flame sooting propensity, suggesting that energy consumption from soot radiation (and possibly soot inception in a minor extent) may play a significant role in the reduction of flame local temperatures. This further proposed that the trade-off of PM/NO_x emissions, typical of exhaust measurements, actually extends to the scale of the flame, converting the latter into a source (possibly the main one) for this well-known issue. Accordingly, RME showed the highest levels of temperature in response to its lower sooting propensity, which is in entire agreement with results of exhaust emissions from the literature.

Finally, a first attempt has been made to evaluate changes in combustion efficiency associated to soot formation, but results cannot be considered

as conclusive because of the large experimental uncertainty. The analysis performed however opens a new possibility for future work.

References

[1] Peters N., *Turbulent Combustion*, Cambridge University Press, 2000.

[2] Pickett L.M., Siebers D.L., "Fuel Effects on Soot Processes of Fuel Jets at DI Diesel Conditions". *SAE Paper 2003-01-3080*, 2003.

[3] Pickett L.M., Siebers D.L., Idicheria C., "Relationship Between Ignition Processes and the Lift-Off Length of Diesel Fuel Jets". *SAE Paper 2005-01-3843*, 2005.

[4] Pickett L.M., Kook S., Persson H., Andersson O., "Diesel fuel jet lift-off stabilization in the presence of laser-induced plasma ignition". *Proc. Combust. Inst.*, Vol. 32, pp. 2793-800, 2009.

[5] Yates A.D.B., Vlljoen C.L., Swarts A., "Understanding the Relation Between Cetane Number and Combustion Bomb Ignition Delay Measurements". *SAE Paper 2004-01-2017*, 2004.

[6] Molina S.A., *Estudio De La Influencia De Los Parametros De Inyeccion Y La Recirculacion De Gases De Escape Sobre El Proceso De Combustion, Las Prestaciones Y Las Emisiones De Un Motor Diesel De 1.8 Litros De Cilindrada*. Tesis Doctoral, Universidad Politécnica de Valencia, Departamento de Máquinas y Motores Térmicos, 2003.

[7] Settles G.S., *Schlieren & Shadowgraph Techniques*, 1^{st} Ed., Springer Verlag, 2001.

[8] Pastor J.V., Payri R., García-Oliver J.M., Nerva J.-G., "Schlieren Measurements of the ECN-Spray A Penetration under Inert and Reacting Conditions". *SAE Paper 2012-01-0456*, 2012.

[9] Rodríguez R.P., Sierens R., Verhelst S., "Ignition delay in a palm oil and rapeseed oil biodiesel fuelled engine and predictive correlations for the ignition delay period". *Fuel*, Vol. 90, pp. 766-72, 2011.

[10] Dec J.E., Coy E.B., "Radical OH Imaging in for DI Diesel Engine and the Structure of the Early Diffusion Flame". *SAE Paper 960831*, 1996.

[11] Nerva J.-G., Genzale C.L., Kook S., García-Oliver J.M., Pickett L.M., "Fundamental spray and combustion measurements of soy methyl-ester biodiesel". *Int J. Engine Res.*, published online 30 August 2012, pp. 1-18, 2012

[12] Venugopal R., Abraham J., "A Review of Fundamental Studies Relevant to Flame Lift-off in Diesel Jets". *SAE Paper 2007-01-0134*, 2007.

[13] Siebers D.L., Higgins B.S., "Flame Lift-Off on Direct-Injection Diesel Sprays Under Quiescent Conditions". *SAE Paper 2001-01-0530*, 2001.

[14] Siebers D.L., Higgins B.S., Pickett L.M., "Flame Lift-Off on Direct-Injection Diesel Fuel Jets: Oxygen Concentration Effects". *SAE Paper 2002-01-0890*, 2002.

[15] Pickett L.M., Siebers D.L., "Soot formation in diesel fuel jets near the lift-off length". *Int. J. Engine Res.*, Vol. 7, pp. 103-30, 2006.

[16] Musculus M.P., Dec J.E., Tree D.R., "Effects of fuel parameters and diffusion flame lift-off on soot formation in a heavy-duty DI diesel engine". *SAE Paper 2002-02-0889*, 2002.

[17] Pickett L.M., Siebers D.L., "Non-Sooting, Low Flame Temperature Mixing-Controlled DI Diesel Combustion". *SAE Paper 2004-01-1399*, 2004.

[18] Benajes J., Molina S., Novella R., Amorim R., "Study on Low Temperature Combustion for Light-Duty Diesel Engines". *Energy Fuels*, Vol. 24, pp. 355-64, 2010.

[19] Pickett L.M., Siebers D.L., "An investigation of diesel soot formation processes using micro-orifices". *Proc. Combust. Inst.*, Vol. 29, pp. 655-62, 2002.

[20] Siebers D.L., Pickett L.M., "Injection Pressure and Orifice Diameter effects on soot in DI diesel fuel jets". *Thermo and fluid-dynamic processes in Diesel engines 2*, Springer-Velag, pp. 253-77, 2004.

[21] Pickett L.M., Siebers D.L., "Soot in Diesel Fuel Jets: Effects of Ambient Temperature, Ambient Density, and Injection Pressure". *Combust. Flame*, Vol. 138, pp. 114-35, 2004.

[22] Mueller C.J., Pitz W.J., Pickett L.M., Martin G.C., Siebers D.L., Westbrook C.K., "Effects of Oxygenates on Soot Processes in DI Diesel Engines: Experiments and Numerical Simulations". *SAE Paper 2003-01-1791*, 2003.

[23] Svensson K.I., Richards M.J., Mackrory A.J., Tree, D.R., "Fuel Composition and Molecular Structure Effects on Soot Formation in Direct-Injection Flames Under Diesel Engine Conditions". *SAE Paper 2005-01-0381*, 2005.

[24] Idicheria C.A., Pickett L.M., "Soot Formation in Diesel Combustion under High-EGR Conditions". *SAE Paper 2005-01-3834*, 2005.

[25] Kook S., Pickett L.M., "Soot volume fraction and morphology of conventional and surrogate jet fuel sprays at 1000-K and 6.7-MPa ambient conditions". *Proc. Combust. Inst.*, Vol. 33, pp. 2911-18, 2011.

[26] Kook S., Pickett L.M., "Soot Volume Fraction and Morphology of Conventional, Fischer-Tropsch, Coal-Derived, and Surrogate Fuel at Diesel Conditions". *SAE Paper 2012-01-0678*, 2012.

[27] Pastor J.V., López J.J., García J.M., Pastor J.M., "A 1D model for the description of mixing-controlled inert diesel sprays". *Fuel*, Vol. 87, pp. 2871-85, 2008.

[28] Dec J.E., "A Conceptual Model of DI Diesel Combustion Based on Laser Sheet Imaging". *SAE Paper 970873*, 1997.

[29] Kosaka H., Aizawa T., Kamimoto T., "Two-dimensional imaging of ignition and soot formation processes in a diesel flame". *Int. J. Engine Res.*, Vol. 6, pp. 21-42, 2005.

[30] Bruneaux G., "Combustion structure of free and wall-impinging diesel jets by simultaneous laser-induced fluorescence of formaldehyde, poly-aromatic hydrocarbons, and hydroxides". *Int. J. Engine Res.*, Vol. 9, pp. 249-65, 2008.

[31] Nerva J.-G., Yamaguchi T., Iguma H., Nishigai H., Kondo K., Takano S., Aizawa T., Genzale C., Pickett L.M., "Transmission Electron Microscopy of Soot Particles sampled directly from a Biodiesel Spray Flame". *SAE Paper 2011-01-2046*, 2011.

[32] Aizawa T., Nishigai H., Kondo K., Yamaguchi T., Nerva J.-G., Genzale C., Kook S., Pickett L.M., "Transmission Electron Microscopy of Soot Particles Directly Sampled in Diesel Spray Flame - A Comparison between US♯2 and Biodiesel Soot". *SAE Paper 2012-01-0695*, 2012.

[33] Lapuerta M., Oliva F., Agudelo J.R., Boehman A.L., "Effect of fuel on the soot nanostructure and consequences on loading and regeneration of diesel particulate filters". *Combust. Flame*, Vol. 159, pp. 844-53, 2012.

[34] Vander Wal R.L., Tomasek A.J., "Soot nanostructure: dependence upon synthesis conditions". *Combust. Flame*, Vol. 136, pp. 129-40, 2004.

[35] Boehman A., Song J., Alam M., "Impact of biodiesel blending on diesel soot and the regeneration of particulate filters". *Energy Fuels*, Vol. 19, pp. 1857-64, 2005.

[36] Song J., Alam M., Boehman A.L., Kim U., "Examination of the oxidation behavior of biodiesel soot". *Combust. Flame*, Vol. 146, pp. 589-604, 2006.

[37] Song J., Alam M., Boehman A.L., "Impact of alternative fuels on soot properties and DPF regeneration". *Combust. Sci. Technol.*, Vol. 179, pp. 1991-2037, 2007.

[38] Di Iorio S., Beatrice C., Guido C., Napolitano P., Vassallo A., Ciaravino C., "Impact of Biodiesel on Particle Emissions and DPF Regeneration Management in a Euro5 Automotive Diesel Engine". *SAE Paper 2012-01-0839*, 2012.

[39] Vander Wal R.L, Mueller C.J., "Initial investigation of effects of fuel oxygenation on nanostructure of soot from a direct-injection Diesel engine". *Energy Fuels*, Vol. 20, pp. 2364-69, 2006.

[40] Xi J., Zhong B.-J., "Soot in Diesel Combustion Systems". *Chem. Eng. Technol.*, Vol. 29, pp. 665-73, 2006.

[41] Tree D.R., Svensson K.I., "Soot processes in compression ignition engines". *Prog. Energy Combust. Sci.*, Vol. 33, pp. 272-309, 2007.

[42] Yamaguchi T., Kondo K., Nishigai H., Takano S., Aizawa T., "Direct Sampling, TEM Analysis and Optical Measurement of Soot Particles at Different Axial Locations in a Transient Spray Flame". *SAE Paper 2011-01-2051*, 2011.

[43] Kondo K., Yamaguchi T., Nishigai H., Takano S., Aizawa T., "High-Resolution Transmission Electron Microscopy of Soot Directly Sampled at Different Axial Locations in Diesel Spray Flame". *SAE Paper 2011-24-0068*, 2011.

[44] Lapuerta M., Armas O., Rodríguez-Fernández J., "Effect of biodiesel fuels on diesel engine emissions". *Prog. Energy Combust. Sci.*, Vol. 34, pp. 198-223, 2008.

[45] Heywood J.B., *Internal Combustion Engine Fundamentals*. McGraw-Hill Publishing, 1988.

[46] Bockhorn H., *Soot formation in combustion - Mechanisms and models*, Springer-Velag, 1994.

[47] Lee K.O., Cole R., Sekar R., Choi M.Y., Kang J.S., Bae C.S., Shin H.D., "Morphological Investigation of the Microstructure, Dimensions, and Fractal Geometry of Diesel Particulates". *Proc. Combust. Inst.*, Vol. 29, pp. 647-53, 2002.

[48] Lapuerta M., Ballesteros R., Martos F.J., "A method to determine the fractal dimension of diesel soot agglomerates". *J. Colloid Interface Sci.*, Vol. 303 pp. 149-58, 2006.

[49] Lapuerta M., Martos F.J., Martin-Gonzalez G., "Geometrical determination of the lacunarity of agglomerates with integer fractal dimension". *J. Colloid Interface Sci.*, Vol. 346, pp. 23-31, 2010.

[50] García-Oliver J.M., *Aportaciones Al Estudio Del Proceso De Combustión Turbulenta De Chorros En Motores Diesel De Inyección Directa*. Tesis Doctoral, Universidad Politécnica de Valencia, Departamento de Máquinas y Motores Térmicos, 2004.

[51] Mueller C.J., Boehman A.L., Martin G.C., "An experimental investigation of the origin of increased NOx emissions when fueling a heavy-duty compression-ignition engine with soy biodiesel". *SAE Paper 2009-01-1792*, 2009.

[52] Musculus M., "Measurements of the Influence of Soot Radiation on In-Cylinder Temperatures and Exhaust NOx in a Heavy-Duty DI Diesel Engine". *SAE Paper 2005-01-0925*, 2005.

[53] Kamimoto T., Murayama Y., "Re-examination of the emissivity of diesel flames". *Int. J. Engine Res.*, Vol. 12, pp. 580-600, 2011.

[54] Monin C., *Caracterizacion Del Proceso De Formación De Hollin En Una Llama De Difusión Diesel De Baja Temperatura*. Tesis Doctoral, Universidad Politécnica de Valencia, Departamento de Máquinas y Motores Térmicos, 2009.

[55] Payri F., Margot X., Gil A., Martin J., *Prediction of heat transfer to the walls in Direct Injection (DI) Diesel engines*. Proceedings of the 2^{nd} EACC - 2005, Frankfurt, June 29-30, 2005.

[56] Payri F., Molina S., Martín J., Armas O., "Influence of measurement errors and estimated parameters on combustion diagnosis". *Appl. Therm. Eng.*, Vol. 26, pp. 226-36, 2006.

[57] Armas O., Rodríguez J., Payri F., Martín J., Agudelo J.R., "Effect of the trapped mass and its composition on the heat transfer in the compression cycle of a reciprocating engine". *Appl. Therm. Eng.*, Vol. 25, pp. 2842-53, 2005.

Chapter 6

Conclusions and future works

Contents

6.1. Introduction

In this final chapter, the objective is to gather the different contributions provided by this experimental work and the corresponding analysis. Beyond a simple and exhaustive listing of the conclusions previously obtained, the idea is also to take a look at the big picture, put such conclusions into their context, anticipate their correlation, and check their relevance with the objectives initially proposed.

Clearly, this work does not have the pretention to resolve all the issues relative to the introduction of alternative fuels. Thus, a proposal of future works is also produced in a second part. Based on several suggestions that have emerged during the analysis, the latter aims at extending the intelligence on the topic and could be somehow considered as an additional result to this work.

6.2. Conclusions

When the time comes to collect, summarize, and take a broader view of the contributions brought about by this study, it might be necessary to first remind ourselves of the global framework and the initial objectives established. As presented in *Chapter 1*, this experimental study has been developed in a difficult context marked by both important energetic and environmental issues. These are manifested respectively by the depletion of fossil resources, further exacerbated by the continuous growth of energetic needs, and contamination matters where cumulated emissions of particles, NO_X and CO_2 remain difficult to reduce simultaneously for any type of combustion devices. In this environment, the possibility of introducing alternative fuels as a replacement for conventional resources in the transport sector has become an increasingly concrete reality, and is seemingly becoming a more and more viable solution, at least as a short and middle term solution. However, the discussion of this document does not focus on the viability of this orientation in itself, but rather on the feasibility and the consequences that would result from the introduction of alternative fuels to combustion processes when supplied into the actual Diesel engine technology. Possibly, a better understanding of the processes involved in their combustion could permit one to extract all the benefits from their properties for their use in a Diesel engine.

The current knowledge of the conventional Diesel combustion has been reviewed in *Chapter 2* by including a detailed description of its processes that were obtained and observed *via* optical techniques. The relatively recent implementation of these techniques permitted great progresses in the intelligence of the flame structure and the whole combustion phenomenology as it occurs in the chamber of a Diesel engine, while revealing the complexity engendered by the numerous physical and chemical processes involved, occurring simultaneously and sometimes interacting. Next, *Chapter 2* approached the current knowledge in regard to alternative fuels when employed directly in Diesel engines. This review raised differences in terms of fuel consumption, combustion efficiency and exhaust emissions, for which a lack of agreement and understanding was evidenced while only few studies appeared to approach their combustion with the level of detail enabled by optical diagnostics. Against this background, it became evident that further insights and quantification into spray and combustion characteristics are fundamental in order to better understand the trends observed in conventional engines, but also with the purpose to extract the maximum benefits from these fuels in the optimization of engine design and calibration, and possibly improve their own design and fabrication.

Several questions and issues about the fuel effect on the combustion processes arose from this review, such that the main interrogations that have been attempted throughout this document could be formulated as follows: *how do fuel properties affect the combustion processes of a conventional Diesel DI engine? What are the mechanisms involved? Which ones are governing?*
As a consequence, the main objective was stated as **improving the understanding and assessing the effect of fuel properties over the physical and chemical mechanisms associated with the processes of combustion and emission formation of a Diesel spray**.
To address this global and quite ambitious assignment, the detail of the combustion process obtained in *Chapter 2* enabled the identification of the key stages and relevant matters where an assessment of the fuel effect is required to better understand both its consequences on the combustion phenomenology, and the resulting performances in terms of combustion and emissions. A framework with the following **intermediate stages** has been defined with a sequential and incremental approach: First, addressing the intrinsic fuel physical and chemical properties at **ambient** conditions, and then addressing sequentially the fuel effect on the **hydraulic behavior** of the injection system, on the evaporative **non-reactive spray**, and finally on the **reactive spray** under Diesel-like conditions.

Such **experimental methodology** has been designed and developed in detail in *Chapter 3* to fulfill both the general and the particular objectives of this work, and could potentially apply to other studies of the same kind:

- Prior to the tests in the high-pressure and high-temperature Diesel environment, five alternative fuels, including biodiesel-derived and Fischer-Tropsch fuels, have been characterized off-engine following a list of selected ASTM/ISO standards. Properties such as fuel density, viscosity, volatility, energy content (LHV) and equivalent formula almost always placed biodiesel and Fischer-Tropsch fuels on both sides of the current conventional diesel (B05). This consequently offered an interesting panel of variables willing to affect all the processes from injection, atomization, and vaporization up to combustion and soot formation.

- As a boundary condition for engine experiments, a solenoid injector was operated and equipped with a small single-hole conical nozzle, sized according to current Diesel engine technology. In particular, this choice presented numerous benefits in respect to a multi-hole nozzle by impeding spray-to-spray interactions and by limiting the amount of fuel-mass injected. The conical shape of the nozzle also meant that cavitation

could be avoided, as well as related issues such as the collapse of the mass flow rate or the alteration of the internal flow pattern. By measuring and combining mass flow rate and momentum flux measurements at the nozzle exit, a hydraulic characterization of the nozzle was obtained, i.e. its hydraulic efficiency compared to an ideal nozzle, allowing the effect of fuel physical properties in this respect to be analyzed.

- For a proper assessment of the fuel effect, steady-state regimes for both the flame and its thermodynamic environment were desirable. This, in fact, represented the target of this study with the objective of simplifying and isolating, as far as was possible, all the processes involved in what had been identified as a very complex problem in *Chapter 2*. Thus, particularly long injections were carried out so the flame would reach the steady-state of a partially premixed turbulent diffusion flame. Under this condition, the spray/flame development also remained quite independent from the injector needle dynamic during injector opening and closing. Then, a test matrix of thermodynamic conditions was created settling different levels of temperature and density. An optical facility permitted the sweep of ambient temperature at constant density, and that of ambient density at constant temperature under quasi-steady conditions. Three levels of injection pressure were performed and all the fuels were injected through the entire test matrix defined accordingly.

- As a first stage of spray optical studies, injections have been operated under inert conditions, while collecting Mie scattering images in order to visualize the liquid-phase of the spray. Prior to an assessment in combustion, this stage mostly focused on the physical aspects of the problem. Thus, the objective was to discuss the fuel effect on the processes of atomization and more particularly liquid vaporization, by evaluating the relevance of fuel property variations in comparison to those of physical variables related to fuel injection and thermodynamic environment. The work was completed by a study performed at Sandia National Lab., including schlieren measurements for inert spray penetration. Although utilized with different fuels, the results on spray development and mixture fraction field formation appeared to extend to the fuels operated in the central thread of this study.

- Under reactive conditions, optical techniques were carefully selected and associated in order to approach the implications of the fuel physico-chemical properties during the combustion process, while intending to detach their influence from the previously accounted inert environment. In this analysis OH-chemiluminescence, laser extinction and 2-color

pyrometry were applied simultaneously to quantify respectively the level of premixing upstream of the flame, the soot formation within the flame and its temperature, with the objective to comment on the differences observed in the literature in terms of PM and NO_x emissions. The work was completed by a study carried out at Meiji University with the observation of soot particles morphology sampled directly from the flame core.

With a clearly defined experimental methodology for the assessment of fuel effect during combustion, the outputs of this work have also been significant on **the experimental techniques** employed:

- Two types of contributions have been developed throughout the distillation curve measurements. Firstly, fuel density variations with temperature have been quantified during the heating phase of distillation tests. This measurement is not common in the literature and does not correspond to any standard yet. Given the important effect observed (nearly -1 $kg.m^{-3}.K^{-1}$), it is believed that this information, associated with fuel compressibility measurements, has a major potential interest for the estimation of fuel state in the nozzle tip region. Accordingly, this association could help in refining both experimental measurements of fuel mass flow rate and fuel conditions at the start of injection for spray modeling. In the absence of compressibility measurements, these results unfortunately did not benefit this study, but the database and the correlations presented do provide a basis for deeper analysis on this topic. Secondly, measurements of distillations curves have been performed in both volume (following the ASTM D86 standard) and mass bases. This association and the close match obtained between the two measurements permitted a discussion of the fuel density self-homogeneity.

- The laser extinction technique for soot quantity measurements has been implemented with success for the first time at CMT-Motores Térmicos. Quite straightforward for atmospheric pressure flames, this technique however requires numerous technical considerations when applied to Diesel-like flames. Among these are the so-called "laser clipping" whose purpose is to account for the transmitted signal contamination created by the collection of flame radiations. In this regard, the optical setup used in this work presented the substantial advantage of not being affected by flame radiation due to the significantly higher power of the laser operated in comparison to other author's work. This allowed a simplification of the optical system and removed both the uncertainties and the heavy coding

for signal treatment associated. In addition, by simultaneously applying laser extinction with the 2-color pyrometry, a comparison was obtained between the two techniques, and showed a good correspondence. This consistency therefore suggested the validity of both methods for the quantification of Diesel-flames sooting propensity, and by extension, for soot temperature *via* the 2-color method.

- The optical arrangement of the 2-color method prioritized the conservation of both the collection angle and the spatial resolution on each channel, in comparison to setups previously employed in the department, where the exact same point of view had been the driving issue. The point of view still remained fairly similar with the remote position of the whole collection system. As suggested above, the 2-color results showed to be consistent in terms of KL in respect to laser extinction, but also in terms of temperature regarding the comparison with *Chemkin* calculations of the adiabatic temperature. Different analyses (0-D and 1-D) further promoted the confidence in the quality of the results obtained with this technique.

From the experimental content point of view, an important number of injections have been performed (∼8250), making this study quite singular on this aspect in respect to others of the same kind. As a consequence, data and images were computationally expensive to process, and therefore required a particular and rigorous effort to extract efficiently the information of interest. Several concerns partly emerged from such high number of tests, but also from the particular functioning of the engine test rig, required to establish a strategy able to overpass these issues. The **methodology for both data processing and results analysis**, based on the following considerations, was successful in this assignment, and even permitted on some occasions to take advantage from some of these boundary conditions which a priori represented a difficulty:

- Under inert conditions, thermodynamic conditions were excessively variable to enable the consideration of steady-state liquid length during the entire injection event. Thus, ambient density and temperature conditions were synchronized with high-speed spray images and their corresponding values of liquid length. This new approach meant that the number of samples could be increased for a more robust statistical analysis, while extending and making the initial test matrix more discreet. Moreover, the comparison with a steady-state approach considering a reduced temporal window, allowed for a discussion of the spray adjustment to its environment under unsteady conditions.

- Under reactive conditions, issues intrinsic to the test rig functioning created highly scattered results and therefore required a consideration of the latter with a cycle-to-cycle approach. Thus, beyond the straightforward analysis based on averages, this cycle-to-cycle analysis, allowed by the simultaneity of optical measurements, permitted further confirmation of the strong connection between lift-off length and soot formation already suggested in the literature.

- Throughout the research conducted, the analysis of the results systematically consisted in two stages. In a first approach, fuels were considered separately in order to check if they each had the same response and the same sensitivity to the variables derived from injection and thermodynamic conditions. This also permitted to address the comparison with conventional diesel, already widely studied in the literature, and to determine if this knowledge was extending to alternative fuels. In a second approach, fuels were all considered together with the objective to identify the most relevant physico-chemical properties, while comparing their effect with the variable issues from the engine functioning, i.e. thermodynamic and injection conditions. The assessment of fuel properties therefore lies in this two-stage analysis and appeared to be essential in the understanding of the fuel effect of the diesel combustion processes.

Finally, after describing the context and both the experimental and methodological contributions, **the main conclusions of this thesis in regard to the assessment of fuel properties throughout the key stages of Diesel spray combustion are summarized as follows**. According to the methodology defined, the sequence follows that of the whole injection/combustion process as it unfolds in time:

- Prior to an assessment at the spray and combustion levels, an evaluation of the fuel effect on the injection system was essential due to its upstream position in respect to the entire process. Accordingly, differences in the hydraulic delay, often referred to as a possible factor responsible for NO_X increase with biodiesel, appeared not to be significant among the five fuels used in this study. In regard to the steady portions of hydraulic measurements, the injector characterization also revealed an overall limited fuel effect on both the mass flow rate and the momentum flux at the nozzle exit. Looking in more detail, both Fischer-Tropsch fuels, however, showed a slightly lower mass flow rate in comparison to biodiesel-derived fuels due to their lower density. Regarding momentum

flux, FT2 appeared to be higher compared to the four other fuels, although none of their properties should theoretically affect this value. This effect is believed to be the result of its lower viscosity, engendering significantly higher Reynolds numbers in the conduct, and thus potentially creating the conditions of nozzle cavitation, as a source of inhomogeneities in the velocity profile at the nozzle exit. In terms of the discharge coefficient (i.e. the hydraulic efficiency in respect to an idealistic nozzle), this propensity to trend towards cavitation was reflected in a decreasing discharge coefficient with Reynolds number, contrary to the general trend displayed by the other fuels, and offsetting the initial advantage of FT2 at lower injection pressure.

- Under inert conditions, measurements of the maximum liquid-phase penetration revealed that Fischer-Tropsch fuels had systematically shorter liquid lengths than RME-derived fuels, for which the latter increased almost proportionally after increasing the RME blending percentage. In the statistical and quantitative assessment, all the fuels appeared to have a similar sensitivity to engine-derived parameters, namely that liquid length was nearly inversely proportional to the cube of ambient temperature, the square root of ambient density, while not being affected by fuel injection pressure. Already widely reported by other authors with conventional diesel, the injection pressure non-effect is significant in that it suggests the extension of the mixing-limited hypothesis to alternative fuels operated under Diesel-like conditions. As regards fuel protagonism in liquid length dissimilarities, fuel density resulted to be the most relevant property, as a mirror of its latent heat of vaporization, but remained insufficient to predict liquid length of realistic fuels involving different chemical compositions and levels of saturation. Therefore, an empirical model based on both fuel density and volatility qualities in addition to thermodynamic and injection conditions has been produced, permitting to estimate the liquid length with 95 % reliability. Next, a comparison between two statistical approaches established that spray liquid-phase adjusts instantaneously to in-cylinder thermodynamic conditions for all the fuels except for RME, suggesting that vaporization processes of the spray can be considered as a succession of steady-states without phenomena of inertia. This result has a particular interest in regard to the hypothesis typically made for spray modeling and enables the use, under unsteady conditions, of empirical models derived from experiments performed within a steady-state environment. Finally, through experiments conducted in collaboration with another laboratory with different fuels and conditions, similar spray penetrations and angles

have been observed, suggesting equivalent qualities of mixing among fuels independently from their properties. This result is most likely to be extendable to the fuels employed in this study and also significant in regard to spray modeling as it shows that variations in the equivalence ratio field while varying fuel origin proceed exclusively from differences in the A/F stoichiometric ratio.

- Under reactive conditions, several key parameters and stages of the combustion process have been considered, including ignition, lift-off length, soot formation, flame temperature and soot radiation. Regarding the processes controlling ignition delay, a statistical analysis specific to each fuel type first established the prominence of chemical kinetics over the quality of spray mixing, by highlighting the low effects of both fuel injection pressure and ambient density. In the hierarchy placing Fischer-Tropsch fuels and RME as respectively the most and the least prone to auto-ignite, fuel density, as the marker of fuel saturation level, appeared to be more predictive than fuel volatility, whilst having significantly less impact than ambient temperature. As regards flame lift-off length, a similar fuel hierarchy was obtained before a statistical analysis further demonstrated the key role played by ignition location in its establishment. Already suggested in the literature, with varying thermodynamic and injection conditions, this relationship between ignition position and lift-off length appeared to also function with varying fuel autoignition quality. Two empirical models were developed, able to predict respectively ignition delay and lift-off length with a high level of accuracy (>95 %). These were based on easily accessible inputs for most applications of Diesel engineering, namely ASTM standards, thermodynamic and injection conditions. As for soot formation, the amount of air entrained upstream of the lift-off length proved to be an overriding factor in the control of flame sooting propensity, as already reflected in the literature. This strong relationship between lift-off and soot formation was verified for each fuel type considered individually and was validated through both an average and a cycle-to-cycle analysis. While both laser punctual and two-dimensional 2-color measurements revealed lower soot levels for RME and equivalent levels for the rest of the fuels, most of them appeared to switch to a non-sooting regime when reaching a fixed value of ϕ_{cl} nearly equal to 2 in the lift-off region. This was independent of the fact that such a lean threshold was achieved thanks to either higher fuel oxygen content, cycle-to-cycle dispersion, or more favorable engine conditions. However, FT1 was off-trend which suggested that cooling effects from

liquid vaporization within the lift-off region may also be considered. This work on fuel effect over soot formation processes was completed by a study in collaboration with Sandia National Lab. and Meiji University. It aimed at observing and characterizing soot particles sampled directly from the core of conventional American diesel and soy-derived biodiesel flames at fixed ambient conditions. Soot particles showed similarity in their evolution throughout the formation/oxidation processes, despite the significantly different amounts of soot formed within each flame. However, diesel aggregates appeared to be slightly more compact and denser than biodiesel thus signifying a more compact structure than biodiesel. Finally, the application of the 2-color method revealed that flame temperature is directly related to flame sooting propensity. In this context, RME showed the highest temperature levels in response to its lower soot formation, in agreement with results of exhaust emissions from the literature. This observation therefore supported the previously reviewed theory which states that energy consumption from soot radiation may play a key role in the reduction of flame local-temperatures. This further suggests that the trade-off of PM/NO_X emissions, typical of exhaust gas measurements, actually extends to the scale of the flame, thus possibly becoming the main source for this well-known issue. To summarize, this study, under reactive conditions, confirmed the successive relationships between ignition, lift-off length, soot formation and flame temperature, whilst providing arguments to better understand the results of exhaust gas emissions using alternative fuels as well as different engine conditions.

6.3. Future works

Throughout the research described in this thesis, several remarks and suggestions about future works were brought to light, which could not be considered either due to hardware limitations, time constraints or budget restrictions. These could potentially provide the basis for prospective studies that would further enhance the application of optical techniques in regard to Diesel spray combustion, as well as providing more accurate and comprehensive investigations into fundamental processes governing Diesel combustion, including that of alternative fuels.

- Firstly concerning optical techniques, the collection angle appeared to be of the utmost importance in their setup. As it is able to adversely affect the results and the success of measurements, it is therefore

deserving of a review in existing literature with recommendations for a proper application. Specifically regarding the schlieren technique, a quantitative assessment of the collection angle, already initiated in [1], could help providing the local temperature of the mixture and would be of particular interest at ignition location. Given the recent progress in the knowledge relating to mixture fraction field, this would be made possible at locations where the spray vanishes by assuming that the refractive index of the fuel mixture is the same as that of surrounding ambient air.

- Several variables of interest were unfortunately not included in this work and could have been considered in order to complete the picture of Diesel combustion. Although their effect is sometimes available in the literature, nozzle-hole diameter, ambient oxygen-concentration (to simulate EGR), and both swirl and tumble levels deserve to be assessed, to enable a more extended application, as well as improved accuracy of the empirical models produced. As regards fuel properties, the use of single-compound fuels, either in pure or blended forms, appears to be the next logical step after this study. These would first permit the connection with the important properties database available in the literature, and be more efficient for the comparison with modeling. Finally, a study dedicated to the comparison between single- and multi-hole injectors would enable the checking of results obtained with single-hole nozzles under more realistic conditions of an engine.

- In view of the important variations of fuel density observed by varying its temperature, deeper investigation on this topic should be performed with the objective to determine the real fuel conditions at the nozzle exit. Associated with the quantification of its compressibility, such an assessment would resolve one of the major remaining unknown concerning Diesel technologies, something which is required for spray modeling.

- To the author's knowledge, few studies approached the maximum length of the spray liquid-phase during combustion. Technically possible, a similar analysis including transient ambient conditions and Mie-scattering high-speed imaging could permit the verification of the instantaneous spray adaptation to its environment, and check the exponent values obtained for both fuel and engine-derived variables (particularly ambient temperature) in the empirical models of liquid length.

- Several contributions remain in order to increase understanding of flame combustion. The employment of Laser Induced Incandescence (LII) could for instance enable the study of soot radial distribution while converting KL into soot volume fraction values. It could also permit a quantification of soot particles escaping from the flame front due to the turbulent character of the flame, and the statement over the relevance of this process in the exhaust PM issue compared to other hypotheses (soot deposit by thermophoresis, etc.). Conclusions obtained through soot sampling that pointed out that oxidation could occur within the flame core should be further tested in order to state categorically the diffusive character of a Diesel flame. Further work on the connection between lift-off length and soot formation, including the effect of liquid vaporization cooling should also be continued. For example, a comparison at iso-LOL, under different conditions of injection or ambient condition by forcing ignition with a laser pulse, could shed more light on this relationship. Finally, the base level for the quantification of soot radiation has been set in this work and was not satisfactory due to the high level of experimental error. The potential was revealed nonetheless to make such assessment, and further accuracy in the application of all the experimental work could lead to the resolution of one of the other major unknowns of Diesel engine combustion.

References

[1] Pastor J.V., Payri R., García-Oliver J.M., Nerva J.-G., "Schlieren Measurements of the ECN-Spray A Penetration under Inert and Reacting Conditions". *SAE Paper 2012-01-0456*, 2012.

References Index

Aizawa T., Kosaka H., "Investigation of early soot formation process in a diesel spray flame via excitation-emission matrix using a multi-wavelength laser source". *Int. J. of Engine Res.*, Vol. 9, pp. 79-97, 2008.

Appears in p. 65 in Chapt. 2-[163]

Aizawa T., Nishigai H., Kondo K., Yamaguchi T., Nerva J.-G., Genzale C., Kook S., Pickett L.M., "Transmission Electron Microscopy of Soot Particles Directly Sampled in Diesel Spray Flame - A Comparison between US♯2 and Biodiesel Soot". *SAE Paper 2012-01-0695*, 2012.

Appears in p. 135, 224 in Chapt. 3-[44] & Chapt. 5-[32]

Aleixandre R., Valderrama J.C., Desantes J.M., Torregrosa A.J., "Identification of information sources and citation patterns in the field of reciprocating internal combustion engines". *Scientometrics*. Vol. 59, pp 321-336, 2004.

Appears in p. 64 in Chapt. 2-[162]

Allocca L., Mancaruso E., Montanaro A., Sequino L., Vaglieco B.M., *Effects of mineral and biodiesel fuel compositions on spray evolution and mixture distribution.* Thermofluidynamic processes in Diesel engines, Valencia, Sept. 14-17, 2010.

Appears in p. 91 in Chapt. 3-[1]

Allocca L., Mancaruso E., Montanaro A., Vaglieco B.M., Vassallo A., "Renewable biodiesel/reference diesel fuel mixtures distribution in non-evaporating and evaporating conditions for diesel engines". *SAE Paper 2009-24-0054*, 2009.

Appears in p. 37 in Chapt. 2-[92]

Allocca L., Montanaro A., Cipolla G., Vassalo A., "Spatial-temporal characterization of alternative fuel sprays from a second-generation common-rail fuel injection system for Euro4 passenger car application". *SAE Paper 2009-01-1856*, 2009.

Appears in p. 170 in Chapt. 4-[21]

Amorim R., *Combustión Por Difusión De Baja Temperatura En Motores Diesel De Pequeña Cilindrada.* Tesis Doctoral, Universidad Politécnica de Valencia, Departamento de Máquinas y Motores Térmicos, 2007.

Appears in p. 7 in Chapt. 1-[20]

Andersson Ö, *Advanced topics in Diesel engine combustion: techniques and concepts*. CMT Internal Seminar Program, 18-22nd July, 2011.

Appears in p. 9 in Chapt. 1-[26]

Arcoumanis C., Kamimoto T., *Flow and Combustion in Reciprocating Engines*. Springer-Verlag, 2010.

Appears in p. 8 in Chapt. 1-[24]

Armas O., Rodríguez J., Payri F., Martín J., Agudelo J.R., "Effect of the trapped mass and its composition on the heat transfer in the compression cycle of a reciprocating engine". *Appl. Therm. Eng.*, Vol. 26, pp. 2842-53, 2005.

Appears in p. 115, 254 in Chapt. 3-[21] & Chapt. 5-[57]

Armas O., Yehliu K., Boehman A.L., "Effect of alternative fuels on exhaust emissions during diesel engine operation with matched combustion phasing". *Fuel*, Vol. 89, pp. 438-456, 2010.

Appears in p. 66 in Chapt. 2-[173]

Arrègle J., *Análisis De La Estructura Y Dinámica Interna De Chorros Diesel*. Tesis Doctoral, Universidad Politécnica de Valencia, Departamento de Máquinas y Motores Térmicos, 1997.

Appears in p. 28, 31, 103 in Chapt. 2-[20] & Chapt. 3-[12]

Arrègle J., Pastor J.V., López J.J., García A., "Insights on postinjection-associated soot emissions in direct injection diesel engines". *Combust. Flame*, Vol. 154, pp. 448-461, 2008.

Appears in p. 54 in Chapt. 2-[136]

Arrègle J., Pastor J.V., Ruiz S., "The Influence of Injection Parameters on Diesel Spray Characteristics". *SAE Paper 1999-01-0200*, 1999.

Appears in p. 32, 38 in Chapt. 2-[48]

Arthozoul S., *Association of premixed and diffusive combustion modes in a Heavy-Duty Diesel engine*. Tesis Doctoral, Universidad Politécnica de Valencia, Departamento de Máquinas y Motores Térmicos, Document under preparation.

Appears in p. 7 in Chapt. 1-[21]

Ashgriz N., *Handbook of atomization and sprays: theory and applications*, Springer, 2011.

Appears in p. 32 in Chapt. 2-[43]

ASTM standard D-4737-03, *Standard Test Method for Calculated Cetane Index by Four Variable Equation*. West Conshohocken, PA: ASTM-International, 2003.

Appears in p. 49 in Chapt. 2-[126]

ASTM standard D-613-01, *Standard Test Method for Cetane Number of Diesel Fuel Oil*. West Conshohocken, PA: ASTM-International, 2001.

Appears in p. 49 in Chapt. 2-[120]

ASTM standard D-6890-04, *Standard Test Method for Determination of Ignition Delay and Derived Cetane Number (DCN) of Diesel Fuel Oils by Combustion in a Constant Volume Chamber*. West Conshohocken, PA: ASTM-International, 2004.
Appears in p. 49 in Chapt. 2-[121]

ASTM standard D-976-91, *Standard Test Methods for Calculated Cetane Index of Distillate Fuels*. West Conshohocken, PA: ASTM-International, 2000.
Appears in p. 49 in Chapt. 2-[125]

Azimov U., Kim K.S., "Visualization of gas-to-liquid (GTL) fuel liquid length and soot formation in the constant volume combustion chamber". *J. Therm. Sci. Technol.*, Vol. 3, pp. 461-73, 2008.
Appears in p. 170 in Chapt. 4-[17]

Badock C., Wirth R., Fath A., Leipertz A., "Investigation of cavitation in real size diesel injection nozzles". *Int. J. of Heat and Fluid Flow*, Vol. 20, pp. 538-544, 1999.
Appears in p. 29 in Chapt. 2-[24]

Baert R., *Advanced topics in engine combustion*. CMT Internal Seminar Program, 6-9th September, 2010.
Appears in p. 9 in Chapt. 1-[25]

Baert R.S.G., Frijters P.J.M., Somers B., Luijten C.C.M., de Boer W., "Design and operation of a high pressure, high temperature cell for HD diesel spray diagnostics: guidelines and results". *SAE Paper 2009-01-0649*, 2009.
Appears in p. 102 in Chapt. 3-[10]

Barlow R.S., Dibble R.W., Chen J.-Y., Lucht R.P., "Effect of Damköler Number on Superequilibrium OH Concentration in Turbulent Nonpremixed Jet Flames". *Combust. Flame*, Vol. 82, pp. 235- 251, 1990.
Appears in p. 52 in Chapt. 2-[133]

Bartok W., Sarofim A.F., *Fossil fuel combustion: a source book*. Wiley, 1991.
Appears in p. 57 in Chapt. 2-[144]

Beatrice C., Bertoli C., Del Giacomo N., Guido C., Migliaccio M., "In-cylinder Soot Evolution Analysis in a Transparent Research DI Diesel Engine Fed by Oxygenated Fuels". *SAE Paper 2002-01-2851*, 2002.
Appears in p. 65, 143 in Chapt. 2-[166] & Chapt. 3-[49]

Beatrice C., Capaldi P., Del Giacomo N., Guido C., Mancaruso E., Vaglieco B.M., "Analysis of Impact of Diesel Fuel/Biodiesel Blends on a Modern Diesel Combustion System Performance by Means of Injection Test Rig, Optical and Real SC Engine Experiments". *SAE Paper 2009-01-0484*, 2009.
Appears in p. 65, 143 in Chapt. 2-[169] & Chapt. 3-[52]

Benajes J., Molina S., De Rudder K., Amorim R.J., "Optimization Towards Low-temperature Combustion in a HSDI Diesel Engine, Using Consecutive Screenings". *SAE Paper 2007-01-0911*, 2007.
Appears in p. 59, 65 in Chapt. 2-[155]

Benajes J., Molina S., Novella R., Amorim R., "Study on Low Temperature Combustion for Light-Duty Diesel Engines". *Energy Fuels*, Vol. 24, pp. 355-64, 2010.
Appears in p. 217 in Chapt. 5-[18]

Benajes J., Novella R., García A., Arthozoul S., "Partially premixed combustion in a Diesel engine induced by a pilot injection at the low-pressure top dead center". *Energy Fuels*, Vol. 23, pp. 2891-902, 2009.
Appears in p. 162, 164 in Chapt. 4-[3]

Benajes J., Novella R., García A., Arthozoul S., "The role of in-cylinder gas density and oxygen concentration on late spray mixing and soot oxidation processes". *Energy*, Vol. 36, pp. 1599-611, 2011.
Appears in p. 162, 164 in Chapt. 4-[4]

Bermúdez V., García J.M., Juliá E., Martínez S., "Engine with Optically Accessible Cylinder Head: a Research Tool for Injection and Combustion Processes". *SAE Paper 2003-01-1110*, 2003.
Appears in p. 113 in Chapt. 3-[20]

Bockhorn H., *Soot formation in combustion - Mechanisms and models*, Springer-Velag, 1994.
Appears in p. 233 in Chapt. 5-[46]

Boehman A., Song J., Alam M., "Impact of biodiesel blending on diesel soot and the regeneration of particulate filters". *Energy Fuels*, Vol. 19, pp. 1857-64, 2005.
Appears in p. 226 in Chapt. 5-[35]

Boehman A.L., Morris D., Szybist J.P., Esen E., "The Impact of the Bulk Modulus of Diesel Fuels on Fuel Injection Timing". *Energy Fuels*, Vol. 18, pp. 1877-1882, 2004.
Appears in p. 30 in Chapt. 2-[29]

Bogin Jr. G.E, DeFilippo A., Chen J.Y., Chin G, Luecke J., Ratcliff M.A., Zigler B.T., Dean A.M., *Modeling the Fuel Spray and Combustion Process of the Ignition Quality Tester with KIVA-3V*. Fall Meeting of the Western States Section of the Combustion Institute, Irvine, Oct. 26-27, 2009.
Appears in p. 49, 50 in Chapt. 2-[124]

Bolis A., "Agrocarburants : un cocktail qui coûte très cher à la pompe". Le Monde, 25th January, 2012.
Appears in p. 14 in Chapt. 1-[36]

Bosch W., "The fuel rate indicator: a new measuring instrument for display of the characteristics of individual injection". *SAE Paper 660749*, 1966.
Appears in p. 102 in Chapt. 3-[11]

Boudy F., Seers P., "Impact of physical properties of biodiesel on the injection process in a common-rail direct injection system". *Energy Convers. Manage.*, Vol. 50, pp. 2905-2912, 2009.
Appears in p. 30 in Chapt. 2-[34]

Bower G.R., Foster D.E., "The effect of split injection on fuel distribution in an engine-fed combustion chamber". *SAE Paper 930864*, 1993.
Appears in p. 33 in Chapt. 2-[74]

BP, *Statistical Review of World Energy*, 2011.
Appears in p. 9, 11, 12, 14 in Chapt. 1-[28]

Bracho G., *Experimental And Theoretical Study Of The Direct Diesel Injection Process At Low Temperatures*. Tesis Doctoral, Universidad Politécnica de Valencia, Departamento de Máquinas y Motores Térmicos, 2011.
Appears in p. 30, 68, 103, 104, 109 in Chapt. 2-[30] & Chapt. 3-[16]

Broadwell J.E., Lutz A.E., "A turbulent jet chemical reaction model: NOx production in jet flames". *Combust. Flame*, Vol. 114, pp. 319-335, 1998.
Appears in p. 59 in Chapt. 2-[146]

Browne K.R., Partridge I.M., Greeves G., "Fuel property effects on fuel/air mixing in an experimental Diesel engine". *SAE Paper 860223*, 1986.
Appears in p. 33, 34, 169 in Chapt. 2-[71] & Chapt. 4-[13]

Bruneaux G., "Combustion structure of free and wall-impinging diesel jets by simultaneous laser-induced fluorescence of formaldehyde, poly-aromatic hydrocarbons, and hydroxides". *Int. J. Engine Res.*, Vol. 9, pp. 249-65, 2008.
Appears in p. 52, 53, 56, 221, 222 in Chapt. 2-[130] & Chapt. 5-[30]

Canaan R.E., Dec J.E., Green R.M., Daly D.T., "The influence of fuel volatility on the liquid-phase fuel penetration in a heavy-duty D.I. diesel engine". *SAE Paper 980510*, 1998.
Appears in p. 34, 169, 176 in Chapt. 2-[82] & Chapt. 4-[14]

Chaves H., Knapp M., Kubitzek A., Obermeier F., Schneider T., "Experimental Study of Cavitation in the Nozzle Hole of Diesel Injectors Using Transparent Nozzles". *SAE Paper 950290*, 1995.
Appears in p. 29 in Chapt. 2-[25]

Cheng A.S., Upatnieks A., Mueller C.J., "Investigation of Fuel Effects on Dilute, Mixing-Controlled Combustion in an Optical Direct-Injection Diesel Engine". *Energy Fuels*, Vol. 21, pp. 1989-2002, 2007.
Appears in p. 65, 143 in Chapt. 2-[168] & Chapt. 3-[51]

Cheng A.S., Upatnieks A., Mueller C.J., "Investigation of the impact of biodiesel fuelling on NOx emissions using an optical direct injection diesel engine". *Int. J. Engine Res.*, Vol.7, pp. 297-318, 2006.
Appears in p. 65, 143 in Chapt. 2-[167] & Chapt. 3-[50]

Chiu W.S., Shahed S.M., Lyn, W.T., "A Transient Spray Mixing Model for Diesel Combustion". *SAE Paper 760128*, 1976.
Appears in p. 54 in Chapt. 2-[139]

Choi M.Y., Mulholland G.W., Hamins A., Kashiwagi T., "Comparisons of the soot volume fraction using gravimetric and light extinction techniques". *Combust. Flame*, Vol. 102, Vol. 161-9, 1995.

Appears in p. 135 in Chapt. 3-[37]

Choi S., Oh Y., "The spray characteristics of unrefined biodiesel". *Renewable Energy*, Vol. 42, pp. 136-139, 2012.

Appears in p. 32 in Chapt. 2-[52]

Coates J., "Interpretation of Infrared Spectra, A Practical Approach", in *Encyclopedia of Analytical Chemistry*, pp. 10815-37, John Wiley & Sons, 2000.

Appears in p. 97 in Chapt. 3-[9]

Comité des Constructeurs Français d'automobile. Press bulletin of 12/10/2010. On behalf of China Daily of 7/10/10.

Appears in p. 11 in Chapt. 1-[30]

Correas D., *Estudio Teórico-Experimental Del Chorro Libre Diesel Isotermo*. Tesis Doctoral, Universidad Politécnica de Valencia, Departamento de Máquinas y Motores Térmicos, 1998.

Appears in p. 28 in Chapt. 2-[19]

Curran H.J., Gaffuri P., Pitz W.J., Westbrook C.K., "A Comprehensive Modeling Study of n-Heptane Oxidation". *Combust. Flame*, Vol. 114, pp. 149-177, 1998.

Appears in p. 42, 47 in Chapt. 2-[111]

David G., *Mesure de la température et de la concentration en suies de flammes Diesel"*. Projet de Fin d'Étude, Institut Supérieur de l'Automobile et des Transports, 2011.

Appears in p. 149 in Chapt. 3-[64]

De Rudder K., *An Approach To Low Temperature Combustion In A Small HSDI Diesel Engine*. Tesis Doctoral, Universidad Politécnica de Valencia, Departamento de Máquinas y Motores Térmicos, 2007.

Appears in p. 7 in Chapt. 1-[17]

Dec J.E., Kelly-Zion P.L., "The effects of injection timing and diluent addition on late-combustion soot burnout in a DI diesel engine based on simultaneous 2-D imaging of OH and soot". *SAE Paper 2000-01-0238*, 2000.

Appears in p. 54 in Chapt. 2-[134]

Dec J.E., "A Conceptual Model of DI Diesel Combustion Based on Laser Sheet Imaging". *SAE Paper 970873*, 1997.

Appears in p. 24, 51, 54, 56, 62, 221, 228 in Chapt. 2-[1] & Chapt. 5-[28]

Dec J.E., Canaan R.E., "PLIF Imaging of NO Formation in for DI Diesel Engine". *SAE Paper 980147*, 1998.

Appears in p. 55 in Chapt. 2-[141]

Dec J.E., Coy E.B., "Radical OH Imaging in for DI Diesel Engine and the Structure of the Early Diffusion Flame". *SAE Paper 960831*, 1996.

Appears in p. 39, 52, 54, 205 in Chapt. 2-[104] & Chapt. 5-[10]

Dec J.E., Espey C., "Chemiluminescence Imaging of Autoignition in for DI Diesel Engine". *SAE Paper 982685*, 1998.
Appears in p. 38, 39, 42, 44, 45, 46 in Chapt. 2-[100]

Dec J.E., Espey C., "Ignition and Early Soot Formation in for D.I. Diesel Engine Using Multiple 2-D Imaging Diagnostics". *SAE Paper 950456*, 1995.
Appears in p. 38, 44, 45, 46 in Chapt. 2-[99]

Desantes J.M., Arrègle J., Pastor J.V., Delage A., "Influence of the Fuel Characteristics on the Injection Process in a D.I. Diesel Engine". *SAE Paper 980802*, 1998.
Appears in p. 30, 32 in Chapt. 2-[32]

Desantes J.M., Arrègle J., Ruiz S., "Characterisation Of The Injection-Combustion Process In A D.I. Diesel Engine Running With Rape Oil Methyl Ester". *SAE Paper 1999-01-1497*, 1999.
Appears in p. 30, 32 in Chapt. 2-[35]

Desantes J.M., Benajes J., Arrègle J., Delage A., *Effect of the properties of several fuels on the injection and combustion in HSDI Diesel engine.* Thermofluidynamic processes in Diesel engines, Valencia, Sept. 13-15, 2000.
Appears in p. 30, 32 in Chapt. 2-[36]

Desantes J.M., Pastor J.V., Payri R., Pastor J.M., "Experimental characterization of internal nozzle flow and diesel spray behavior. Part II. Evaporative conditions". *Atomization Sprays*, Vol. 15, pp. 517-43, 2005.
Appears in p. 166 in Chapt. 4-[11]

Desantes J.M., Payri R., Salvador F.J., De la Morena J., "Influence of cavitation phenomenon on primary break-up and spray behaviour at stationary conditions". *Fuel*, Vol. 89, pp. 3033-3041, 2010.
Appears in p. 29 in Chapt. 2-[26]

Desantes J.M., Payri R., Salvador F.J., Gil A., "Development and validation of a theoretical model for diesel spray penetration". *Fuel*, Vol. 85, pp. 910-917, 2006.
Appears in p. 37 in Chapt. 2-[90]

Desantes J.M., Payri R., Salvador F.J., Gimeno J., "Measurements of Spray Momentum for the Study of Cavitation in Diesel Injection Nozzles". *SAE Paper 2003-01-0703*, 2003.
Appears in p. 106 in Chapt. 3-[18]

Di Iorio S., Beatrice C., Guido C., Napolitano P., Vassallo A., Ciaravino C., "Impact of Biodiesel on Particle Emissions and DPF Regeneration Management in a Euro5 Automotive Diesel Engine". *SAE Paper 2012-01-0839*, 2012.
Appears in p. 226 in Chapt. 5-[38]

Diesel R., *Arbeitsverfahren und Ausführungsart für Verbrennungskraftmaschinen*, Deutsches Reichspatent Nr. 67207, 1892.
Appears in p. 2 in Chapt. 1-[1]

Diesel R., *Die Entstehung des Dieselmotors*. Springer, 1913.
Appears in p. 2 in Chapt. 1-[2]

Diesel R., *Theorie und Konstruktion eines rationellen Wärmemotors zum Ersatz der Dampfmaschinen und der heute bekannten Verbrennungsmotoren*. Springer, 1893. Reprint: VDI-Verlag, 1986.
Appears in p. 2 in Chapt. 1-[3]

DieselNet Technology Guide, "www.dieselnet.com/tech".
Appears in p. 13 in Chapt. 1-[33]

DieselNet: Diesel Emissions Online, *Information available at http://www.dieselnet.com /standards*.
Appears in p. 5, 6, 8 in Chapt. 1-[7]

Directive 2003/30/EC of the European Parliament and of the Council of 8 May 2003. Official Journal L123, 42-46, 2003.
Appears in p. 13 in Chapt. 1-[34]

Directive 2009/28/EC of the European Parliament and of the Council of 23 April 2009. Official Journal L140, 16-62, 2009.
Appears in p. 13 in Chapt. 1-[35]

Drake M.C., Fansler T.D., Solomon A.S., Szekely G.A., "Piston fuel films as a source of smoke and hydrocarbon emissions from a wall-controlled spark-ignited direct-injection engine". *SAE Paper 2003-01-0547*, 2003.
Appears in p. 33 in Chapt. 2-[68]

DuMouchel W.H., O'Brien F.L., *Integrating a Robust Option into a Multiple Regression Computing Environment*. Computer Science and Statistics: Proceedings of the 21^{st} Symposium on the Interface, Alexandria, VA, 1989.
Appears in p. 131 in Chapt. 3-[29]

Edwards C.F., Siebers D., Hoskin D.H., "A Study of the Autoignition Process of diesel Spray via High Speed Visualization". *SAE Paper 920108*, 1992.
Appears in p. 44, 45 in Chapt. 2-[114]

Ejim C.E., Fleck B.A., Amarfazli A., "Analytical study for atomization of biodiesels and their blends in a typical injector: Surface tension and viscosity effects". *Fuel*, Vol. 86, pp. 1534- 1544, 2007.
Appears in p. 32 in Chapt. 2-[53]

EN ISO standards 4264:2007, *Petroleum products - Calculation of cetane index of middle-distillate fuels by the four-variable equation*, Geneva, Switzerland: International Organization for Standardization, 2007.
Appears in p. 49 in Chapt. 2-[127]

Espey C., Dec J.E., "The effect of TDC temperature and density on the liquid-phase fuel penetration in a DI Diesel engine". *SAE Paper 952456*, 1995.
Appears in p. 33, 34 in Chapt. 2-[75]

EU, 2006. "Biofuels in the European Union - A vision for 2030 and Beyond", European Union, *Final report of the Biofuels Research Advisory Council*, EUR 22066, 2006.

Appears in p. 15 in Chapt. 1-[40]

Faeth G.M., "Current Status of Droplet and Liquid Combustion". *Prog. Energy Combust. Sci.*, Vol. 3, pp. 191-224, 1977.

Appears in p. 54 in Chapt. 2-[137]

Fang T., Coverdill R.E., Lee C.F., White R.A., "Smokeless combustion within a small-bore HSDI diesel engine using a narrow angle injector". *SAE Paper 2007-01-0203*, 2007.

Appears in p. 33 in Chapt. 2-[70]

Fang T., Lee C.F., "Bio-Diesel Effects on Combustion Processes in an HSDI Diesel using Advanced Injection Strategies". *Proc. Combust. Inst.*, Vol. 32, pp. 2785-92, 2009.

Appears in p. 65, 143 in Chapt. 2-[171] & Chapt. 3-[54]

Fang T., Lin Y.-C., Foong T.M., Lee C.-F., "Biodiesel combustion in an optical HSDI diesel engine under low load premixed combustion conditions". *Fuel*, Vol. 88, pp. 2154-62, 2009.

Appears in p. 65, 143 in Chapt. 2-[164] & Chapt. 3-[47]

Faria M.D.C., Valle M.L.M., Pinto R.R.C., "The influence of physic-chemical properties of diesel/biodiesel mixtures on atomization quality in diesel direct injection engines". *SAE Paper 2005-01-4154*, 2005.

Appears in p. 37 in Chapt. 2-[94]

Fisher B.T., Knothe G., Mueller C.J., "Liquid-phase penetration under unsteady incylinder conditions: soy- and cuphea-derived biodiesel fuels versus conventional diesel". *Energy Fuels*, Vol. 24, pp. 5163-80, 2010.

Appears in p. 162, 170, 174 in Chapt. 4-[1]

Fisher B.T., Mueller C.J., "Liquid penetration length of heptamethylnonane and trimethylpentane under unsteady in-cylinder conditions". *Fuel*, Vol. 89, pp. 2673-96, 2010.

Appears in p. 33, 162, 173, 174 in Chapt. 2-[62] & Chapt. 4-[2]

Flynn P.F., Durret R.P., Hunter G.L., zur Loye A.O., Akinyemi O.C., Dec J.E., Westbrook C.K., "Diesel Combustion: An Integrated View Combining Laser Diagnostics, Chemical Kinetics and Empirical Validation". *SAE Paper 1999-01-0509*, 1999.

Appears in p. 42, 51, 54 in Chapt. 2-[106]

Flynn P.F., Mizusawa M., Uyehara O.A., Myers P.S., "An Experimental Determination of the Instantaneous Potential Radiant Heat Transfer Within an Operating Diesel Engine". *SAE Paper 720022*, 1972.

Appears in p. 63 in Chapt. 2-[159]

García A., *Estudio De Los Efectos De La Post-Inyección Sobre El Proceso De Combustión Y La Formación De Hollín En Motores Diesel*. Tesis Doctoral, Universidad Politécnica de Valencia, Departamento de Máquinas y Motores Térmicos, 2009.

Appears in p. 5, 6, 25, 27 in Chapt. 1-[6] & Chapt. 2-[5]

García-Oliver J.M., *Aportaciones Al Estudio Del Proceso De Combustión Turbulenta De Chorros En Motores Diesel De Inyección Directa*. Tesis Doctoral, Universidad Politécnica de Valencia, Departamento de Máquinas y Motores Térmicos, 2004.
Appears in p. 25, 28, 34, 145, 150, 165, 172, 240, 244 in Chapt. 2-[4], Chapt. 3-[56], Chapt. 4-[6] & Chapt. 5-[50]

Gaydon A.G., "The Spectroscopy of Flames". *Chapman and Hall Ltd.*, 1974.
Appears in p. 39 in Chapt. 2-[103]

Genzale C.L., Pickett L.M., Kook S., "Liquid penetration of diesel and biodiesel sprays at late-cycle post-injection conditions". *SAE Paper 2010-01-0610*, 2010.
Appears in p. 170, 181 in Chapt. 4-[18]

Gill S.S., Tsolakis A., Dearn K.D., Rodríguez-Fernández J., "Combustion characteristics and emissions of Fischer-Tropsch diesel fuels in IC engines". *Prog. Energy Combust Sci.*, Vol. 37, pp. 503-523, 2011.
Appears in p. 64, 67 in Chapt. 2-[161]

Gimeno J., *Desarrollo y Aplicación De La Medida Del Flujo De Cantidad De Movimiento De Un Chorro Diesel*. Tesis Doctoral, Universidad Politécnica de Valencia, Departamento de Máquinas y Motores Térmicos, 2008.
Appears in p. 28, 29, 103, 107 in Chapt. 2-[14] & Chapt. 3-[15]

Glassman I., Yetter R., *Combustion*, 4^{th} Ed., Academic Press, 2008.
Appears in p. 26 in Chapt. 2-[10]

Gray W.A., Muller R., *Engineering Calculations in Radiative Heat Transfer*, Permagon Press, 1974.
Appears in p. 146 in Chapt. 3-[63]

Grondin O., Stobart R., Chafouk H., Maquet J., "Modelling the Compression Ignition Engine for Control: Review and Future Trends". *SAE Paper 2004-01-0423*, 2004.
Appears in p. 6 in Chapt. 1-[13]

Hardy W.L., Reitz R.D., "A study of the effect of high EGR, high equivalence ratio, and mixing time on emissions levels in a heavy-duty diesel engine for PCCI combustion". *SAE Paper 2006-01-0026*, 2006.
Appears in p. 33 in Chapt. 2-[69]

Haynes B.S., Wagner H.G., "Soot formation". *Prog. Energy Combust Sci.*, Vol. 7, pp. 229-73, 1981.
Appears in p. 57 in Chapt. 2-[143]

Hermens S., *Influence Of Diesel Injector Nozzle Geometry On The Injection And Combustion Process*. Tesis Doctoral, Universidad Politécnica de Valencia, Departamento de Máquinas y Motores Térmicos, 2008.
Appears in p. 28, 103 in Chapt. 2-[16] & Chapt. 3-[14]

Heywood J.B., *Internal Combustion Engine Fundamentals*. McGraw-Hill Publishing, 1988.
Appears in p. 6, 25, 26, 46, 54, 63, 233 in Chapt. 1-[15], Chapt. 2-[6] & Chapt. 5-[45]

Higgins B., Siebers D., Aradi A., "Diesel-Spray Ignition and PremixedBurn Behaviour". *SAE Paper 2000-01-0940*, 2000.
Appears in p. 38, 39, 40, 42, 43, 45, 46 in Chapt. 2-[101]

Higgins B., Siebers D.L., "Measurement of the Flame Lift-Off Location on DI Diesel Sprays Using OH Chemiluminescence". *SAE Paper 2001-01-0918*, 2001.
Appears in p. 133 in Chapt. 3-[33]

Higgins B.S., Mueller C.J., Siebers D., "Measurements of fuel effects on liquid-phase penetration in DI sprays". *SAE Paper 1999-01-0519*, 1999.
Appears in p. 34, 35, 165, 166, 169, 174, 176 in Chapt. 2-[80] & Chapt. 4-[10]

Hiroyasu H., Arai M., "Structures of Fuel Sprays in Diesel Engines". *SAE Paper 900475*, 1990.
Appears in p. 32, 37, 38 in Chapt. 2-[47]

Hiroyasu H., Arai M., Tabata M., "Empirical equations for the Sauter mean diameter of diesel spray". *SAE Paper 890464*, 1989.
Appears in p. 32 in Chapt. 2-[46]

Hiroyasu H., Kadota T., "Fuel droplet size distribution in Diesel combustion chamber". *SAE Paper 740715*, 1974.
Appears in p. 32 in Chapt. 2-[45]

Hodges J.T., Baritaud T.A., Heinze T.A., "Planar liquid and gas fuel and droplet size visualization in a DI Diesel engine". *SAE Paper 910726*, 1991.
Appears in p. 33 in Chapt. 2-[73]

Holland P.W., Welsch R.E., "Robust Regression Using Iteratively Reweighted Least-Squares". *Commun. Statis.-Theor. Method.*, Vol. A6, pp. 813-27, 1977.
Appears in p. 131 in Chapt. 3-[30]

Hottel D.C., Broughton F.P., "Determination of true temperature and total radiation from luminous gas flames". *Ind. Eng. Chem.*, Vol. 4, pp. 166-75, 1932.
Appears in p. 146 in Chapt. 3-[59]

Huber P.J., *Robust Statistics*. John Wiley & Sons, 1981.
Appears in p. 131 in Chapt. 3-[31]

Hurn R.K., Hughes K.J., "Combustion Characteristics of Diesel Fuels as Measured in a Constant Volume Bomb". *SAE Paper 520210*, 1952.
Appears in p. 38 in Chapt. 2-[98]

Idicheria C., Pickett L., "Formaldehyde Visualization Near Lift-off Location in a Diesel Jet". *SAE Paper 2006-01-3434*, 2006.
Appears in p. 42, 56, 59, 61 in Chapt. 2-[107]

Idicheria C.A., Pickett L.M., "Ignition, soot formation, and end-of-combustion transients in diesel combustion under high-EGR conditions". *Int. J. Engine Res.*, Vol. 12, pp. 376-392, 2011.
Appears in p. 42 in Chapt. 2-[108]

Idicheria C.A., Pickett L.M., "Soot Formation in Diesel Combustion under High-EGR Conditions". *SAE Paper 2005-01-3834*, 2005.
Appears in p. 59, 60, 65, 218 in Chapt. 2-[153] & Chapt. 5-[24]

Ikegami M., Kamimoto T., "Conventional Diesel Combustion", in *Flow and Combustion in Reciprocating Engines*, Chapter 6, Springer-Verlag, 2009.
Appears in p. 130 in Chapt. 3-[28]

International Energy Agency, *Technology Roadmap. Biofuels for Transport*, OECD Publications, 2011.
Appears in p. 12, 13, 16 in Chapt. 1-[32]

International Energy Agency. *World Energy Outlook 2009*. OECD Publications, 2009.
Appears in p. 5, 9, 10, 11, 14, 15 in Chapt. 1-[5]

Iyer V.A., Post S.L., Abraham J., "Is the liquid penetration in diesel sprays mixing controlled?". *Proc. Combust. Inst.*, Vol. 28, pp. 1111-18, 2000.
Appears in p. 34 in Chapt. 2-[87]

Jääskeläinen H., *Biodiesel Standards & Properties*. DieselNet Technology Guide. "http://www.dieselnet.com/tech".
Appears in p. 92 in Chapt. 3-[2]

Jerrett, M., Finkelstein, M.M., Brook, J.R., Arain, M.A., Kanaroglou, P., Stieb, D.M., Gilbert, N.L., Verma, D., Finkelstein, N., Chapman, K.R., Sears, M.R., "A Cohort Study of Traffic-Related Air Pollution and Mortality in Toronto, Ontario, Canada". *Environmental Health Perspectives*, Vol. 117, pp. 772-777, 2009.
Appears in p. 6 in Chapt. 1-[9]

Juliá J.E., *Medida De Concentraciones De Combustible En Chorros Diesel Mediante Tecnicas De Fluorescencia Inducida Por Laser*. Tesis Doctoral, Universidad Politécnica de Valencia, Departamento de Máquinas y Motores Térmicos, 2003.
Appears in p. 33 in Chapt. 2-[78]

Kamimoto T., Murayama Y., "Re-examination of the emissivity of diesel flames". *Int. J. Engine Res.*, Vol. 12, pp. 580-600, 2011.
Appears in p. 146, 249 in Chapt. 3-[60] & Chapt. 5-[53]

Kamimoto T., Yokota H., Kobayashi H., "Effect of high pressure injection on soot formation processes in a rapid compression machine to simulate Diesel flames". *SAE Paper 871610*, 1987.
Appears in p. 33, 34 in Chapt. 2-[72]

Kashdan J.T., Mendez S., Bruneaux G., "On the origin of unburned hydrocarbon emissions in a wall-guided, low NOx diesel combustion system". *SAE Paper 2007-01-1836*, 2007.
Appears in p. 33 in Chapt. 2-[64]

Kegl B., Kegl M., Pehan S., "Optimization of an injection system for diesel and biodiesel usage". *Energy Fuels*, Vol. 22, pp. 1046-1054, 2008.
Appears in p. 30 in Chapt. 2-[27]

Kim H.J., Park S.H., Suh H.K., Lee C.S., "Atomization and Evaporation Characteristics of Biodiesel and Dimethyl Ether Compared to Diesel Fuel in a High-Pressure Injection System". *Energy Fuels*, Vol. 23, pp. 1734-1742, 2009.
Appears in p. 32 in Chapt. 2-[59]

Kim H.J., Suh H.K., Park S.H., Lee C.S., "An Experimental and Numerical Investigation of Atomization Characteristics of Biodiesel, Dimethyl Ether, and Biodiesel-Ethanol Blended Fuel". *Energy Fuels*, Vol. 22, pp. 2091-2098, 2008.
Appears in p. 32 in Chapt. 2-[57]

Kimura S., Aoki O., Kitahura Y., Aiyoshizawa E., "Ultra-Clean Combustion Technology Combining a Low-Temperature and Premixed Combustion Concept for Meeting Future Emissions Standards". *SAE Paper 2001-01-0200*, 2001.
Appears in p. 7 in Chapt. 1-[18]

Kinast J.A., *Production of Biodiesels from Multiple Feedstocks and Properties of Biodiesels and Biodiesel/Diesel Blends*, Prepared for U.S. Department of Energy, NREL Report, NREL/SR-510-31460, 2003.
Appears in p. 92 in Chapt. 3-[3]

Klein-Douwel R.J.H., Donkerbroek A.J., Van Vliet A.P., Boot M.D., Somers L.M.T., Baert R.S.G., Dam N.J., Ter Meulen J.J., "Soot and chemiluminescence in diesel combustion of bio-derived, oxygenated and reference fuels". *Proc. Combust. Inst.*, Vol. 32, pp. 2817-25, 2009.
Appears in p. 65, 143 in Chapt. 2-[170] & Chapt. 3-[53]

Kondo K., Yamaguchi T., Nishigai H., Takano S., Aizawa T., "High-Resolution Transmission Electron Microscopy of Soot Directly Sampled at Different Axial Locations in Diesel Spray Flame". *SAE Paper 2011-24-0068*, 2011.
Appears in p. 228 in Chapt. 5-[43]

Kook S., Pickett L.M., "Liquid length and vapor penetration of conventional, Fischer-Tropsch, coal-derived, and surrogate fuel sprays at high-temperature and high-pressure ambient conditions". *Fuel*, Vol. 93, pp. 539-48, 2012.
Appears in p. 17, 181, 182 in Chapt. 1-[41] & Chapt. 4-[24]

Kook S., Pickett L.M., "Soot volume fraction and morphology of conventional and surrogate jet fuel sprays at 1000-K and 6.7-MPa ambient conditions. *Proc. Comb. Inst.*, Vol. 33, pp. 2911-18, 2011.
Appears in p. 135, 218 in Chapt. 3-[40] & Chapt. 5-[25]

Kook S., Pickett L.M., "Soot Volume Fraction and Morphology of Conventional, Fischer-Tropsch, Coal-Derived, and Surrogate Fuel at Diesel Conditions". *SAE Paper 2012-01-0678*, 2012.
Appears in p. 135, 218 in Chapt. 3-[41] & Chapt. 5-[26]

Kosaka H., Aizawa T., Kamimoto T., "Two-dimensional imaging of ignition and soot formation processes in a diesel flame". *Int. J. Engine Res.*, Vol. 6, pp. 21-42, 2005.
Appears in p. 42, 56, 57, 221, 222 in Chapt. 2-[109] & Chapt. 5-[29]

Kosaka H., Drewes V.H., Catalfamo L., Aradi A.A., Iida N., Kamimoto T., "Two-Dimensional Imaging of Formaldehyde Formed During the Ignition Process of Diesel Fuel Spray". *SAE Paper 2000-01-0236*, 2000.
Appears in p. 38, 42, 46 in Chapt. 2-[102]

Kuo K.K., *Principles of Combustion*. Wiley & Sons, pp. 589-594, 1986.
Appears in p. 54 in Chapt. 2-[138]

Lapuerta M., Agudelo J.R., Prorok M., Boehman A.L., "Bulk Modulus of Compressibility of Diesel/Biodiesel/HVO Blends". *Energy Fuels*, Vol. 26, pp. 1336-43, 2012.
Appears in p. 30 in Chapt. 2-[31]

Lapuerta M., Armas O., Rodríguez-Fernández J., "Effect of biodiesel fuels on diesel engine emissions". *Prog. Energy Combust Sci.*, Vol. 34, pp. 198-223, 2008.
Appears in p. 64, 65, 66, 67, 230, 248 in Chapt. 2-[160] & Chapt. 5-[44]

Lapuerta M., Ballesteros R., Martos F.J., "A method to determine the fractal dimension of diesel soot agglomerates". *J. Colloid Interface Sci.*, Vol. 303 pp. 149-58, 2006.
Appears in p. 233 in Chapt. 5-[48]

Lapuerta M., Canoira L., Ráez J., "Improved Method for Determining the Atmospheric Distillation Curve of Biodiesel Fuels from Reduced Pressure". *Ind. Eng. Chem. Res.*, Vol. 50, pp. 7041-48, 2011.
Appears in p. 93 in Chapt. 3-[4]

Lapuerta M., Martos F.J., Martin-Gonzalez G., "Geometrical determination of the lacunarity of agglomerates with integer fractal dimension". *J. Colloid Interface Sci.*, Vol. 346, pp. 23-31, 2010.
Appears in p. 233, 234 in Chapt. 5-[49]

Lapuerta M., Oliva F., Agudelo J.R., Boehman A.L., "Effect of fuel on the soot nanostructure and consequences on loading and regeneration of diesel particulate filters". *Combust. Flame*, Vol. 159, pp. 844-53, 2012.
Appears in p. 225, 226 in Chapt. 5-[33]

Lapuerta M., Rodríguez-Fernández J., Armas O., "Correlation for the estimation of the density of fatty acid esters fuels and its implications. A proposed biodiesel cetane index". *Chem. Phys. Lipids*, Vol. 163, pp. 720-727, 2010.
Appears in p. 49 in Chapt. 2-[128]

Lapuerta M., Rodríguez-Fernández J., Font de Mora E., "Correlation for the estimation of the cetane number of biodiesel fuels and implications on the iodine number". *Energy Policy*, Vol. 37, pp. 4337-4344, 2009.
Appears in p. 49 in Chapt. 2-[129]

Lee C.S., Park S.W., Kwon S.I., "An Experimental Study on the Atomization and Combustion Characteristics of Biodiesel-Blended Fuels". *Energy Fuels*, Vol. 19, pp. 2201-2208, 2005.
Appears in p. 32, 37 in Chapt. 2-[54]

Lee K.O., Cole R., Sekar R., Choi M.Y., Kang J.S., Bae C.S., Shin H.D., "Morphological Investigation of the Microstructure, Dimensions, and Fractal Geometry of Diesel Particulates". *Proc. Combust. Inst.*, Vol. 29, pp. 647-53, 2002.
Appears in p. 233 in Chapt. 5-[47]

Leohold J., *Vision for future mobility - Volkswagen fuel and powertrain strategy*, SYNBIOS II Conference, Stockholm, Sweden, May 23-24, 2007.
Appears in p. 10 in Chapt. 1-[27]

Levy N., Amara S., Campoussin J.-C., Guerrassi N., "Non-Reactive Diesel Spray Computations Supported by PDA Measurements". *SAE Paper 970049*, 1997.
Appears in p. 32 in Chapt. 2-[49]

López J.J., *Estudio teórico-experimental del chorro libre Diesel no evaporativo y de su interacción con el movimiento del aire*. Tesis Doctoral, Universidad Politécnica de Valencia, Departamento de Máquinas y Motores Térmicos, 2003.
Appears in p. 28 in Chapt. 2-[22]

Lyn W.T., *Study of Burning Rate and Nature of Combustion in Diesel Engines*. 9^{th} Symposium (International) on Combustion, pp. 1069-1082, 1963.
Appears in p. 44, 54 in Chapt. 2-[113]

Maestrelli P., Canova C., Scapellato M.L., Visentin A., Tessari R., Bartolucci G.B., Simonato L., Lotti M., "Personal exposure to particulate matter is associated with worse health perception in adult asthma". *Journal of Investigational Allergology and Clinical Immunology*, Vol. 21, pp. 120-128, 2011.
Appears in p. 6 in Chapt. 1-[12]

Maly R., Schaefer V., Hass H., Cahill G., Rouveirolles P., Röj A., Wegener R., Montagne X., Di Pancrazio A., Kashdan J., "Optimum Diesel Fuel for Future Clean Diesel Engines". *SAE Paper 2007-01-0035*, 2007.
Appears in p. 8 in Chapt. 1-[23]

Martin G.C., Mueller C.J., Milam D.M., Radovanovic M.S., Gehrke C.R., "Early direct-injection, low-temperature combustion of diesel fuel in an optical engine utilizing a 15-hole, dual-row, narrow-included-angle nozzle". *SAE Paper 2008-01-2400*, 2008.
Appears in p. 33 in Chapt. 2-[66]

Martínez S., *Desarrollo de una instalación experimental para el estudio de chorros diesel evaporativos en atmósfera inerte y reactiva*. Tesis Doctoral, Universidad Politécnica de Valencia, Departamento de Máquinas y Motores Térmicos, 2003.
Appears in p. 33, 34 in Chapt. 2-[79]

Matsui Y., Kamimoto T., Matsuoka S., "A study on the time and space resolved measurement of flame temperature and soot concentration in a DI diesel engine by the two-color method". *SAE Paper 790491*, 1979.
Appears in p. 145 in Chapt. 3-[58]

Molina S.A., *Estudio De La Influencia De Los Parametros De Inyeccion Y La Recirculacion De Gases De Escape Sobre El Proceso De Combustion, Las Prestaciones Y Las Emisiones De Un Motor Diesel De 1.8 Litros De Cilindrada*. Tesis Doctoral, Universidad Politécnica de Valencia, Departamento de Máquinas y Motores Térmicos, 2003.
Appears in p. 7, 25, 46, 200 in Chapt. 1-[16], Chapt. 2-[8] & Chapt. 5-[6]

Mollenhauer K., Tschöke H., *Handbook of Diesel Engines*. Springer-Verlag, 2010.
Appears in p. 2, 3, 4, 5, 8 in Chapt. 1-[4]

Monin C., *Caracterizacion Del Proceso De Formación De Hollin En Una Llama De Difusión Diesel De Baja Temperatura*. Tesis Doctoral, Universidad Politécnica de Valencia, Departamento de Máquinas y Motores Térmicos, 2009.
Appears in p. 253 in Chapt. 5-[54]

Mueller C.J., Boehman A.L., Martin G.C., "An experimental investigation of the origin of increased NOx emissions when fueling a heavy-duty compression-ignition engine with soy biodiesel". *SAE Paper 2009-01-1792*, 2009.
Appears in p. 65, 66, 143, 244 in Chapt. 2-[165], Chapt. 3-[48] & Chapt. 5-[51]

Mueller C.J., Martin G.C., "Effects of oxygenated compounds on combustion and soot evolution in a DI diesel engine: Broadband natural luminosity imaging". *SAE Paper 2002-01-1631*, 2002.
Appears in p. 65, 145 in Chapt. 2-[172] & Chapt. 3-[55]

Mueller C.J., Martin G.C., Briggs T.E., Duffy K.P., "An experimental investigation of in-cylinder processes under dual-injection conditions in a DI diesel engine". *SAE Paper 2004-01-1843*, 2004.
Appears in p. 33 in Chapt. 2-[63]

Mueller C.J., Pitz W.J., Pickett L.M., Martin G.C., Siebers D.L., Westbrook C.K., "Effects of Oxygenates on Soot Processes in DI Diesel Engines: Experiments and Numerical Simulations". *SAE Paper 2003-01-1791*, 2003.
Appears in p. 217, 239 in Chapt. 5-[22]

Murray J., King D., "Climate policy: Oil's tipping point has passed". *Nature*, Vol. 481, pp. 433-435, 2012.
Appears in p. 10 in Chapt. 1-[29]

Musculus M.P.B., "Measurements of the Influence of Soot Radiation on In-Cylinder Temperatures and Exhaust NOx in a Heavy-Duty DI Diesel Engine". *SAE Paper 2005-01-0925*, 2005.
Appears in p. 63, 66, 249 in Chapt. 2-[157] & Chapt. 5-[52]

Musculus M.P.B., Dec J.E., Tree D.R., "Effects of fuel parameters and diffusion flame lift-off on soot formation in a heavy duty DI Diesel engine". *SAE Paper 2002-01-0889*, 2002.
Appears in p. 59, 65, 217 in Chapt. 2-[149] & Chapt. 5-[16]

Musculus M.P.B., "Entrainment waves in decelerating transient turbulent jets". *J. Fluid Mech.*, Vol. 638, pp. 117-40, 2009.
Appears in p. 34, 165, 174, 181 in Chapt. 2-[86] & Chapt. 4-[9]

Musculus M.P.B., "Measurements of the Influence of Soot Radiation on In-Cylinder Temperatures and Exhaust NO_2 in a Heavy-Duty Diesel Engine". *SAE Paper 2005-01-0925*, 2005.
Appears in p. 146, 150 in Chapt. 3-[61]

Musculus M.P.B., Kattke K., "Entrainment Waves in Diesel Jets". *SAE Paper 2009-01-1355*, 2009.
Appears in p. 27, 34, 165, 174, 181 in Chapt. 2-[12] & Chapt. 4-[8]

Musculus M.P.B., Lachaux T., Pickett L.M., Idicheria C., "End-of-Injection Over-Mixing and Unburned Hydrocarbon Emissions in Low-Temperature-Combustion Diesel Engines". *SAE Paper 2007-01-0907*, 2007.
Appears in p. 27 in Chapt. 2-[13]

Musculus M.P.B., Pickett L.M., "Diagnostic considerations for optical laser-extinction measurements of soot in high-pressure transient combustion environments". *Combust. Flame*, Vol. 141, pp. 371-91, 2005.
Appears in p. 134, 138, 139, 140, 141, 142 in Chapt. 3-[35]

Naber J.D., Siebers D.L., "Effects of Gas Density and Vaporization on Penetration and Dispersion of Diesel Sprays". *SAE Paper 960034*, 1996.
Appears in p. 37, 38, 179 in Chapt. 2-[91] & Chapt. 4-[22]

Nerva J.-G., Genzale C.L., Kook S., Garcia-Olivier J.M., Pickett L.M., "Fundamental Spray and Combustion Measurements of Soy Methyl-Ester Biodiesel". *Int. J. Engine Res.*, published online 30 August 2012, pp. 1-18, 2012.
Appears in p. 135, 170, 178, 208, 209, 218, 223 in Chapt. 3-[42], Chapt. 4-[19] & Chapt. 5-[11]

Nerva J.-G., Yamaguchi T., Iguma H., Nishigai H., Kondo K., Takano S., Aizawa T., Genzale C., Pickett L.M., "Transmission Electron Microscopy of Soot Particles sampled directly from a Biodiesel Spray Flame". *SAE Paper 2011-01-2046*, 2011.
Appears in p. 135, 223, 224 in Chapt. 3-[43] & Chapt. 5-[31]

No S.-Y., "How vegetable oils and their derivatives affect spray characteristics in CI engines - A review". *Atomization Sprays*, Vol. 21, pp. 87-105, 2011.
Appears in p. 37 in Chapt. 2-[93]

Novella R., *Estudio De La Influencia De Los Ciclos Atkinson Y Miller Sobre El Proceso De Combustion Y Las Emisiones Contaminantes En Un Motor Diesel*. Tesis Doctoral, Universidad Politécnica de Valencia, Departamento de Máquinas y Motores Térmicos, 2009.
Appears in p. 24, 25, 27, 54, 59 in Chapt. 2-[2]

Novella R., García A., Pastor J.M., Domenech V., "The role of detailed chemical kinetics on CFD diesel spray ignition and combustion modelling". *Math. Comput. Model.*, Vol. 54, pp. 1706-1719, 2011.
Appears in p. 45 in Chapt. 2-[116]

Opat R., Ra Y., Gonzalez M.A., Krieger R., Reitz R.D., Foster D.E., Durrett R.P., Siewert R.M., "Investigation of mixing and temperature effects on HC/CO emissions for highly dilute low temperature combustion in a light-duty diesel engine". *SAE Paper 2007-01-0193*, 2007.

Appears in p. 33 in Chapt. 2-[65]

Orfanidis S.J., *Introduction to Signal Processing*, Prentice-Hall, 1996.

Appears in p. 130 in Chapt. 3-[27]

Owen K., Coley T., *Automotive Fuels Reference Book*. SAE International, 1995.

Appears in p. 8 in Chapt. 1-[22]

Park S.H., Kim H.J., Suh H.K., Lee C.S., "A study on the fuel injection and atomization characteristics of soybean oil methyl ester (SME)". *Int. J. Heat Fluid*, Vol. 30, pp. 108-116, 2009.

Appears in p. 30, 32 in Chapt. 2-[33]

Park S.H., Suh H.K., Lee C.S., "Effect of Bioethanol-Biodiesel Blending Ratio on Fuel Spray Behavior and Atomization Characteristics". *Energy Fuels*, Vol. 23, pp. 4092-4098, 2009.

Appears in p. 32, 37 in Chapt. 2-[58]

Park S.H., Suh H.K., Lee C.S., "Effect of cavitating flow on the flow and fuel atomization characteristics of biodiesel and diesel fuels". *Energy Fuels*, Vol. 22, pp. 605-613, 2008.

Appears in p. 30, 32 in Chapt. 2-[39]

Park S.H., Suh H.K., Lee C.S., "Nozzle flow and atomization characteristics of ethanol blended biodiesel fuel". *Renewable Energy*, Vol. 35, pp. 144-150, 2010.

Appears in p. 32 in Chapt. 2-[60]

Park S.W., Kim S., Lee C.S., "Effect of Mixing Ratio of Biodiesel on Breakup Mechanisms of Monodispersed Droplets". *Energy Fuels*, Vol. 20, pp. 1709-1715, 2006.

Appears in p. 32 in Chapt. 2-[56]

Pastor J.V., Arrègle J., García J.M., Zapata L.D., "Segmentation of diesel spray images with loglikelihood ratio test algorithm for non-Gaussian distributions". *Appl. Opt.*, Vol. 46, pp. 888-99, 2007.

Appears in p. 127 in Chapt. 3-[26]

Pastor J.V., Arrègle J., Palomares A., "Diesel spray image segmentation with a likelihood ratio test". *Appl. Opt.*, Vol. 40, pp. 1-10, 2001.

Appears in p. 127 in Chapt. 3-[25]

Pastor J.V., López J.J., García J.M., Pastor J.M., "A 1D model for the description of mixing-controlled inert diesel sprays". *Fuel*, Vol. 87, pp. 2871-85, 2008.

Appears in p. 34, 37, 165, 174, 221, 238 in Chapt. 2-[85], Chapt. 4-[7] & Chapt. 5-[27]

Pastor J.V., Pastor J.M., Gimeno J., Nerva J.-G., "The effect of biodiesel fuel blend rate on the liquid-phase fuel penetration in diesel engine conditions". *SAE Paper 2009-24-0051*, 2009.

Appears in p. 117, 126, 169, 170 in Chapt. 3-[23] & in Chapt. 4-[16]

Pastor J.V., Payri R., García-Oliver J.M., Nerva J.-G., "Schlieren Measurements of the ECN-Spray A Penetration under Inert and Reacting Conditions". *SAE Paper 2012-01-0456*, 2012.

Appears in p. 201, 214, 216, 275 in Chapt. 5-[8] & Chapt. 6-[1]

Pastor J.V., Payri R., Gimeno J., Nerva J.-G., "Experimental Study on RME Blends: Liquid-Phase Fuel Penetration, Chemiluminescence, and Soot Luminosity in Diesel-Like Conditions". *Energy Fuels*, Vol. 23, pp. 5899-915, 2009.

Appears in p. 48, 117, 170 in Chapt. 2-[119], Chapt. 3-[24] & Chapt. 4-[20]

Payri F., Arrègle J., Fenollosa C., Belot G., Delage A., Schaberg P., Myburgh I., Botha J., "Characterisation Of The Injection-Combustion Process In A Common Rail D.I. Diesel Engine Running With Sasol Fischer-Tropsch Fuel". *SAE Paper 2000-01-1803*, 2000.

Appears in p. 32 in Chapt. 2-[61]

Payri F., Bermúdez V., Payri R., Salvador F.J., "The influence of cavitation on the internal flow and the spray characteristics in diesel injection nozzles". *Fuel*, Vol. 83, pp. 419-431, 2004.

Appears in p. 28 in Chapt. 2-[18]

Payri F., Desantes J.M., Arrègle J., "Characterization of D.I. Diesel Sprays in High Density Conditions". *SAE Paper 960774*, 1996.

Appears in p. 38 in Chapt. 2-[97]

Payri F., Desantes J.M., *Motores de combustión interna alternativos*, 1^{era} Ed., Editorial Reverté, 2011.

Appears in p. 6, 25, 63 in Chapt. 1-[14] & Chapt. 2-[7]

Payri F., Margot X., Gil A., Martin J., *Prediction of heat transfer to the walls in Direct Injection (DI) Diesel engines.* Proceedings of the 2^{nd} EACC - 2005, Frankfurt, June 29-30, 2005.

Appears in p. 254 in Chapt. 5-[55]

Payri F., Molina S., Martín J., Armas O., "Influence of measurement errors and estimated parameters on combustion diagnosis". *Appl. Therm. Eng.*, Vol. 26, pp. 226-36, 2006.

Appears in p. 115, 254 in Chapt. 3-[22] & Chapt. 5-[56]

Payri F., Pastor J.V., García-Oliver J.M., Pastor J.M., "Contribution to the application of two-colour imaging to diesel combustion". *Meas. Sci. Technol.*, Vol. 18, pp. 2579-98, 2007.

Appears in p. 145, 146, 150 in Chapt. 3-[57]

Payri R., García A., Domenech V., Durrett R., Plazas A.H., "An experimental study of gasoline effects on injection rate, momentum flux and spray characteristics using a common rail diesel injection system". *Fuel*, Vol. 97, pp. 390-9, 2012.

Appears in p. 181 in Chapt. 4-[23]

Payri R., García J.M., Salvador F.J., Gimeno J., "Using spray momentum flux measurements to understand the influence of diesel nozzle geometry on spray characteristics". *Fuel*, Vol. 84 pp. 551-61, 2005.

Appears in p. 28, 106, 108, 109 in Chapt. 2-[15] & Chapt. 3-[19]

Payri R., Salvador F.J., Gimeno J., Bracho G., "A new methodology for correcting the signal cumulative phenomenon on injection rate measurements". *Experimental Techniques*, Vol. 32, pp. 46-49, 2008.

Appears in p. 103 in Chapt. 3-[13]

Payri R., Salvador F.J., Gimeno J., Bracho G., "The effect of temperature and pressure on thermodynamic properties of diesel and biodiesel fuels". *Fuel*, Vol. 90, pp. 1172-80, 2011.

Appears in p. 104 in Chapt. 3-[17]

Perlack R.D., Wright L.L., Turhollow A., Graham R.L., Stokes B., Erbach D.C., *Biomass as feedstock for a bioenergy and bioproducts industry: the technical feasibility of a billion-ton annual supply.* U.S. Department of Energy and U. S. Department of Agriculture, 2005.

Appears in p. 15 in Chapt. 1-[39]

Peters N., *Turbulent Combustion*, Cambridge University Press, 2000.

Appears in p. 193, 210, 211 in Chapt. 5-[1]

Pickett L.M., Caton J.A., Musculus M.P.B., Lutz A.E., "Evaluation of the equivalence ratio-temperature region of diesel soot precursor formation using a two-stage Lagrangian model". *Int. J. Engine Res.*, Vol. 7, pp. 349-370, 2006.

Appears in p. 58, 59 in Chapt. 2-[145]

Pickett L.M., Idicheria C.A., *Effects of ambient temperature and density on soot formation under high-EGR conditions.* Thermofluidynamic processes in Diesel engines, Valencia, Sept. 13-15, 2006.

Appears in p. 59, 60, 65 in Chapt. 2-[154]

Pickett L.M., Kook S., Persson H., Andersson O., "Diesel fuel jet lift-off stabilization in the presence of laser-induced plasma ignition". *Proc. Combust. Inst.*, Vol. 32, pp. 2793-800, 2009.

Appears in p. 193, 212, 215 in Chapt. 5-[4]

Pickett L.M., Kook S., Williams T., "Visualization of Diesel Spray Penetration, Cool-Flame, Ignition, High-Temperature Combustion, and Soot Formation Using High-Speed Imaging". *SAE Paper 2009-01-0658*, 2009.

Appears in p. 43 in Chapt. 2-[112]

Pickett L.M., Siebers D.L., "An investigation of diesel soot formation processes using micro-orifices". *Proc. Combust. Inst.*, Vol. 29, pp. 655-62, 2002.
Appears in p. 59, 65, 217, 218, 239 in Chapt. 2-[150] & Chapt. 5-[19]

Pickett L.M., Siebers D.L., "Fuel Effects on Soot Processes of Fuel Jets at DI Diesel Conditions". *SAE Paper 2003-01-3080*, 2003.
Appears in p. 141, 193, 211, 217, 218, 237 in Chapt. 3-[46] & Chapt. 5-[2]

Pickett L.M., Siebers D.L., "Non-Sooting, Low Flame Temperature Mixing-Controlled DI Diesel Combustion". *SAE Paper 2004-01-1399*, 2004.
Appears in p. 7, 59, 65, 217 in Chapt. 1-[19], Chapt. 2-[151] & Chapt. 5-[17]

Pickett L.M., Siebers D.L., "Soot formation in diesel fuel jets near the lift-off length". *Int. J. Engine Res.*, Vol. 7, pp. 103-130, 2006.
Appears in p. 56, 59, 61, 141, 217, 218 in Chapt. 2-[142], Chapt. 3-[45] & Chapt. 5-[15]

Pickett L.M., Siebers D.L., "Soot in Diesel Fuel Jets: Effects of Ambient Temperature, Ambient Density, and Injection Pressure". *Combust. Flame*, Vol. 138, pp. 114-35, 2004.
Appears in p. 59, 65, 217, 218 in Chapt. 2-[152] & Chapt. 5-[21]

Pickett L.M., Siebers D.L., Idicheria C., "Relationship Between Ignition Processes and the Lift-Off Length of Diesel Fuel Jets". *SAE Paper 2005-01-3843*, 2005.
Appears in p. 193, 203, 211 in Chapt. 5-[3]

Pitz W.J., Mueller C.J., "Recent progress in the development of diesel surrogate fuels". *Prog. Energ. Combust.*, Vol. 37, pp 330-350, 2011.
Appears in p. 35, 62, 167 in Chapt. 2-[88] & Chapt. 4-[12]

Plee S.l., Ahmad T., "Relative Roles of Premixed and Diffusion Burning in Diesel Combustion". *SAE Paper 831733*, 1983.
Appears in p. 26 in Chapt. 2-[9]

Poinsot T., Veynante D., *Theoretical and Numerical Combustion*, 3^{rd} Ed., R.T. Edwards, 2012.
Appears in p. 41 in Chapt. 2-[105]

Reitz R.D, Bracco F.V., "On the Dependence of the Spray Angle and Other Spray Parameters on Nozzle Design and Operating Conditions". *SAE Paper 790494*, 1979.
Appears in p. 38 in Chapt. 2-[95]

Reitz R.D., Bracco F.V., "Mechanism of atomization of a liquid jet". *Phys. Fluids*, Vol.25, pp. 1730-42, 1982.
Appears in p. 31 in Chapt. 2-[41]

Reitz R.D., Bracco F.V., "Mechanisms of Breakup of Round Liquid Jets". *The Encyclopedia of Fluid Mechanics*, Vol. 3, Chapter 10, pp. 233-249, 1986.
Appears in p. 31 in Chapt. 2-[42]

Rodríguez Fernández J., *Estudio bibliográfico y experimental de las emisiones y prestaciones de un motor trabajando con biodiesel*. Tesis Doctoral, Universidad de Castilla-La Mancha, Departamento de Mecánica Aplicada e Ingeniería de Proyectos, 2007.
Appears in p. 97 in Chapt. 3-[7]

Rodríguez R.P., Sierens R., Verhelst S., "Ignition delay in a palm oil and rapeseed oil biodiesel fuelled engine and predictive correlations for the ignition delay period". *Fuel*, Vol. 90, pp. 766-72, 2011.
Appears in p. 203 in Chapt. 5-[9]

Ruiz S., *Estudio Teórico-Experimental De Los Procesos De Atomización Y De Mezcla En Los Chorros Diesel D.I.*. Tesis Doctoral, Universidad Politécnica de Valencia, Departamento de Máquinas y Motores Térmicos, 2003.
Appears in p. 28 in Chapt. 2-[21]

Ryan III T.W., "Correlation of Physical and Chemical lgnition Delay to Cetane Number". *SAE Paper 852103*, 1985.
Appears in p. 49 in Chapt. 2-[123]

Sadeghbeigi R., *Fluid Catalytic Cracking Handbook: An Expert Guide to the Practical Operation, Design, and Optimization of FCC Units*, 3rd Ed., Gulf Publishing Company, 2012.
Appears in p. 93 in Chapt. 3-[5]

Salvador F.J., *Estudio Teorico Experimental De La Influencia De La Geometria De Toberas De Inyección Diesel Sobre Las Carateristicas Del Flujo Interno Y Del Chorro*. Tesis Doctoral, Universidad Politécnica de Valencia, Departamento de Máquinas y Motores Térmicos, 2003.
Appears in p. 28 in Chapt. 2-[17]

Sawyer R.F., "Science based policy for addressing energy and environmental problems". *Proceeding of the Combustion Institute*, Vol. 32, pp. 45-56, 2009.
Appears in p. 11 in Chapt. 1-[31]

Schefer R.W., Namazian M., Kelley J., *CH, OH and CH4 Concentration Measurements in a Lifted Turbulent-Jet Diffusion Flame*. 23^{rd} Symposium (International) on Combustion, The Combustion Institute, pp. 669-676, 1990.
Appears in p. 52 in Chapt. 2-[132]

Settles G.S., *Schlieren & Shadowgraph Techniques*, 1^{st} Ed., Springer Verlag, 2001.
Appears in p. 201, 214 in Chapt. 5-[7]

Siebers D., "Ignition Delay Characteristics of Alternative Diesel Fuels: Implications on Cetane Number". *SAE Paper 852102*, 1985.
Appears in p. 49 in Chapt. 2-[122]

Siebers D., "Liquid-phase fuel penetration in Diesel sprays". *SAE Paper 980809*, 1998.
Appears in p. 33, 34, 169, 176, in Chapt. 2-[76] & Chapt. 4-[15]

Siebers D., "Scaling Liquid-Phase Fuel Penetration in Diesel Sprays Based on Mixing-Limited Vaporization". *SAE Paper 1999-01-0528*, 1999.
Appears in p. 33, 34, 94, 164, 171, 174, 184 in Chapt. 2-[77], Chapt. 3-[6] & Chapt. 4-[5]

Siebers D.L., Higgins B.S., "Flame Lift-Off on Direct-Injection Diesel Sprays Under Quiescent Conditions". *SAE Paper 2001-01-0530*, 2001.
Appears in p. 24, 59, 65, 210 in Chapt. 2-[3] & Chapt. 5-[13]

Siebers D.L., Higgins B.S., Pickett L.M., "Flame Lift-Off on Direct-Injection Diesel Fuel Jets: Oxygen Concentration Effects". *SAE Paper 2002-01-0890*, 2002.
Appears in p. 59, 60, 65, 217 in Chapt. 2-[147] & Chapt. 5-[14]

Siebers D.L., Pickett L.M., "Injection Pressure and Orifice Diameter effects on soot in DI diesel fuel jets". *Thermo and fluid-dynamic processes in Diesel engines 2*, Springer-Velag, pp. 253-77, 2004.
Appears in p. 59, 65, 217 in Chapt. 2-[148] & Chapt. 5-[20]

Sietzman J.M., Üngüt A., Paul P.H., Hanson R.K., *Imaging and Characterization of OH Structures in a Turbulent Nonpremixed Flame*. 23^{rd} Symposium (International) on Combustion, The Combustion Institute, pp. 637-644, 1990.
Appears in p. 52 in Chapt. 2-[131]

Singh S., Reitz R.D., Musculus M.P.B., "2-Color Thermometry Experiments and High-Speed Imaging of Multi-Mode Diesel Engine Combustion". *SAE Paper 2005-01-3842*, 2005.
Appears in p. 146 in Chapt. 3-[62]

Smallwood G.J., Gülder Ö.L., "Views on the Structure of Transient Diesel Sprays". *Atomization and Sprays*, Vol. 10, pp. 355-386, 2000.
Appears in p. 31 in Chapt. 2-[44]

Smyth K.C., Shaddix C.R., "Elusive History of m=1.57-0.56i for the Refractive Index of Soot. Brief Communication". *Combust. Flame*, Vol. 107, pp. 314-20, 1996.
Appears in p. 135 in Chapt. 3-[39]

Soare V.T., *Phase Doppler Measurements In Diesel Dense Sprays: Optimization Of Measurements And Study Of The Orifice Geometry Influence Over The Spray At Microscopic Level*. Tesis Doctoral, Universidad Politécnica de Valencia, Departamento de Máquinas y Motores Térmicos, 2007.
Appears in p. 32 in Chapt. 2-[50]

Soid S.N., Zainal Z.A., "Spray and combustion characterization for internal combustion engines using optical measuring techniques - A review". *Energy*, Vol. 36, pp. 724-741, 2011.
Appears in p. 30 in Chapt. 2-[37]

Solbrig C.E., Litzinger T.A., "The Effect of Intake Charge Temperature on Combustion and Emissions in an Optically Accessible DI Diesel Engine with and without Swirl". *SAE Paper 902060*, 1990.
Appears in p. 45 in Chapt. 2-[115]

Song J., Alam M., Boehman A.L., "Impact of alternative fuels on soot properties and DPF regeneration". *Combust. Sci. Technol.*, Vol. 179, pp. 1991-2037, 2007.
Appears in p. 226 in Chapt. 5-[37]

Song J., Alam M., Boehman A.L., Kim U., "Examination of the oxidation behavior of biodiesel soot". *Combust. Flame*, Vol. 146, pp. 589-604, 2006.
Appears in p. 226 in Chapt. 5-[36]

Sou A., Hosokawa S., Tomiyama A., "Effects of cavitation in a nozzle on liquid jet atomization". *International Journal of Heat and Mass Transfer*, Vol. 50, pp. 3575-3582, 2007.
Appears in p. 29 in Chapt. 2-[23]

Stieb D.M., Judek S., Burnett R.T., "Meta-Analysis of Time-Series Studies of Air Pollution and Mortality: Effects of Gases and Particles and the Influence of Cause of Death, Age, and Season". *Journal of the Air & Waste Management Association*, Vol. 52, pp. 470-484, 2002.
Appears in p. 6 in Chapt. 1-[8]

Stieb D.M., Szyszkowicz M., Rowe B.H., Leech J.A., "Air pollution and emergency department visits for cardiac and respiratory conditions: a multi-city time-series analysis". *Environmental Health*, pp. 8:25, 2009.
Appears in p. 6 in Chapt. 1-[11]

Street J.O., Carroll R.J., Ruppert D., "A Note on Computing Robust Regression Estimates *via* Iteratively Reweighted Least Squares". *The American Statistician*, Vol. 42, pp. 152-154, 1988.
Appears in p. 131 in Chapt. 3-[32]

Struwe F.J., Foster D.E., "In Cylinder Measurement of Particulate Radiant Heat Transfer in a Direct Injection Diesel Engine". *SAE Paper 2003-01-0072*, 2003.
Appears in p. 63 in Chapt. 2-[158]

Suh H.K., Park S.H., Lee C.S., "Atomization Characteristics of Dimethyl Ether Fuel as an Alternative Fuel Injected through a Common-Rail Injection System". *Energy Fuels*, Vol. 20, pp. 1471-1481, 2006.
Appears in p. 32 in Chapt. 2-[55]

Suh H.K., Park S.H., Lee C.S., "Experimental investigation of nozzle cavitating flow characteristics for diesel and biodiesel fuels". *Int. J. Automot. Techn.*, Vol. 9, pp. 217-224, 2008.
Appears in p. 30, 32 in Chapt. 2-[40]

Suh H.K., Roh G.H., Lee C.S., "Spray and combustion characteristics of biodiesel/diesel blended fuel in a direct injection common-rail diesel engine". *Trans. ASME J. Eng. Gas. Turbines Power*, Vol. 130, pp. 2807-15, 2008.
Appears in p. 30, 32 in Chapt. 2-[38]

Suppes G.J., Rui Y., Rome A.C., Chen Z., "Cetane-Improver Analysis and Impact of Activation Energy on the Relative Performance of 2-Ethylhexyl Nitrate and Tetraethylene Glycol Dinitrate". *Ind. Eng. Chem. Res.*, Vol. 36, pp. 4397-4404, 1997.
Appears in p. 48 in Chapt. 2-[118]

Svensson K.I., Richards M.J., Mackrory A.J., Tree, D.R., "Fuel Composition and Molecular Structure Effects on Soot Formation in Direct-Injection Flames Under Diesel Engine Conditions". *SAE Paper 2005-01-0381*, 2005.
Appears in p. 59, 217 in Chapt. 2-[156] & Chapt. 5-[23]

Szybist J.P., Boehman A.L., "Behavior of a diesel injection system with biodiesel fuel". *SAE Paper 2003-01-1039*, 2003.
Appears in p. 30 in Chapt. 2-[28]

Szybist J.P., Boehman A.L., Haworth D.C., Koga H., "Premixed ignition behavior of alternative diesel fuel-relevant compounds in a motored engine experiment". *Combust. Flame*, Vol. 149, 112-128, 2007.
Appears in p. 42, 48 in Chapt. 2-[110]

Szybist J.P., Song J., Alam M., Boehman A.L., "Biodiesel combustion, emissions and emission control". *Fuel. Process. Technol.*, Vol. 88, pp. 679-691, 2007.
Appears in p. 66 in Chapt. 2-[174]

Takeda Y., Keiichi N., Keiichi N., "Emission characteristics of premixed lean diesel combustion with extremely early staged fuel injection". *SAE Paper 961163*, 1996.
Appears in p. 33 in Chapt. 2-[67]

Taylor D.C., Katavic V., Zou J., MacKenzie S.L., Keller W.A., An J., Friesen W., Barton D.L., Gossen K.K., Giblin E.M., Ge Y., Dauk M., Luciw T., Males D., "Field-testing of transgenic rapeseed cv. Hero transformed with a yeast sn-2 acyltransferase results in increased oil content, erucic acid content and seed yield". *Molecular Breeding*, Vol. 8, pp. 317-322, 2002.
Appears in p. 15 in Chapt. 1-[37]

Taylor J., McCormick R., Clark W., *Report on the relationship between molecular structure and compression ignition fuels, both conventional and HCCI.* Prepared for U.S. Department of Energy, *available online*, 2004.
Appears in p. 48 in Chapt. 2-[117]

Thomas A., "Fats and Fatty Oils", in *Ullmann's Encyclopedia of Industrial Chemistry*, John Wiley & Sons, 2007.
Appears in p. 97 in Chapt. 3-[8]

Thring M.W., Newby M.P., *Combustion length of enclosed turbulent jet flames.* 4^{th} Symposium International on Combustion, pp. 789-796, 1952.
Appears in p. 34 in Chapt. 2-[83]

Tree D.R., Svensson K.I., "Soot processes in compression ignition engines". *Prog. Energy Combust. Sci.*, Vol. 33, pp. 272-309, 2007.
Appears in p. 54, 56, 58, 59, 228 in Chapt. 2-[135] & Chapt. 5-[41]

Turns S.R., *An introduction to combustion*, 2^{nd} Ed., McGraw-Hill Publishing, 2000.
Appears in p. 6, 26 in Chapt. 1-[10] & Chapt. 2-[11]

Vander Wal R.L, Mueller C.J., "Initial investigation of effects of fuel oxygenation on nanostructure of soot from a direct-injection Diesel engine". *Energy Fuels*, Vol. 20, pp. 2364-69, 2006.
Appears in p. 226 in Chapt. 5-[39]

Vander Wal R.L., Tomasek A.J., "Soot nanostructure: dependence upon synthesis conditions". *Combust. Flame*, Vol. 136, pp. 129-40, 2004.
Appears in p. 226 in Chapt. 5-[34]

Varde K., Popa D., "Diesel Fuel Spray Penetration at High Injection Pressures". *SAE Paper 830448*, 1983.
Appears in p. 38 in Chapt. 2-[96]

Venugopal R., Abraham J., "A Review of Fundamental Studies Relevant to Flame Lift-off in Diesel Jets". *SAE Paper 2007-01-0134*, 2007.
Appears in p. 54, 59, 210 in Chapt. 2-[140] & Chapt. 5-[12]

Verhoeven D., Vanhemelryck J.L., Baritaud T., "Macroscopic and ignition characteristics of high-pressures sprays of single-component fuels". *SAE Paper 981069*, 1998.
Appears in p. 34 in Chapt. 2-[81]

Vigeolas H., Waldeck P., Zank T., Geigenberger P., "Increasing seed oil content in oil-seed rape (Brassica napus L.) by over expression of a yeast glycerol-3-phosphate dehydrogenase under the control of a seed-specific promoter". *Plant Biotechnology Journal*, Vol. 5, pp. 431-441, 2007.
Appears in p. 15 in Chapt. 1-[38]

Wakuri Y., Fujii M., Amitani T., Tsuneya R., "Studies on the penetration of fuel spray in a diesel engine". *Bulletin of Japan Society of Mechanical Engineers*, Vol. 3, pp. 123-130, 1960.
Appears in p. 37 in Chapt. 2-[89]

Wang X., Huang Z., Kuti O.A., Zhang W., Nishida K., "Experimental and analytical study of biodiesel and diesel spray characteristics under ultra-high injection pressure". *Int. J. Heat Fluid Fl.*, Vol. 31, pp.656-666, 2010.
Appears in p. 32 in Chapt. 2-[51]

Williams T.C., Shaddix C.R., Jensen K.A., Suo-Anttila J.M., "Measurement of the Dimensionless Extinction Coefficient of Soot within Laminar Diffusion Flames". *Int. J. Heat Mass Trans.*, Vol. 50, pp. 1616-30, 2007.
Appears in p. 134, 135 in Chapt. 3-[36]

Xi J., Zhong B.-J., "Soot in Diesel Combustion Systems". *Chem. Eng. Technol.*, Vol. 29, pp. 665-73, 2006.
Appears in p. 228 in Chapt. 5-[40]

Yamaguchi T., Kondo K., Nishigai H., Takano S., Aizawa T., "Direct Sampling, TEM Analysis and Optical Measurement of Soot Particles at Different Axial Locations in a Transient Spray Flame". *SAE Paper 2011-01-2051*, 2011.
Appears in p. 228 in Chapt. 5-[42]

Yates A.D.B., Vlljoen C.L., Swarts A., "Understanding the Relation Between Cetane Number and Combustion Bomb Ignition Delay Measurements". *SAE Paper 2004-01-2017*, 2004.
Appears in p. 194 in Chapt. 5-[5]

Yeh C., Kamimoto T., Kobori S., Kosaka H., "2-D imaging of fuel vapor concentration in a Diesel spray via Exciplex-based fluorescence technique". *SAE Paper 932652*, 1993.
Appears in p. 34 in Chapt. 2-[84]

Zhao H., Ladommatos N., "Optical diagnostics for soot and temperature measurement in diesel engines". *Prog. Energy Combust. Sci.*, Vol. 24, pp. 221-55, 1998.
Appears in p. 134, 146 in Chapt. 3-[34]

Zhu J., Choi M.Y., Mulholland G.W., Gritzo L.A., "Soot Scattering Measurements in the Visible and Near-Infrared Spectrum". *Proc. Combust. Inst.*, Vol. 28, 439-46, 2000.
Appears in p. 135 in Chapt. 3-[38]